UNIVERSITÀ DEGLI STUDI DI TRIESTE

XXX CICLO DEL DOTTORATO DI RICERCA IN

SCIENZE DELLA TERRA E MECCANICA DEI FLUIDI

MORPHODYNAMICS OF MASS MOVEMENTS IN THE CROTONE-SPARTIVENTO FOREARC BASIN, SOUTHERN ITALY, THROUGH GEOLOGICAL AND GEOPHYSICAL DATA INTEGRATION

Settore scientifico-disciplinare: GEO/02
GEOLOGIA STRATIGRAFICA E SEDIMENTOLOGIA

DOTTORANDO / A
OLIVIERO CANDONI

COORDINATORE
PROF. PIERPAOLO OMARI

SUPERVISORE DI TESI
DR. CERAMICOLA SILVIA

TUTOR
PROF. CHRISTIAN GORINI

ANNO ACCADEMICO 2017/2018

UNIVERSITA DEGLI STUDI DI TRIESTE

XXXI CICLO DEL DOTTORATO DI RICERCA IN

SCIENZE DELLA TERRA E MECCANICA DEI FLUIDI

Morphodynamics of mass movements in the Crotone-Spartivento forearc basin, southern Italy, through geological and geophysical data integration

PhD Student

Oliviero Candoni

Thesis Supervisor

Dr. Silvia Ceramicola

Tutor

Prof. Christian Gorini

PhD program Coordinator

Prof. Pierpaolo Omari

ACADEMIC YEAR 2017/2018

Table of Contents

Abstract

Morphodynamics of mass movements in the Crotone-Spartivento forearc basin, Southern Italy, through geological and geophysical data integration

Submarine mass movements are widely present in marine environments, shaping the seafloor in all water depths and are major mechanisms by which sediments are transferred from shallow water areas across slopes into deep waters. In the last decades, improvements in geophysical methods used to image the seafloor and the subsurface have allowed a better characterization of submarine mass movements and the processes responsible for their occurrence. Particular attention is given by the scientific community to unravel the dynamics of complex mass movements in order to identify and characterize the factors that precondition certain areas to failure and thus trigger mass movements.

This study investigates the occurrence and the controlling factors of mass movements through a morphological characterization and then correlates them with the Plio-Quaternary geodynamics of the tectonically active margin of the Crotone-Spartivento forearc basin (Ionian Sea, Italy).

The study combines and integrates all available geophysical and geological data acquired over the last decades within the study area. Geophysical data are represented by swath multibeam data, sub-bottom profiles and multichannel seismic reflection data. In addition, the study makes use of vintage multichannel seismic data and public exploration wells.

The Crotone-Spartivento forearc basin has formed since the late Miocene as part of the Calabrian accretionary prism (CAP), characterized by the subduction of the African plate beneath the European plate. The tectonic history of the CAP has been dominated by Neogene episodes of rapid rollback of the African plate linked to back-arc spreading of the Tyrrhenian Sea, as well as by recent km-scale uplift of Calabria that has exposed parts of the inner Crotone basin on land. Recent studies of the CAP have provided evidence of recurrent mass movements during the Plio-Quaternary within the Crotone-Spartivento basin.

Based on differences in morphological features and spatial and temporal distribution, three types of mass movements are identified within the Crotone-Spartivento forearc basin: 1) Submarine landslides (SLs), 2) Headwall and sidewall canyon slides (HSSs), 3) Slope parallel stratified ridges (SPSRs). SLs are mainly located on slopes with gradients >5° and are characterized by 236 arcuate seafloor slide scars ranging from ca. 300 m to 16 km in length above mass transport deposits (MTDs) of different forms commonly occurring stacked at multiple levels within the stratigraphic succession. The two largest features occur on the Punta Stilo high, and are represented by previously recognized Assi failure and the newly identified Punta Stilo failure. HSSs are recognized as 847 arcuate and nested slide scarps ranging from tens of meter to ca. 3 km in lengths, that generally affect areas of steep slopes (>10°) on the headwalls and sidewalls of the canyon systems that incise the continental slope. SPSRs are represented by slope stratified ridges of km scale in length and tens of

meters in high and are interpreted as slow gravity gliding mass movements triggered by subsurface diapir structure and fault systems.

Stratigraphic analysis performed on newly and old multichannel seismic data allow the identification of three main unconformities (named MU, MPSU and MPCU) bounding four seismic units (units named A-D from the oldest to the youngest) on the Plio-Quaternary stratigraphic succession of the forearc basin. The unconformities and seismic units have been correlated to available wells and to stratigraphic units within the adjacent onshore Crotone basin. The three major unconformities have been tentatively dated to top of the Miocene (MU unconformity ~ 5.3 Ma), Middle Pliocene (MPCU unconformity ~ 3.4-3.6 Ma) and Middle Pleistocene (MPSU unconformity ~ 1.1-1.2 Ma) and associated to the Late Messinian / Plio-Quaternary tectonic major events that affected the Calabrian Arc.

The combination of the morphological characterization and the stratigraphic reconstruction shows that mass movements are widespread in the Crotone-Spartivento basin and that they occur above the MPSU unconformity. Analyzing the spatial and temporal distribution of the three types of identified mass movements respect to the stratigraphic succession of the basin, a relation between the tectonic events occurred during Plio-Quaternary times and the initiation of the mass movements is proposed: mass movements occur above the MPSU unconformity, that marks the initiation of a tectonic phase characterized by a ultra-rapid uplift of the Calabria margin, that coupled with a general subsidence of the Crotone-Spartivento fore arc basin led to an increased slope steepness of the continental slope and basin seafloor areas, thus causing the initiation of mass movements.

1 Introduction

This chapter is intended to provide information necessary for the reader to understand the scientific aims treated in this thesis. This will be achieved by presenting a general overview of the main scientific topic, that is mass movements in submarine environments, followed by explanation of why the Crotone-Spartivento forearc basin has been chosen as a relevant study area. The chapter is divided into three sub-chapters, intended to provide a general overview of submarine mass movements (1.1.1), a review of the preconditioning and triggering factors that cause mass movements (1.1.2) and a summary of how mass movements can be identified on geophysical data through the recognition of kinematic indicators (1.1.3).

Scientific and societal importance: interest in submarine mass movements and their consequences is increasing among the scientific community (Chiocci et al., 2011; Clare et al., 2016; Masson et al., 2010; Moscardelli and Wood, 2008; Urgeles and Camerlenghi, 2013). Thanks to multidisciplinary approaches and new advances in the technologies of geophysical exploration and in situ measurements, our understanding of mass movements has significantly advanced in the last decades. Nonetheless, further studies are necessary for a better comprehension of these phenomena, their relationship with the sedimentary dynamics of the continental margins on which they occur, and the factors that influence their development and emplacement.

Submarine mass movements are one of the main processes through which sediments are transported from shallow areas to deeper basins and through which the seafloor is shaped. In addition, some mass movements, such as submarine landslides, represent marine geohazards and have received wide attention, because of their potential impacts on both coastal areas and offshore infrastructures. For these reasons, it is important to understand the geological processes that govern the initiation and development of mass movements, the understanding of the failure kinematics, the failure history and the link between mass movements and the evolution of the margin on which they occur.

Scientific question and aim: this PhD focus on the Crotone Spartivento forearc basin, in the Ionian Sea, which forms part of the Calabrian accretionary prism (CAP) that has developed as a consequence of on-going subduction of the African beneath the European plates. Since the late Miocene, the CAP has experienced different forms of tectonic activity: episodes of rapid advance and thickening in the Pliocene and Pleistocene, followed by late Quaternary differential uplift that has resulted in exposure of the inner parts of the forearc basin on land in Calabria. The Crotone Spartivento basin and the entire Ionian Calabrian margin has been shown to be prone to mass movements (Ceramicola et al., 2014a, 2012; Coste, 2014; Morelli et al., 2011). However, questions remain open, regarding the spatial distribution and timing of mass movements, their linkages with subsurface tectonic, the triggers and pre-conditioning factors that could have caused them and if any relations are possible between the geological evolution of the margin and the occurrence of mass movements. To answer these questions, research has been undertaken into the seafloor and subsurface distribution and character of mass movements features within the Plio-Quaternary succession of the Crotone-Spartivento basin. The study is based on an extensive geophysical dataset, comprising different types of data, including swath multibeam bathymetric data, sub-bottom profiles and 2D multichannel seismic reflection data. The overall aim is to investigate the occurrence of mass movements in the Crotone-Spartivento basin, performing morphological, morphometric, echofacies and seismostratigraphic analyses to characterize the different types of mass movements, their spatial and temporal distribution and evaluate their possible relationship to the geologic evolution of the margin.

1.1 Submarine mass movements: processes and features

Mass movement is a generic term that refers to a geomorphic process in which a bulk downslope movement of soil or rock takes place driven by the force of gravity. From a mechanical point of view, mass failure occurs when the shear stress applied to a given material, such as marine sediment, exceeds its shear strength (Figure 1-1).

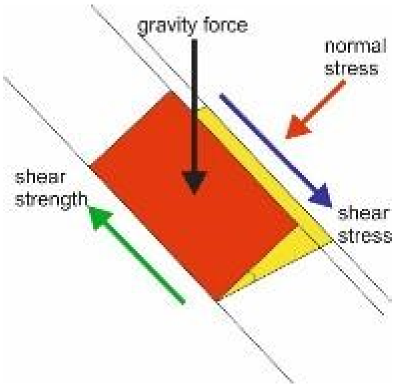

Figure 1-1: simplified schematic view of the forces acting on a portion of material in an inclined plane. Green arrow represents the shear strength, the blue arrow the shear stress, the red arrow the normal stress and the black arrow the gravity force. When the shear stress exceeds the shear strength, a failure occurs.

The essential features that characterize a submarine landslide are a shear or rupture surface and a displaced mass of sediment or rock (Hampton et al., 1996a); the rupture surface is where the failure took place and downward movements originates, while the displaced mass is the material that moves downward (Hampton et al., 1996a) and is defined as the mass transport deposit (MTD). The rupture surface may correspond to a discrete layer characterized by low shear strength, for example permeable sand layers, porous tephra layers or sand and clay interbeds. A variety of both compressional and extensional features are associated with mass movements. Extensional features are commonly present in the upper part of the slide, in the headwall domain, in the form of normal or listric faults perpendicular to the slide direction. In contrast, compressional features are present at the front of the slide, where internal deformation may be associated with folds and imbricate thrust slices. The main driving force for all types of mass movements is gravity.

Mass movements occur both on land and in marine environments and result in a wide variety of erosional and depositional features (Hampton et al., 1996a). Mass movements are widespread along continental margins, both on active and passive margins (McAdoo et al., 2000; Urgeles and Camerlenghi, 2013). They tend to occur in specific areas that have been recognized to be prone to mass movements, notably where thick bodies of sediments are present, where steep slopes and/or load exerted by the environment are high. These conditions are satisfied in areas like fjords, submarine canyon-fan systems, active river deltas on the continental shelf and on the open continental slope, where 50% of currently known landslides occur. As a consequence, the global distribution of submarine mass movements is not uniform (Lee et al., 2009; Mulder and Cochonat, 1996).

Different classes of submarine mass failures are recognized (Figure 1-2), related to the type of transport process in terms of mechanical behavior (Fei, 2013; Hampton et al., 1996a; Masson et al., 2006; Nardin et al., 1979; Shanmugam, 2016; Varnes, 1978) (Figure 1-3) or to observed relationships between slope mass failures, sourcing regions, dimensions and geometries (Moscardelli and Wood, 2015, 2008)(Figure 1-4).

From a mechanical point of view mass movements may be divided into slides, slumps, debris flows, debris avalanches and turbidity currents. Sliding involves brittle deformation of a coherent mass that translates along a planar glide plane (Figure 1-2). Slumping is a form of plastic deformation in which a coherent mass of sediments bounded on all sides by failure planes translates over a concave-up glide plane (Figure 1-2): the internal structure of the removed material is largely undisturbed, and displacement is limited. Slides and slumps can transform into debris flows or turbidity currents (Figure 1-2), due to increasing water content in the sliding material and disintegration of coherent blocks. Debris flow involves a plastic or laminar flow (Figure 1-2): the failed material is composed of heterogeneous sediment that may include large clasts supported by a mixture of water and mud, resulting in an internal structure that is poorly sorted and highly disturbed (Figure 1-2). A debris avalanche refers to the rapid flow of cohesionless rock fragments, blocks and clasts with a loss of energy due to the impact between the grains. Turbidity currents (Figure 1-2) are gravity flows in which the sediment is supported by the upward component of fluid turbulence and involve a continuous movement of a fluid body with a uniform velocity in a given direction. Turbidity currents are often formed by the disintegration of slides of debris flow, although they also may be generated independently of other gravity-driven processes (Mulder, 2011; Mulder and Cochonat, 1996). Different types of submarine mass movements produce different gravity-induced deposits (Figure 1-3) which may be used to reconstruct the likely type of submarine mass movement (Hampton et al., 1996b; Lee et al., 2009; Moscardelli et al., 2008; Shanmugam, 2016).

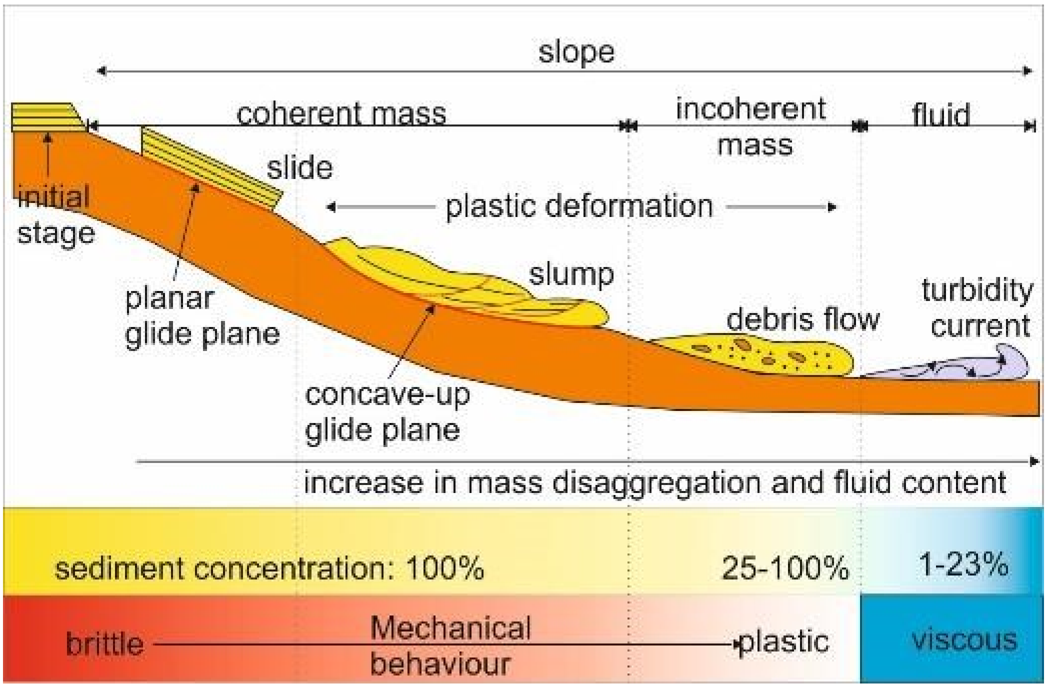

Figure 1-2: schematic cartoon showing the four common types of submarine mass movements and how gravity failures can evolve during their failure. A slide represents a coherent translational mass transport of a block on a glide planar plane (basal shear surface) with no internal deformation. A slide may evolve into a slump, i.e. a coherent rotational mass transport of a block or strata gliding on a rotational glide plane (basal shear surface) with internal deformation. If the mass moving downslope enriches in fluids, the slumped material may transform into a debris flow, which transports sediment as an incoherent chaotic body in which intergranular movements predominated over shear-surface movements. A debris flow acts as a plastic laminar flow with strength. If the fluid content increases, the flow could eventually evolve into a turbidity current. Slumps and debris flows dominated the upper slope. However, some turbidity currents may evolve directly from sediment failures. The sediment concentration is variable in gravity-driven processes, from a 100% for slides and slumps and decreasing up to 25% in debris flow, and to 1-23% only for the turbidity currents (Shanmugam et al. 2016). Based on mechanical behavior, gravity-driven mass transport can have more brittle behavior in the case of slides and slumps to more plastic behavior in the case of slumps and debris flows. Turbidity currents are not included, because they have a viscous behavior (modified from Shanmugam et al., 2016).

A second classification, proposed by Moscardelli et al., (2008) is based on the relationship between slope mass failures, sourcing regions, dimensions and geometries of mass movements to better understand the causal mechanisms and the pre-failure conditions: 1) shelf-attached MTDs (Figure 1-4a), 2) slope-attached MTDs (Figure 1-4b), 3)detached MTDs (Figure 1-4c,Figure 1-4d,Figure 1-4e).

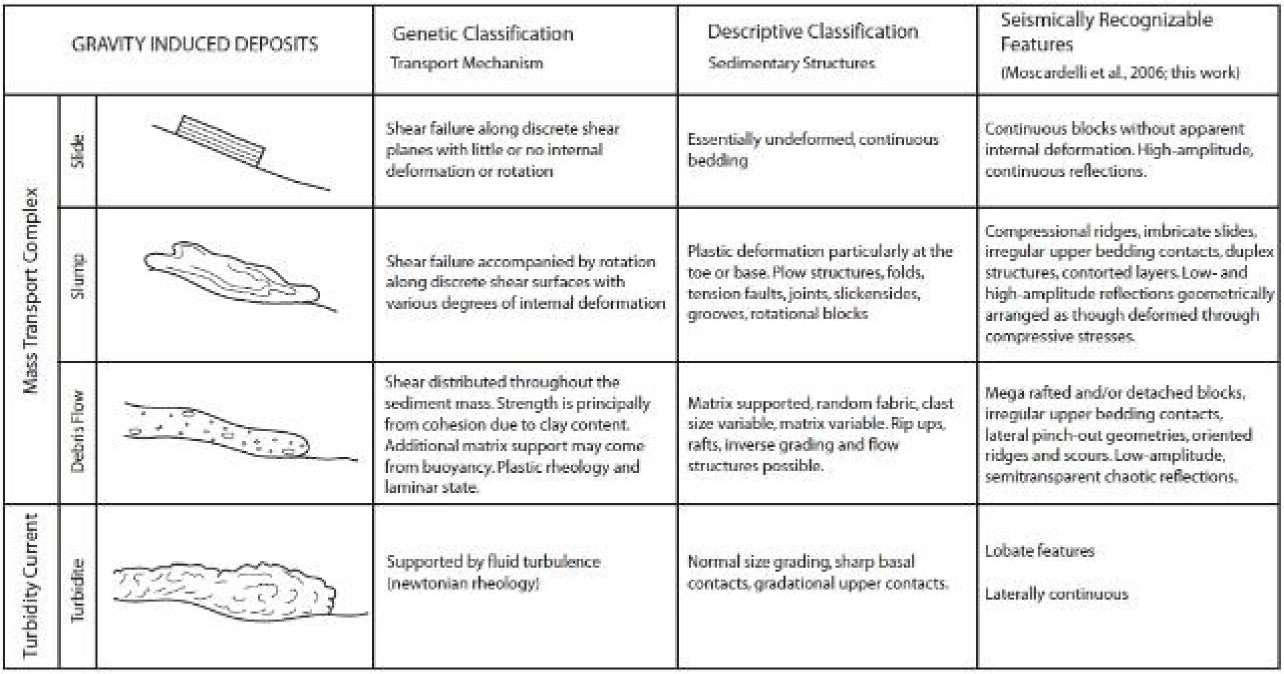

GRAVITY INDUCED DEPOSITS		Genetic Classification Transport Mechanism	Descriptive Classification Sedimentary Structures	Seismically Recognizable Features (Moscardelli et al., 2006; this work)
Mass Transport Complex	Slide	Shear failure along discrete shear planes with little or no internal deformation or rotation	Essentially undeformed, continuous bedding	Continuous blocks without apparent internal deformation. High-amplitude, continuous reflections.
	Slump	Shear failure accompanied by rotation along discrete shear surfaces with various degrees of internal deformation	Plastic deformation particularly at the toe or base. Flow structures, folds, tension faults, joints, slickensides, grooves, rotational blocks	Compressional ridges, imbricate slides, irregular upper bedding contacts, duplex structures, contorted layers. Low- and high-amplitude reflections geometrically arranged as though deformed through compressive stresses.
	Debris Flow	Shear distributed throughout the sediment mass. Strength is principally from cohesion due to clay content. Additional matrix support may come from buoyancy. Plastic rheology and laminar state.	Matrix supported, random fabric, clast size variable, matrix variable. Rip ups, rafts, inverse grading and flow structures possible.	Mega rafted and/or detached blocks, irregular upper bedding contacts, lateral pinch-out geometries, oriented ridges and scours. Low-amplitude, semitransparent chaotic reflections.
Turbidity Current	Turbidite	Supported by fluid turbulence (newtonian rheology)	Normal size grading, sharp basal contacts, gradational upper contacts.	Lobate features Laterally continuous

Figure 1-3: classification of gravity-induced deposits according to a sedimentological point of view. For each gravity induced deposits type, are reported the genetic classification, a description based on the sedimentary structures and the seismically recognizable features (from Moscardelli et., 2008).

Attached MTDs (Figure 1-4a, Figure 1-4b) may be quite large, up to thousands of square km in area and hundreds of meters in thickness with source areas usually related to extra basinal systems like shelf-edge deltas and zones of collapse present in the upper-slope region and are generated by regional basin scale events, like earthquakes, relative sea-level changes, the occurrence of gas-hydrate dissociation, high sedimentation rates, storms and hurricanes and longshore currents. On the other hand, detached MTDs (Figure 1-4c,Figure 1-4d,Figure 1-4e) are smaller in size (areas <10 km^2), and their cause is mostly related to local gravitational instabilities that can be related to seismicity, oversteepening of slope or diapir / volcano activities (Moscardelli and Wood, 2008)

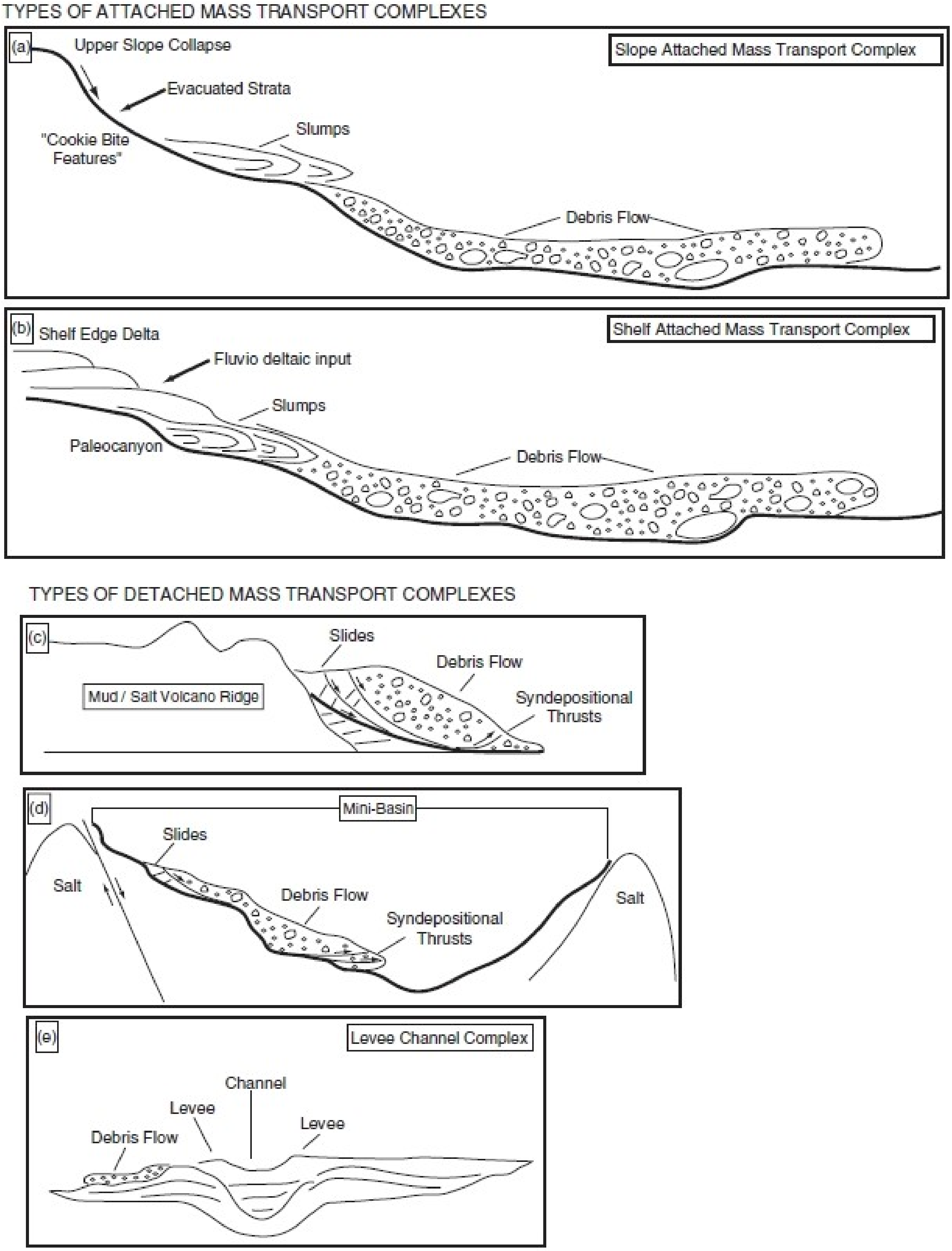

Figure 1-4: a schematic view of the three different types of MTDs and the processes associated with their genesis. A) Slope- attached mass transport complex sediments originated from the collapse of the upper slope. B) Shelf-attached mass transport complex sediments are delivered by shelf-edge deltas and are released into the deep-marine basin. C) Detached mass transport complex whose genesis is related with the collapsing flank of a mud-volcano ridge. D) Detached mass transport complex whose genesis is related with oversteepening of one of the margins of a deep-water basin. E) Detached mass transport complex whose genesis is related with a levee-channel complex (from Moscardelli et al., 2008).

1.2 Pre-conditioning factors and triggering mechanisms

The process of downslope sliding of a mass begins when the shear stress applied to the sediment exceeds its shear strength thereby causing failure. The process is argued to be controlled by long-term pre-conditioning factors and short-term trigger mechanisms (Locat and Lee, 2002; Sultan et al., 2004a)(Figure 1-5).

Pre-conditioning factors can be defined as the physical and geotechnical properties of sediments resulting from initial deposition and post-depositional alteration, which can contribute to instability (Ercilla and Casas, 2012), but do not necessarily initiate the failure. Examples of pre-conditioning factors discussed below are high sedimentation rates, the existence of a weak layer deposited over time, climate change over hundreds of years, slope steepening and presence of diapiric processes (Masson et al., 2006). Triggering mechanisms are defined as an external stimulus that initiates the slope instability process (Sultan et al., 2004a): examples of triggering mechanisms discussed below are earthquakes/seismic loading, storm wave loading, gas hydrate and gas hydrate dissociation, fluid flow and seepage (Locat and Lee, 2002). The distinction between pre-conditioning and triggering factors is not always simple but understanding their relative importance and the role played by each is of importance to advance our knowledge of submarine landslide processes.

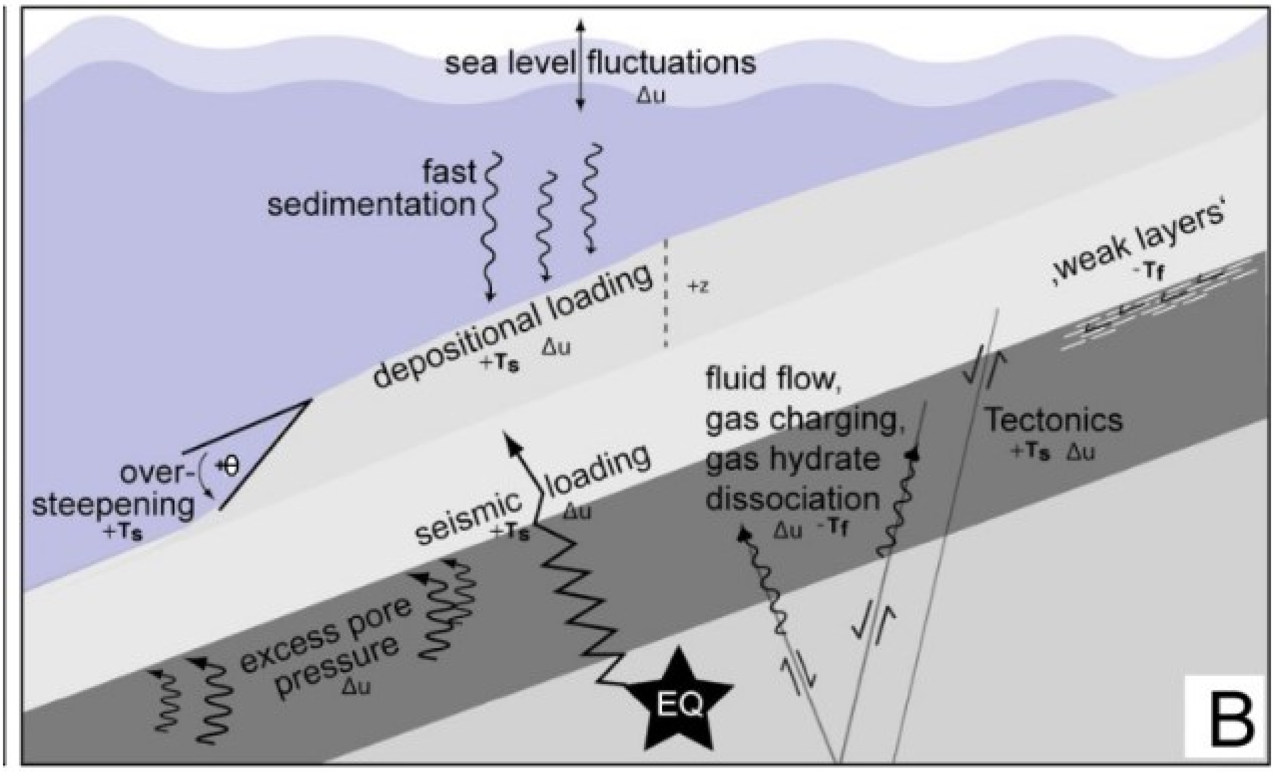

Figure 1-5: schematic diagram showing how different geological processes affect slope instability (from Strozyk, 2009).

1.2.1 Pre-conditioning factors

Sedimentation rates

Spatial and temporal variations in sedimentation rates influence the shear resistance of sedimentation. High sedimentation rates, for example, generate overpressures (pressure in excess of hydrostatic) and so reducing the effective stress. Sediment properties such as grain size, structural arrangements and permeability affect the dissipation of internal overpressures in the sediments (Laberg and Camerlenghi, 2008). At high latitudes, variations in sedimentation rate during alternations of glacial and interglacial periods seems to have been a main pre-conditioning factor for slope failure along the northwestern European continental margin (Bellwald et al., 2016; Laberg et al., 2003). In low latitudes, rivers may discharge large quantities of sediment to relatively localized areas on the continental margins, with high sedimentation rates (Lee, 2005). Thick, often under consolidated sediments can fail even on very gentle slope angles (<1°).

Weak layer

Weak layers play a major role in the development of many submarine landslides. A weak layer has been defined as "layer (or band) consisting of sediment or rock that has strength potentially or sufficiently lower than that of adjacent units (strength contrast) to provide a potential focus for the development of a surface of rupture (Figure 1-6). Such a layer or a band can follow stratigraphic horizons, but this is not a requirement. In addition, weak layers can develop in strain softening sediments where progressive failure can generate a surface of rupture without the need to invoke the role of excess pore pressures" (Locat et al., 2014).

An open question regarding weak layers is whether they existed prior to the landslide or resulted from the failure mechanism. A rupture phase takes place where an existing surface with lower resistance or reduction in the shearing resistance exists, and it cannot resist the gravitational driving forces. In marine environments such weak layers are often linked with sediments characterized by some level of stratification (or layering) or they may result from landslide re-activation on a pre-existing surface of rupture (Locat et al., 2014). In seismic data, failure surfaces commonly follow the stratigraphic horizons identified by strong reflectors (Levesque, 2004; Masson et al., 2010). Table 1-1 presents a compilation of weak layers observed in submarine landslides studies. It is worth noting how various types of sediments and failure processes involved a weak layer.

Weak layers can result from various processes: sedimentological (e.g. layering), geotechnical (e.g. strain softening) and geochemical (e.g. leaching) (Locat et al., 2014). According to the definition provided above, Locat et al (2014) recognized two types of weak layers: inherited and induced (Figure 1-7). An inherited weak layer is a layer (or stratigraphic horizon) where strength was already low before landslide initiation (Locat et al., 2014): examples are weak layers developed as part of an older landslide, long-term weathering, presence of joints or aligned pockmarks. An induced weak layer is a layer in which the strength is reduced during the slide process (Locat et al., 2014), as in the case of external forces (e.g. earthquakes), local liquefaction, gas hydrate dissociation, development of strain softening behavior, cementation.

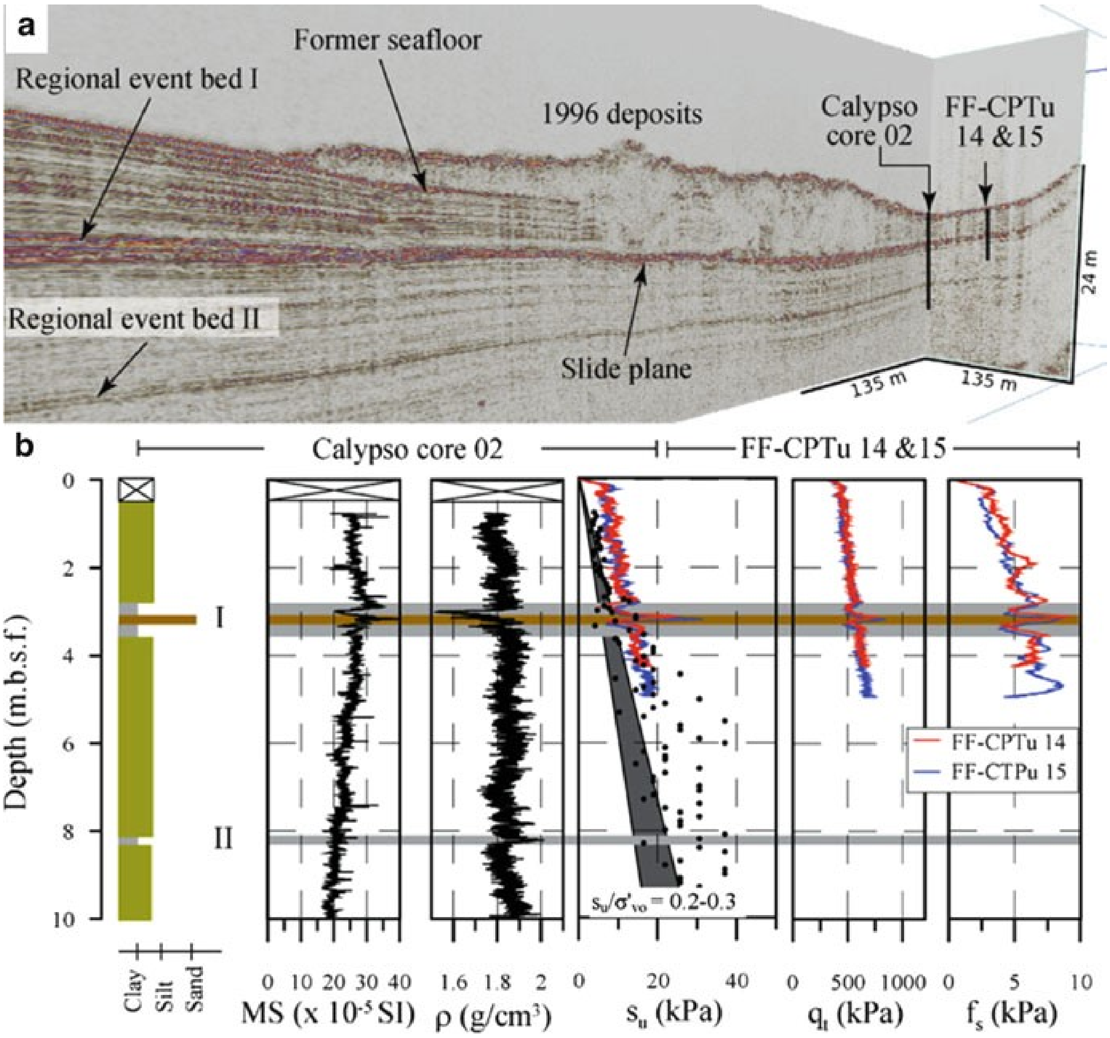

Figure 1-6: Example of a surface of rupture (a and b) identified as an event layer comprised between more resistant layers. The origin of the landslide is ascribed to a slide plane located in the Holocene sedimentary succession and related to a weak layer composed of highly sensitive clays (quick clays) (from L'Heureux et al., 2012).

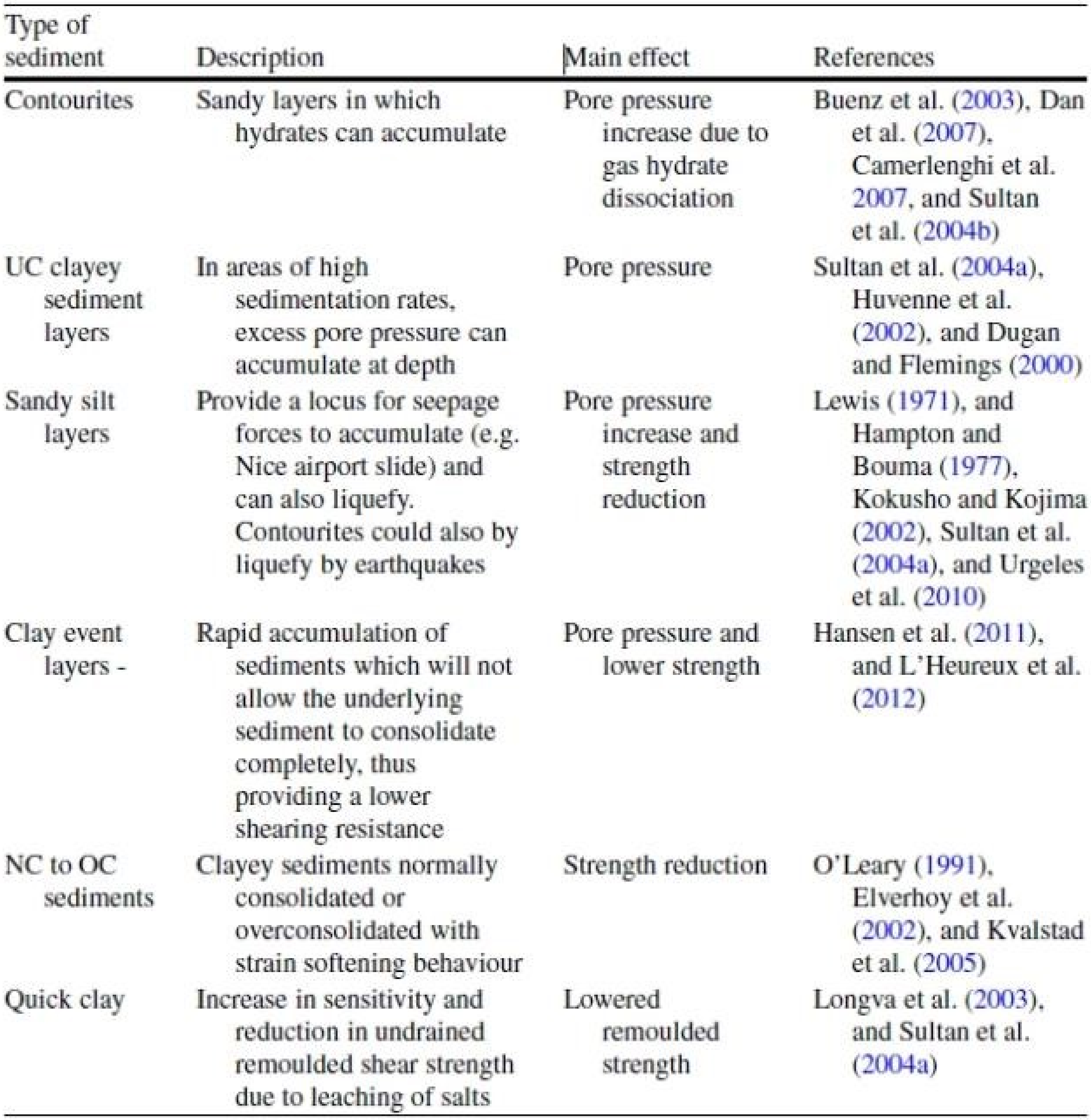

Type of sediment	Description	Main effect	References
Contourites	Sandy layers in which hydrates can accumulate	Pore pressure increase due to gas hydrate dissociation	Buenz et al. (2003), Dan et al. (2007), Camerlenghi et al. 2007, and Sultan et al. (2004b)
UC clayey sediment layers	In areas of high sedimentation rates, excess pore pressure can accumulate at depth	Pore pressure	Sultan et al. (2004a), Huvenne et al. (2002), and Dugan and Flemings (2000)
Sandy silt layers	Provide a locus for seepage forces to accumulate (e.g. Nice airport slide) and can also liquefy. Contourites could also by liquefy by earthquakes	Pore pressure increase and strength reduction	Lewis (1971), and Hampton and Bouma (1977), Kokusho and Kojima (2002), Sultan et al. (2004a), and Urgeles et al. (2010)
Clay event layers -	Rapid accumulation of sediments which will not allow the underlying sediment to consolidate completely, thus providing a lower shearing resistance	Pore pressure and lower strength	Hansen et al. (2011), and L'Heureux et al. (2012)
NC to OC sediments	Clayey sediments normally consolidated or overconsolidated with strain softening behaviour	Strength reduction	O'Leary (1991), Elverhoy et al. (2002), and Kvalstad et al. (2005)
Quick clay	Increase in sensitivity and reduction in undrained remoulded shear strength due to leaching of salts	Lowered remoulded strength	Longva et al. (2003), and Sultan et al. (2004a)

Table 1-1: Examples of weak layers that have been related to submarine slide studies in relation to the type of sediment involved (Buenz et al., 2003; Camerlenghi et al., 2007; Dan et al., 2007; Dugan and Flemings, 2000; Elverhøi et al., 2002; Hampton and Bouma, 1977; Hansen et al., 2011; Huvenne et al., 2002; Kokusho and Kojima, 2002; Kvalstad et al., 2005; Lewis, 1971; L'Heureux et al., 2012; Locat et al., 2014; Longva et al., 2003; O'Leary, 1991; Sultan et al., 2004a, 2004b; Urgeles et al., 2010).

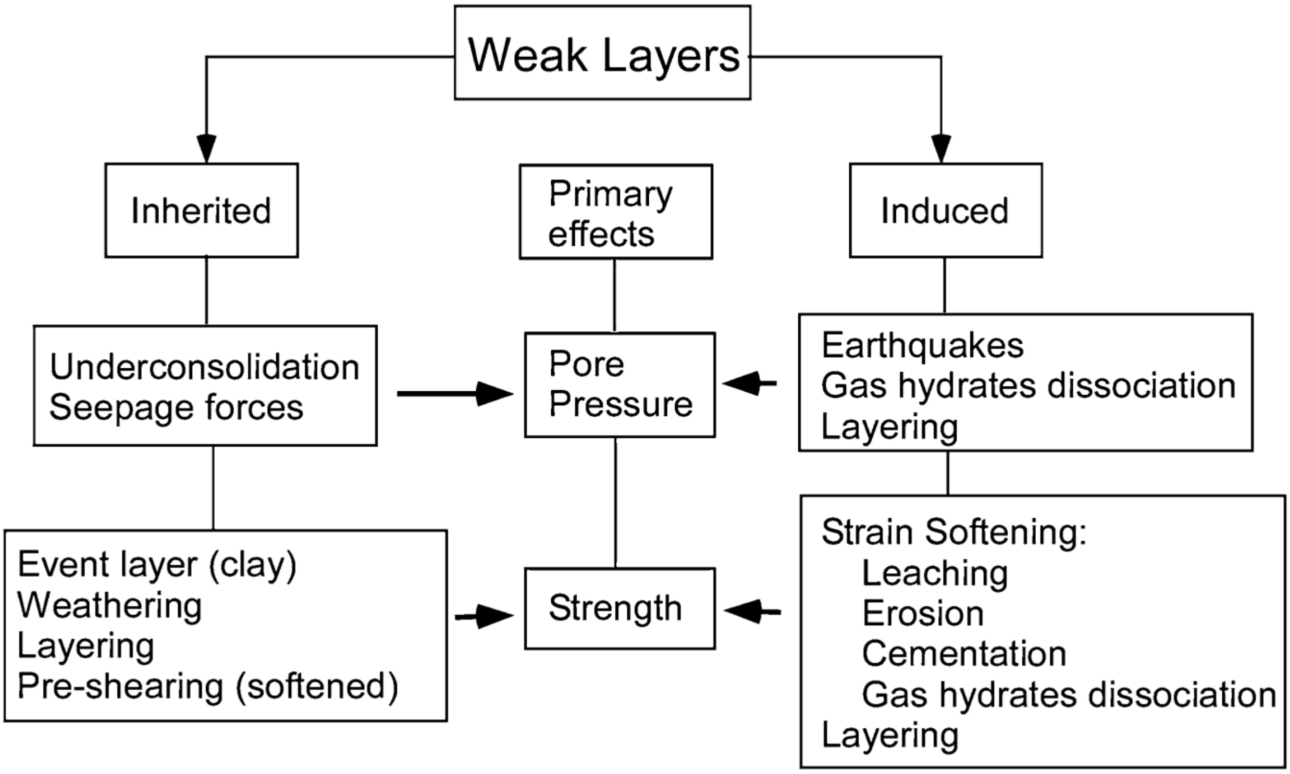

Figure 1-7: image showing a combined sedimentological and geotechnical classification system for weak layers. The horizontal arrows point in towards the direction of the primary effect of the process involved (from Locat et al., 2014)

Climate change

Climate is an important pre-conditioning factor because it influences other factors, e.g. changes is sea level, water temperature, gas hydrate stability or sedimentation rates. Owen et al., (2007) demonstrate how Late Pleistocene submarine mass movements on the North Atlantic area have been influenced by climatic change, through a combination of isostatic and sedimentary processes related to the sea level oscillation. A correlation between largest failures and low stand periods have been suggested for the Mediterranean region too (Urgeles and Camerlenghi, 2013). Rising sea level during interglacial periods can enhance water loading on continental margins thus leading to overpressures in sediments (Kremer et al., 2017), like for the Holocene Storegga Slide (Smith et al., 2013a), or have the potential to cause bending stresses that could lead to enhanced seismicity (Brothers et al., 2013). Glacial cycles due to the climate change leave distinct sedimentary columns. During interglacial periods pelagic sedimentation tends to dominate, producing clays, silts and muds which are sediments associated with high water content. During glacial periods and particularly during deglaciation, glaciogenic sedimentation dominates. Deposited on top of soft pelagic muds, the glaciogenic sediment will compact them and force the pore fluids out of the pore spaces and into migration leading to a generation of a weak layer (Owen et al., 2007a). Changes in the water temperature can produce an upward shift of the gas hydrate stability zone, resulting in a hydrate dissociation and consequently produce weak layers within the sediments. On the other hand, an increase of the pressure by the water column at the seafloor due to sea level rise would shift the base of the hydrate stability zone downward (Kremer et al., 2017). It is worth nothing that the influence of climate change on submarine mass movements is still debated and recent studies (Urlaub et al., 2013a) shows that there is not a clear correlation between the frequency of major slope failures on passive margins and sea level oscillation.

Slope steepening

Slope steepening is usually related to an interplay between two adjacent areas, one characterized by uplift and the other by subsidence: this could be due to tectonic activity with faults displacing the seafloor, salt tectonics in which upward migration of diapir lead to steeper flanks locally. All such differential activity leads to a steepening of the intervening slopes and thus generating a potential pre-conditioning factor. Slope steepening has been invoked by Strozyk et al., (2010) for landslide occurrences along the Hellenic forearc basin and the northeastern Cretan margin, or by Leslie and Mann (2016) for giant submarine landslides on the Colombian margin. Another element that could lead to slope over-steepening is high sedimentation rates (Leslie and Mann, 2016) However, there is disagreement among the scientific community on the role played by slope steepening. According to some authors like McAdoo et al., (2010), Urlaub et al., (2013), a steep slope is not necessarily a pre-conditioning factor, since it has been demonstrated how submarine landslides can take place on slopes of less than 3°.

Diapiric processes

Diapirism can influence the occurrence of mass movement with the consequences such as slope steepening that increases the likelihood of slope failure (Lee et al., 2009a), or hydrate dissociation caused by a salt rise (Sawyer et al., 2015). Mud or salt diapirs have been invoked as potential triggering factors, for example in the Gulf of Mexico, where halokinetic processes are known to occur (E. Tripsanas et al., 2004; Tripsanas et al., 2003) or in the Espírito Santo Basin, SE Brazil (Gamboa et al., 2012). Another example of the interplay between salt diapirs and mass movements occurrence is provided by Akinci and Sawyer (2016) offshore North Carolina in the Carolina Trough, where a breached salt diapir is thought to have caused the Cape Fear slide (Akinci and Sawyer, 2016). Subsidence of salt basins and the uplift of salt diapirs have been invoked as the factors that lead to an over-steepening of the basin flanks, thus generating extensive and widespread rotational slump complexes: the mass transport deposits at the foot and lower parts of the flanks leads to a successive development of retrogressive translational slump and slides (Tripsanas et al., 2003) (Figure 1-8)

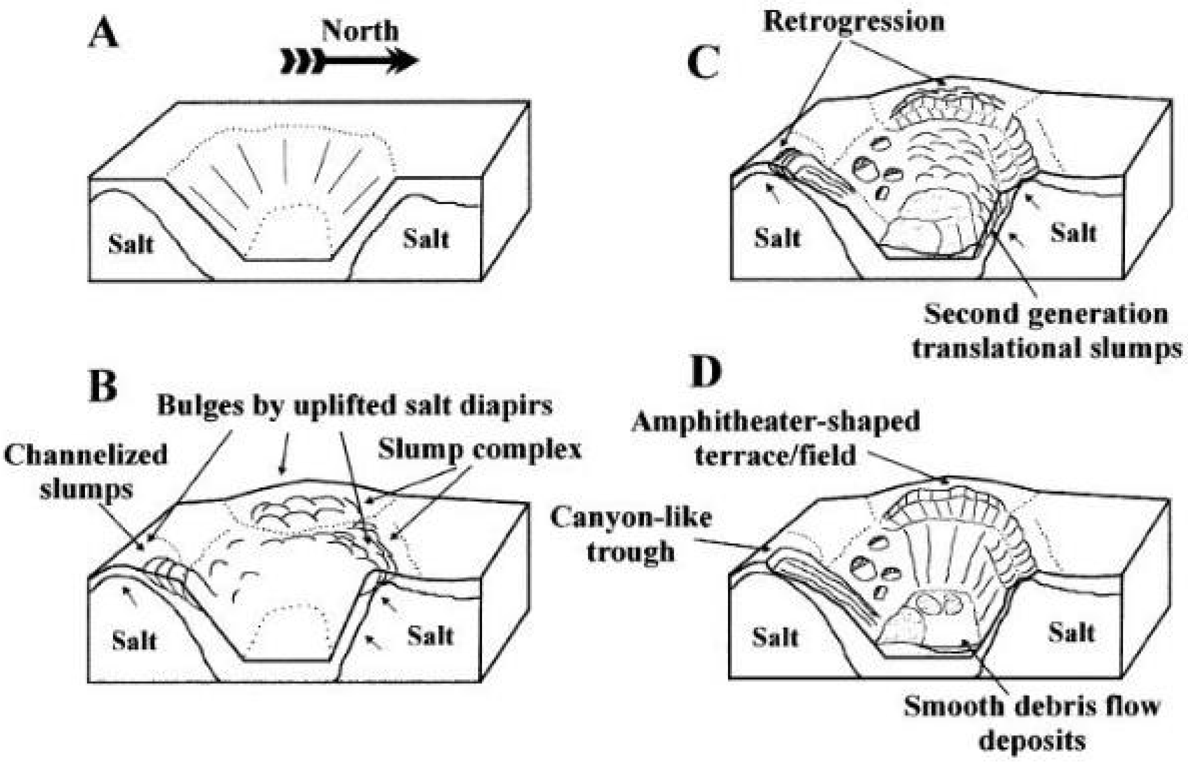

Figure 1-8: cartoon of the evolution of the Beaumont basin, the Gulf of Mexico due to salt activity. A) initial stage, B) mobilization of salt masses produce an increase of the flank gradients leading to development of deep rotational slump complexes, C) deposition of mass-transport deposits at the foot and lower parts of flanks leads to the development of successive sets of retrogressive translational slump/slides, D) present morphology, with major part of the failures translated in debris flows which filled the basin floors (from Tripsanas et al., 2003)

Mobilization of subsurface sediments is not limited to halokinetic processes but may also take place in shale-rich sedimentary environments. On accretionary prisms and deep fans, subsurface sediment mobilization can be widespread and produce a wide variety of structures, from deep buried anticlines, to seafloor active mud volcanoes. In shale tectonics, fluid dynamics exert a control on the shale mobilization and sediment liquefaction, generating overpressure that weakens the sediments above diapir structures. An example is found in the Niger Delta, where submarine slides are associated to regional compressional gravity driven deformation (Sultan et al., 2007). The Niger Delta is characterized by imbricate thrust structures affected by several submarine landslides, coinciding with known anticlines and faults (Figure 1-9).

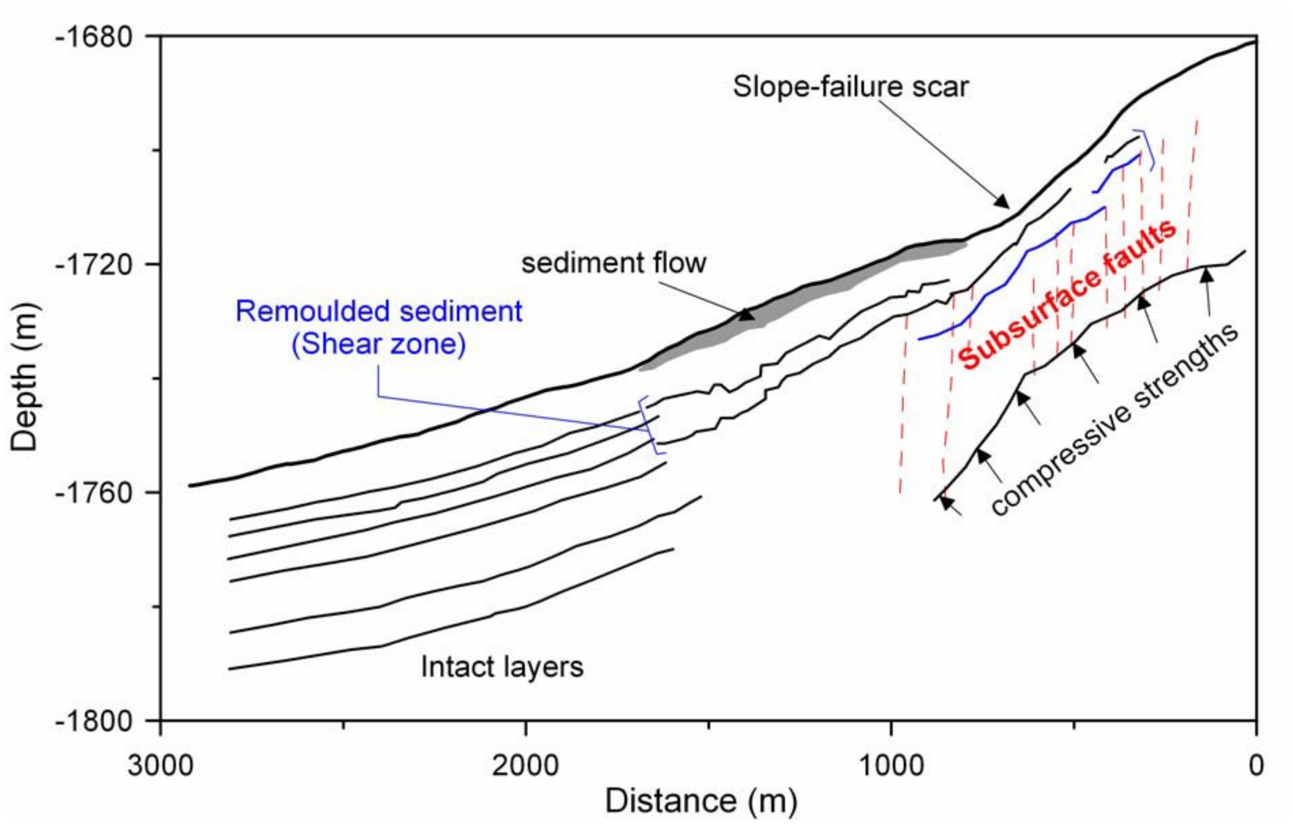

Figure 1-9: cartoon showing the internal architecture of the failure zone, where compressive strengths coupled with subsurface faults are related to the seafloor failure zone (from Sultan et al., 2007)

1.2.2 Triggering factors

Earthquakes/ Seismic Loading

Earthquakes are an important triggering factor, mainly resulting from plate tectonic activity. The seismic energy induced by plate tectonics is released through displacements in the Earth's crust, generating faults. Earthquakes influence the sediments in increasing the driving stress through seismic accelerations and also may trigger sediment liquefaction of coarse-grained, cohesionless sediments (Sultan et al., 2004). A better understanding of how earthquakes can trigger slope failure is provided by Nadim (2012), who presented three possible scenarios: 1) failure occurring during the earthquake because of the degradation of the shear strength due to excess pore pressure generated by cycling stress that the slope is not able to sustain the static shear stress; 2) post-earthquake failure, when the excess pore pressure generated by the cycling stress migrate from deeper layers into critical areas leading to slope instability; 3) after-earthquake failure due to creeping, believed to be the most common mechanism for clay-rich slopes (Fei, 2013).

Storm-wave loading

This mechanism is related to the generation of adjacent zones of relatively high and low pressure beneath the crests and troughs of waves, respectively, which in turn generate zones of higher shear stress halfway between the crests and troughs (Hampton et al., 1996). The induced shear stress is a function of wave characteristics and depth in the sediment column (Seed and Rahman, 1978). Storm waves can generate sediment failure only in relative shallow water, i.e. on the continental shelf and uppermost continental slope. This type of trigger mechanism seems to be particularly efficient and active in submarine canyons, because it generates sediment gravity flows, especially in canyon heads regions that affect the continental shelf (Puig et al., 2004).

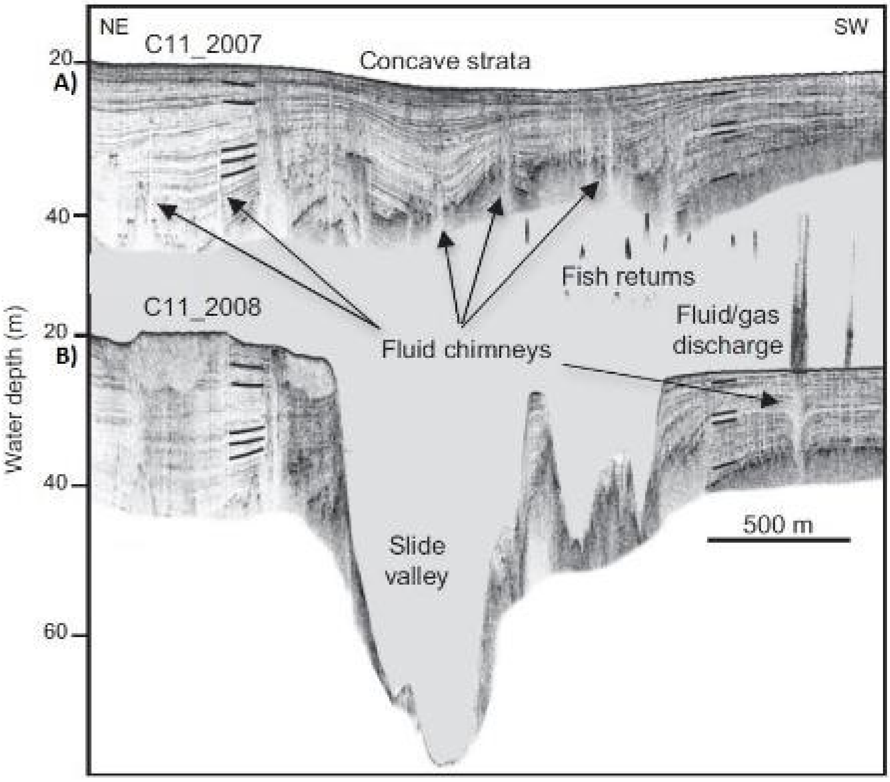

Figure 1-10: comparison of pre (A)-and post (B) -storm sonar images from a high resolution seismic profile along the northwestern canyon rim of No Ground submarine canyon, Bay of Bengal: liquefaction and massive slide valley formed due to the storm event (Rogers and Goodberg, 2010)

Rogers and Goodberd (2010) reported a mass failure over the Swath of No Ground submarine canyon at the Bay of Bengal due to a large tropical cyclone (Figure 1-10). They reported mass sediments flows interpreted as liquefied strata that formed in response to the hydrostatic loading and cyclic wave pumping during the storm. Sediment gravity flows related to storms and wave loading are also discussed in Puig et al., (2004) who analyzed the Eel Canyon, offshore California: storms lead to the development of excess pore pressure which causes liquefaction of sediment deposited at the head of the canyon.

Presence of Gas hydrate

Gas hydrates are solid crystalline compounds that encage gas molecules inside a water molecule lattice (Sloan, 2003). Gas hydrates form at relatively high pressures and low temperatures, such that in submarine settings they may occur within a subsurface zone of stability that is present in most places below depths of 300-700 m below sea level, and that generally thickens seaward to reach thicknesses that may exceed 1 km (e.g. Buffett, 2000). Gas charging affects sediment strength through the development of excess pore pressure. Perturbation of the system can cause the dissociation of gas hydrates, releasing both gas and water into the sediments and so greatly reducing their strength. The dissociation of gas hydrate may take place due to environmental changes: for example sea-level lowering reduces the stability zone of the gas hydrates, destabilizing the base of the gas hydrate zone, the part of the sediment column that is closest to the gas-hydrate equilibrium (Lee et al., 2009a). However, recent research (Elger et al., 2018) supports a link between gas hydrates and slope stability where climate-driven changes are not needed to trigger gas migration: gas hydrates reduce sediment permeability causing a build-up of overpressure at the base of the gas hydrate stability zone (Figure 1-11A). As a result, hydro-fracturing forms pipe structures allowing overpressure fluids to migrate upward (Figure 1-11B): when they reach a shallower permeable layer, the overpressure is transferred laterally and destabilize the slope (Figure 1-11C).

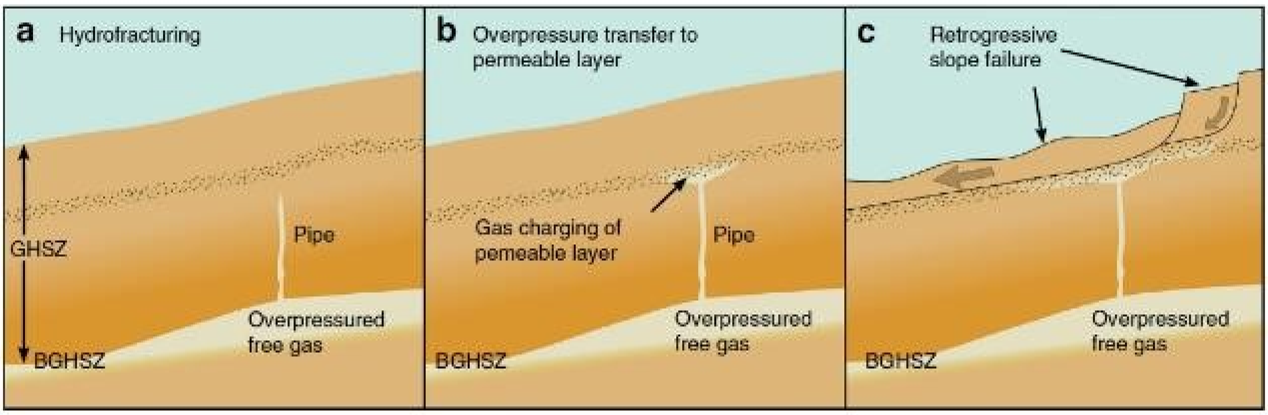

Figure 1-11: schematic model showing the evolution of retrogressive slope failure due to over pressured gas below the gas hydrate stability zone (from Elger et al., 2018).

Fluid flow

The presence of fluids within sediments may act as a triggering factor for failure, through geological and hydrological processes that cause excess pore pressure, thus reducing the shear strength of the sediments. Elements such as margin stratigraphy and permeability architecture are recognized to induce flow focusing and development of fluid overpressure, thus pre-conditioning low-angle slopes for failure (Yamada et al., 2012). However, the presence of the fluids and the generation of overpressures is not always enough to initiate slope failure: for example, in low-sedimentation passive margins, layers of anomalous low permeability that prevent fluid migration, or high permeability layers that allow more rapid lateral flow are needed. Another element could be the presence of weak layers (Urlaub et al., 2012). The presence of tectonic structures, like faults, can be important in relation to fluid flow, because they act as a preferential pathways for fluid migration, and thus leading to low slope instability conditions (Anasetti et al., 2012; Kawamura et al., 2012). Pockmarks or fields of pockmarks are commonly found in proximity of the headwall scarps (Casalbore et al., 2016)(Figure 1-12), typically often upslope of the slides in the undisturbed sediments (Hovland et al., 2002), suggesting a correlation between fluid migration and the destabilization of the upper sediment layers (Deiana et al., 2015; Lastras et al., 2004a; Lee et al., 2009). Pockmarks may increase the pore pressure of a weak reflector, or because they represent a bedding discontinuity, they can reduce shear resistance along potential failure planes (Lastras et al., 2004a).

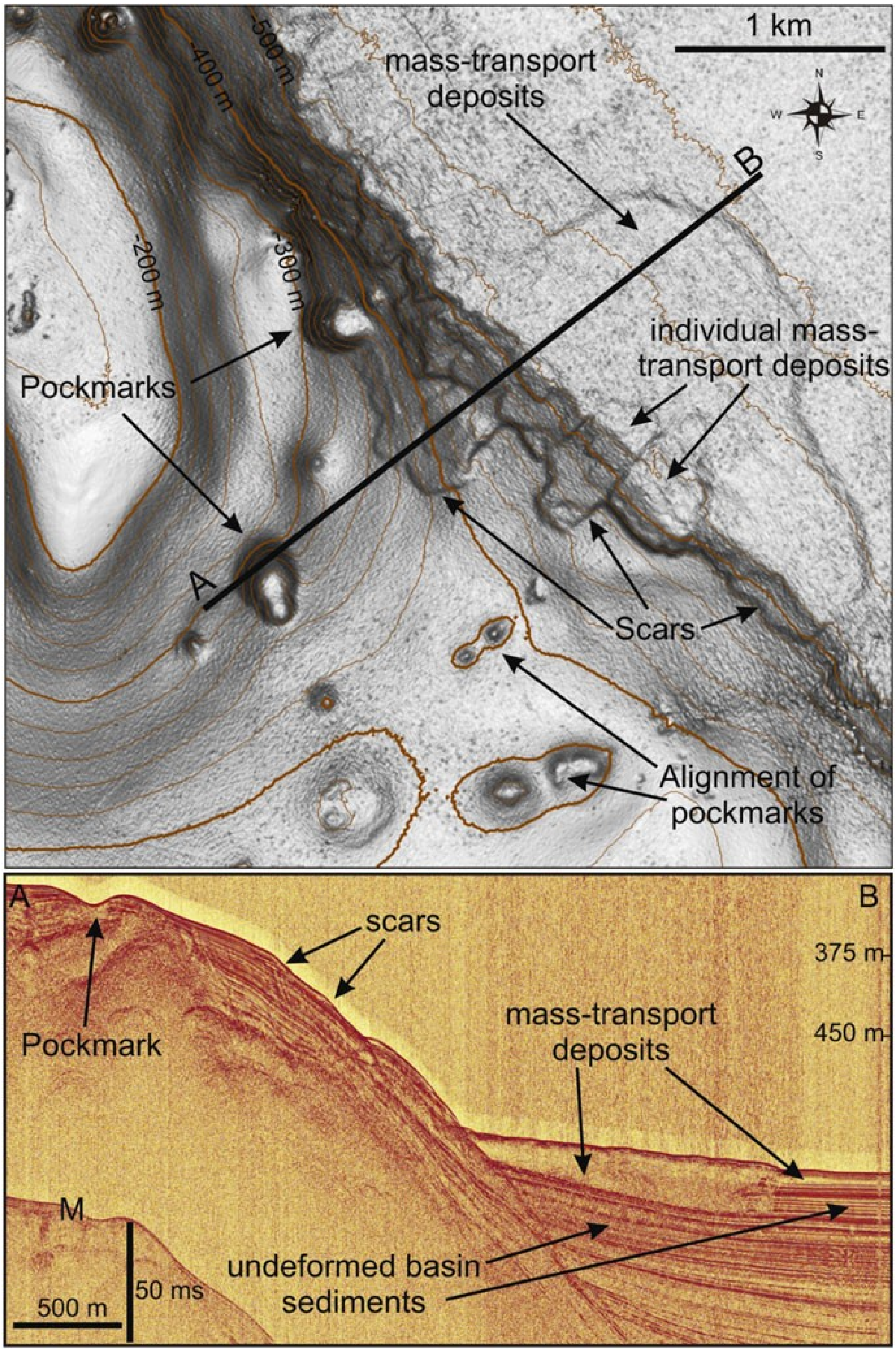

Figure 1-12: bathymetry and sub-bottom profile (position on the bathymetry) from the south- eastern flank of the Palmarola ridge, largely affected by slide scars and presence of pockmarks on the upper slope beyond the slide scars (from Casalbore et al., 2016).

1.3 Kinematic indicators from mass movements using geophysical data

As mentioned in Chapter 1.1, mass movements can be classified according to their mechanical behavior. The reconstruction of a mass movement can be analyzed through the recognition of certain kinematic indicators, defined as geological structures or features that the direction, mode, geometry and magnitude of a mass movement to be constrained (Bull et al., 2009a). The occurrence of such kinematic indicators is valid both on land and in marine environments. Below are presented kinematic indicators with reference to marine environments examined through the use of geophysical data.

Generally speaking, mass movements can be divided in three major domains: 1) the headwall domain, 2) the translational domain and 3) the toe or depositional domain (Figure 1-13 from Bull et al., 2009) These domains are not always easy to identify, because some overlap is possible. However, a clearly defined classification scheme allows a better comprehension of the investigated phenomena.

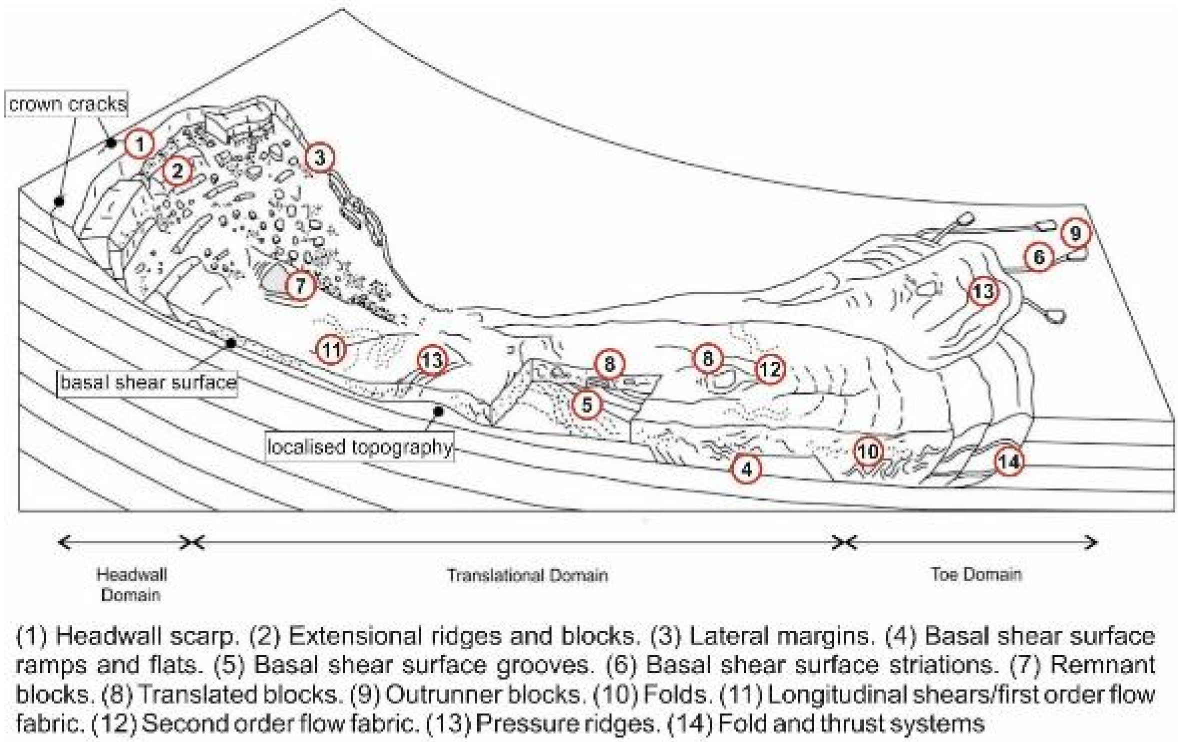

(1) Headwall scarp. (2) Extensional ridges and blocks. (3) Lateral margins. (4) Basal shear surface ramps and flats. (5) Basal shear surface grooves. (6) Basal shear surface striations. (7) Remnant blocks. (8) Translated blocks. (9) Outrunner blocks. (10) Folds. (11) Longitudinal shears/first order flow fabric. (12) Second order flow fabric. (13) Pressure ridges. (14) Fold and thrust systems

Figure 1-13: schematic representation of a mass movement and the likely associated kinematic indicators relative to the three domains (from Bull et al., 2009)

Headwall domain: This encompasses the upslope, extension dominated region of the mass movement. Two important kinematic indicators are found here: the headwall scarp and the extensional ridges and blocks (Figure 1-13). Headwall scarps can be defined as the boundary or scarp marking the upslope margin of a MTD, where the basal shear surface ramps up to cut stratigraphically higher, younger strata and intersects the surface (Bull et al., 2009b). These are features that can be easily recognized both in seismic and bathymetric data (Bull et al., 2009b). Their shapes, lengths and heights vary from slide to slide. The headwall scarp develops parallel to slope and perpendicular to the direction of the landslide movement, thus suggesting the direction of failure.

Headwall scarps are steeply dipping, with inclinations ranging from 10° to 35°. Another feature present in the headwall domain are crown-cracks, subtle, elongate depressions, that appear as linear features in planform while in seismic section are seen to be small scale faults or fractures (Frey-Martínez et al., 2006). Crown-cracks occur in the vicinity undeformed and undisplaced strata of the headwall scarp and form because of the extensional stresses related to the upslope propagation of a retrogressive failure.

Extensional ridges and blocks can be found within the area of failure of the headwall scarp, where the basal shear plane may be exposed or barely depleted. They represent discrete, detached units of translated material that have retained a high degree of internal coherency. Blocks may occur in a variety of scales and may undergo varying degrees of translation, with spacing, deformation and disintegration tending to increase with the distance away from the headwall scarp (Gee et al., 2007). Blocks are typically elongated along-strike direction, due to their association with normal faults oriented parallel-to-sub-parallel to the headwall scarp. However, with increasing distance downslope from the headwall scarp, they can disaggregate and reorient, decreasing in size and continuity and changing in direction, from parallel to the headwall to parallel to the general transport direction (Bull et al., 2009b). In seismic data, blocks can be identified as localized packages of undisrupted, continuous reflections bounded by normal-listric faults and which may be separated from the headwall scarp or other blocks by considerable gaps depending on the degree of translation (Bull et al., 2009b).

Translational domain: this domain comprises the main translated body of the mass movement, between the up and downslope extremes. The typical features are lateral margins, basal shear surface, internal body and top surface of a MTD.

Lateral margins are the side boundaries of a MTD, which form parallel to the gross flow direction and offer a primary constraint on the general transport direction. Lateral margins are associated with a transtensional or transpressional deformation, respectively if the MTD scar widens or narrows (Martinsen, 1994). In plan form, the upper part of a lateral margin commonly appears as a scarp or nonlinear feature roughly parallel to the slope direction. They can also be expressed as raised, positive features due to localized or net accumulation of material in the translational or toe domain of the MTD (Prior et al., 1984; Trincardi and Normark, 1989). A seismic section across a lateral margin, commonly reveals a contrast between undeformed strata and those disrupted by failure process, although this may be more difficult to detect where the translational domain does not exhibit a high degree of disruption (Bull et al., 2009b).

The basal shear surface or detachment surface, is one of the most important kinematic indicators because it yields important information about the dynamic emplacement of such events (Gee et al., 2007). In seismic data it usually appears as a continuous reflector that is concordant to the sediment bedding, but that may be affected by faults, bedding plane or material variations (Varnes, 1978). The basal shear surface is often assumed to correspond to a weak layer within which the shear stresses exceeded the shear strength, thus leading to the mass failure.

Ramps and flats describe vertical displacements of the basal shear surface. A ramp is defined as a segment of the basal shear surface that cuts discordantly across bedding, whereas the ‘flat’ sections are bedding-parallel segments of the basal shear surface (Bull et al., 2009b). In seismic sections, ramps are easily identifiable in the same manner as faults or the headwall scarp from truncation of underlying strata. Ramps can occur both parallel and perpendicular to the transport direction. Ramps can connect different basal shear surfaces if they are present (Bull et al., 2009b).

Grooves, named also furrows, are incisions with V shaped cross-sections that can extend for kilometers downslope and may merge seaward. These features are interpreted to be the result of the erosion by coherent blocks of translated material transported at the base of a debris-like flow (Gee et al., 2007, 2006; Posamentier and Kolla, 2003a). The identification of grooves is of particularly interest because they record the translation across the basal shear surface, providing information on the transport direction and an indication of the dominant process active during the development of the MTD (Bull et al., 2009b).

Striations also affect the basal shear surface. In contrast to grooves, they are linear, continuous features with a wider, flat bottom cross-section and no downslope divergence. As for grooves, they are associated with the translation of intact blocks of coherent material that “plough” the basal shear surface (Gee et al., 2006a), but in this case the striations represent ‘glide-tracks’ left by intact blocks that detach from the leading edge of the MTD and move downslope ahead of it and beyond it (Bull et al., 2009b).

Blocks and folds are also detectable within the translated MTD body and may have no expression on the top or bounding basal surfaces. These translational features can provide useful information about the flow direction. Rafted or intact blocks are coherent masses of sediment that have been transported within or in front of the failed mass and are often deposited within the translational domain (Bull et al., 2009b).

Depositional domain

The depositional domain represents the downslope region of the MTD that includes the downslope termination point, or “toe”, characterized by compressional regimes. The failed body often has an overall convex-downslope morphology that contains two main kinematic indicators corresponding to compressional features, i.e. pressure ridges and thrust and fold systems. Frey Martinez et al. (2006) suggested that the depositional domain can be divided into two categories: “frontally confined” and “frontally emergent”. The former is when the translated mass is buttressed downslope against stratigraphically equivalent undisturbed strata, the latter when the translated mass is able to ramp up from the original level of the basal shear surface and move freely across the seafloor (Frey-Martínez et al., 2006). Frontally confined MTDs are characterized by the development of large-scale thrust and fold system, whilst frontally emergent MTDs are characterized by pressure ridges. These two categories represent the end members of a range of possible intermediate situations.

2 Geological setting

2.1 Geodynamics of the Mediterranean Sea

2.1.1 Plate tectonic evolution

The formation of the Western and Central Mediterranean are related to the slow convergence (4-10 mm/yr) of the African and Eurasian plates (Royden and Faccenna, 2018). Subduction of the African beneath the European plate and a general SE migration of the trench has resulted in the opening of the Western Mediterranean as back-arc basins. The western Mediterranean started opening around 30 Ma ago in the Late Oligocene (Figure 2-1a), with the opening of the Liguro-Provençal back-arc basin followed by counterclockwise rotation and separation of the Corso-Sardinia-Calabro Peloritani block from the Iberian region between 20 to 10 Ma ago (Gueguen et al., 1998, Figure 2-1b). In Late Burdigaglian (ca. 15 Ma ago) this block separated into the Corso-Sardinia and the Calabro-Peloritani blocks (Gueguen et al., 1998) the latter of which moved to its present position between Sicily and Apulia at a rates of up to 6-8 cm/y (Goes et al., 2004). Between ca. 12-10 Ma ago separation of the two blocks was accompanied by back arc extension to form the Tyrrhenian Sea (Faccenna et al., 2001; Guillaume et al., 2010) via a series of extensional episodes that led to the formation of Vavilov back-arc basin during the Pliocene, ca. 4.3-2.6 Ma ago (Figure 2-2c), and the Marsili basin between 2 and 1 Ma ago (Gueguen et al., 1998, Figure 2-1d ; Guillaume et al., 2010). The latter Early Quaternary episode of back-arc extension was ultra-fast up to 19 cm/yr for the Marsili basin (Guillaume et al., 2010). Back-arc extensional episodes were accompanied by the advance and thickening of the sedimentary wedges of the Apennine-Maghrebide accretionary system to the east and south, generating large-scale thrusting and folding (Gueguen et al., 1998). The last 5 Ma (Figure 2-1d) are characterized by the opening of the Vavilov and Marsili basins, the southern Apennines collision with the thicker continental crust of the Apulian platform, halting the migration of the subduction front while in the northern and central Apennines subduction of the thin Adriatic oceanic lithosphere allowed the prosecution of slab retreat. From the Early Pliocene, subduction occurred only in the Ionian basin generating the Ionian foreland basin (Catalano et al., 2001; Cavazza and Barone, 2010). During the Pleistocene, uplift events took place throughout the Calabrian accretionary prism, causing subsidence of the basins and uplift of the Calabrian region, at rates more than 1 mm/y (Sartori, 2003).

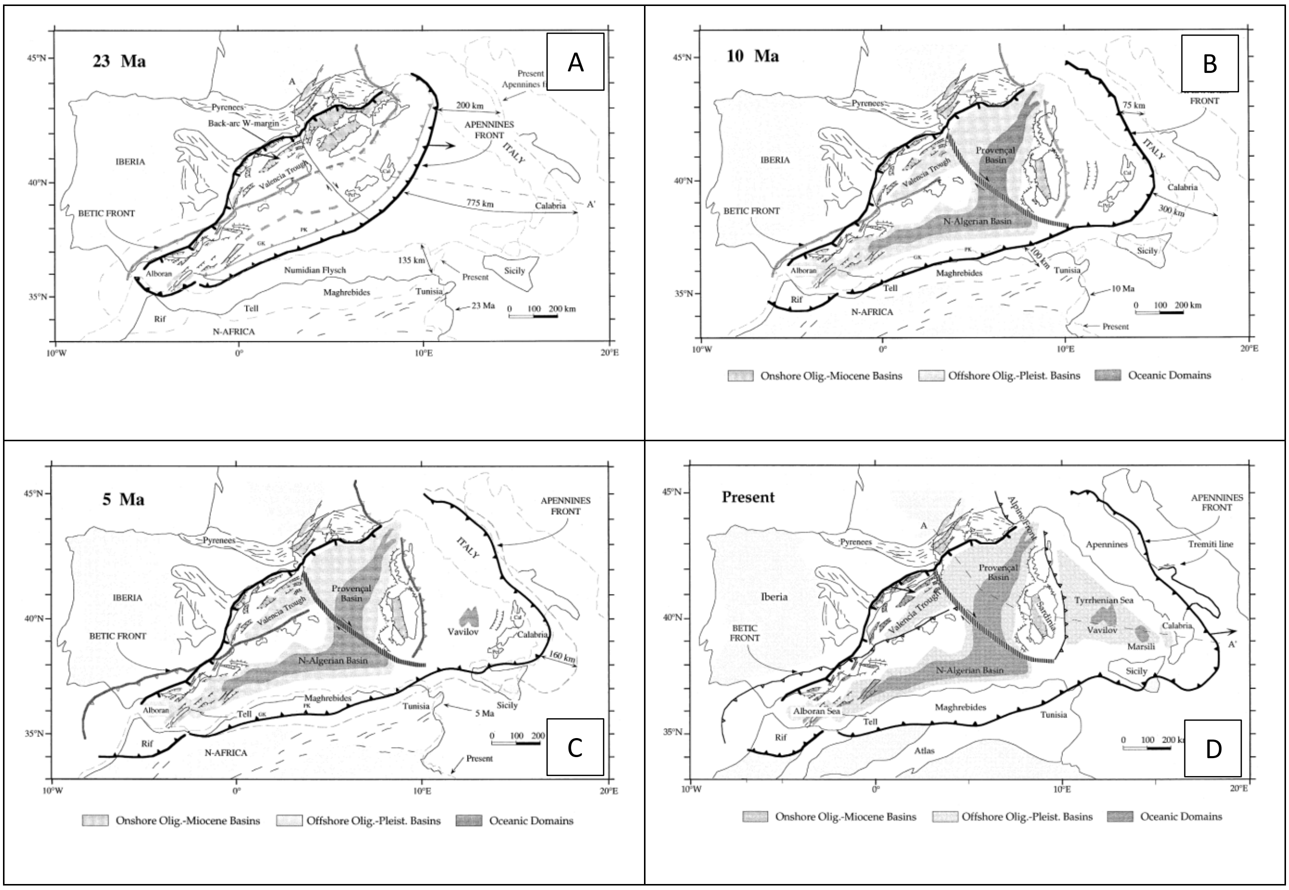

Figure 2-1: Late Oligocene to present evolution of the Mediterranean basin represented in four main steps from 23 Ma to present (modified from Gueguen et al., 1998)

The driving mechanism of the back-arc extension and trench migration is interpreted to be episodic trench roll-back and abrupt fragmentation of the subducting lithosphere due to the slab narrowing (Guillaume et al., 2010). According to Faccenna et al., (2010) three main stages can be depicted in the evolution of subduction in the western-central Mediterranean: the first lasted from 80 to 30-35 Ma and corresponded to initiation of subduction of the African Plate (Figure 2-2a); this was followed by slab development between 30 – 35 to 15 Ma with an increase in the subduction velocity and the development of back-arc basins (Figure 2-1b); while from 15 Ma to the present a slow-down convergence took place due to slab detachment and the opening of the Tyrrhenian back-arc basin (Figure 2-1c); the last phase is characterized by two episodes of rapid back-arc spreading (Faccenna et al., 2001; Gueguen et al., 1998; Malinverno and Ryan, 1986).

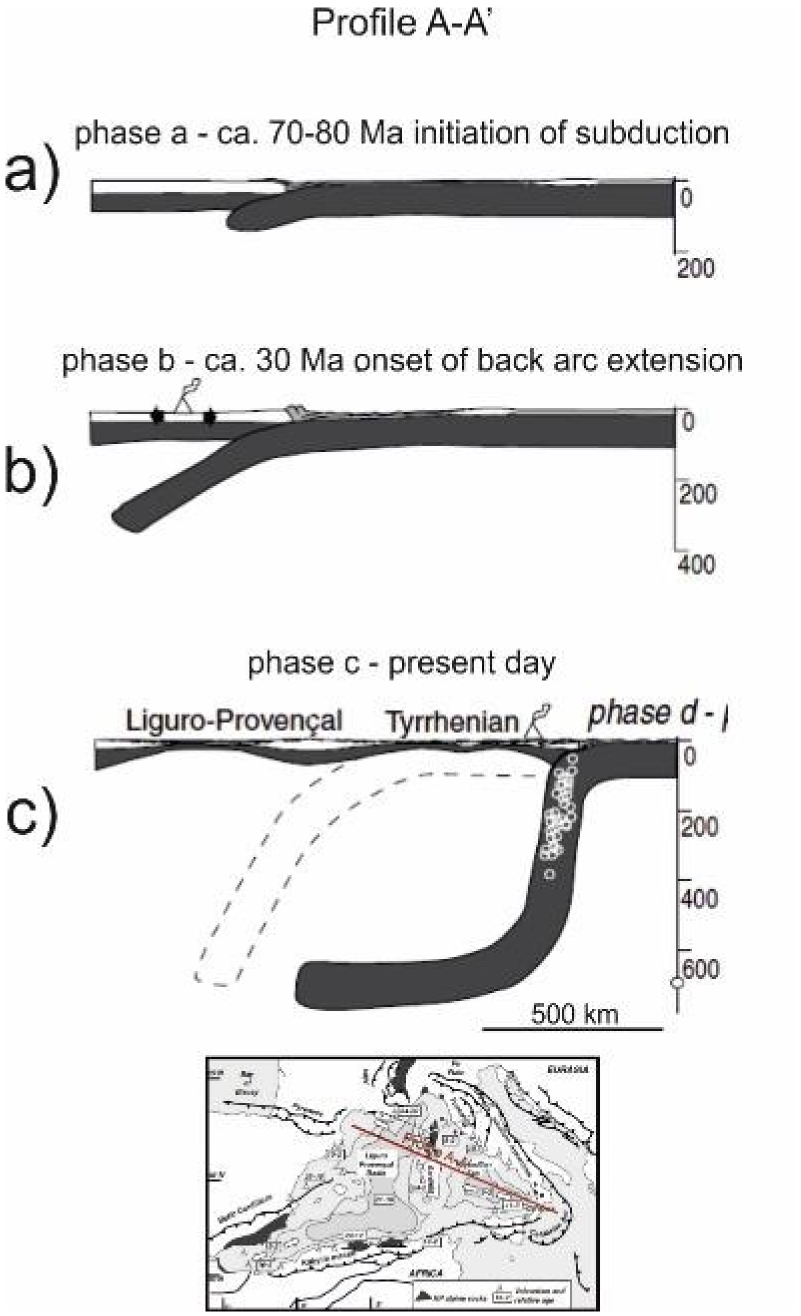

Figure 2-2: cross section showing the four-stage reconstruction of the subduction processes in the west-central Mediterranean (modified from Faccenna et al., 2001). For profile location see the inset in the figure.

2.1.2 The Messinan Salinity Crisis

The Messinian Salinity Crisis (hereafter referred to MSC, Hsu et al., (2003) represented a dramatic sea level fall that affected the entire Mediterranean basin in a relatively brief time span between 5.96 to 5.32 Ma (Duggen et al., 2003; Gautier et al., 1998; Krijgsman et al., 1999). The sea level fall was a response to the progressive closure of gateways between the Atlantic ocean and the Mediterranean Sea due to the convergence of the African and the European plates (Garcia-Castellanos and Villaseñor, 2011; Govers et al., 2009; Ryan, 2011, 2009) and an overall tectonic uplift of ca. 1 km in the Gibraltar strait area between 6.3 and 4.8 Ma (Duggen et al., 2003; Govers et al., 2009), . Thus the MSC is primarily attributed to a combination of tectonic events rather than a climatic change (Gargani and Rigollet, 2007; Jolivet et al., 2006).

The maximum sea level fall associated with the MSC is estimated to be from 1200 m to 2500 m (Gargani and Rigollet, 2007). The sea level drop led to subaerial exposure of most of the continental slopes generating a significant subaerial erosion all around the Mediterranean regions (Ryan, 1976). Furthermore, due to evaporation of the sea water, a huge amount of evaporitic layers (dolomite, gypsum, anhydrite and halite) were deposited in the basins, with thicknesses around 1 km or even more, i.e. 1.5 to 1.8 km in the deep basins for a volume estimated at ca. 1 million of m^3 (Lofi et al., 2005; Roveri et al., 2014; Ryan, 2009)(Figure 2-3).

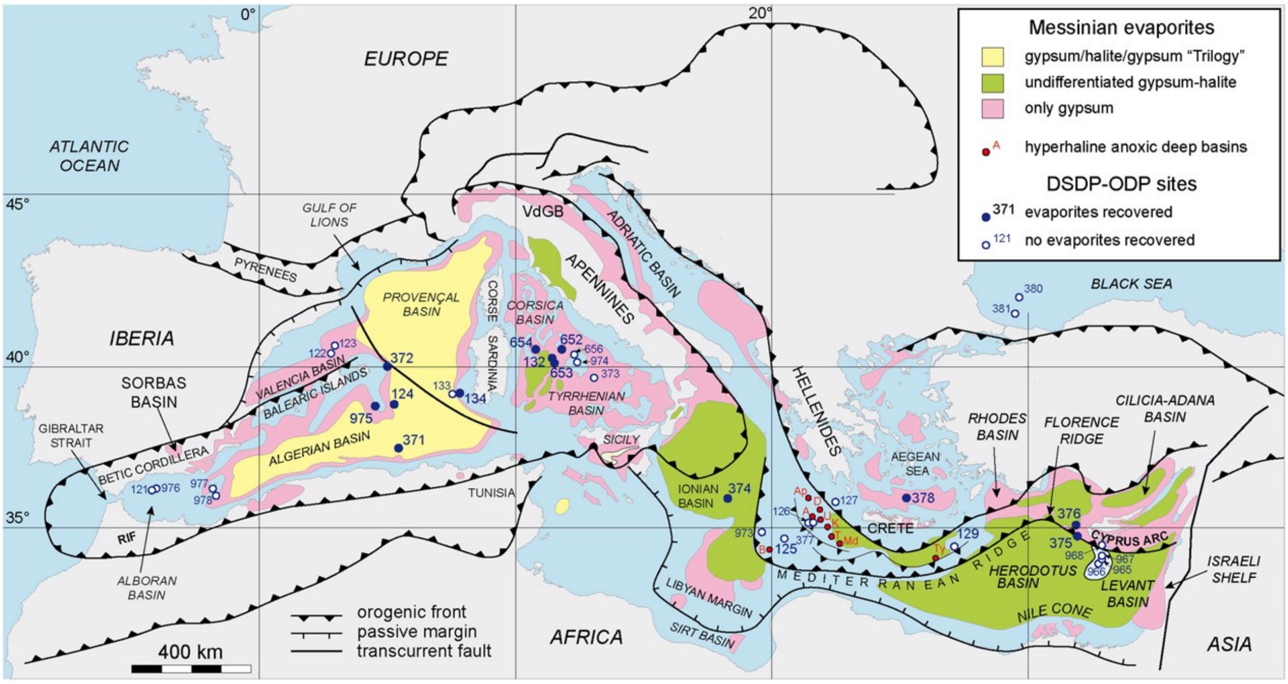

Figure 2-3: distribution of the Messinian evaporites in the Mediterranean Sea (from Roveri, 2014)

The MSC lasted up to the Zanclean times, when reflooding of the system occurred, due to the reconnection of the Mediterranean sea and the Atlantic ocean through the strait of Gibraltar (Blanc, 2002; Garcia-Castellanos et al., 2009; Hsü et al., 1973; Micallef et al., 2018).

Evidence of this pan-Mediterranean event is identifiable in outcrops onshore, such as in Sicily or the Apennines but also in offshore basins, in both the western and eastern Mediterranean. The key to unravelling the history of the crisis are the Messinian erosional surfaces, considered the Rosetta Stone of the MSC in the onshore areas (Ryan, 2009). Onshore Messinian successions usually correspond to marginal or peripheral basins, whereas offshore the deep, central basins of the Mediterranean sea contain deep-water deposits (Feng et al., 2017; Gorini et al., 2015; Roveri et al., 2014); intermediate basins ranging in water depths between 200-1000 m are classified within the onshore basins.

In offshore basins the MSC has been examined mainly using seismic reflection data that also allows the identification of regional units and unconformities, the most characteristic of which are the Mobile Unit (MU) and the Messinian Erosional Surface (MES) (Lofi et al., 2012). The MU differs in character between the Western and Eastern Mediterranean. The western part is characterized by a known “MSC trilogy ” of the Lower Unit (LU), Mobile Unit (MU) and Upper Unit (UU) (Lofi et al., 2012; Roveri et al., 2014)(Figure 2-4c), whereas eastern part is characterized by a thick undifferentiated MU (Figure 2-4d).

In the Western Mediterranean, the offshore LU could be correlated onshore to either the RLG unit described in the intermediate basins (Roveri et al., 2014) or to a complex unit made of mass transport deposits, and turbidites deposited in an hypersaline basin before salt precipitation (Gorini et al., 2015; Ryan, 2011, 2009). The MU corresponds to the Messinian salt, and is easily recognizable due to its transparent acoustic facies: MU appears almost undisturbed in the western Mediterranean basins with a ca. < 1.2 km thick, while in the eastern basins is thicker, up to ca. 2.1 km. The UU consists of parallel and fairly continuous reflections of relatively high amplitude generally bounded on top by a concordant surface (TS Figure 2-4). Other units are the Complex Unit (CU), generally absent on shelves and rarely observed on the upper part of the continental slope (Lofi et al., 2012). A Bedded Unit (BU), consist of sub-parallel reflectors generally observed in topographic lows and geometrically disconnected from the other deep basin Messinian units, with a thickness up to 350 m and often bounded by a top erosional surface (TES)

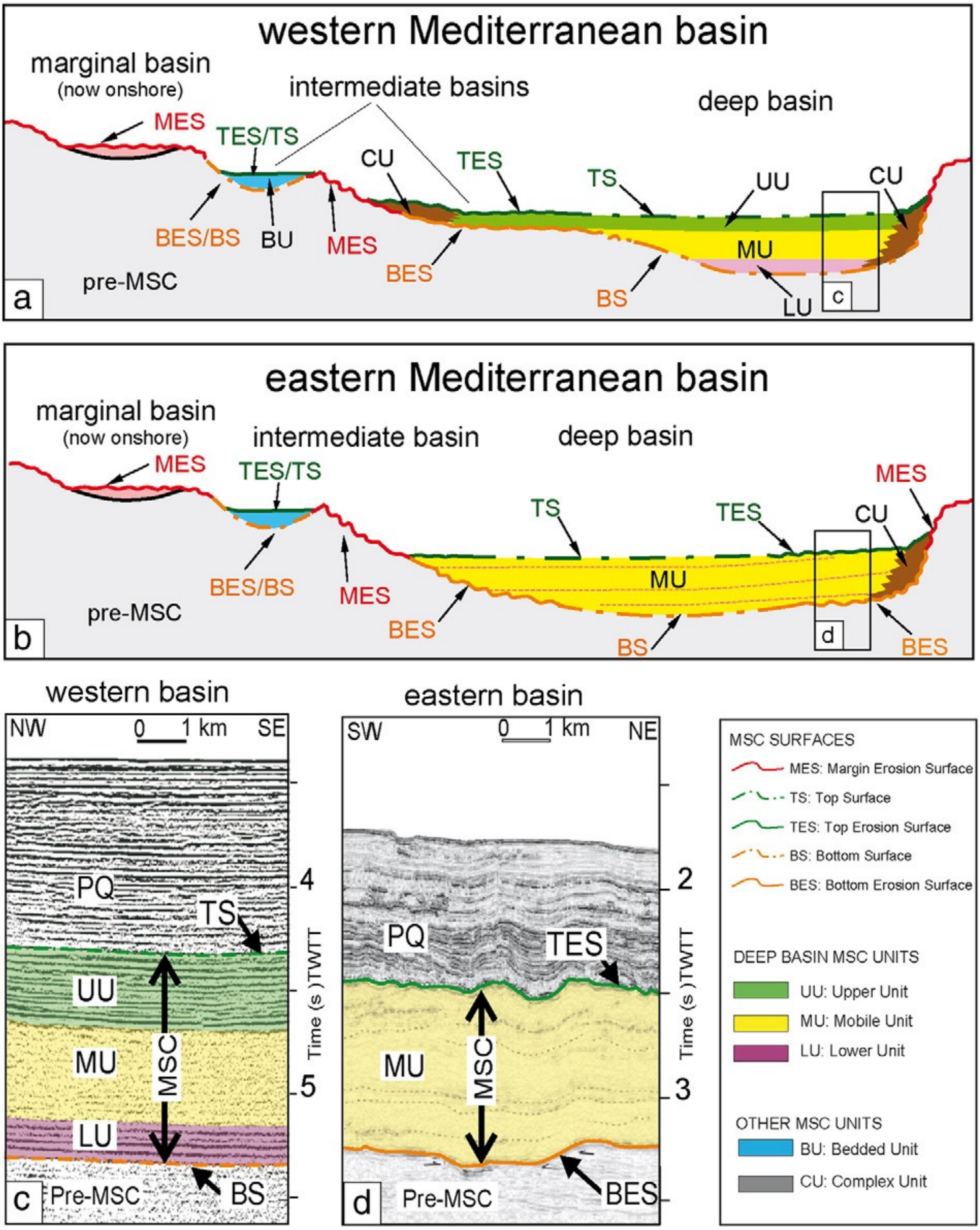

Figure 2-4: schematic sketches showing the western (a) and eastern (b) Mediterranean basins and the relative MSC seismic markers from the shallower areas down to the deep basins at the end of the MSC. Seismic profiles from the western (c) and eastern (d) Mediterranean basins illustrating the differences between the present day MSC seismic records (from Roveri et al., 2014)

2.2 The Calabrian accretionary prism

The Calabrian Accretionary Prim (CAP) is located above a 300 km wide subduction zone and a Wadati-Benioff plane (Selvaggi and Chiarabba, 1995). The origin and evolution of the CAP is mainly controlled by the southeastward migration of the Apennine chain, the Calabro-Peloritani block and the Calabrian subduction zone, due to episodes of roll-back and trench retreat. Furthermore, a vertical axis rotation from Miocene to Quaternary times is responsible for the arcuate shape of the CAP (Polonia et al., 2011). GPS measurements evidence residuals directed toward the Ionian Sea, thus indicating that a crustal compression and an outward migration of the CAP may be active at present.

2.2.1 The Ionian slab

The Calabrian Arc is the apex of an arcuate Africa -Eurasia convergence zone in the Central Mediterranean, that connects the Sicilian Maghrebian chain with the Southern Apennines (Figure 2-6b). Seismic tomographic imaging (Argnani et al., 2016; Maesano et al., 2017; Scarfì et al., 2018; Selvaggi and Chiarabba, 1995) shows an extremely narrow (<200 km), deep (>400 km) and steep (70°) Wadati-Benioff plane dipping beneath the Calabrian Arc and the Southeast Tyrrhenian Sea (Selvaggi and Chiarabba, 1995). The subduction zone is bounded on the northeast by the Apulian platform, on the west by the Hyblean platform (Minelli and Faccenna, 2010), and to the northwest is bounded by active volcanoes, i.e. Etna, Aeolian Islands, Vesuvio (Scarfì et al., 2018)(Figure 2-5). The oceanic lithosphere beneath the Ionian abyssal plain (IAP, Figure 2-6).

According to Maesano et al., (2017) and Scarfì et al., (2018), a combination of deformation processes occurring at its edges and the slab gravitational pull are leading to a progressive narrowing and necking of the slab. On the southwestern boundary slab breakoff and lithospheric vertical shear are occurring due to the sinking and retrograde motion of the slab (Figure 2-5); vertical shear propagates to the upper plate along a NW-SE oriented fault system, the Aeolian-Tindari Letojanni Fault System (ATLFS) (Scarfì et al., 2018). Towards the southeastern edge, in the Hyblean-Ionian sector, the lithosphere is not broken as in the southwest, but only flexed (Figure 2-5): on top of this flexed sector are reported fault systems (North and South Alfeo System in Gutscher et al., 2017, 2015; Alfeo-Etna fault and the Ionian Fault in Polonia et al., 2016) that are thought to accommodate the deformation by lithospheric flexing of the shallow crust in an incipient slab edge bending and tearing. The northern edge of the slab is narrowing, progressively broken in a parallel direction respect the trench and the horizontal tear may propagate southwards (Figure 2-5)(Scarfì et al., 2018).

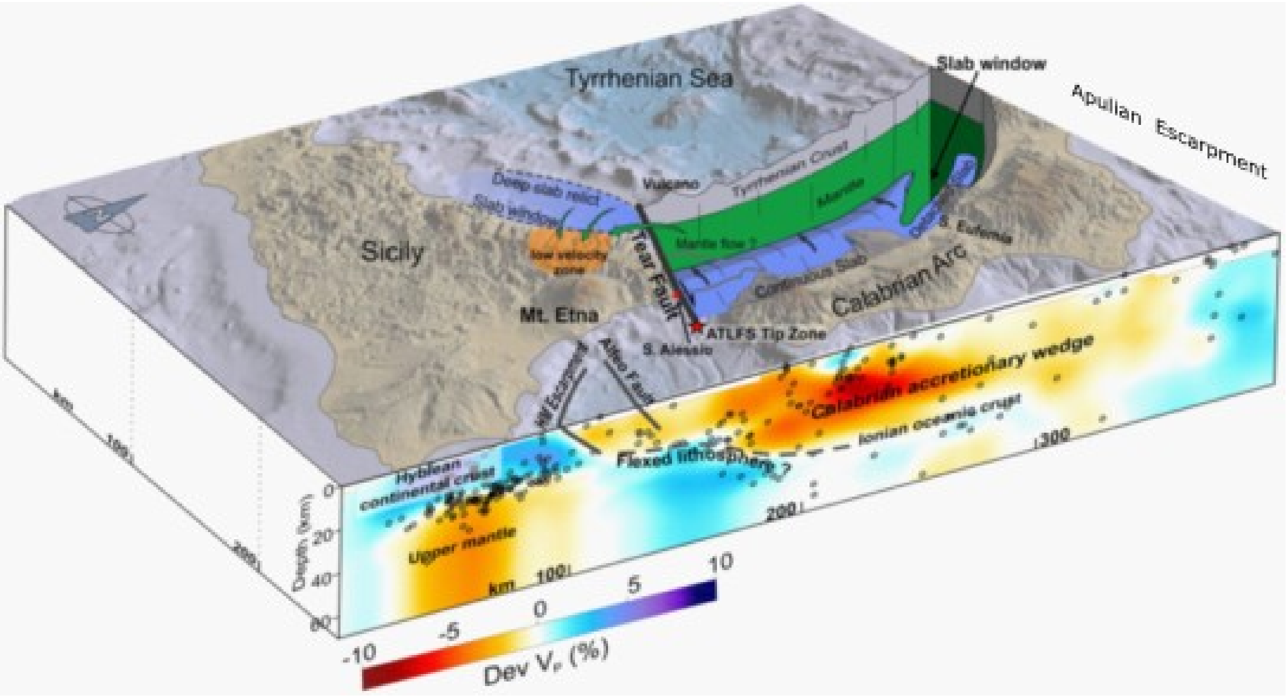

Figure 2-5: 3D model summarizing the main features of the Ionian subduction zone (from Scarfì et al., 2018).

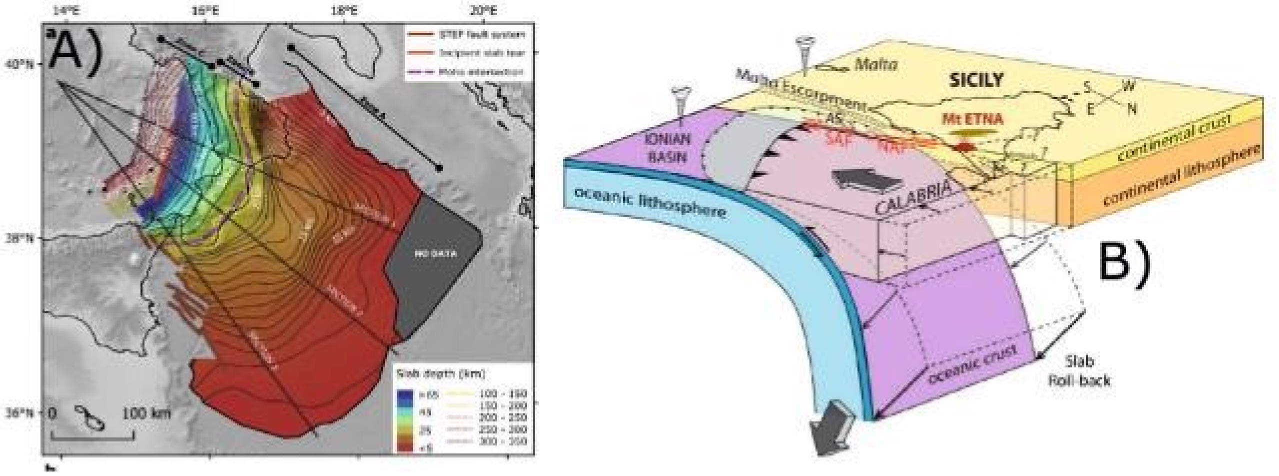

Figure 2-6: a) plan view of the slab (from Maesano et al., 2017), and b) sketch model of the subduction zone beneath the Calabrian Arc (from Gutscher et al., 2015)

2.2.2 Stratigraphy and geodynamics of the Calabrian accretionary prism

The CAP represents the SE apex of the arcuate Apenninic-Maghrebian fold and thrust belt. The CAP is a large accretionary complex, 400 km long and 300 km wide, that is composed by an outcropping onshore part and an offshore prosecution: it extends from Calabria region up to 1000 m height to the Ionian abyssal plain at water depths of 4000 m. The onshore part of the Calabrian Arc is due to the Quaternary uplift that lead to the exposure of more than 2000 m of thick sedimentary succession that spans from Oligocene to Quaternary ages (Cavazza et al., 1997).

The onshore part of the Calabrian accretionary prism is composed of an inner core made up of a nappe stack of metamorphic and sedimentary units that includes Hercynian and pre-Hercynian continental basement and

Jurassic to Early Cretaceous sequences (Bonardi et al., 2001), emplaced on Mesozoic sedimentary and metasedimentary terranes during Oligocene to early Miocene times (Bonardi et al., 2001; Tortorici, 1982; van Dijk et al., 2000). The Calabrian basement is made up of crystalline Paleozoic to Mesozoic – Lower Miocene deposits characterizing the Sila, Serre and Aspromonte massifs of Calabria (Figure 2-8), while the Oligocene to Quaternary sequence crops out in the rest of the Calabria terrane. This inner core is overlain by a variety of Plio-Quaternary basins, present both on the Tyrrhenian and Ionian sides of Calabria (Figure 2-8). These Plio-Quaternary basins developed both parallel and transversal to the direction of thrust propagation in the Apennine chain linked to progressive eastward migration of the Calabrian Arc (Zecchin et al., 2015) and record phases of subsidence interrupted by episodes of tectonic uplift associated with contractional-transgressive events, related to the reorganization of the Apennine-Maghrebian chain (Patacca et al., 1990; Roda, 1964; Sartori, 1990, p. 90; van Dijk, 1991, 1990; van Dijk and Okkes, 1991; Zecchin et al., 2012). In particular, three regional-scale unconformities are recognized, of mid-Pliocene, early Pleistocene and middle Pleistocene age (MPCU, EPSU and MPSU respectively) (Longhitano et al., 2014; Massari and Prosser, 2013; Roda, 1964; van Dijk, 1990; Zecchin et al., 2015). The MPCU is interpreted to have formed as a response to the Pliocene opening of the Vavilov basin and interference of the Calabrian Arc with the Apulian plate or an episode of out-of-sequence thrusting within the accretionary wedge during slab retreat (Longhitano et al., 2014; Massari and Prosser, 2013; Roda, 1964; van Dijk, 1990; Zecchin et al., 2015). The EPSU and MPSU are correlated to the ultra-fast opening of the Marsili basin in relation to a phase of basin collapse in northern Calabria (the Gelasian drowning event) and pauses in the subduction retreat, with the EPSU associated to minor contraction-transpression events and the MPSU formed during the reduction in Arc migration and result of transpressional activation of NW-trending shear zones (Longhitano et al., 2014; Massari and Prosser, 2013; Roda, 1964; van Dijk, 1990; Zecchin et al., 2015).

The offshore part of the Calabrian Arc can be described as formed by the submerged Crotone-Spartivento fore arc basin composed of Oligocene to Quaternary sediments, an inner clastic or accretionary wedge (Figure 2-8) characterized by an Upper Cretaceous to pre-Messinan sedimentary sequence and an outer or external wedge (Figure 2-8) formed only by Messinian and Plio-Quaternary deposits. A basal detachment occurring at the Messinian bottom boundary layer, separated by “splay fault”, i.e. out of sequence thrust (Polonia et al., 2011) or by a “main external ramp” (Minelli and Faccenna, 2010) locally expressed by a change in seafloor morphology (Gutscher et al., 2017) or by a Central Transition Zone (CTZ). The main morpho structural domains in the longitudinal direction of the prism are represented by the Crotone-Spartivento forearc basin (Figure 2-8), the inner accretionary wedge, the outer accretionary wedge and the Ionian abyssal plain (Figure 2-8) (Gutscher et al., 2017; Minelli and Faccenna, 2010; Polonia et al., 2011; Rossi and Sartori, 1981). Besides this longitudinal classification, the offshore Calabrian Arc can also be divided into separate lateral domains: a NE and SW lobe (Figure 2-8). This classification was first proposed by Polonia et al., (2011) where the boundary between the two lobes occur along a NW-SE lineament, the “Ionian Fault” (Figure 2-8).

The Ionian Abyssal Plain (IAP) is a deep foreland basin with a triangular shape that lies in water depths around 4000 m (Figure 2-8). The northern edge of the IAP, is bounded by front of the Calabrian accretionary prism (CAP) and beyond by the Western Mediterranean Ridge (WMR).

The Calabrian outer accretionary wedge or post-Messinian wedge is bounded by the deformation front of the CAP that separates it from the IAP and to a scarp around the 3000 isobath, known as splay 1 (Polonia et al., 2011) (Figure 2-8). Anticlinal structures are separated by small elongated syncline basins. This morphology changes moving westward, where folds are less well-expressed and small-scale asperities affect the seafloor morphology.

Moving towards Calabria, the 3000-isobath small scarp represents the seaward boundary of the Inner accretionary wedge or pre-Messinian wedge (Figure 2-8). It is characterized by an arcuate shape, 130-140 km long and 280-300 km, with a western depressed area and an eastern elevated area, the former corresponding to a wide nearly flat basin (Gallais et al., 2012) and the latter affected by SW-NE trending egg-shaped depressions (Gallais et al., 2012). These two areas correspond to the lateral division into two major lobes, the eastern and western lobe firstly proposed by Polonia et al., (2011). The wedge is made up of extremely deformed nappe stack of pre-Messinian units scraped off from the down going plate. It is characterized by several NE-SW oriented thrust dipping to the north, deforming Messinian and Plio-Quaternary units.

The stratigraphy of the offshore area has been mainly imaged by seismic data and when available calibrated with well logs. Five main seismostratigraphic units have been identified (Minelli and Faccenna, 2010 and references therein)(Figure 2-8): a Plio-Quaternary Unit (PQ), a Messinian Unit (ME), Pre-Messinian Unit (PM) a Miocene Unit (MC) separated by regional reflectors (A, B, K and S). Both the seismic units and the unconformities were detected in the foreland basin, where it was possible to calibrate them with stratigraphic data from DSDP (site 374, Messina).

The PQ unit was described as subparallel, high frequency with low amplitude reflectors derived from terrigenous and turbidite deposits of Plio-Quaternary age (Figure 2-8). The average thickness in the wedge domain is about 200 to 400 ms TWT, while it reaches up to 2 s TWT in the Crotone-Spartivento basin. This unit appears almost undeformed in the IAP while it is folded and faulted in the internal part of the prism. The unit is bounded on the bottom by a high amplitude reflector, the A reflector, easily recognizable throughout the basin, that represent the base of the PQ unit.

The ME unit is bounded by the A and B reflectors and is recognizable both in the inner and outer portions of the CAP (Figure 2-8). In the foreland basin, the average thickness is around 0.4 s TWT, and consists of two seismic units: an upper high velocity-layer related to the upper evaporitic Messinian sequence and a lower less reflective unit. According to the new classification proposed by Lofi et al., (2012) the upper unit can be associated the Messinian Upper Unit while the lower unit can be associated with the Mobile Unit. The base of the ME unit is represented by the B reflector, a planar, high amplitude reflector (Figure 2-8).

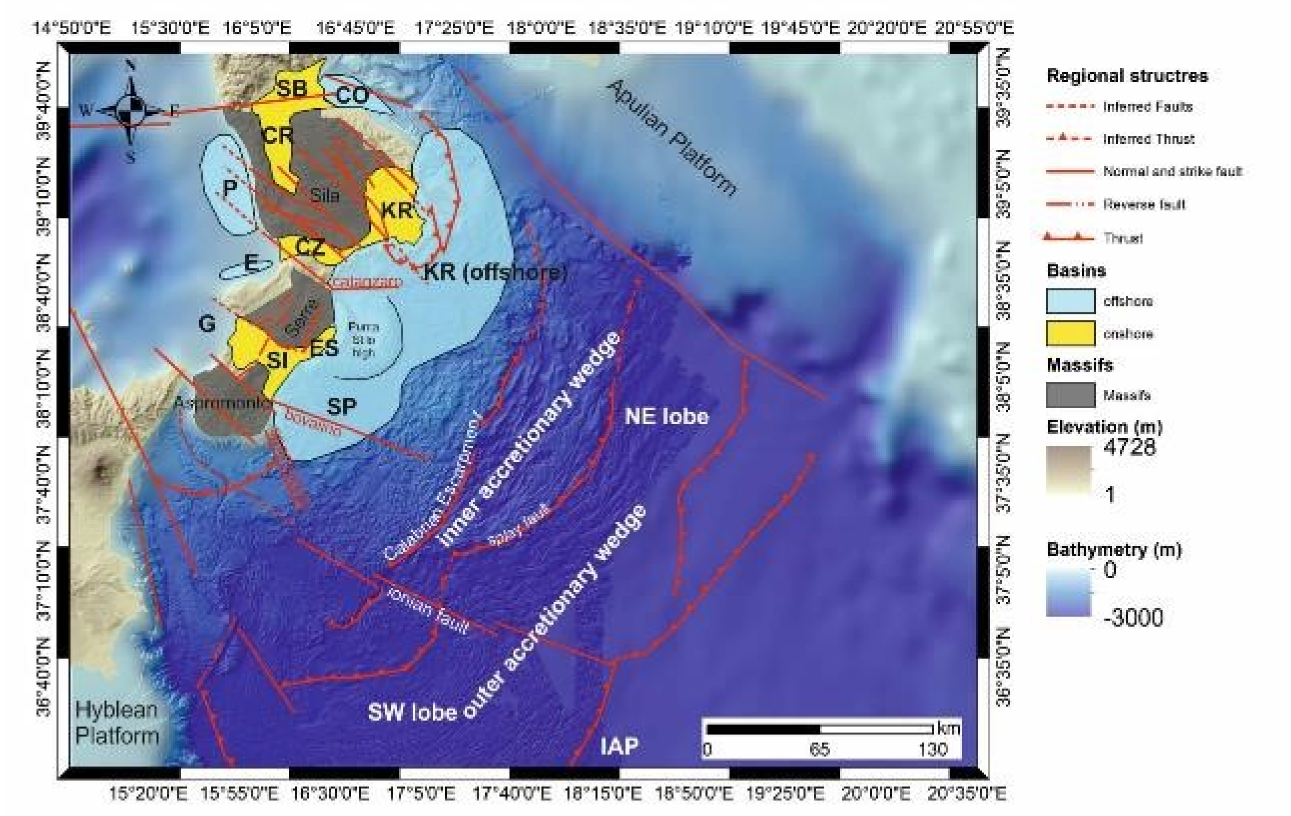

Figure 2-7: Architecture of the Calabrian Arc. Major structural boundaries, active faults and the basins are indicated. CO: Corigliano Basin, SB: Sibari Basin, CR: Crati Basin; KR: Crotone Basin, CZ: Catanzaro Basin, E: S. Eufemia Basin, P: Paola Basin, G: Gioia Basin, ES: East Serre Basin, SI: Siderno Basin, SP: Spartivento Basin, IAP: Ionian Abyssal Plain

The pre-Messinian units (Figure 2-8) are well layered and poorly reflective sequences, associated to deep water clays and marls. The unit is deformed in the Ionian basin, with variable thicknesses from 1.5 to 0.4 s TWT. Moving landward, the unit is progressively incorporated into the Calabrian wedge; the lower boundary is represented by the K reflector that corresponds to the top of the Mesozoic carbonate unit (MC) (Figure 2-8). The MC unit is composed of strong, quite continuous and low-frequency reflectors with an average thickness of ca. 1.5 s TWT. The unit lies above the S reflector, commonly described as the top of the acoustic basement, that lies around 8 s TWT in the mostly undeformed foreland basin.

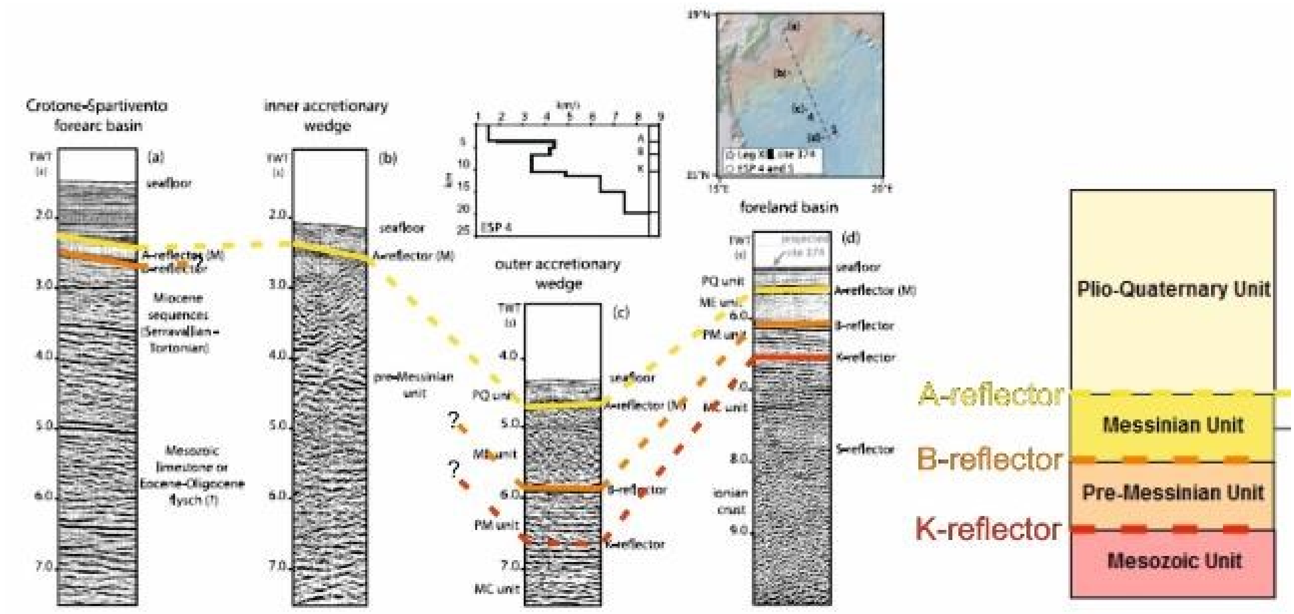

Figure 2-8: seismic stratigraphy of the sedimentary section in the Ionian offshore aligned along a general NW-SE cross section from the Crotone Spartivento basin to the IAP. Vertical scale in s TWT (modified from Minelli and Faccenna 2010).

The evolution of the CAP can be depicted through five main stages (Minelli and Faccenna, 2010), since the Late Miocene to present:

A first phase occur between 15 to 10 Ma when it is inferred the Calabrian wedge was already growing and the foreland basin was experiencing intraplate compressive deformation and shortening; in this time interval, between the end of the Liguro-Provençal basin and the first episodes of back-arc extension to form the Tyrrhenian Sea, the central Mediterranean underwent a decrease in the subduction and roll-back velociy and intraplate shortening (Minelli and Faccenna, 2010).

The second phase occurred between 10 to 6 Ma and is characterized by active subduction and the growth of the inner portion of the wedge, accommodated along several thrust faults and frontal accretion of the sedimentary sequences at the CAP toe. The growing phase of the prism is related to shortening due to rapid plate rollback that accommodated the inner wedge for a total subduction of 140 km, divided in 40 km of net convergence and 100 of retreat (Minelli and Faccenna, 2010).

The third stage coincides with the MSC (chapter 2.1.2) that represents an important event in the evolution of the CAP, through a sea level drop, likely related to an isostatic rebound, and deposition of thick clastic and evaporitic sequences. “Salty” Messinian units crop out in the Crotone basin in thicknesses reaching 500 m but also offshore, in the foreland basin, with an estimated maximum thickness of ca. 1 km. The deposition of this clastic and evaporitic sequence lead to an upward and forward propagation of the CAP on a décollement layer within that sequence. The development of a décollement layer and the associated fast forward growth of more than 100 km led to a lowering of the CAP profile.

The fourth stage occurred between 5-3 Ma, after the MSC: the entire CAP experienced a fast foreland propagation above the weak salt décollement layer localized at the base of the Messinian sequence. The fast foreland propagation reduced the wedge taper and increased the total length of the wedge to 200 km. At this time the outer wedge was experiencing a continuous deformation of the Messinian and Plio-Quaternary units that shaped it through internal shortening, folding and vertical thickening. Furthermore, in this time interval other events punctuated the evolution of the CAP, such the reactivation of the out-of-sequence thrusts in the inner portion of the wedge, the uplift of the Calabrian belt attested by the progressive onlapping unconformity of the Messinian-Pliocene unit onto the basement accompanied by a strong subsidence of the Crotone-Spartivento forearc basin. The upward migration of the basal décollement produced underplating of the Ionian sedimentary cover. The total amount of subduction was 190 km, with 10 km of convergence and 180 km of roll-back accommodating back-arc opening of the Vavilov basin.

The last stage (3 Ma to present) was mainly driven by localized and very fast subduction and trench rollback of ca. 100 km. The inner part of the wedge was characterized by activation of out-of-sequence thrust, the outer wedge by thickening, while the Crotone-Spartivento forearc basin was under subsidence. Underplating was still active and might be associated to the reshaping of the wedge topography.

2.2.3 Architecture and stratigraphy of the Crotone-Spartivento forearc basin

The Crotone Spartivento forearc basin extends both offshore and onshore Calabria, filled by middle-upper Miocene to Quaternary sediments resting on a Calabrian crystalline basement on the inner part while moving seaward on Tertiary and Meso-Cenozoic sediments and on the fore-arc outer thrust of the accretionary prism (Catalano et al., 2001; Cernobori et al., 1996; Minelli and Faccenna, 2010 ; Polonia et al., 2011; Rossi and Sartori, 1981). The forearc basin is divided into two sub-basins (the Crotone basin and the Spartivento basin) by a morphological high located off Punta Stilo (Figure 2-7). Seaward the limit of the basin corresponds to a post-Messinian SE verging-arc outer thrust, the Calabrian Escarpment, that on the seafloor appears as a topographic scarp with relief up to 750 m. Because of the outcropping inner part due to Neogene-Quaternary uplift of the Crotone basin, it is possible to correlate the onshore and offshore stratigraphic sequences. The Plio-Quaternary unit is affected by synsedimentary normal faulting, tilted blocks and rollovers (Minelli and Faccenna, 2010) and by diapiric structures in the inner part of the basin (Capozzi et al., 2012; Minelli and Faccenna, 2010) and compressive structures in the outer sector. Associated to this compressive structures are sliding and slumping features, like the largest gravitational structure in the Crotone peninsula (Minelli et al., 2013; Minelli and Faccenna, 2010; Zecchin et al., 2018).

The onshore Crotone basin stratigraphy is well documented by numerous works (Massari et al., 2010; Massari and Prosser, 2013; Roda, 1964; van Dijk, 1990; Zecchin et al., 2015). According to Capozzi et al., (2012) (Figure 2-9), five depositional units can be traced into the offshore Squillace basin: the entire sedimentary sequence rapidly thickens from the basin margin to the depocenter located offshore with a maximum thickness of ca. 5.6 km (Capozzi et al., 2012). This sedimentary sequence lies on top on a strongly deformed unit represented by a stack of the Calabrian tectonic units (Figure 2-9). Starting from the bottom and moving upward, the series is characterized as follows: two lowermost sequences (S1 and S2 in Capozzi et al., (2012) Figure 2-9) described as a non-reflective and poorly stratified units, followed by the upper units (S3, S4 and S5 in Capozzi et al., (2012) Figure 2-9) which are well stratified and characterized by high to low amplitude reflectors with good to low continuity. S1 and S2 are interpreted to be equivalent to the uppermost Chattian-Langhian Capo d'Orlando Fm the former and the "unnamed unit" of Serravallian-Tortonian age the latter. S2 is characterized by sandstone and conglomerates that moving upward and seaward passes to thicker clay and marl successions especially during Tortonian. The S3 correspond to the Messinian Sequence that reaches a thickness of up to 2000 m in the depocenter of the basin and shows an internal distinction into two sub-units, a well upper stratified unit and a lower poorly stratified and deformed unit. Looking at the correlations with the available offshore wells (Videpi wells), Capozzi et al., (2012) showed the variable thickness of the Late Miocene to recent sedimentary sequence that occurs in the Squillace area (Figure 2-9).

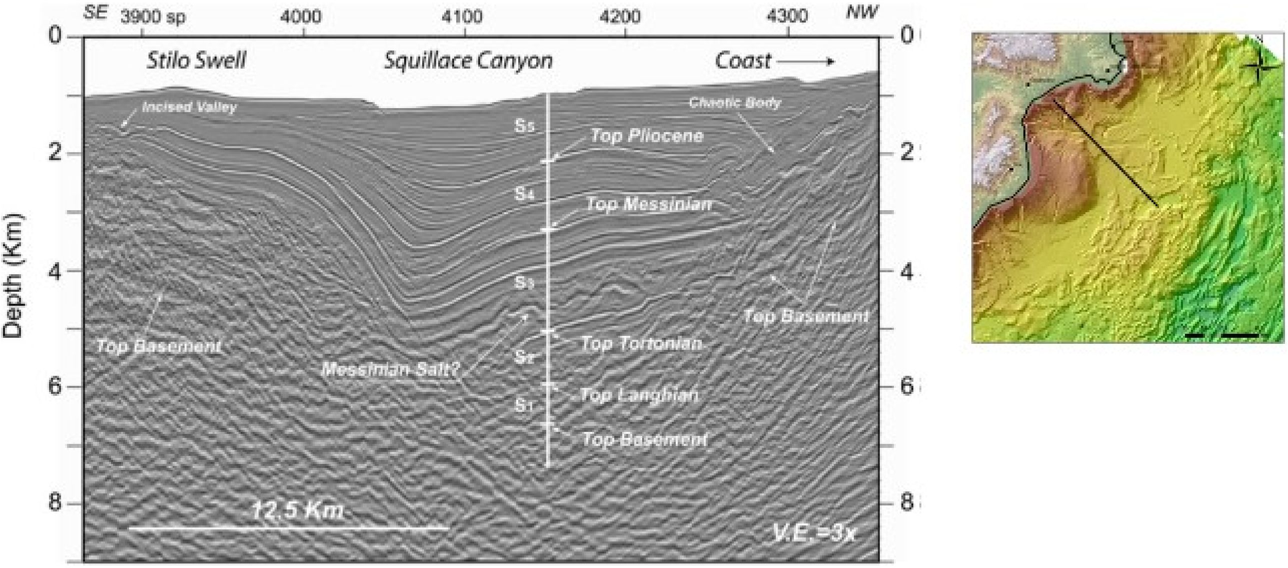

Figure 2-9:Seismic profile crossing in NE-SE direction the central part of the Crotone basin on which are reported the five depositional sequences (S1 to S5), bounded by four major unconformities identified on a cross-correlation between wells and field stratigraphic data, overlain a strongly deformed acoustic basement (from Capozzi et al., 2012).

On the Crotone basin, and in particular on its onshore counterpart and northern sector, Zecchin et al., (2015) provide a new stratigraphic reconstruction of the Plio-Pleistocene sedimentary succession of the Crotone basin, based on the recognition of three major unconformities through a correlation between outcropping and offshore basin (Figure 2-10): these three unconformities have been recognized in most of the basins of the Calabrian Arc mentioned above and are inferred to record interruptions of subsidence by phases of uplift and deformation, in relation to the tectonic events linked the trench migration and slab fragmentation. One unconformity (MPCU), has been dated to mid-Pliocene and associated with uplift and deformation of the Ionian flank of the Calabrian Arc, then interrupted by a phase of subsidence of the basin related to the opening of the Vavilov back-arc basin. The second and third unconformities, respectively Early Pleistocene (EPSU) and Middle Pleistocene (MPCU) in age are related to a phase of basin collapse in the northern Calabrian sector coeval with the ultra-fast opening of the Marsili back arc basin and associated to uplift and contractional-transpressional deformation of the Calabro-Peloritani block. On the Spartivento basin a Mid-Pliocene unconformity is also reported by Praeg et al., (2009) and correlated with the outcropping part of the Crotone basin.

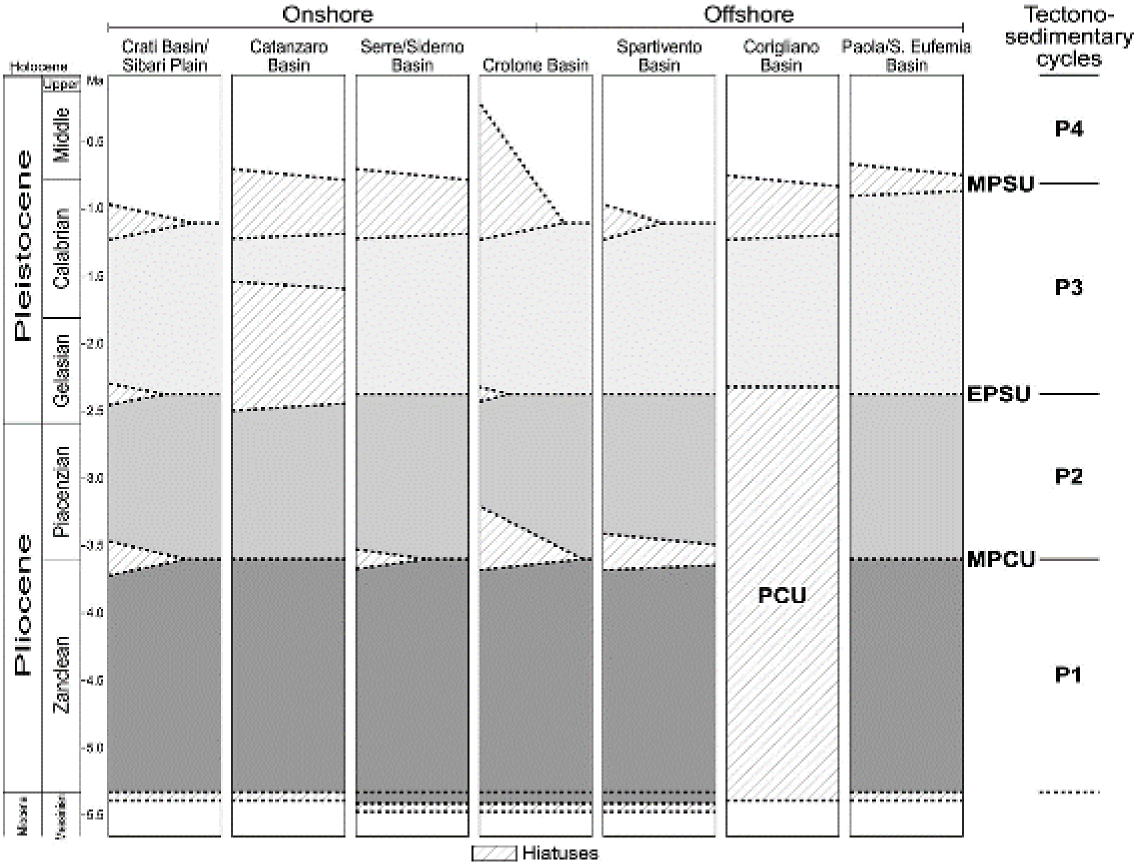

Figure 2-10: image depicting the three major unconformities recognized by Zecchin et al., (2015) in the Crotone basin and in the other onshore and offshore basins of southern Italy. The unconformities and their correlative conformities separate four tectono-sedimentary cycles (P1-P4) related to the Plio-Quaternary evolution of the Central Mediterranean (from Zecchin et al., 2015).

3 Methods and Data

This chapter presents the methods and data used for the study. Chapter 3.1 introduces the physical principles that rules of marine geophysical of seafloor features and subsurface structures based on the propagation of acoustic. Chapter 3.2 provides an overview of the geophysical dataset, with details about the acquisition parameters and data resolution and coverage; chapter 3.3 presents the well logs used to calibrate the seismostratigraphic analysis; chapters 3.4, 3.5, 3.6 describe the methods applied to the geophysical and well data of chapters 3.2 and 3.3.

3.1 Acoustic principles and geophysical methods

The basic principle of acoustic methods and exploration seismology is the generation of an acoustic pulse at a given time, that propagates through the water column and/or to the subsurface media and is reflected (or refracted) back to the surface where it can be detected as a returning signal. The elapsed time between the source being triggered and the arrival of the returning signal is used to determine the depth of the seafloor or the nature of the subsurface layers and is known as *two way travel time (TWT)*, where the real distance can be obtained through the formula:

Distance = Velocity x TWT time x (1/2)

The method requires a controlled seismic source of energy, a receiver to “listen” the reflected acoustic signal, and a system to record and store the data. The acoustic pulse travels in water in a moving series of pressure fronts as a compressional wave (Figure 3-1). These pressure fronts propagate with a sound speed in water that can change depending on the physical properties of the water, such as pressure, temperature and salinity. The typical average compressional wave speed in water is about 1500 m/s.

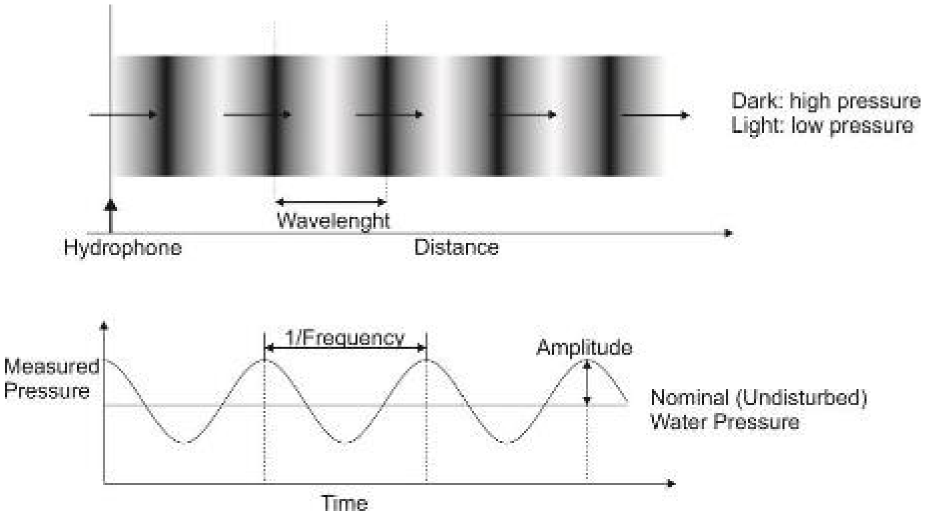

Figure 3-1: components of a sound wave

The physical distance between two pressure fronts in a traveling sound wave is known as wavelength (Figure 3-1). Given a stationary point, the number of pressure fronts that pass the stationary point in a unit time is called frequency (Figure 3-1). Sound speed, frequency and wavelength are related with the formula:

Speed of sound = frequency x wavelength

A sound wave is capable of transfer acoustic energy that can be measured by a receiver, like a hydrophone or a piezo-electric ceramic made project, which are sensible to the pressure oscillations when passed by a pressure front of a sound wave. When perturbed by an acoustic wave they start to oscillate and converts the pressure wave in an electric signal. The size of the oscillations measures the amplitude of the wave. The amplitude is related to the acoustic energy being transmitted in the wave, the higher the amplitude, the higher the energy, as expressed by the formula:

Energy of sound = Amplitude^2

During its propagation, part of the sound pulse is reflected off by the seafloor, while the rest penetrates within the seafloor subsurface and is reflected and refracted. The reflected signal is sensible to the sub-substrate different density of the sediments. Thus, boundaries of layers of different sediments below the seafloor are detected because of the different acoustic impedance (Z), expressed as the product of the density (ρ) and the speed of sound (v) of each layer (Figure 3-2).

$$Z = \frac{\rho}{v} \qquad RC = \frac{(Z_2 - Z_1)}{(Z_2 + Z_1)}$$

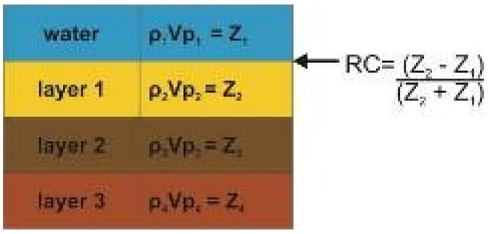

Figure 3-2: different acoustic impedance Z in relation to ρ (density) and v_p (P wave velocity) different values

The higher the acoustic impedance, the higher the strength of the reflected signal. The reflected signal is recorded by an array of hydrophones towed behind the vessel, or by a transducer/receiver system hull mounted on the vessel. Lower frequency pulses achieve greater penetration but loose in resolution, while higher frequency pulses are less penetrative but have a high resolution. The relationship between penetration and resolution is not linear but it is constant, allowing real-time adaptation of the frequency interval.

For this study, three different types of instrumentations have been used: swath multibeam echo sounder, sub-bottom profiler and multichannel seismic reflection.

Multibeam

Multibeam echo sounder system (MBES) is a device that allows the measurement of water depths. The result is a bathymetric map of the seafloor that is typically presented as a digital terrain model (DTM) of the seafloor. MBES systems consist of a pair of orthogonally mounted linear acoustic arrays: the Transmitter (Tx) and a Receiver (Rx) (Figure 3-3A); a Control and Display system, integrated with a global positioning information system (i.e. GPS); a gyroscope for the system orientation over time; the Reference Motion Unit sensor of the ship that measures the three spatial components of vessel oscillation (roll, pitch and heave) and finally a vertical probe to measure the speed of sound in the water column. MBES can be hull-mounted on the ship, or autonomous underwater vehicle (AUV) deployed in the water and remotely controlled on the ship.

The MBES determines the ocean floor depth simultaneously in several directions by the transmission and reception of beams (Figure 3-3B), based on the travel time of the acoustic waves (swath) emitted, released at high frequencies: a typical frequency operation for a hull-mounted MBES is around 12 to 40 kHz, while in case of autonomous underwater vehicles it can range between 200 to 400 kHz. The beams form a swath perpendicular to the ship directions. The swath operates with wide angles ranging from 50° to 160° degrees perpendicular to the ship's course and with narrow angles, from 0.1° to 2°, parallel to the ship's track Figure 3-3C).

The area covered by the MBES can vary from three to more than seven times the depth of water, with a resolution depending on the depth of the seafloor and operating frequency of the source emitter, because of the energy loss by acoustic wave when propagating: the deeper the seafloor, the lower the resolution.

A spherical acoustic wave is sent in a single beam, with an opening of 50° to 150° perpendicular to the ship's track and an opening of 0.1° to 1.8° parallel to the ship's track.

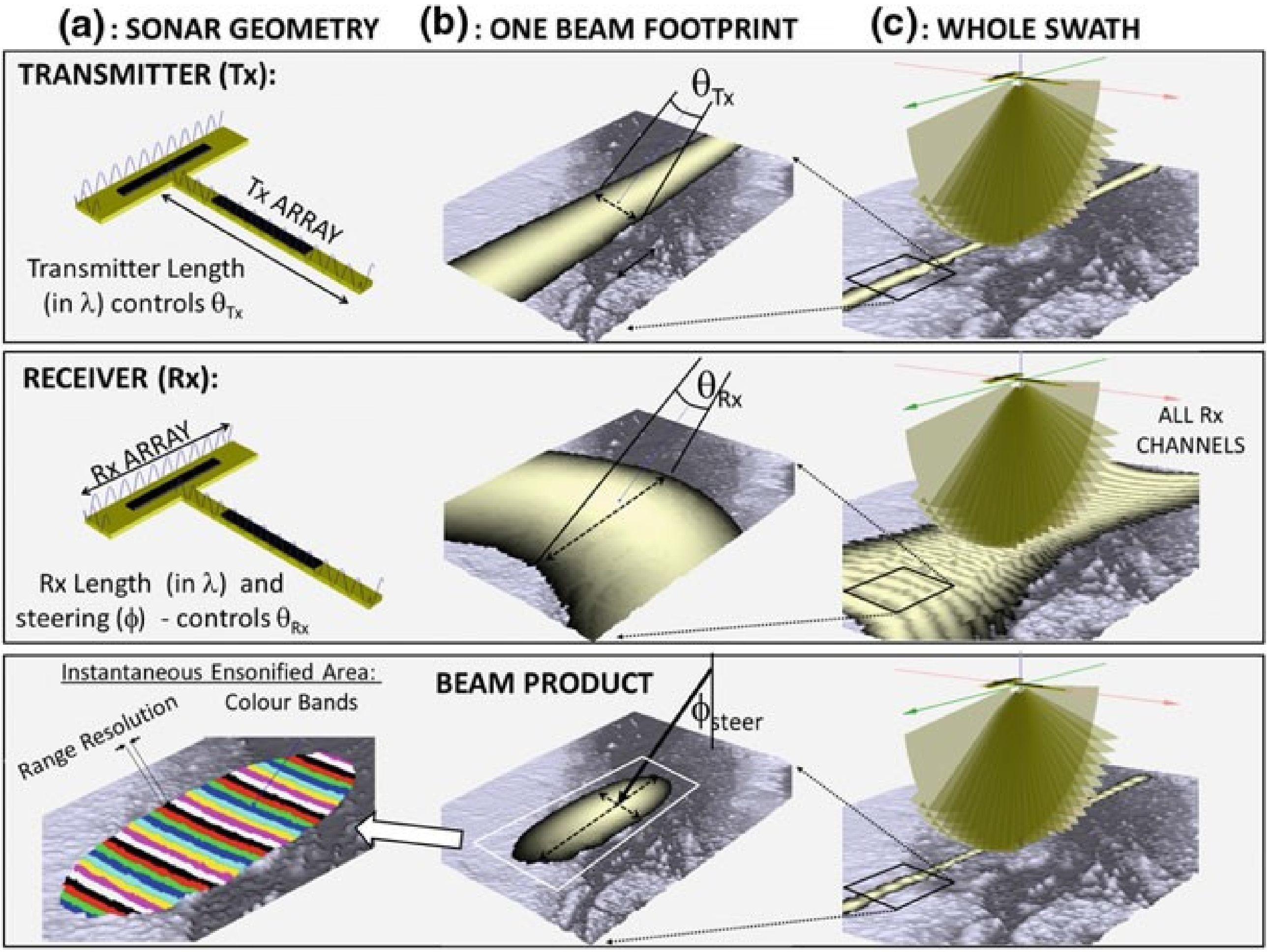

Figure 3-3: combination of the transmitter (Tx) and multiple receiver (Rx) beam foot prints to generate a across track swath of multiple narrow beams (from Hughes Clarke 2018)

Sub-bottom profiler

A sub-bottom profiler is an echo sounder used to investigate the shallower part (maximum 100 m depth) of the seafloor subsurface (Figure 3-4). It operates around a central frequency that is swept across a range between 2 kHz to 16 kHz that is capable of penetrating the seafloor.

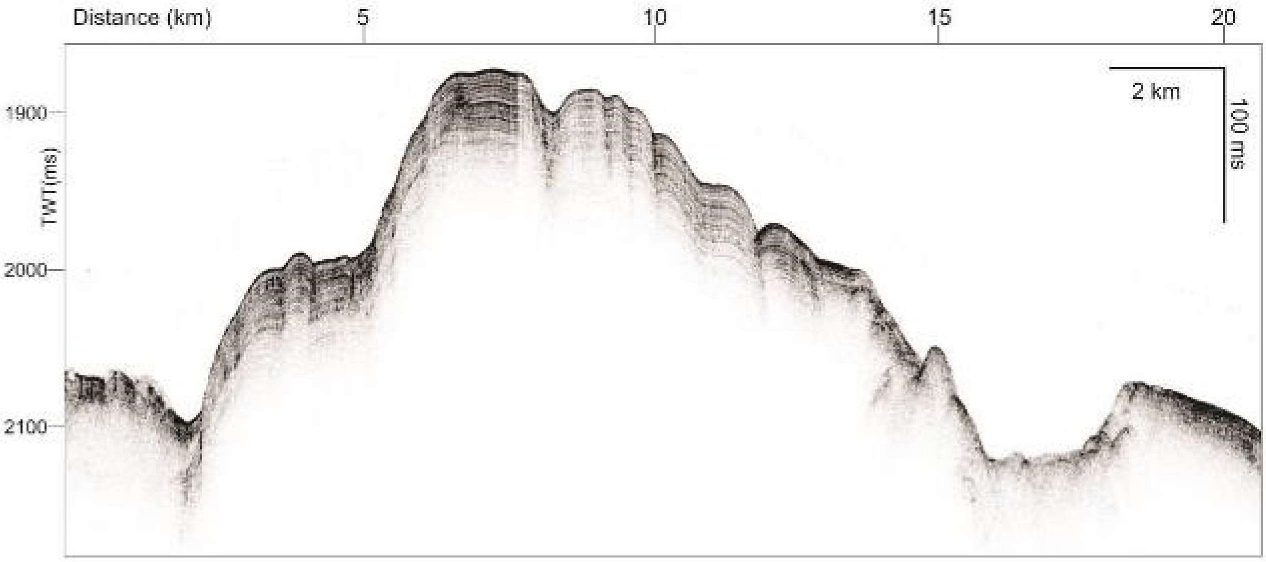

Figure 3-4: example of a sub-bottom profile

The arrival time and intensity of successive pulses provide information about subsurface layers (Edelmann, 1968). Sub-bottom profiles are influenced by several physical parameters that can be modified during acquisition, such output power, signal frequency, and pulse length; the opportunity to modify and module these parameters makes sub-bottom profilers a useful instrument in various marine environments (McGee, 2000). Increased output power and lower emitted frequencies allow a greater vertical penetration into sedimentary substrates. However, when attempting to survey harder substrates (e.g., gravels or highly compacted sands) or areas of very shallow water, higher output power will most likely result in multiple reflections and more background scattered noise, or potential error in the data (Grant and Schreiber, 1990). On the contrary higher frequencies systems (i.e. up to 20 kHz) produce high definition images of sediment layers, able to discriminate cm-scale layers between layers that are close together (e.g., 10's of cm) (Mosher and Simpkin, 1999). Longer pulse length transmissions, known as 'pings', yield more energy and result in greater penetration of substrate (Hutchins et al., 1976). However, they decrease the system resolution. The depth of penetration is also dependent on the hardness of the upper layer, i.e. sand layers are less penetrative, or and can be significantly limited by the presence of gas (Hardage, 1985).

Seismic reflection

Seismic reflection investigates deeper in the earth's subsurface, to km scale. In this case the seismic source generates an acoustic wave in form of a seismic pulse that propagates to the water column and then through the seafloor subsurface. An example of marine seismic source is the air gun (Figure 3-5), a pneumatic source that releases compressed air previously filled in a chamber, provided by a shipboard compressor (Figure 3-5). The volume of the compressed air is dependent of the energy needed, the more energy is required the bigger the volume of compressed air is, and so the air gun chamber. To increase the penetration, it possible to use arrays of seismic sources.

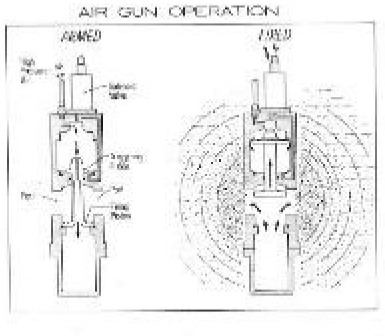

Figure 3-5: schematic view of an air gun

For seismic reflection, receivers are represented by hydrophones (Figure 3-6 and Figure 3-7). The hydrophone registers the reflected wave from the seafloor and the subsurface under it. The hydrophones are usually deployed in large numbers in the form of a linear array within a cable called a streamer (Figure 3-6 and Figure 3-7). The streamer is deployed behind the vessel, at a certain depth below the sea surface. More than one streamer can be deployed, generating an array of streamers. Special devices called "fish" control the depth of the streamer (Figure 3-6 and Figure 3-7). This geometry of deploying arrays of hydrophones is used to increase the signal to noise ratio.

The deployment of the seismic source and the streamers is regulated by the geometry of acquisition, i.e. the distances between the source and the streamers, the interval distance between each hydrophone, the towing depth under the sea level (Figure 3-7). This parameter has a key role to get a correct seismic reflection acquisition.

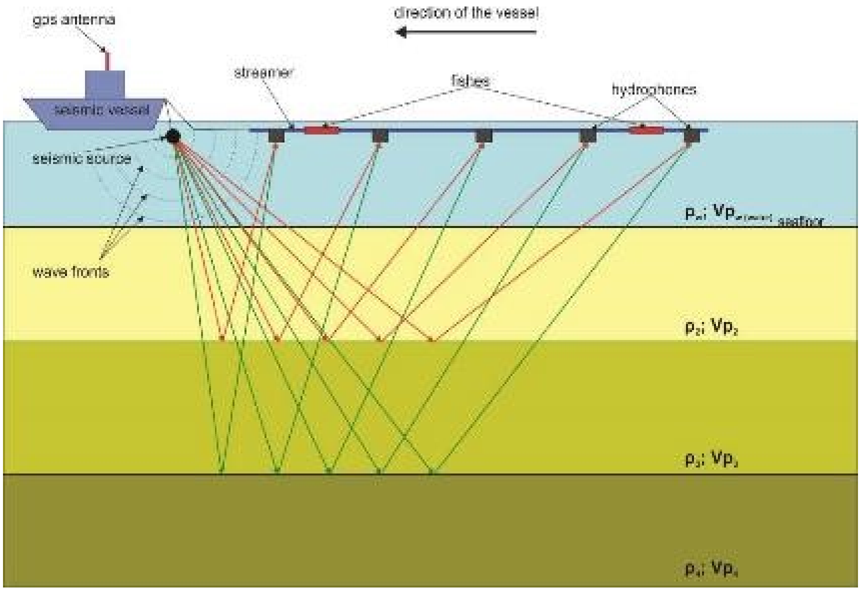

Figure 3-6: seismic reflection method. Red and green lines represent the reflected ray paths from the different subsurface layers resulted from a single shot by the seismic source.

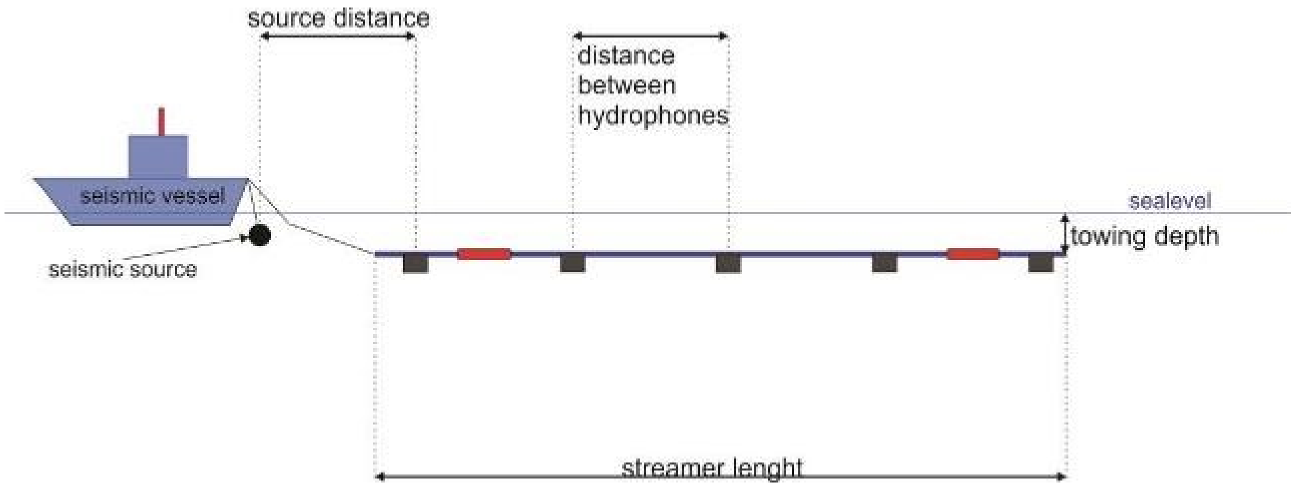

Figure 3-7:geometry of acquisition

3.2 Geophysical Dataset

The study is based on an extensive dataset, collected during different research cruises in the last decades, the most recent in 2014 and 2015 (Table 3-1). Two main datasets are used: one composed of swath multibeam bathymetric data and one of seismic profiles of two types, higher resolution (sub-bottom profiles) and lower resolution (multichannel seismic reflection data).

The multibeam bathymetric dataset is composed of a mosaic of DTMs of varying resolution, for a total coverage of 16500 km^2. The DTMs are of 5x5, 10x10, 20x20 and 50x50 m grid size (Figure 3-8), acquired during several research cruises (Table 3-2). Higher resolution DTMs are found at relative shallow water depths while lower resolution DTMs cover deeper areas.

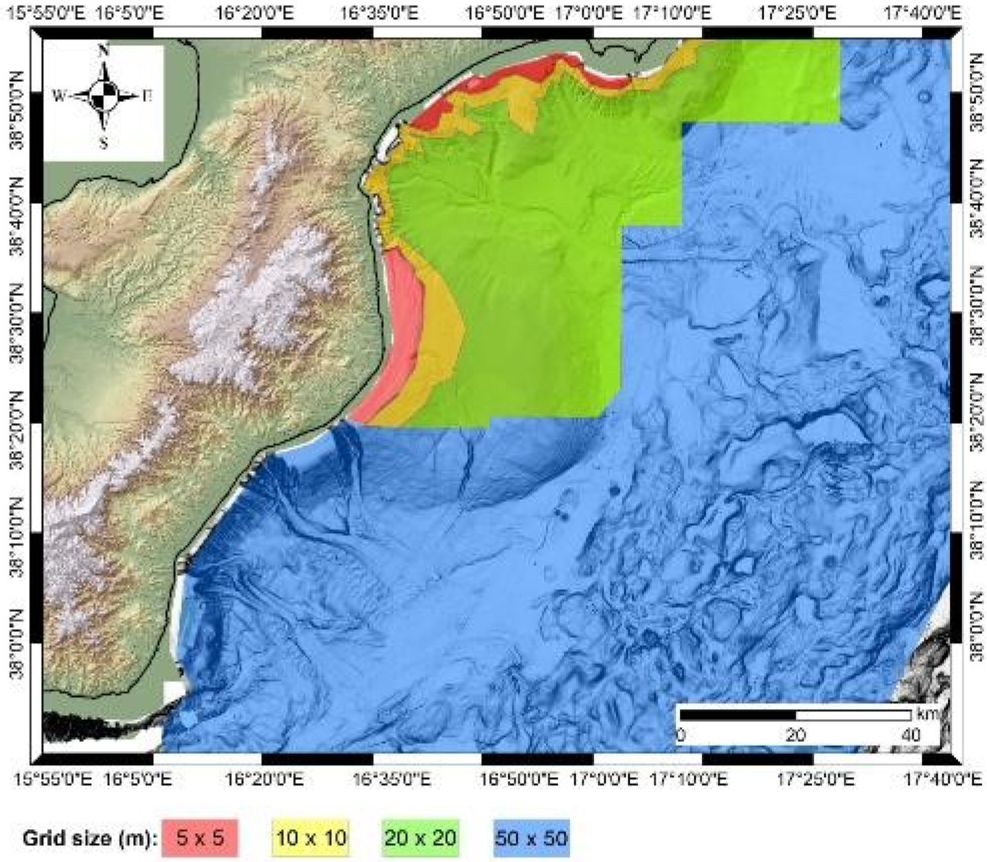

Figure 3-8: image showing the different DTM classified by their different grid size (refer to the legend for DTM colors).

The seismic dataset is composed of more than 10000 km (Figure 3-9) of sub-bottom profiles (SBP) and ca. 4400 km of multichannel seismic reflection data (MCS) (Figure 3-10). MCS dataset is composed of profiles with different resolution and penetration, that allow investigations of the subsurface of the study area at vertical resolutions from 15 m up to 2 m (Table 3-4).

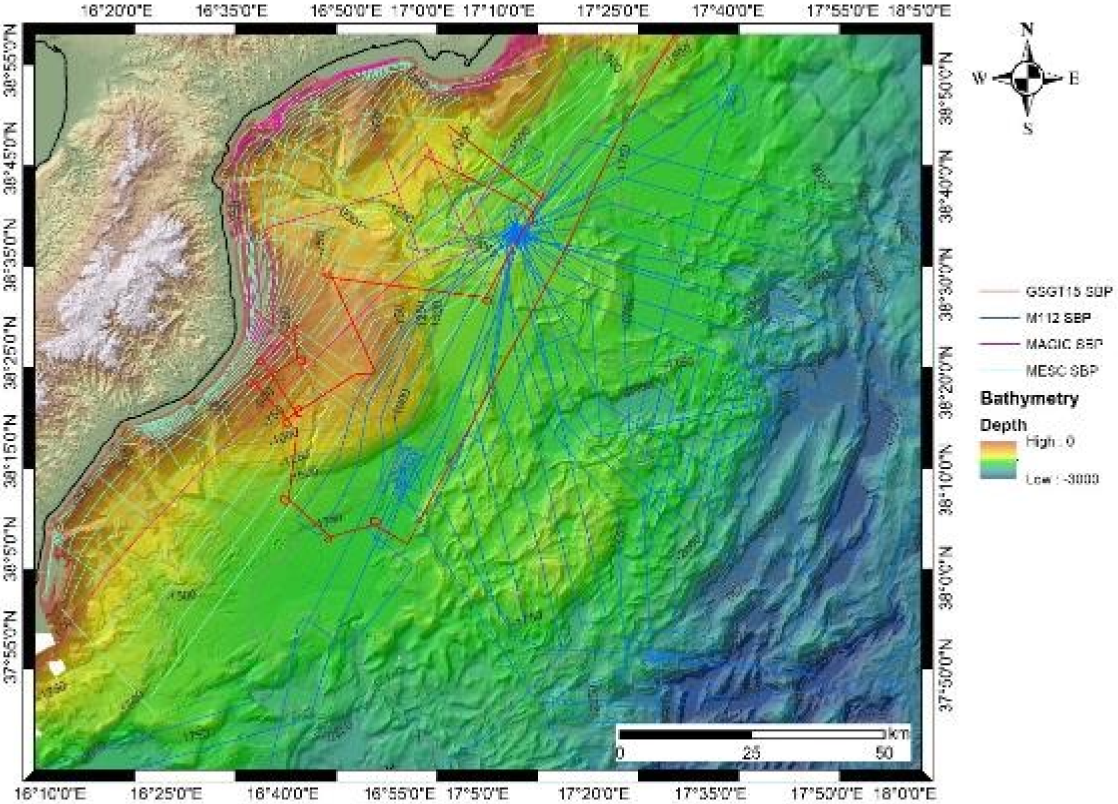

Figure 3-9: bathymetric map with superimposed the SBP dataset used for this study.

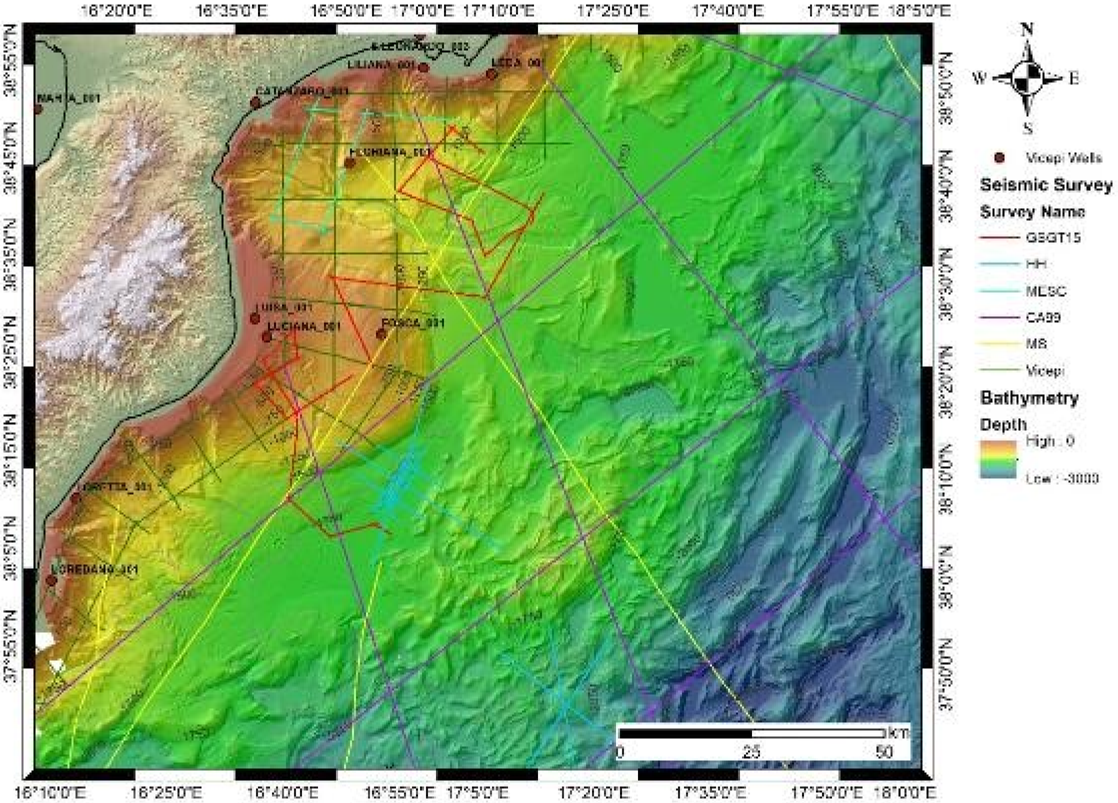

Figure 3-10: bathymetric map with superimposed the MCS dataset used for this study; red dots represents well logs used for calibration with the MCS dataset and correlation purposes.

Table 3-1: table summarizing the different campaigns composing the used dataset. For each campaign are reported the datatypes acquired and used for this study. Table 3-2, Table 3-3 and Table 3-4 report details of each datatype.

Project Name	Organization	Research Vessel	Date	Data type
MESC	OGS / University of Trieste	OGS Explora	2005	Bathymetric data, Sub-bottom profiles, multichannel seismic reflection profiles
MAGIC	OGS / Italian Civil Protection	OGS Explora	2005 & 2009	Bathymetric data, Sub-bottom profiles
Hermes - Hydramed	OGS	OGS Explora	2005	Bathymetric data, multichannel seismic reflection profiles
M112	University of Bremen	Meteor	2014	Bathymetric data, Sub-bottom profiles
GSGT15	OGS	OGS Explora	2015	Bathymetric data, Sub-bottom profiles, multichannel seismic reflection profiles
CA99	Industrial data			Seismic reflection profiles
ViDEPI	Oil companies	Various vessels	1970-1990	multichannel seismic reflection profiles and wells

Table 3-2: table showing the different DTMs grid size and acquisition parameters

Cruise	MBES	Depth range (m)	Operating frequency	Configuration (°)	Swath angle (°)	MBES grid size
Magic, Mesc	Reason Seabat 8111	0 – 150	100 kHz	1,5°	150°	5 x 5
Magic, Mesc	Reason Seabat 8111	150 – 400	100 kHz	1,5°	150°	10 x 10
Magic, Mesc	Reson SeaBat 8150	250 – 1500	12 kHz	2°	150°	20 x 20
M112	Kongsberg EM122	> 1500	12 kHz	1 – 2°	130°	50 x 50

Table 3-3: table showing the different SBP and their acquisition parameters

Cruise	SBP	Operating frequency
GSGT15	Benthos Chirp II	2- 7 kHz
M112	Parasound P70	4 kHz
Magic	Benthos Chirp II	2- 7 kHz
Mesc	Benthos Chirp II	2- 7 kHz

Table 3-4: table showing the different MCS and their acquisition parameters. Vertical and lateral resolution are calculated on a velocity of 1500 m/s. Lateral resolution is calculated at 1s as a radius of the area

Survey name	**Source**	**Streamer Length (m)**	**Dominant Frequency (Hz)**	**Vertical Resolution (m)**	**Lateral resolution (m)**	**Tot. length (km)**
CA99	n.a.	n.a.	70	5.0	90	2000
GSGT15	GI gun + Mini GI gun	300	200	2.0	53	260
HH	Sodera Air guns	600	100	4.0	75	163
MESC	n.a.	n.a.	120	3.5	68	90
MS	Flexotir (explosive)	2400	40	15.0	120	1025
Videpi	Vapor choc	2400	40	10	120	837

3.3 Well data

Well data are represented by log data from five raster hydrocarbon exploration wells (Figure 3-11) carried out in the study area during the last 40 years by Italian oil companies. Well logs provide a lithological description of the stratigraphic succession and the age constrains. They were for stratigraphic reconstruction purposes. In a first step the 5 raster well logs were correlated in order to evaluate the occurrence of stratigraphic patterns (in terms of age and recognized stratigraphic sequences) within the Neogene-Quaternary succession of the study area and then correlated to the multichannel seismic facies and reflectors, using average time-depth relationships. The wells describe the stratigraphic succession of the Crotone-Spartivento forearc basin. However, for the Plio-Quaternary succession well-logs provide only partial information, because of the total or partial absence of log data for the Plio-Quaternary interval. Figure 3-11 shows the 5 exploration well logs. Only Luciana well log provides information of the Pleistocene, while Fosca, Luisa, Floriana and Catanzaro interrupt at Early to Middle Pliocene.

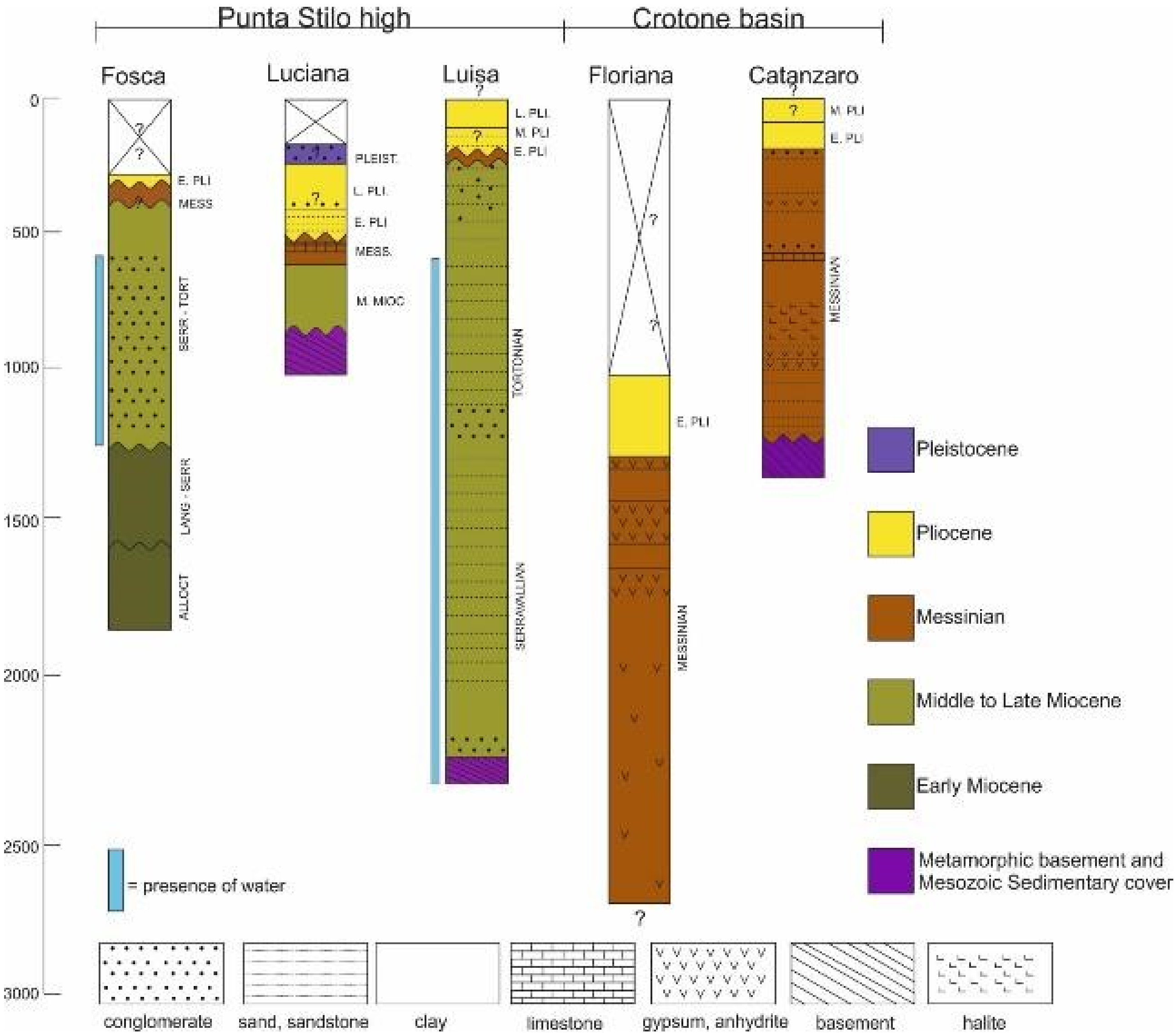

Figure 3-11: image reporting the five well-logs used for this study. For location of the profiles refer to figure 3-10.

3.4 Seabed mapping

Seabed mapping is a technique to map and identify geomorphic features of the seafloor detected using multibeam bathymetry. The results are maps that show the geomorphic features present on the seafloor and through their interpretation it is possible to identify and describe physiographic domains of the seafloor and the geological processes that are shaping the seafloor. In this study seabed mapping was intended to describe the study area in terms of its regional morphologies and to map the occurrence, distribution of geomorphic features related to mass movements occurring at the seafloor, like the presence of slope scarps, canyon head scarps and gravity flow deposits. The result is the creation of a thematic map based on a three level layers: Physiographic domains (PD), Morphological domains (MorD) and Morphobathymetric elements (ME). PD include regional or sub-regional features represented by physiographic domains like continental shelf, continental slope, intra-slope reliefs or small basins, volcanoes and regional-wide erosional areas. MorD represents the envelope of broad, sub-regional areas dominated by a dominant feature types that can be associated to specific geological processes, like submarine canyons, volcanic areas, or seafloor areas characterized by seepage or turbiditic flows. ME represents a detailed mapping of the seafloor morphologies by identifying and tracing geomorphological features of the seafloor related to mass movements, like slope scarps, canyon headwall scarps. This method of regional-scale seafloor mapping has been used for geohazard assessment of the Italian Coasts, during the MaGIC project through high-resolution multibeam bathymetry (Chiocci and Ridente, 2011). In this study the same method was applied, but focusing on the seafloor mass transport features, notably scarps, slide deposits, headwall and sidewall canyon slide scarps.

Seabed mapping was started by generating digital morphometric maps using a Geographic Information System (GIS): shaded relief map (using 3x exaggeration and NW illumination), slope gradient maps (in degrees), slope aspect maps (in degrees) and curvature maps (in degrees^{-1}). The attributes were extracted using a 3x3 cell neighborhoods sampling. Shaded relief map allows to have a first overview of the main seafloor features. Slope gradient map is a valuable tool in the description of the various physiographic domains, while curvature maps were useful to emphasize seafloor abrupt changes in the seafloor topography, like scars and slide scarps.

3.5 Morphometric analysis

Morphometric analysis was conducted on the MTDs identified in the study area in order to evaluate morphological properties such as geometry, shape, area and volume. Geometry was defined considering the different shapes of the MTDs inferred from seismic profiles, area was obtained by interpolation between the profiles on which each MTDs was identified. Volume was estimated using two different approaches: in one case using the area obtained from the interpolation of the seismic profiles crossing the same MTD, multiplied by the mean thickness of the MTD (previously converted from TWT to m using a interval velocity for the MTD of 1500 m/s); where data coverage was sufficient, the top and bottom surfaces of MTDs were picked on each seismic profile using the Kingdom Suite interpretation software to calculate an isopach map of the MTDs subsequently converted from TWT to m using an interval velocity of 1500m/s.

3.6 Echofacies analysis

Echofacies analysis is a method for to the study of the very shallow (up to 100 m depth) seafloor subsurface. This method is based on the recognition of different echo-types characterizing the shallow subsurface that can be related to sedimentary processes and variations between coarser to softer sediments. Echo-types can be divided into two principal classes based on their acoustic signature, distinct echoes and indistinct echoes, based on the attitude or absence of sub-bottom reflectors. According to Damuth et al., (1980), echofacies mapping can reveal the distribution and abundance of sediments deposited by down slope processes such as turbidity currents or slope instabilities like slide and slumps. The discrimination and classification has been conducted using the classification criteria found in the available literature about echofacies analysis and description of echofacies (Damuth, 1975, 1980a; Embley, 1976; Jacobi, 1976; Loncke et al., 2009). The outcome is a compiled map that shows the distribution of the echo-types. Of particular interest in this study was the recognition of acoustically low reflectivity bodies, that can be interpreted as MTDs.

3.7 Seismostratigraphic analysis

The procedures for seismic stratigraphic interpretation followed three main principles: 1) seismic sequence analysis, 2) seismic facies analysis, 3) interpretation of depositional environments and lithofacies (Vail et al., 1977). Seismic sequences analysis involves the identification of major reflection “packages” that are bounded by recognizable surfaces of discontinuity, known as *unconformities*. Unconformities can be recognized by the interpretation of seismic patterns of reflection terminations along discontinuity surfaces, of which four types are recognized: truncation, downlap, toplap and onlap (Mitchum and Vail, 1977; Vail et al., 1977; Veeken, 2006). Unconformities represent surfaces of erosion and/or non-deposition which constitute time-gaps in the geological record (Dunbar and Rodgers, 1957). Packages of reflectors between two unconformities form a time *seismic unit*. Where well logs were available, they have been used to calibrate the seismostratigraphic analysis, providing age and lithological information of the seismic units identified. In the absence of well data, unconformities were correlated to regional tectonic events on the basic information available from a bibliographic review regarding the onshore and offshore basins (Longhitano et al., 2014; Minelli and Faccenna, 2010; Praeg et al., 2009; Zecchin et al., 2015).

Seabed mapping, morphometric analysis and seismostratigraphic analysis have been conducted using the Kingdom Suite interpretational software and the ArcGIS software.

4 Results

This chapter is subdivided into three sub-chapters addressing the main themes of the study. Chapter 4.1 present an analysis of seafloor morphologies based on seabed mapping on swath multibeam data and sub-bottom data in order to characterize the range of sedimentary processes affecting the margins of the Crotone-Spartivento basin. Chapter 4.2 presents to the Plio-Quaternary stratigraphy of the Crotone-Spartivento forearc basin, based on the identification of unconformity-bound seismic units and their correlation with available well data. Chapter 4.3 is on the features and processes of mass wasting failures, presenting a classification of the different mass movements in three different types, based on differences in features and dynamics.

4.1 Seabed mapping and echofacies analysis

This chapter presents an analysis of seafloor morphologies mapped based on multibeam data. The overall aim of the chapter is to characterize the range of seafloor and subsurface morpho-sedimentary features within the forearc basin, in order to identify those that are the associated with mass movements The chapter is divided into three sub-chapters, that reflects the three division of physiographic domains (PD), morphological domains (MorD) and morphological elements (ME) described in chapter 3.4. The results first provide a description of regional physiographic domains of the Crotone-Spartivento basin and then focus on the distribution within them of morphological features that can be associated to mass movements that affect the margin.

4.1.1 Physiographic domains (PD)

The study area ranges between water depths of < 100 m to 2500 m below sea level (b.s.l.) (Figure 4-1) and is dominated by slope gradients ranging from less than 3° to 5°, to steeper areas with gradients > 5° (Figure 4-3). The area is divided into 4 main physiographic domains, corresponding to a 1) continental shelf, 2) continental slope, 3) forearc basin floor and 4) corrugated area (Figure 4-4).

Continental shelf domain

The continental shelf (Figure 4-4) corresponds to a gently seaward dipping platform (gradients less than 3° Figure 4-2), that ranges from a few hundreds of meters to a maximum of 7 km in width and up to 250m in depth (Figure 4-4). The shelf mimics the shape of the Ionian Calabrian coast: in the north along the Gulf of Squillace it is concave seaward while across the Punta Stilo high it is concave landward and in the south it is more rectilinear, with a NE-SW orientation (Figure 4-4). The continental shelf is wider on the Punta Stilo high, with values ranging between 5 to 7 km while in the northern and southern part it is very indented with widths between hundreds of meters to few kilometers (< 5 km).

Continental slope domain

The continental slope ranges from depths of 200-250 m down to 1500 – 1600 m b.s.l. (Figure 4-4). The shelf break is an abrupt change in slope gradient from less than 3° to more than 5° on the upper slope, and in places to over 10° on the lower slope. It is possible to divide the slope into three sectors: southern, central and northern. The southern sector has a steep slope with gradients from 10° to 15° (Figure 4-3), steeper on the upper slope (Figure 4-2-profile 3). The central sector is represented by the Punta Stilo high (Figure 4-4), a southeastern oriented relief with a lobate shape, characterized by gradients of 2°- 3° on the upper slope that steepen to 10° - 15° downslope (Figure 4-3); the top of the Punta Stilo high includes a N-S oriented depression 10 km wide and 40 m deep ca. (Figure 4-2-profile 2). The northern sector is represented by high gradients (10°- 25° Figure 4-2-profile 1) on the upper slope between 100 and 700 m b.s.l. that decreases downslope with an average steepness of 3° (Figure 4-4and Figure 4-3). The northern sector is characterized by a morphological relief here called "Squillace high" (Figure 4-4) dominated on the east by an upper slope (between 200 to 800-1000 m b.s.l.) with gradients ranging between 15° and 25° (Figure 4-3) while the lower slope is gentler, with gradients ranging from 3° to 5° (Figure 4-2 profile 3).

Forearc basin floor

The forearc basin floor is characterized by gently corrugated areas corresponding to the floors of the Crotone and the Squillace basins, separated by the Punta Stilo high (Figure 4-4). The basin floor extends from the base of the continental slope, around ca. 1500-1600 m b.s.l. and gently dips seaward up to ca. 1750 m b.s.l. with gradients between 2° to 3° (Figure 4-3). It is roughly elongated SW-NE and narrows at the base of the Punta Stilo high, that divides the forearc basin floor into two wider areas, corresponding respectively to the southern offshore part of the offshore Crotone basin on the northern sector and to the Spartivento basin on the southern sector. The seaward limit of this area is approximated by the 1750 m isobath, where the first reliefs and morphological highs start to appear.

Corrugated domain

To seaward lies the more corrugated domain of the forearc basin floor (Figure 4-4), characterized by the presence of morphological reliefs and subcircular to variously elongated basins. Morphological reliefs vary with dimension of tens of kilometers in length with heights up to thousands of meters while sub circular to variously elongate basins vary from tens to thousands of km^2 in area (Figure 4-4).

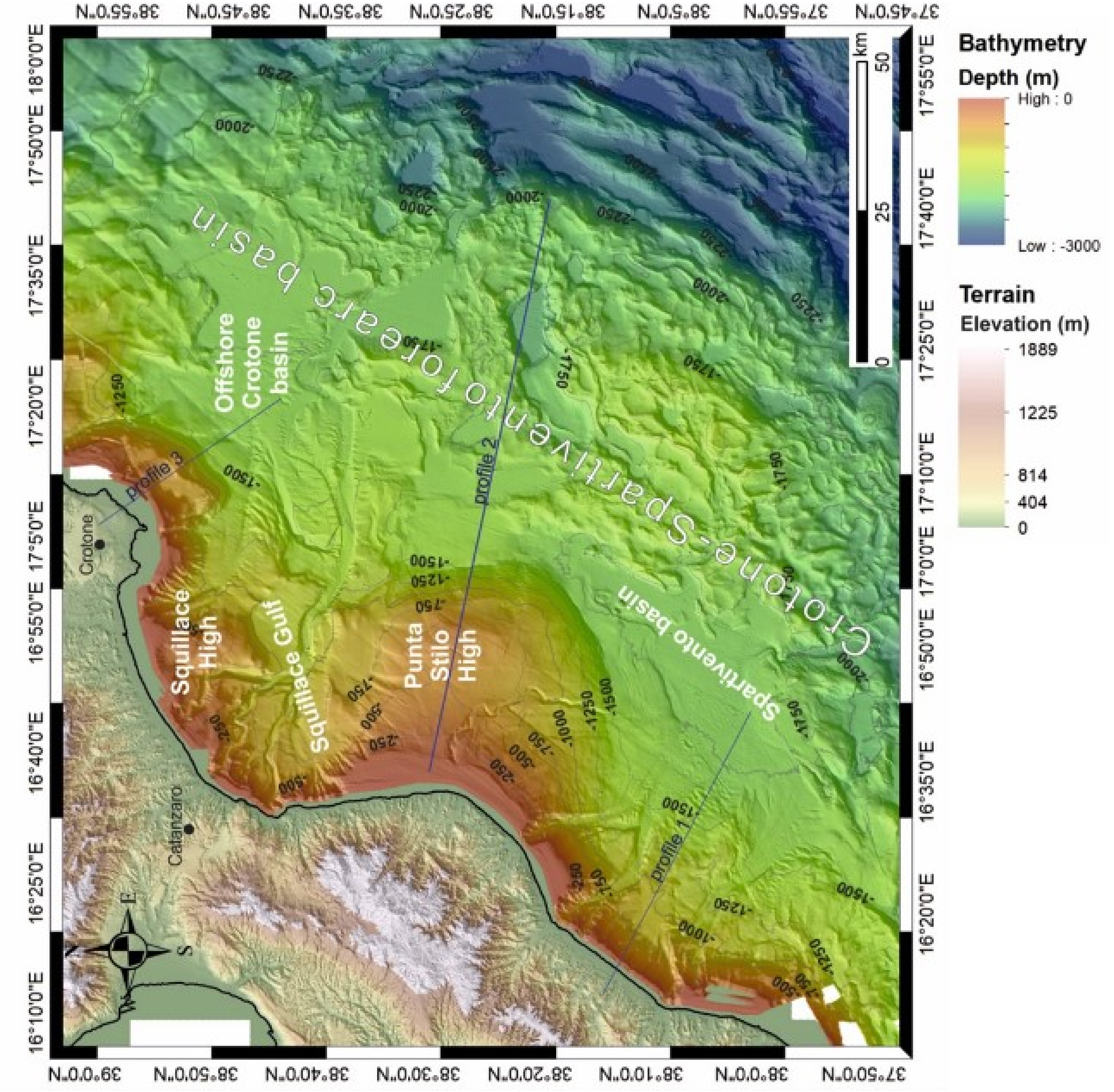

Figure 4-1: bathymetry of the Crotone-Spartivento fore arc basin with the main physiographic features indicated. Contours lines every 250m.

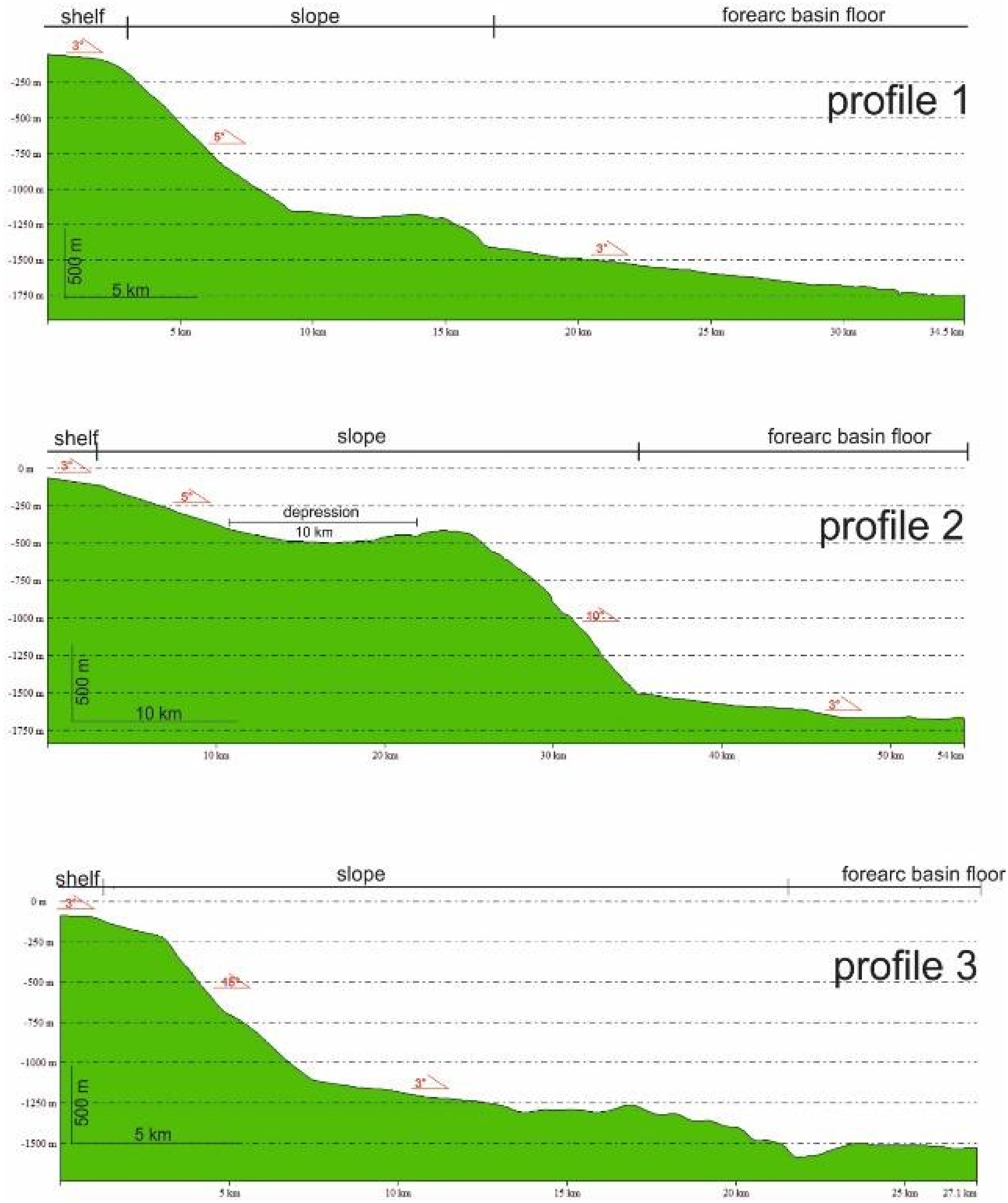

Figure 4-2: bathymetric profiles crossing the four physiographic domains. For locations refer to figure 4.1. Profile 1 is from the Spartivento offshore basin, profile 2 crosses the Punta Stilo high and profile 3 crosses the Crotone basin.

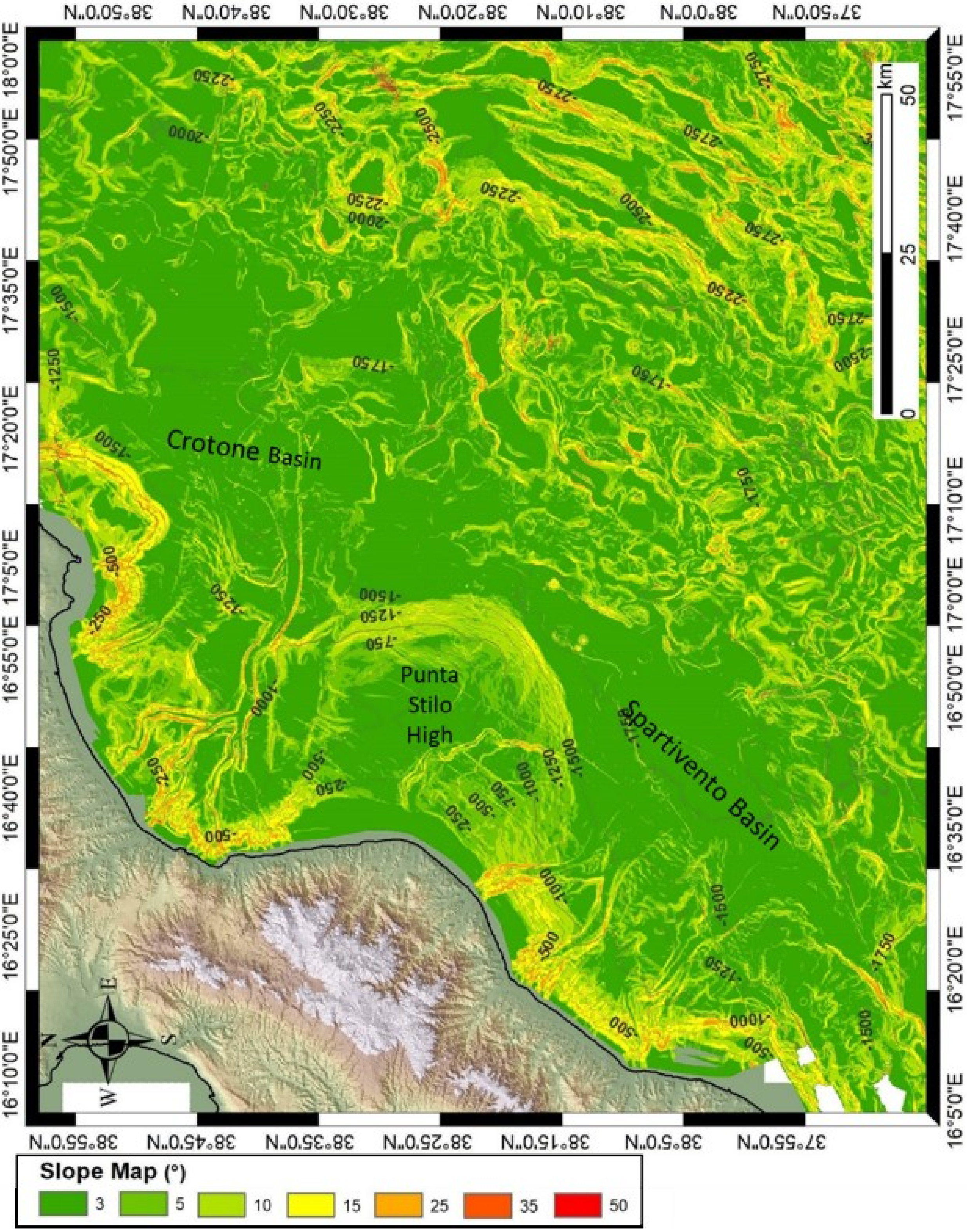

Figure 4-3: slope map of the study area. Light green to yellow and red areas represents steeper slopes (>10°) while the dark green areas represent gentler to flat areas (from 0 to 5°). Contour lines represent isobaths every 250 m.

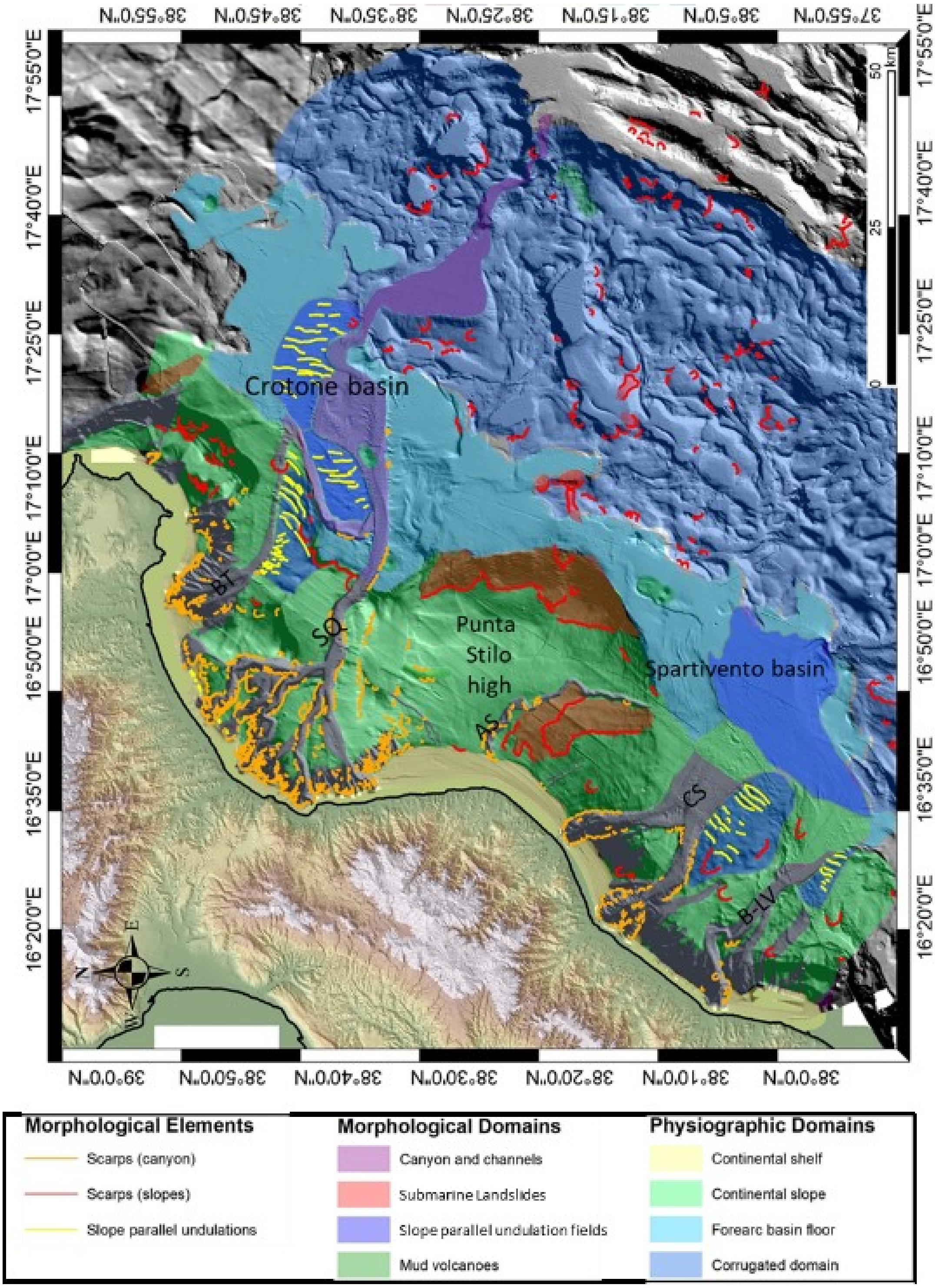

Figure 4-4: Morphological map of the study area, showing: the physiographic domains represented by continental shelf, continental slope, forearc basin floor and corrugated domain; the morphological units represented by canyon and channels, submarine landslides, slope parallel undulation fields and mud volcanoes; the morphological elements that are associated to mass movements are represented by the scarps and the slope parallel undulations. Letters in caps lock refer to the canyon systems names: BT = Bottricello canyon, SQ = Squillace canyon, AS = Assi canyon, CS = Caulonia Siderno canyon, B-LV = Bovalino La Verde canyon

4.1.2 Morphological domains (MorD) and Morphological elements (ME)

Morphological domains (MorD) refer to areas defined by a dominant feature type. Each domain is associated with specific morphological elements, that can be related to different geological process. Four morphological domains are identified: submarine landslides, canyon and channels, slope parallel undulation fields and mud volcanoes. Mud volcanoes occur in this area, and even they are not directly correlated to mass movements, are briefly presented and for sake of completeness. Morphological elements (ME) represent individual morphological features, linked to a specific geological process. Here attention is given to those linked to mass movements, described below as scarps, single or multiple slope failures, slope parallel undulations.

Submarine landslides domain

This domain corresponds to areas where it is possible to identify several scarps, i.e. arcuate morphologies that create an abrupt step in the seafloor, in plan usually concave downslope (Lee et al., 2009; Moscardelli and Wood, 2008; Shanmugam, 2016). Submarine landslides are identified by the presence of an headwall slide scarp upslope of an evacuation area and a mass transport deposit downslope. In the study area, the main submarine landslides occur along the flanks of the Punta Stilo high (Figure 4-4). On the southern flank of the Punta Stilo high, headwall scarps are found between 250-500 m b.s.l. On its eastern flank, a headwall scarp with an irregular shape extends along slope for 16 km, in water depths between 850-1000 m b.s.l. Smaller headwall scarps are also observed in the corrugated area and at the eastern flank of the Crotone continental slope (Figure 4-4), without any other kinematic indicators.

Submarine canyons and channels domain

Canyon systems are channelized areas that transport sediments from the continental shelf and slope to the deeper basins. Canyons are defined landward by a headwall scarp and seaward by the mouth of the canyon. In this domain morphological scarps are also reported, in particular in the headwall and sidewall slopes of canyon systems (Figure 4-4).

The domain is represented by six main canyon systems that characterize the Crotone-Spartivento forearc basin. They are, from north to south: Bottricello, Squillace, Assi, Caulonia-Siderno and 5) Bovalino-La Verde canyon systems (Figure 4-5).

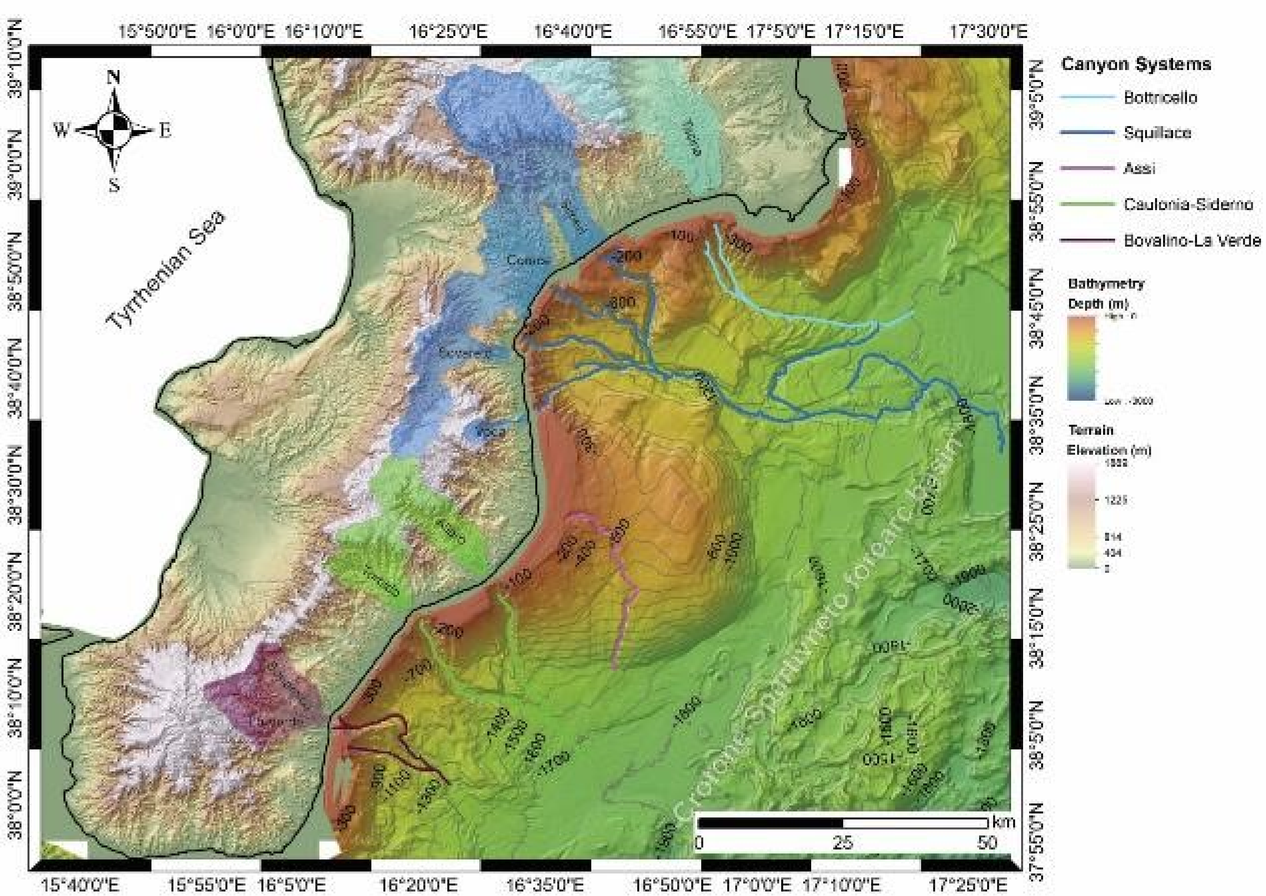

Figure 4-5: Bathymetric map of the study area with the six canyon systems and the subaerial basins to which they area connected. Subaerial watershed colors are the same of the canyon system to which they are connected (see legend for colors). Isobaths every 100 m.

The Bottricello canyon system is located at the northern part of the Gulf of Squillace (Figure 4-5). It is ca. 40 km long and roughly oriented NW-SE and it extends from the continental shelf through the continental slope, from < 50 m b.s.l to 1060 m b.s.l. It is characterized by two tributaries (Bottricello 1 and Bottricello 2 from Coste, 2014) (Figure 4-6A) that together create a headwall domain 10 km wide that deeply incise the continental shelf, 2.8 to 4.5 km from the coastline (Figure 4-6B). The headwall domain is affected by the presence of numerous morphological scarps (Figure 4-6B)

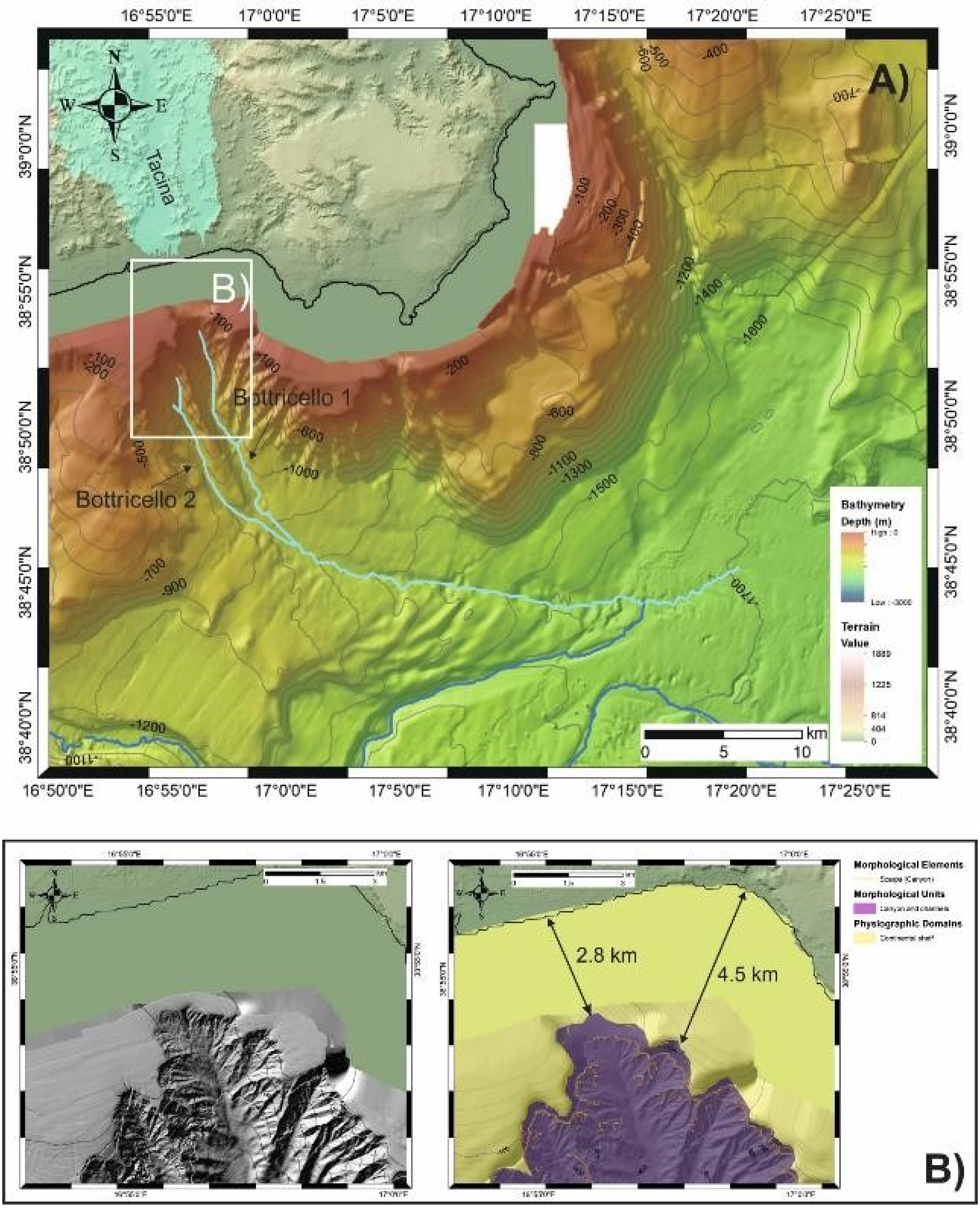

Figure 4-6: A) bathymetric map showing the Bottricello canyon and its two tributaries; contour lines every 100 m (refer to Figure 4-5for location). B) shaded relief map and interpreted map of the Bottricello headwall canyon with the classification in PD, MorD and ME (see text of chapter 4 for the legend classification).

The Squillace canyon (Figure 4-7A) has the widest headwall domain (40 km) of all the canyons of the Crotone Spartivento fore arc basin (Figure 4-5). It extends from 50 m b.s.l. to the forearc basin floorup to 1700-1800 m b.s.l. with a general WNW-ESE direction (Figure 4-7A). It is composed of a main channel, the Squillace channel through which four different tributary canyons merge at around 1070 m depth, named from north to south: Sellia, Catanzaro, Squillace and Badolato (Coste, 2014) (Figure 4-7A). The Sellia extends from ca. 60 m b.s.l. to the lower continental slope at 1060 m b.s.l. (Figure 4-7B) with the headwall limits up to 1.6 km close to the coastline (Figure 4-7B). The Catanzaro canyon extends from the continental shelf to the continental slope from 70 m to 1070 m b.s.l. with its headwall ca. 1.9 km far from the coastline (Figure 4-7C). The Squillace canyon extends from the continental shelf from ca. 60 m b.s.l. through the lower continental slope up to 1070 m b.s.l. with its headwall 0.6 to 1.5 km from the coast (Figure 4-7D). The Badolato canyon extends from ca. 70 m b.s.l. through the lower continental slope up to 1080 m b.s.l with its headwall between 1.5 to 1.65 km from the coast (Figure 4-7E). To seaward the four tributaries merge to form the Squillace channel (Figure 4-7). The Squillace channel widens in proximity of Venere mud volcanoes, dividing into two separated branches, which converge at ca. 1750 m b.s.l (Figure 4-7). At 1500 m b.s.l. from the north flank of the Squillace channel departs a minor channel, called channel annexe. The tributaries are characterized by the presence of numerous and diffuse morphological scarps (Figure 4-7B, Figure 4-7C and Figure 4-7D).

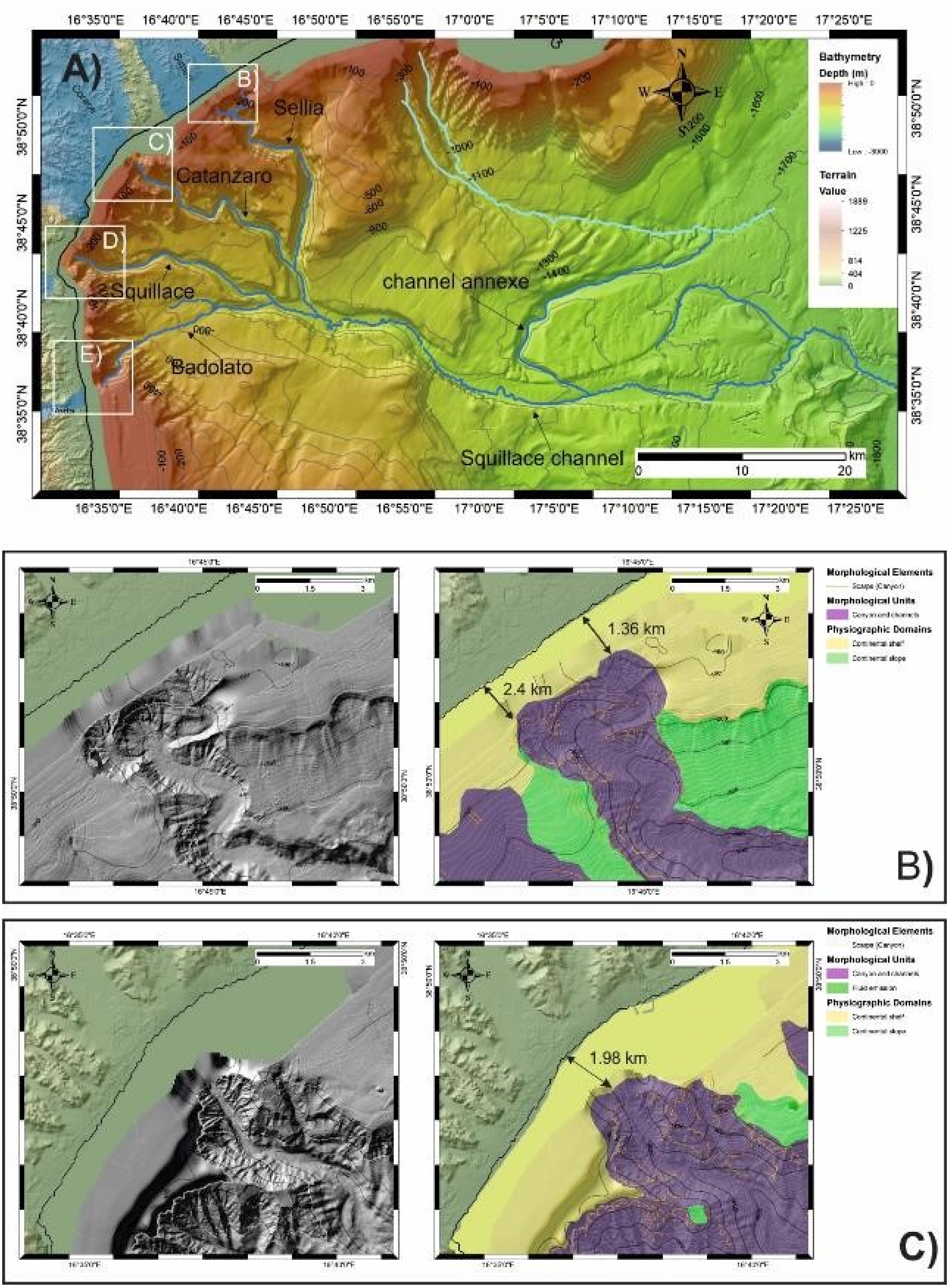
A)
B)
C)
D)
E)
Sellia
Catanzaro
Squillace
Badolato
channel annexe
Squillace channel
Bathymetry
Depth (m)
High : 0
Low : -3000
Terrain
Value
1889
1225
614
404
0
km
0
10
20
16°35'0"E
16°40'0"E
16°45'0"E
16°50'0"E
16°55'0"E
17°0'0"E
17°5'0"E
17°10'0"E
17°15'0"E
17°20'0"E
17°25'0"E
38°50'0"N
38°45'0"N
38°40'0"N
38°35'0"N
N
S
W
E
1.36 km
2.4 km
1.98 km
Morphological Elements
Scarps (Canyon)
Morphological Units
Canyon and channels
Fluid emission
Physiographic Domains
Continental shelf
Continental slope

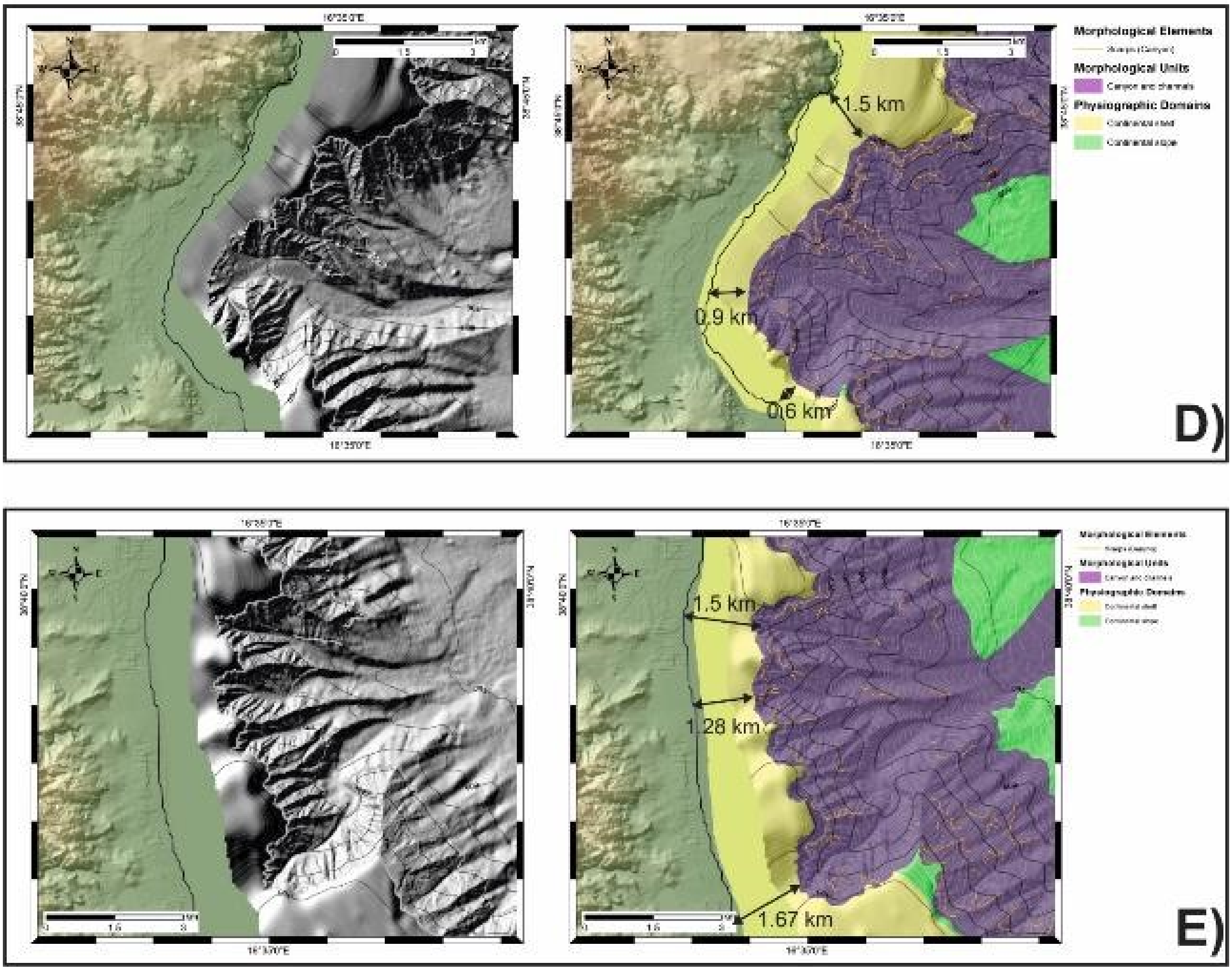

Figure 4-7: A) bathymetric map showing the Squillace canyon and its four tributaries; contour lines every 100 m (refer to Figure 4-5 for location). B) shaded relief map and interpreted map of the Sellia headwall canyon with the classification in PD, MorD and ME (see text of chapter 4 for the legend classification; C) shaded relief map and interpreted map of the Catanzaro headwall canyon with the classification in PD, MorU and ME (see text of chapter 4 for the legend classification; D) shaded relief map and interpreted map of the Squillace headwall canyon with the classification in PD, MorU and ME (see text of chapter 4 for the legend classification; E) shaded relief map and interpreted map of the Badolato headwall canyon with the classification in PD, MorU and ME (see text of chapter 4 for the legend classification.

The Assi canyon is an isolated feature on the southern flank of the Punt Stilo high (Figure 4-5). It is the smallest canyon of the Crotone Spartivento basin. It extends across the continental slope, from 110 m to 1500 m b.s.l. It breaches the shelf but is the only canyon that does not incise it, with its headwall lying 5 km from the coastline (Figure 4-8). It is NNW-SSE oriented in its upper part and becomes N-S moving downslope.

The Caulonia-Siderno canyon system (Figure 4-5) is located south from the Punta Stilo high and debouches in the Spartivento basin. It extends from < 50 m b.s.l. to ca. 1700 m at the base of the continental slope with a general NW-SE direction. In the upper part it is characterized by two tributary channels, the Caulonia and Siderno canyons, that merge downslope into a main channel (Figure 4-9A). The Caulonia and

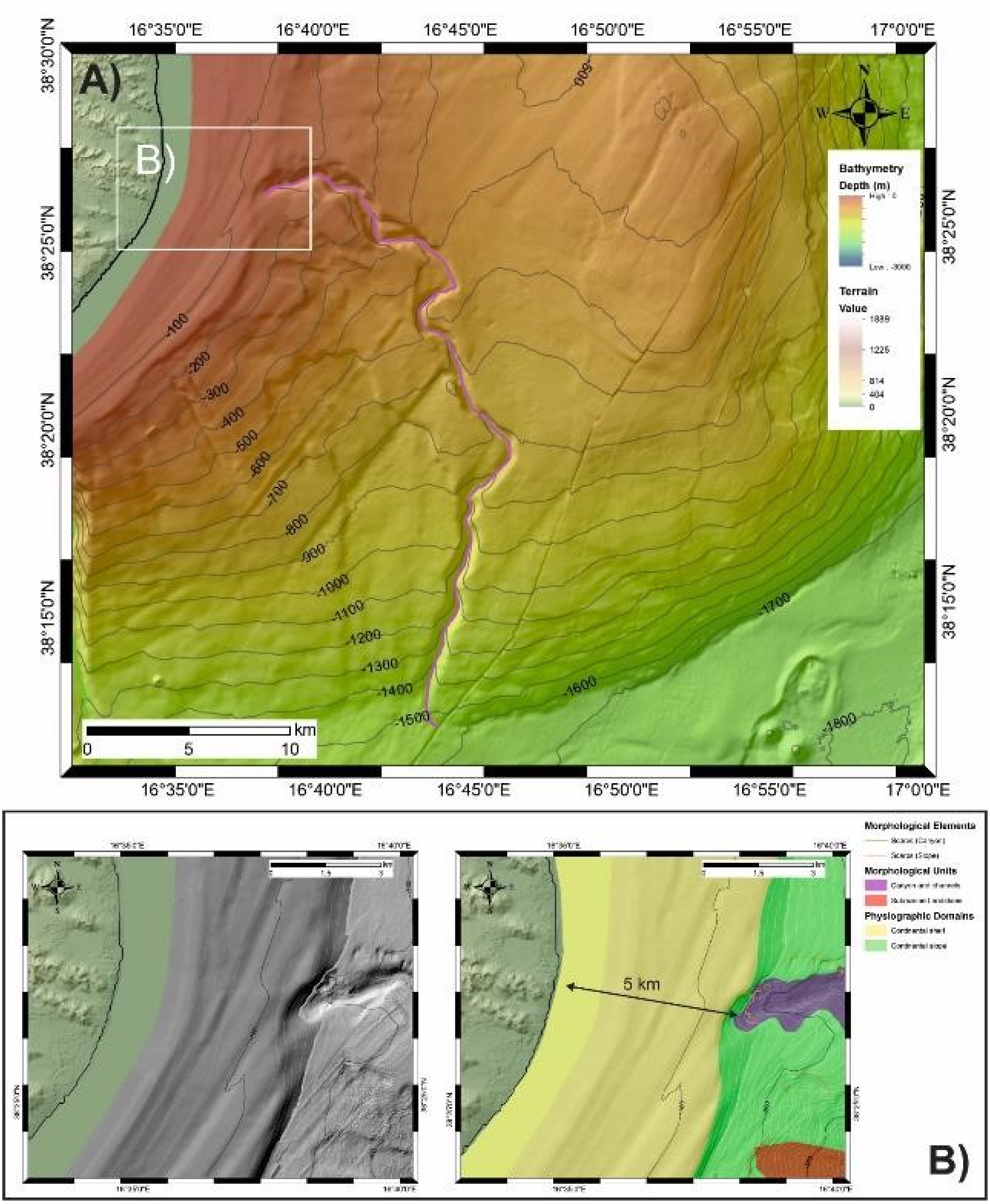

Figure 4-8: A)bathymetric map showing the Assi canyon; contour lines every 100 m (refer to Figure 4-5 for location). C) shaded relief map of and interpreted map of the Assi headwall canyon with the classification in PD, MoD and ME (see text of chapter 4 for the legend classification).

Siderno tributary canyons have their upper headwall respectively 1 km and 1.5 km from the coastline (Figure 4-9B and Figure 4-9C). At 1400 m b.s.l. the two tributaries merge into a single section (and Figure 4-9A). The two tributaries are affected by numerous morphological scarps on their headwalls and sidewalls (Figure 4-9B and Figure 4-9C).

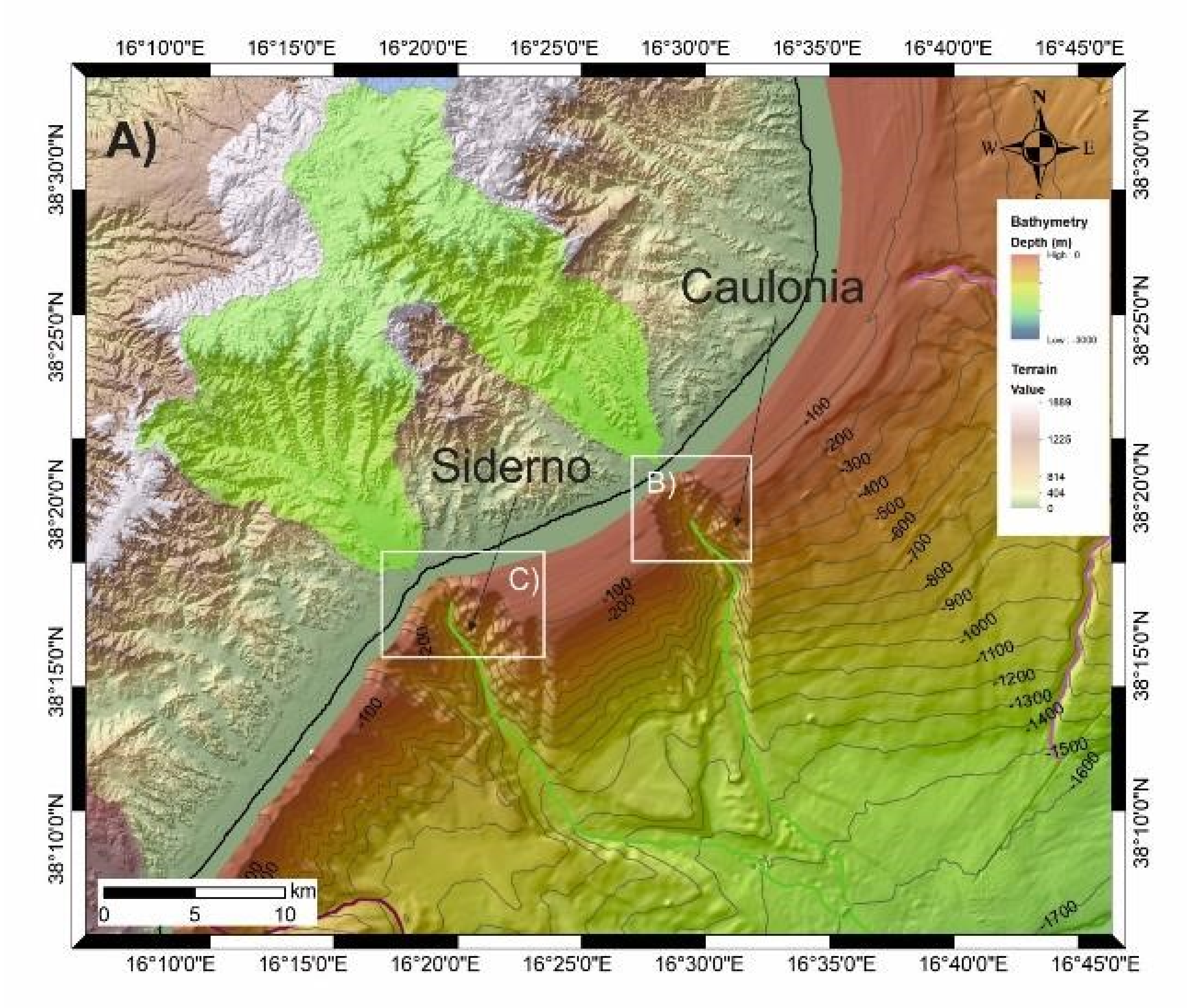

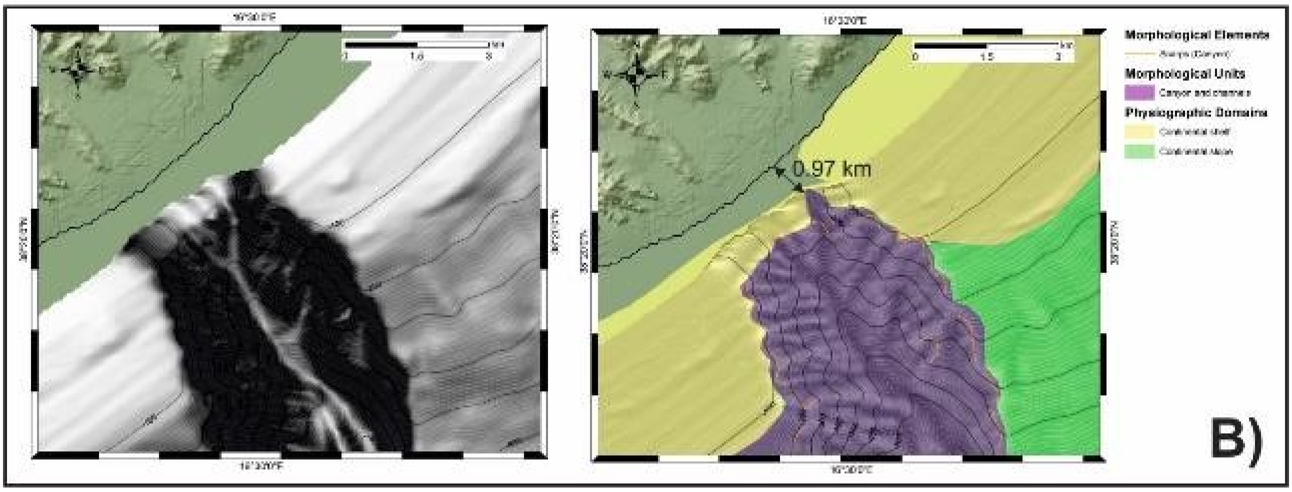

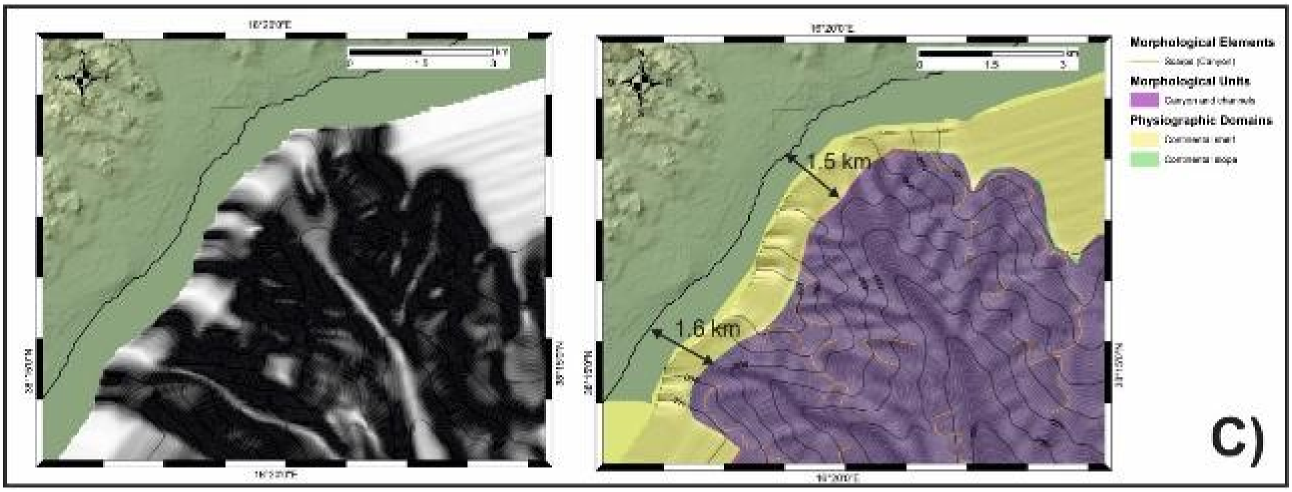

Figure 4-9: A)bathymetric map showing the Caulonia Siderno canyon and its two tributaries; contour lines every 100 m (refer to Figure 4-5 for location). B) shaded relief map and interpreted map of the Caulonia headwall canyon with the classification in PD, MorU and ME (see text of chapter 4 for the legend classification; C) shaded relief map and interpreted map of the Siderno headwall canyon with the classification in PD, MorU and ME (see text of chapter 4 for the legend classification

The Bovalino-La Verde system is located ca. 10 km south of the Caulonia-Siderno canyon system (Figure 4-5). It extends from < 50 m to 1700-1750 m b.s.l. with a general direction NW-SE except for the seaward part that is more NNW-SSE directed (Figure 4-10A). It is composed of two tributaries that merge downslope, the Bovalino in the north and the La Verde in the south (Figure 4-10A). Both tributaries incise the continental shelf, the Bovalino canyon headwall canyon lying 400 m from the coast (Figure 4-10B) and the La Verde canyon 2.4 km from the coast (Figure 4-10C). The headwalls and sidewalls of the two tributaries are marked by the presence of morphological scarps.

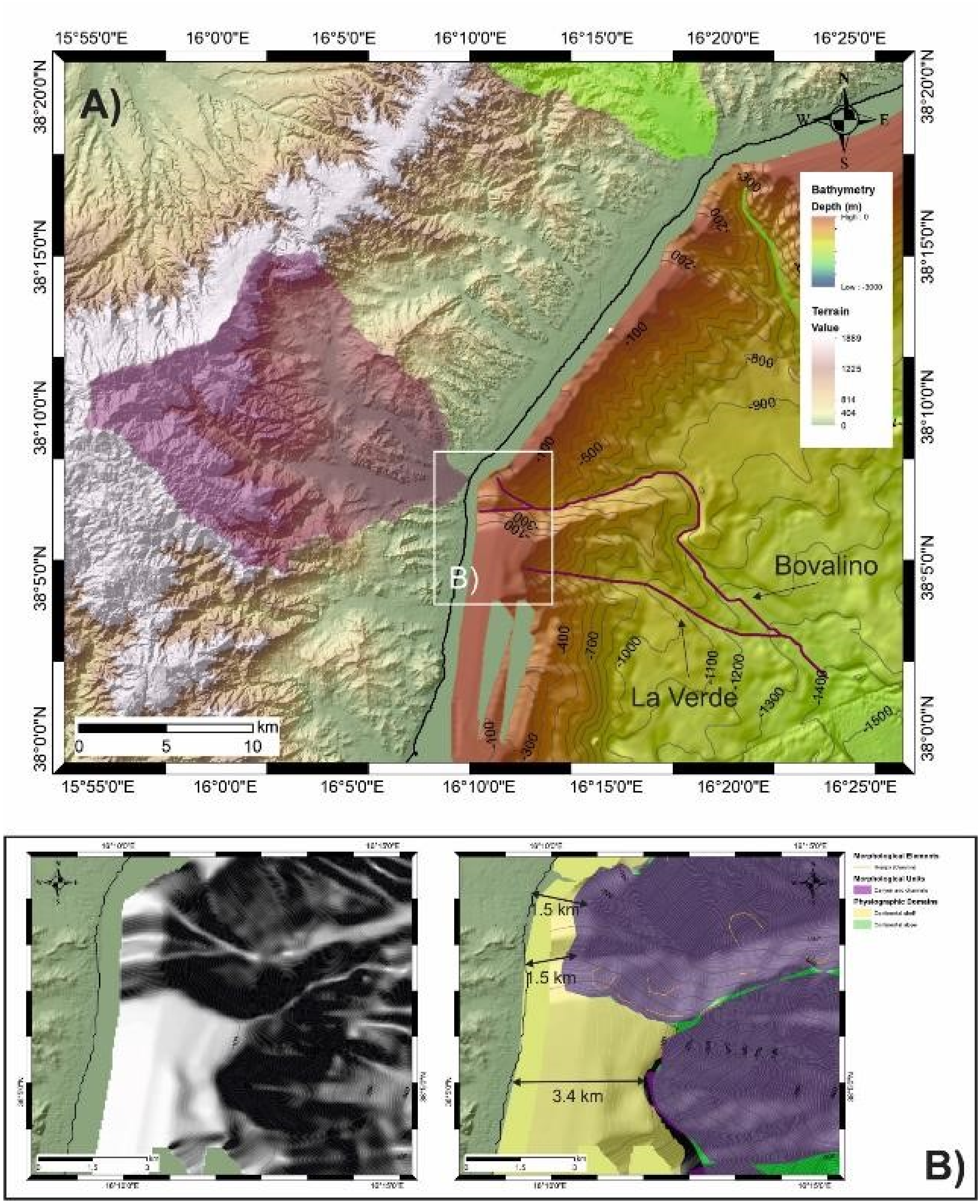

Figure 4-10: A) bathymetric map showing the Bovalino La Verde canyon and its two tributaries; contour lines every 100 m (refer to Figure 4-5 for location). B) shaded relief map and interpreted map of the Bovalino headwall canyon with the classification in PD, MorD and ME (see text of chapter 4 for the legend classification; C) shaded relief map and interpreted map of the La Verde headwall canyon with the classification in PD, MorU and ME (see text of chapter 4 for the legend classification

Areas affected by incisions in form of closely-spaced, V-shaped gullies are widespread on the continental slope: they affect the front of the Crotone Megaslide (Figure 4-11A), the southern sector of the Squillace canyon system headwall (Figure 4-11B) and the southern sector of the continental slope between the Caulonia Siderno and Bovalino La Verde canyons (Figure 4-11C). In the northern sector they occur on the east respect to the Bottricello canyon: in water depths from 150 to 200 m down to 800 m on the western side and 1000 m on the eastern side (Figure 4-11A) with gradients > 25° (Figure 4-3). They are V-shaped with widths ranging from 700 m to 1480 m, and incision depths from 20 m to 100 m (Figure 4-12A). In the southern sector they occur between the Caulonia Siderno and Bovalino-La Verde canyons, in water depths from 100 m to 900 m b.s.l. (Figure 4-12B), on slope gradients >25°(Figure 4-3). They have a V shape and vary from 480 to 1360 m width and 105 m to 10 m depth incision (Figure 4-12B). On the southern part of the Squillace canyon head system, they occur in water depths from 150 to 650 m b.s.l (Figure 4-12C) on slopes with gradients >25° (Figure 4-3). They are closely spaced with width between ca. 730 to 539 m and incision depth between 32 to 34 m (Figure 4-12C).

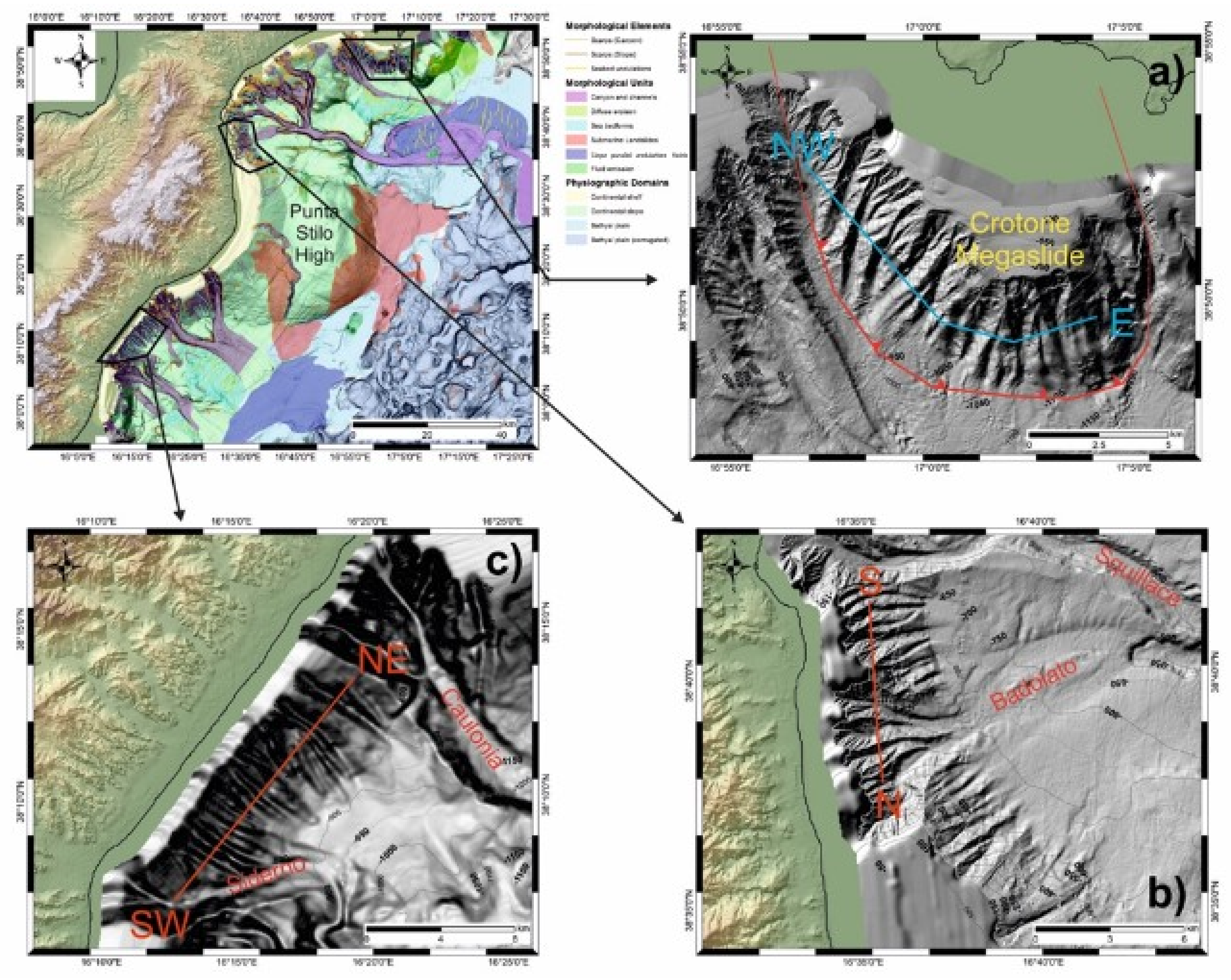

Figure 4-11: on the top left the map of the study area with the PD, MorD and ME classification. A) shaded relief map of the elongated depressions at the front of the Crotone Megaslide; red line shows the position of the profile of Figure 4-12. B) shaded relief map showing the elongated depression on the continental slope south of the Squillace canyon; red line shows the position of

the profile of Figure 4-12. C) shaded relief map showing the elongated depression on the continental slope between the Caulonia Siderno and Bovalino La Verde canyon systems; red line shows the position of the profile of Figure 4-12.

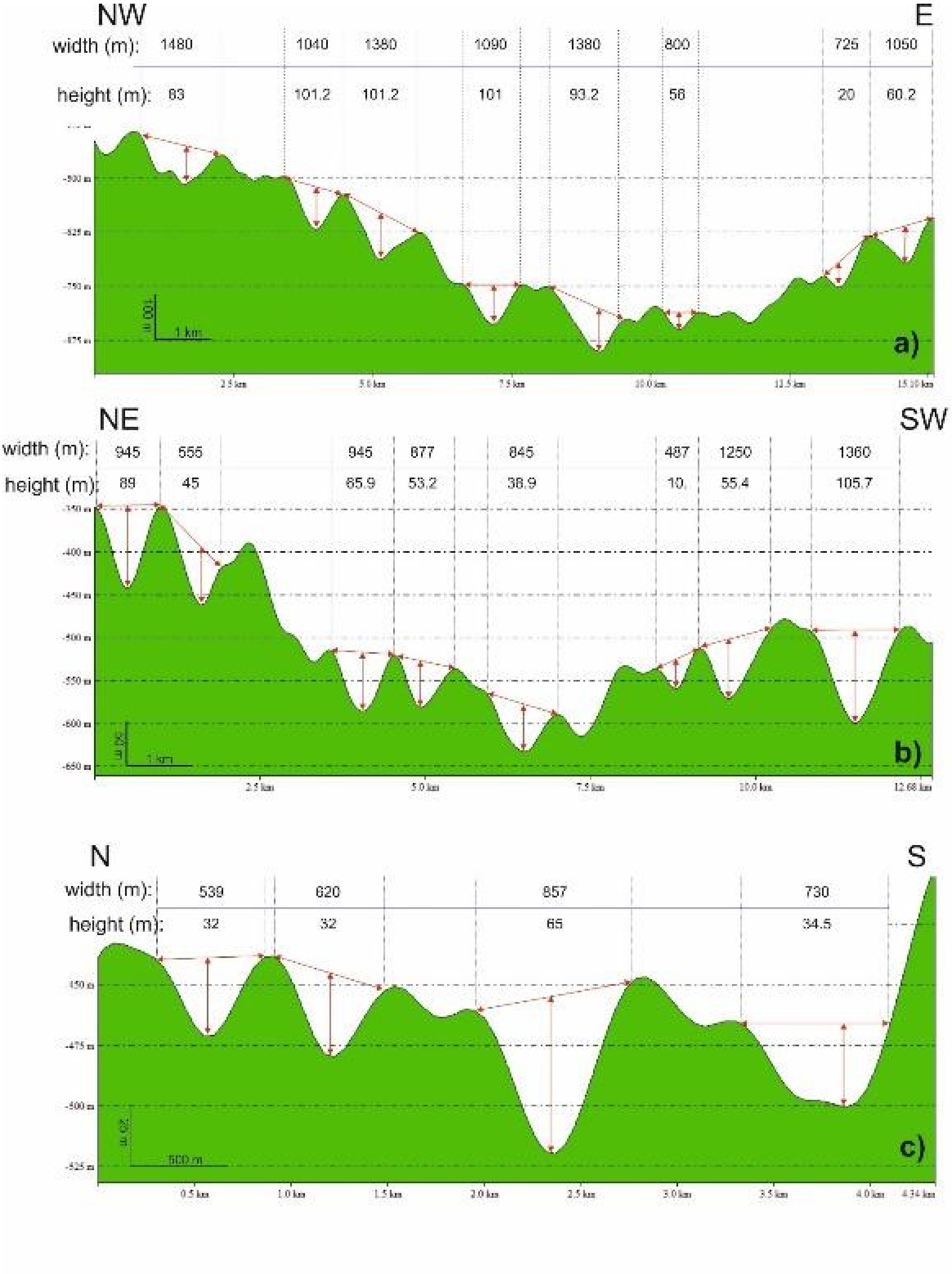

Figure 4-12: A) bathymetric profile across the elongated depression on the steep slope of the western part of the Crotone Megaslide front (see Figure 4-11A for location).B) bathymetric profile across the elongated depressions on the steep slope on the southern area respect between the Squillace and Catanzaro canyons (see Figure 4-11B for location. C) bathymetric profile across the elongated depressions on the steep slope between the Caulonia Siderno and Bovalino La Verde canyons (see Figure 4-11C for location).

Slope parallel undulation fields

Three areas are characterized by fields of slope parallel undulation (<5°): in the Crotone offshore basin at mouth of the Squillace canyon system and in the Spartivento basin at the mouth of the Caulonia-Siderno and Bovalino La Verde canyon systems (Figure 4-4).

In the offshore Crotone basin, the domain is bordered on the north by the Botricello canyon, that marks its northern edge and to the southeast by the channel annexe of the Squillace channel. This area is 27 km long and ca. 8 km wide: it occurs on the lower continental slope, with gradients of 3° to 5° between 800 to 1600 m b.s.l (Figure 4-13A). Slope parallel undulation are N-S oriented in the western part of this area and more NE-SW oriented in the eastern part (Figure 4-13A). The amplitude of the undulations increases from W to E, from 5 m to 35 m height with increasing spacing from hundreds of meters up to 1.8 km with a length in the order of 2 to 8 km with a general lee side steeper than the stoss side (Figure 4-13B).

A second field characterized by undulations lies south of the above field, bordered in the north by the channel annexe of the Squillace channel and in the south by the Squillace channel itself (Figure 4-14A). It extends approximately, between 1400 to 1650 m b.s.l. across slope with gradients from 1° to 3° (Figure 4-14B). The area is 16 km long and 6 km wide, with slope parallel undulations between 1 to ca. 2 km wide and tens of meter high (Figure 4-14B), N-S oriented. At the mouth of the Squillace channel, an area 20 km long and 7 km between 1640 m to 1770 m b.s.l. with gradients of 3° is affected by low amplitude with irregular shape N-S oriented parallel undulations (Figure 4-15A), between 1 to 2 km wide and between 5 to 12 m high (Figure 4-15B).

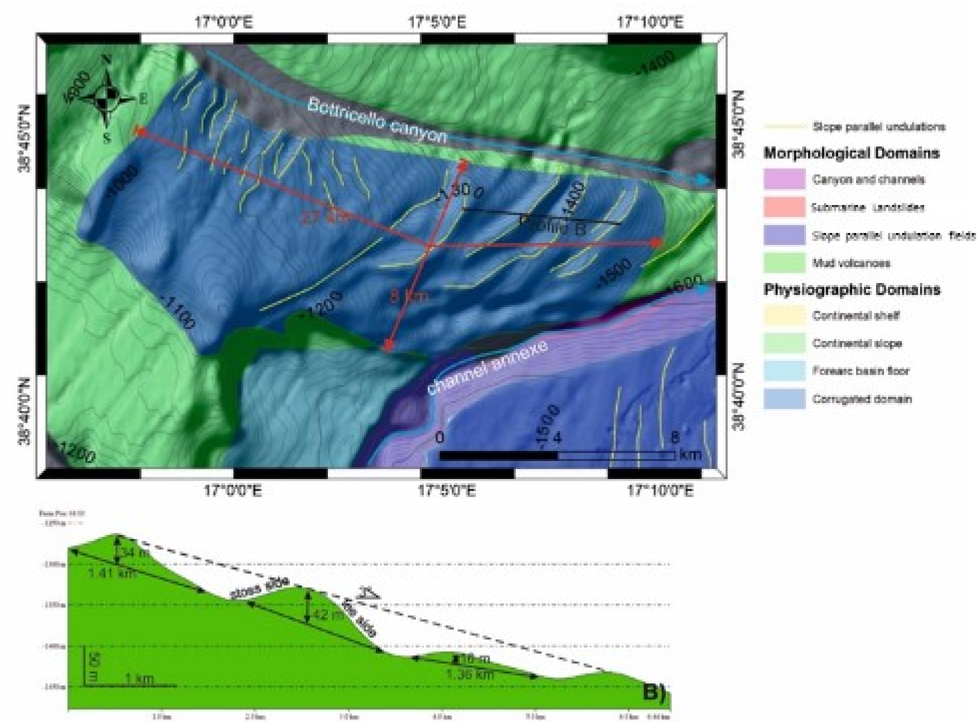

Figure 4-13: A) image showing the slope parallel undulation identified between the Botricello canyon system and the annexe channel of the Squillace canyon system. B) profile crossing the slope parallel undulation (see fig. A for location of the profile).

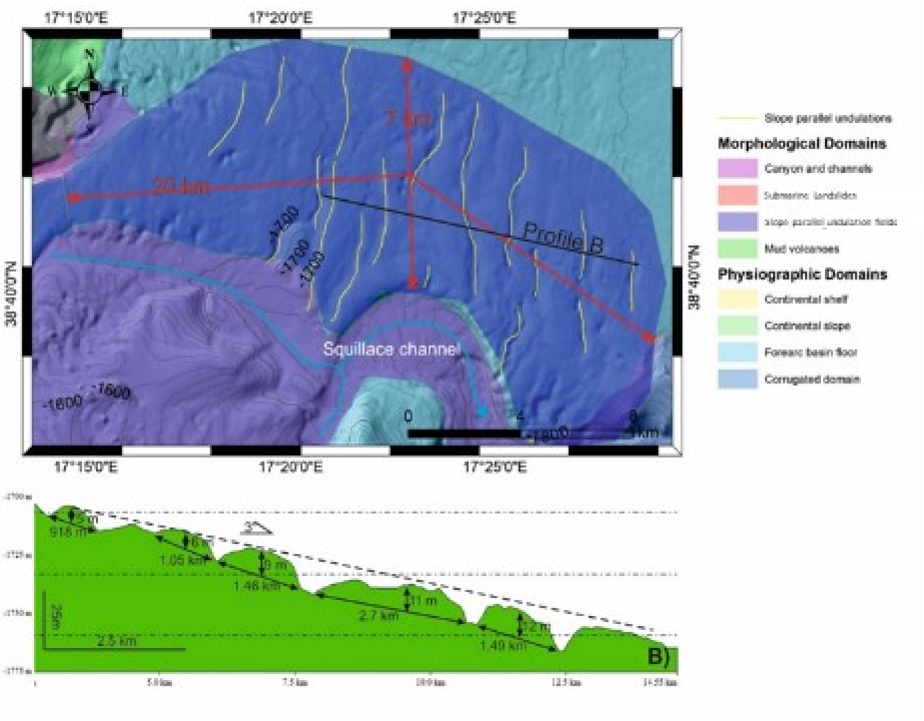

Figure 4-14: A) image showing the slope parallel undulation identified between the annexe channel of the Squillace channel and the Squillace channel itself. B) profile crossing the slope parallel undulation (see fig. A for location of the profile).

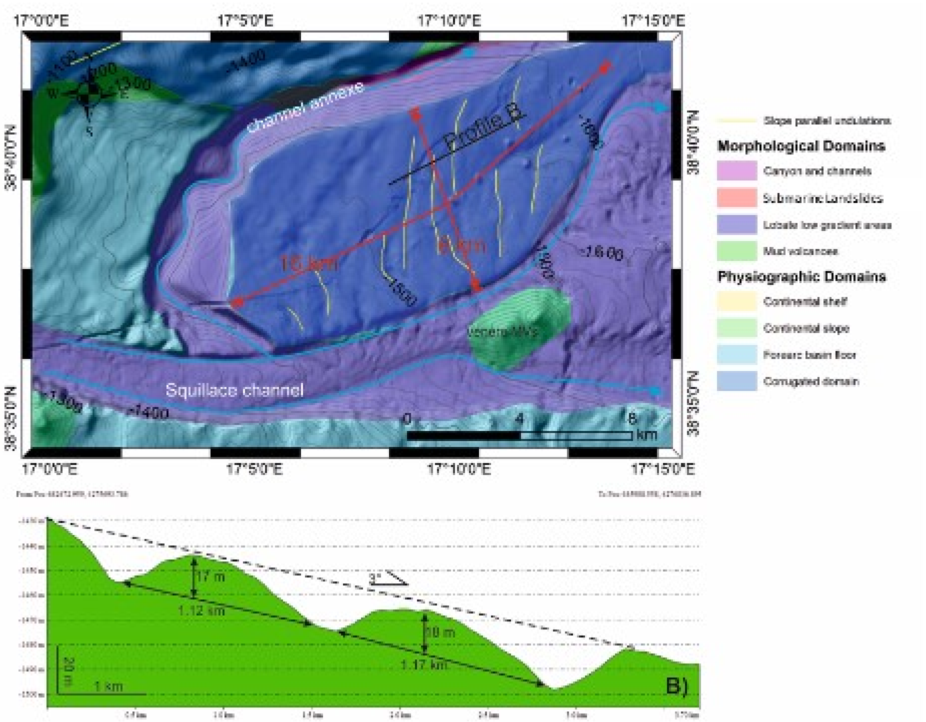

Figure 4-15: A) image showing the slope parallel undulation identified at the Squillace channel. B) profile crossing the slope parallel undulation (see fig. A for location of the profile). C) Sub-bottom profile showing the subsurface expressions of the slope parallel undulations (see fig. A for the location of the profile).

The third field is located on the lower continental slope of the Spartivento basin, bordered in the north by the Caulonia Siderno canyon system and in the south by the Bovalino La Verde canyon system, in water depths between 1000 m to 1700 m (Figure 4-16A), with slope gradients from 2° to 10°(Figure 4-16B). Here slope parallel undulations extend across an area ca. 20 km downslope and 8 km wide (Figure 4-16A). They are 20 to 30 m high and between 700 to 900 m long with a less steep upslope stoss side Figure 4-16B).

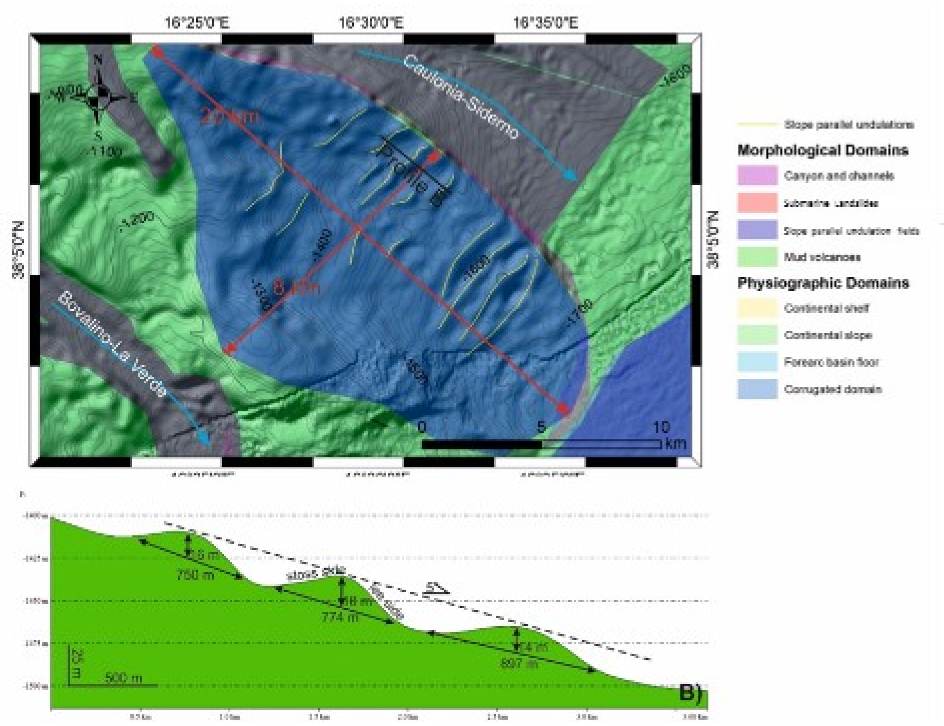

Figure 4-16: A) image showing the slope parallel undulation identified on the Spartivento basin, between the Caulonia-Siderno and Bovalino-La Verde canyon systems. B) profile crossing the slope parallel undulation (see fig. A for location of the profile)

Mud volcanoes domain

Numerous mud volcanoes (Bohrmann et al., 2016; Ceramicola et al., 2014b; Loher et al., 2018a; Praeg et al., 2009) are present in low densities within the Crotone-Spartivento forearc basin, from the shallow water of the continental shelf to the deeper areas of the forearc basin floor. They appear in different forms, from isolated cones, like the Catanzaro MV, to the twin cones of the Venere site or the Madonna dello Ionio MV, to more pie-like structures, like Pythagoras and Sartori MV. They mainly occur on the basin floors and are scarce in the continental slope and continental shelf, except for the Catanzaro MV, which is located on the northern flank of the Catanzaro canyon.

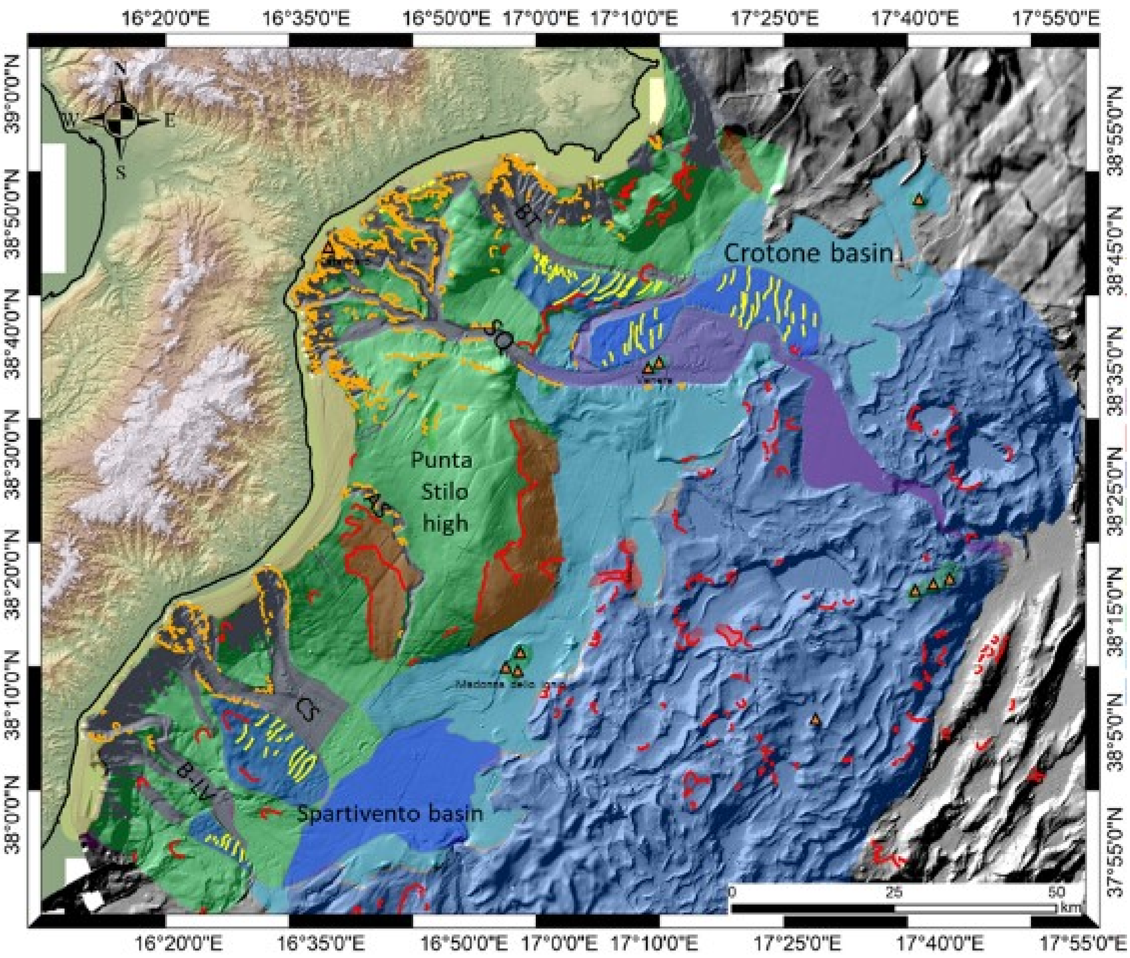

Figure 4-17: map showing the location of mud volcanoes, highlighted by the orange triangle. For the legend refer to Figure 4-4.

4.1.3 Echo-facies analysis

An echofacies analysis was conducted using the ca. 10000 km of sub-bottom profiles, which allowed the identification of eight different echo-types (Figure 4-18)

Bedded: this echofacies is characterized by a continuous sharp bottom echo with mostly horizontal to sub-horizontal, parallel to sub parallel continuous, sharp, alternating from low to high amplitude reflectors (Figure 4-18). In some case onlap terminations are observed.

Discontinuous bedded: this echo type is characterized by continuous sharp bottom echo with mostly parallel to sub parallel sharp, with low to high amplitude reflectors (Figure 4-18). Reflectors drapes the seafloor morphology and are frequently interrupted by lateral discontinuities, interpreted to be faults or in some cases chimneys of fluid migration.

Rough bedded: continuous sharp bottom reflector with highly reflective parallel to sub parallel discontinuous near surface reflectors. This echofacies is characterized by poor penetration (Figure 4-18).

Rough: continuous sharp high amplitude bottom echo without any sub-bottom reflector (Figure 4-18). This type of echofacies is associated to the presence of coarse sediments like sand or gravel deposits on the seafloor or in the canyon thalwegs. The energy absorption because of the gravel sediments prevents any penetration of the sub-bottom echo masking any possible reflector below the bottom echo.

Hyperbolic: large irregular overlapping or single overlapping hyperbolae with widely varying vertex elevation above the seafloor (Figure 4-18). According to Damuth (1980) and Damuth (1994), the occurrence of hyperbolas is mainly linked to the degree of roughness of the seafloor topography or with deposits and surface structuration generated by mass-wasting processes.

Hyperbolic (slope): large irregular overlapping hyperbolas, with vertex approximately tangent to the seafloor (Figure 4-18).

Chaotic: rough and strong bottom echo with sub bottom discontinuous, irregular with medium to low amplitude reflector and sub-bottom fuzzy with undistinguishable reflectors (Figure 4-18).

Transparent: this echofacies include all the echo types characterized by weak bottom echoes and a transparent sub-bottom unit, with absence of any internal reflectors. Sometimes transparent units show an irregular reflective base, interpreted to be an erosional surface. According to their position on the subsurface, they have been classified into two sub-categories: buried and recent transparent echofacies. Buried transparent sub-bottom units are embedded within the sediments (Figure 4-18). Recent acoustically transparent bodies refer to those that are not covered by draping sedimentation (Figure 4-18). The transparent facies are mostly found at the downslope areas in correspondence of the submarine landslides MorD and in sedimentary basins fills. It is usually associated with mass transport deposits related to destabilization and transformation of debris flows or fine-grained distal turbidites (Tripsanas et al., 2003b). The distinction between buried and recent transparent facies is important because allows to make some hypothesis on the spatial and temporal distribution of them. Indeed, recent transparent echofacies could be associated to recent event of failure or mass transport processes because of the absence of any draping sediments on their top, while buried transparent facies is inferred to represent events occurred in the past and for this buried by a sedimentation drape.

Each of the echo facies identified can be associated to different types of sediments and different depositional processes (Table 4-1).

Bedded echo-type and bedded discontinuous are commonly attributed to sediments with alternating sandy and silty beds related respectively to hemipelagic sedimentation (Gaullier and Bellaiche, 1998) or deposition of sediments related to turbidity currents (Damuth, 1980b). In the case of the bedded echo-type it represents undisturbed sediments, while in the case of the bedded discontinuous it is deformed by the presence of lateral discontinuities inferred to represent shallow subsurface faults. This suggests that this echofacies has recorded or is recording recent fault activity.

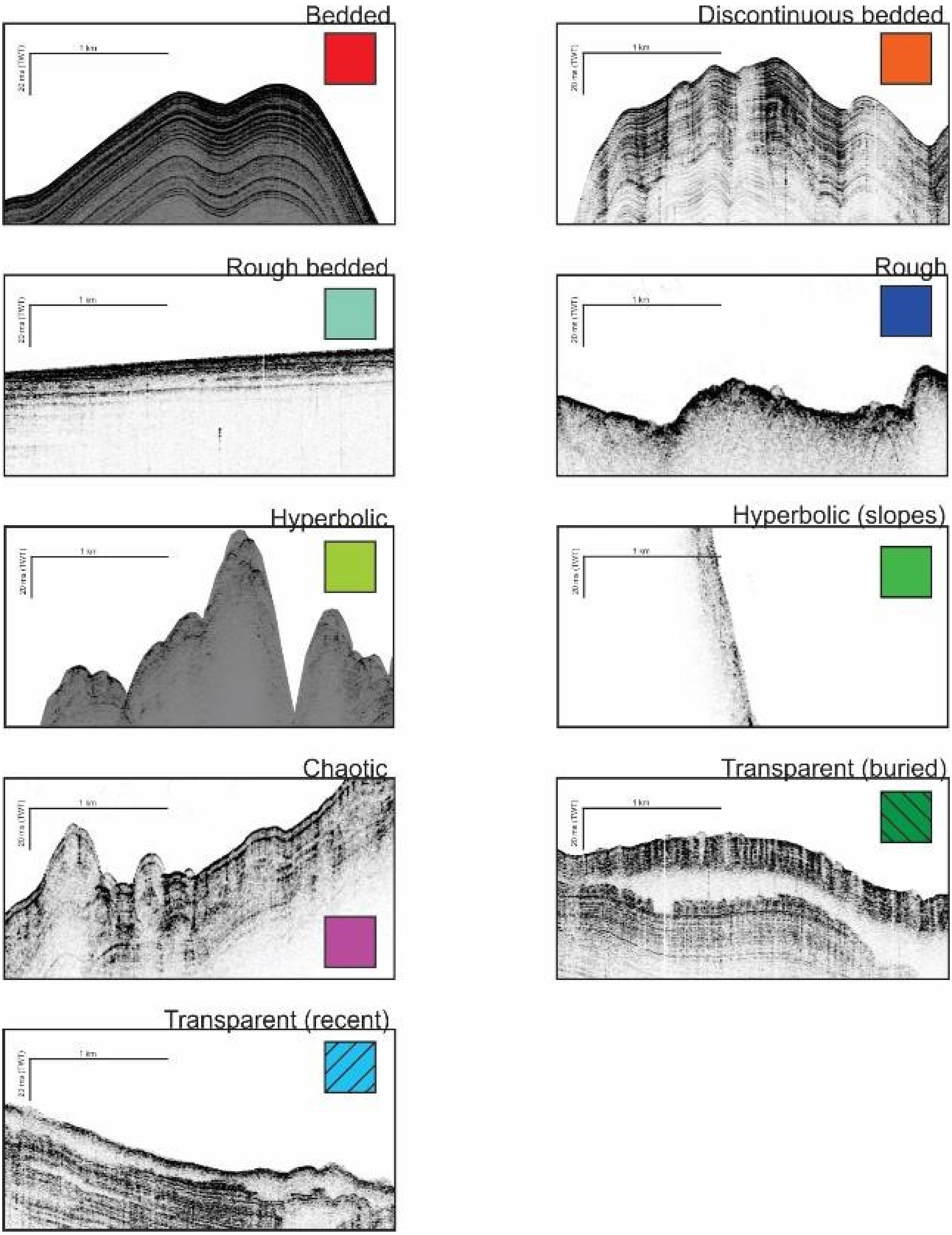

Figure 4-18: Echofacies classification. Note that transparent echo-type has been divided into transparent (recent) and transparent (buried). Colors refers to the echofacies map (Figure 4-20)

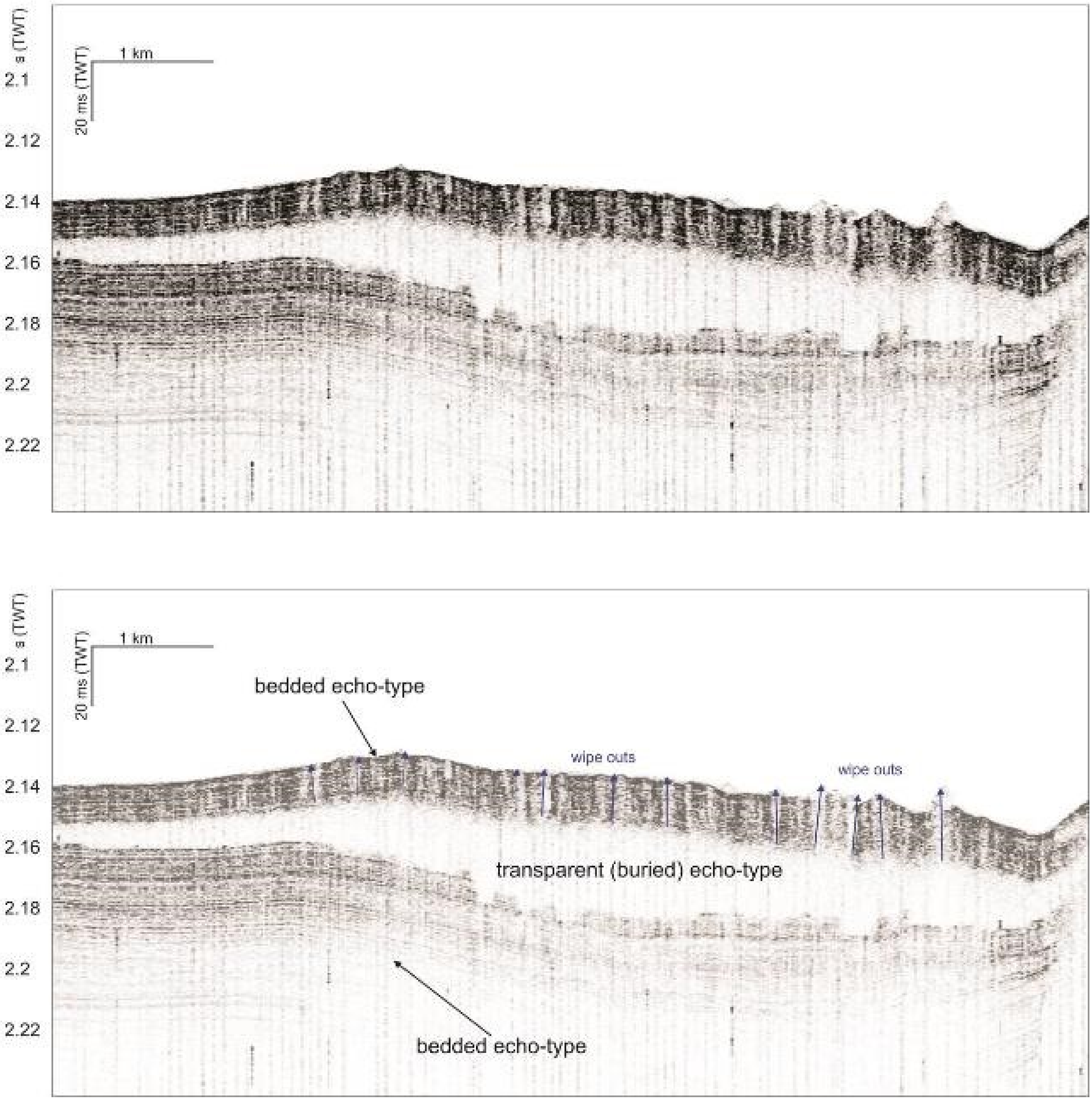

Figure 4-19:) Uninterpreted and interpreted SBP profile showing the occurrence of wipe-outs (blue arrows) in the overlying bedded sediments on top to a transparent buried echo-type.

Rough bedded echo-type is interpreted to represent turbidities with prevalent coarser sediments than the bedded echo-types. Damuth (1975) and Damuth and Hayes (1977) demonstrated that there is a quantitative relationship between the amount of coarser, bedded terrigenous sediments, i.e. sand/silt/ and gravel, in the upper few meters of the seafloor and the bedded, rough bedded and rough echofacies. According to their results, regions characterized by a rough echofacies have a higher content of coarser terrigenous sediments for example in the distal lobes connected with the canyon systems. On the other hand, regions characterized by the two other echo-types, i.e. the bedded and rough bedded have less coarse sediments. Alternatively, the rough echofacies can also be attributed to areas where erosional process is dominant, like for example in canyon thalweg or canyon headwalls.

Hyperbolic echo-characters are related to the hyperbolae size, shape and distribution. Large, irregular hyperbolae are generally associated to rugged slopes, which mask the underlying echo-facies. Small regular hyperbolae of the hyperbolic echo-type is commonly linked with deposits and surface structuration related to mass-wasting processes (Damuth, 1980a, 1980b, 1994; Loncke et al., 2009).

Chaotic echo-characters are related to highly disorganized sediments that are generally produced by mass movements like slumps or debris flow (Damuth, 1994; Pratson and Laine, 1989)

Transparent echo-type is usually referred to deposits related to mass movements, for example, most debris flows return relatively diffuse, fuzzy echo-types from their upper surfaces. Their internal structure is characterized by the absence of any coherent reflectors and thus appears acoustically transparent (Damuth, 1980a, 1980b, 1994; Loncke et al., 2009) while the erosive base are reflective. These transparent echo-types can also characterize basinal fine-grained turbidites (E. K. Tripsanas et al., 2004), but in this case no erosive base is observed (Loncke et al., 2009)

Table 4-1: Table with the 3.5 kHz echo-types and the relative interpretation for the study area. Each echo-type refers to a specific sediment type generated by a specific sedimentary process.

CLASS	**INTERPRETATION**	
	SEDIMENT TYPE OR SPECIFIC SETTING	**SEDIMENTARY PROCESS**
Bedded	Turbidites or Hemipelagites	Turbiditic currents or hemipelagic sedimentation
Bedded-discontinuous	Turbidites or Hemipelagites	Turbiditic currents or hemipelagic sedimentation, creeping
Bedded-rough	Basinal Turbidites or distal lobes	Turbidity currents
Rough	Erosion or sand and gravel inside canyons.	Turbidity currents

Chaotic	Debris flows, creeping masses or erosion in canyon headwalls	Mass movements
Hyperbolic	Erosion, debris flows or seafloor roughness	Mass movements, creeping, erosion
Hyperbolic (slope)	Slumps, Debris flows, slope artifacts	Mass movements, erosion
Transparent (buried)	Mass Transport Deposit (MTD)	Mass movements
Transparent (recent)	Mass Transport Deposit (MTD)	Mass movements

Echofacies analysis allowed the identification of the transparent echofacies, that represents mass transport deposits (MTDs), i.e. the failed material of a gravity flow. MTDs are found to be present at the downslope area of the Punta Stilo high, except for one MTDs identified on top of it, in the basins that characterize the corrugated area, in the forearc basin floorin the Crotone offshore basin and few cases in the headwall domain of the Squillace canyon. For these MTDs, a morphometric analysis has been carried out to evaluate the shape, area, thickness, and the thickness of the overlying sediments for the buried MTDs. The area has been calculated interpolating the sub-bottom profiles on which the same transparent body could be detected, according to its geographic location and position within the sedimentary fill. The thickness has been measured at the maximum thickness section of the MTDs on the sub-bottom profile. Then a rough estimation of the volume has been performed using the thickness and the width of the transparent bodies. In few cases, the top and bottom boundaries of these transparent bodies have been mapped in order to obtain a more precise calculation of the volume

4.1.4 Seafloor processes of the Crotone-Spartivento basin

The combination of seabed mapping and echofacies analysis has allowed the identification of different seafloor processes. In particular, the spatial distribution of the echofacies and the correlation with the morphologies mapped, allowed to depict the major seafloor morphodynamics that are shaping the seafloor. The main morphodynamics are represented by mass movements, canyon systems, and mud volcanoes.

From a general point of view, the area seems to be characterized by an extensive occurrence of the bedded-discontinuous echo-type, like on top of the Punta Stilo high, in the fore arc basin floor area and in the Crotone basin. The continental shelf is mostly characterized by the occurrence of the hyperbolic echo-type where it is incised by the canyon systems and by the bedded echo-type where unperturbed.

Mass movements can be inferred in areas characterized by the presence of scarps and MTDs. These features occur mostly in areas characterized by the presence of the hyperbolic, hyperbolic (slope) and chaotic echo-types (Figure 4-20 and Table 4-1). In some cases, morphological scarps are clearly imaged by sub-bottom profiles. Areas characterized by mass movements and those echo-types are the headwall domain of the six canyon systems and in particular the Punta Stilo high. Diffuse MTDs are observed at the base of the continental slope and within depressions on the forearc basin floor and the corrugated area.

Canyon systems are shaping the seafloor from the continental shelf to the forearc basin floor. They are characterized by the hyperbolic echo-type and in the case of the Squillace canyon and the Bottricello by the rough echo-type. These echofacies can be associated with coarse sediments (Damuth, 1980a, 1980b, 1994) likely transported after being eroded on the headwall domains. The occurrence of the rough echo-type at the mouth of the canyons, in particular the Squillace canyon, suggests that coarse sediments are deposited on the forearc basin floor.

The presence of fluids is inferred on the continental shelf, where seismic anomalies are observed to occur within the shallow stratigraphic succession. The anomalies correspond to diffuse acoustic blanking that masks underlying reflectors, with an irregular top surface sealed by thin parallel to sub-parallel high amplitude and high frequency bedded reflectors (Figure 4-21). In some cases, the top surface of the acoustic blanking occurs at the depth of the U unconformity (Figure 4-22). In this cases, inferred fluid migration pathways occur at the parallel to sub-parallel high amplitude and high frequency bedded reflectors above the acoustic blanking (Figure 4-22). The acoustic anomaly extends from 0.035 ms (TWT) to 0.2 ms (TWT) (Figure 4-23), at a velocity of 1500 m/s correspond from 26 m to 168 m below seafloor. The anomaly is shallower in the inner part of the continental shelf and deepens seaward. In a few cases, acoustic anomalies in form of seismic wipe-outs reach the seafloor (Figure 4-22), although a good correlation with the underlying blanking is not always present. The anomalies are not observed in the canyon head domains, but on the portions of continental shelf that lies between the canyon systems.

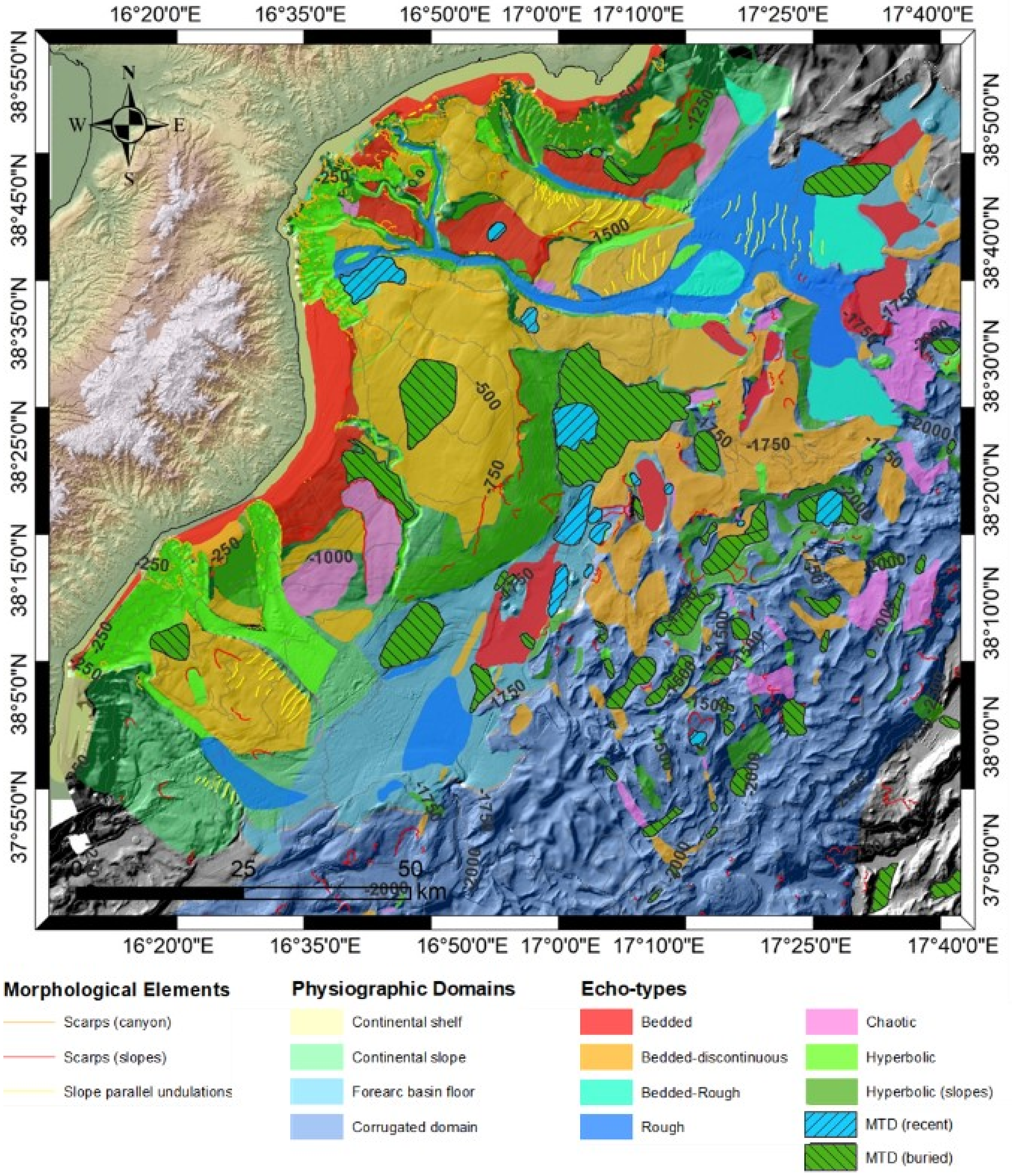

Figure 4-20:seafloor processes detected through the combination of echofacies analysis and seabed mapping

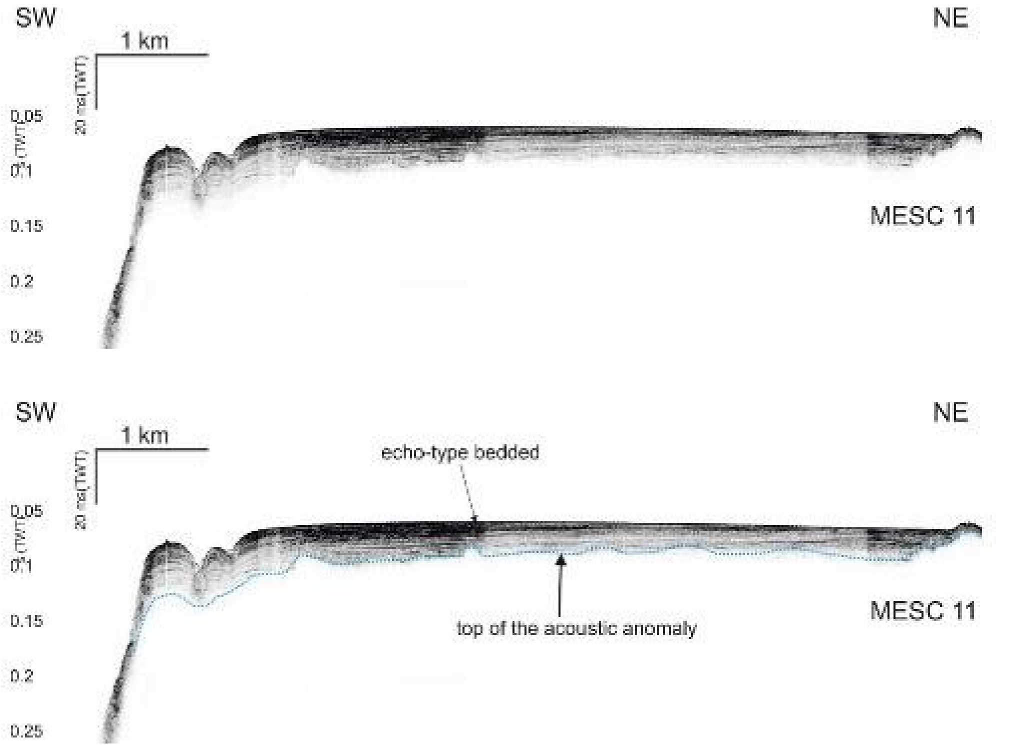

Figure 4-21: uninterpreted and interpreted MESC 11 sub-bottom profile showing seismic acoustic anomaly inferred to be related presence of fluids. Refer to Figure 4-23for location of the profile. In the interpreted profile, the dotted light blue line represents the irregular top surface of the acoustic anomaly, that masks the underlying stratigraphy

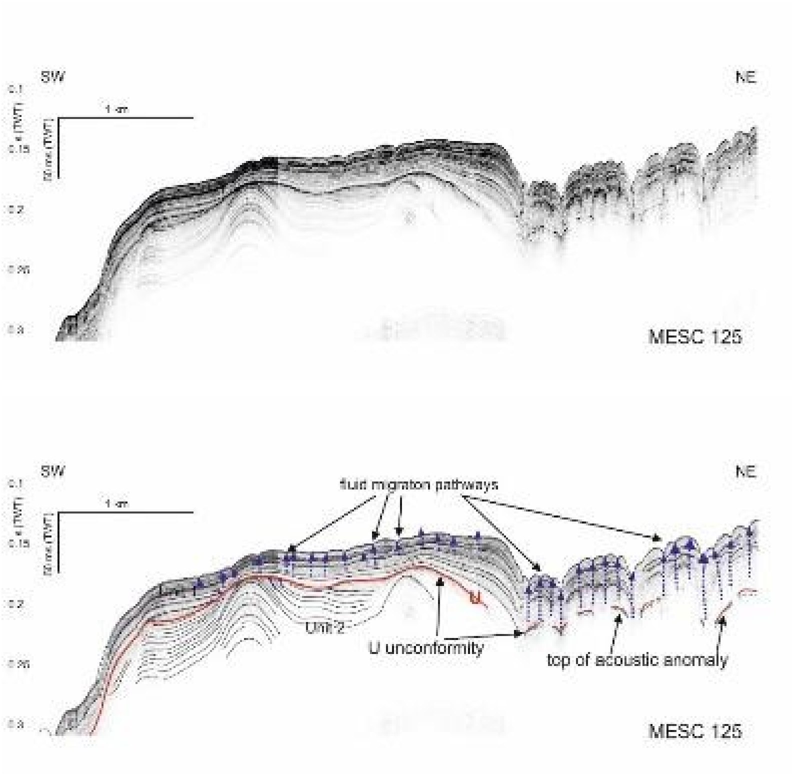

Figure 4-22: uninterpreted and interpreted MESC 125 sub-bottom profile showing U unconformity and vertical pipe structures inferred to be related to fluid migration pathways, represented by the blue dotted arrows. Refer to Figure 4-23 for location of the profile.

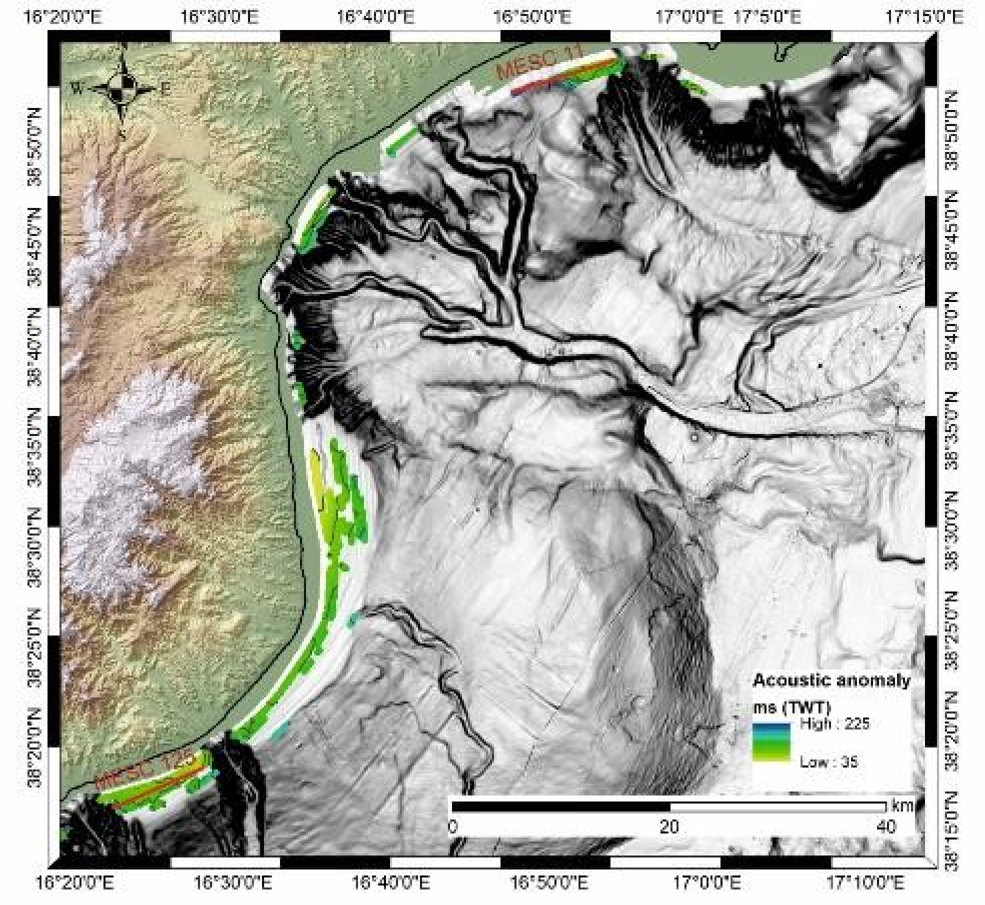

Figure 4-23: map showing the top of the acoustic anomaly mapped in the study areas. Note how the anomaly is mostly present on the undisturbed continental shelf on the central sector on the Punta Stilo high, and in the portions of the unperturbed continental shelf between the heads of the tributary canyon systems

4.2 Plio-Quaternary stratigraphy of the Crotone – Spartivento forearc basin

A seismostratigraphic analysis of the Plio-Quaternary succession of the Crotone Spartivento basin was undertaken using SBP and MCS profiles, subsequently correlated to well log data from near-shore areas (Figure 4-24). Seismostratigraphic analysis was conducted with two major purposes: to constrain the age of the mass movements detected, and to investigate a relationship between the mass movements identified and the evolution of the margin.

The stratigraphic analysis allowed the identification of four unconformities and six seismic units. A shallow unconformity and two shallow units were identified in the SBP data while three major unconformities and four seismic units were identified in the MCS data.

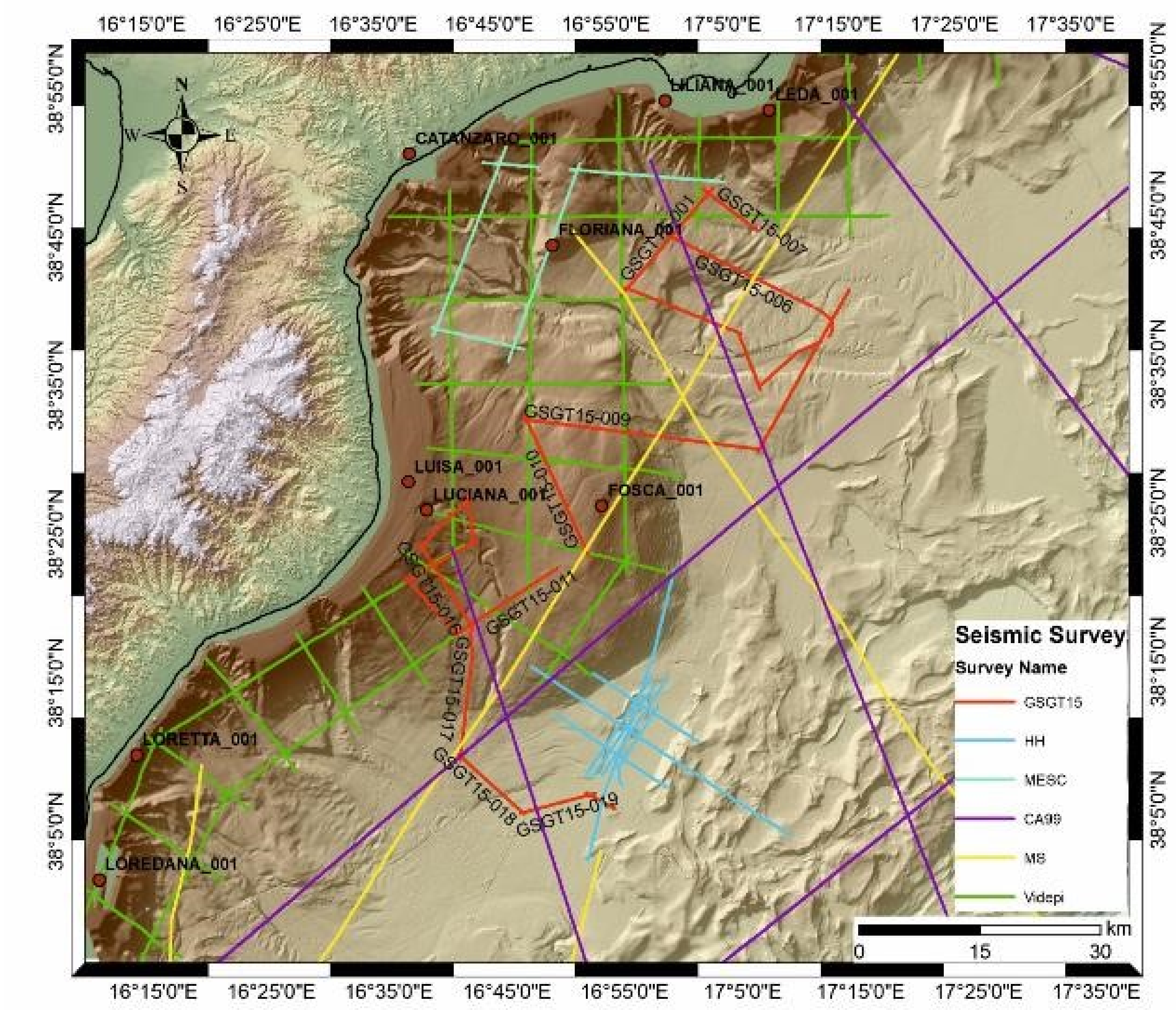

Figure 4-24: bathymetric map with the location of seismic profiles and available wells.

4.2.1 Seismic Unconformities

MU: is characterized by a high amplitude, discontinuous reflector. In some cases, it can be recognized as an erosional surface as in the Punta Stilo high, where it truncates underlying reflectors (see profile GSGT15-009, from shot point 1000 to 1300,Figure 4-25). This unconformity is observed from the upper continental slope to the forearc basin floor (Figure 4-26). It has been traced in the Crotone basin and on the Punta Stilo high (as shallow as 0.6 s TWT). It deepens moving seaward, in the Crotone and Spartivento offshore basin up to 4 s TWT (Figure 4-26). In the Crotone basin the unconformity depicts an elongated depression E-W oriented and coincident with the position of the Squillace canyon. Correlation with available wells Fosca, Luciana and Luisa on the Punta Stilo high and Floriana on the Crotone basin (Figure 4-33), indicate a Late Messinian / Early Pliocene age of the MU unconformity, dated around 5.3 Ma. A clear unconformity is reported on the Fosca well around 765 m b.s.l.f. (below sea level floor) and coincident to the end of the Messinian and to the base of the Pleistocene (Figure 4-33). This result is consistent with previous studies that identified and mapped the MU unconformity in the Ionian basin as well as in the entire Mediterranean and that is known to be coincident with the end of the MSC and the onset of the Plio-Quaternary succession (Cita and Corselli, 1990; Minelli and Faccenna, 2010; van Dijk, 1990, 1991; van Dijk and Okkes, 1991; Zecchin et al., 2013b, 2013a).

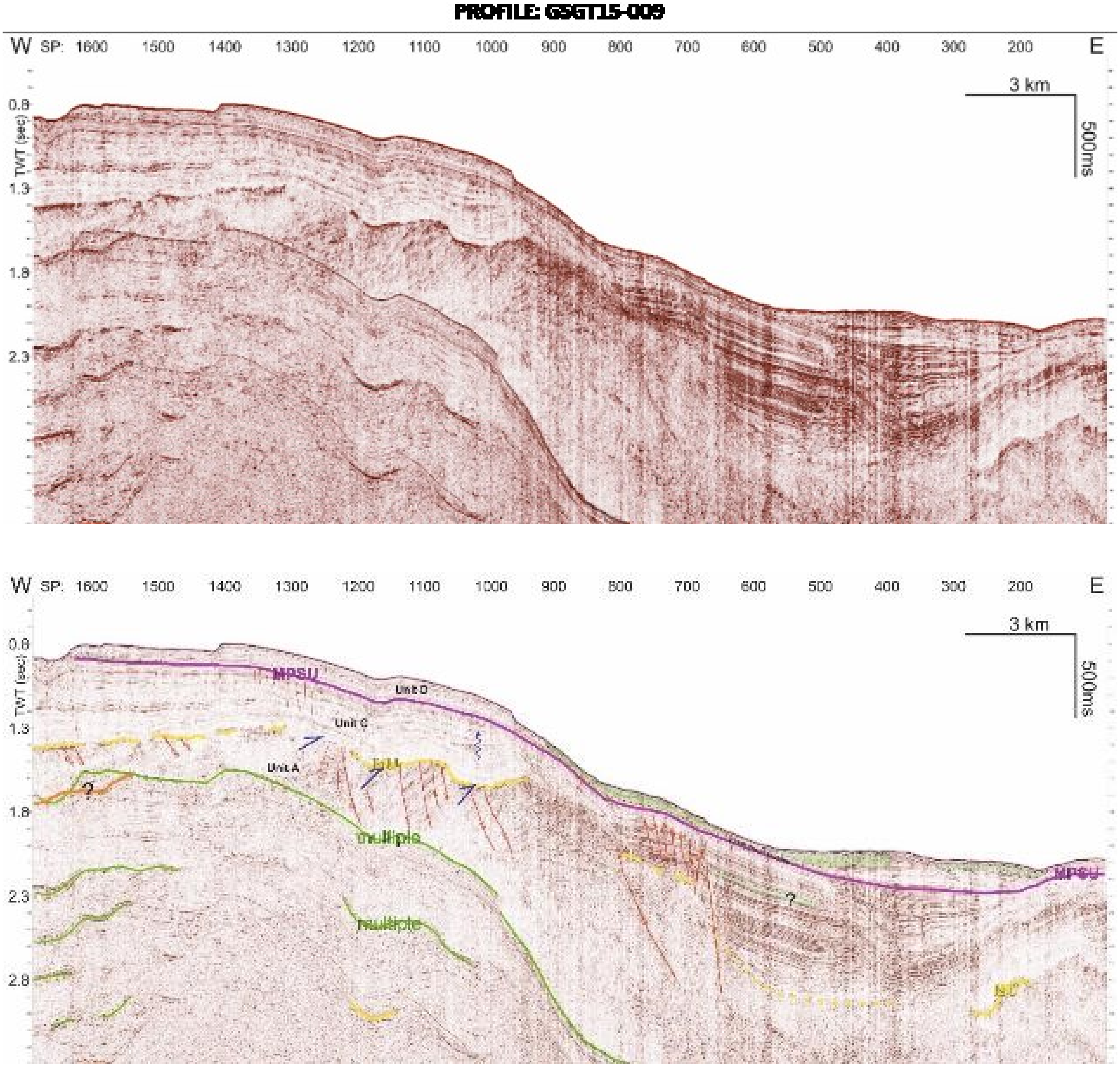

Figure 4-25: seismic profile GSGT15-009. On top the uninterpreted profile, on the bottom the interpreted profile with main unconformities and seismic units (see Figure 4-24 for the location of the profile).

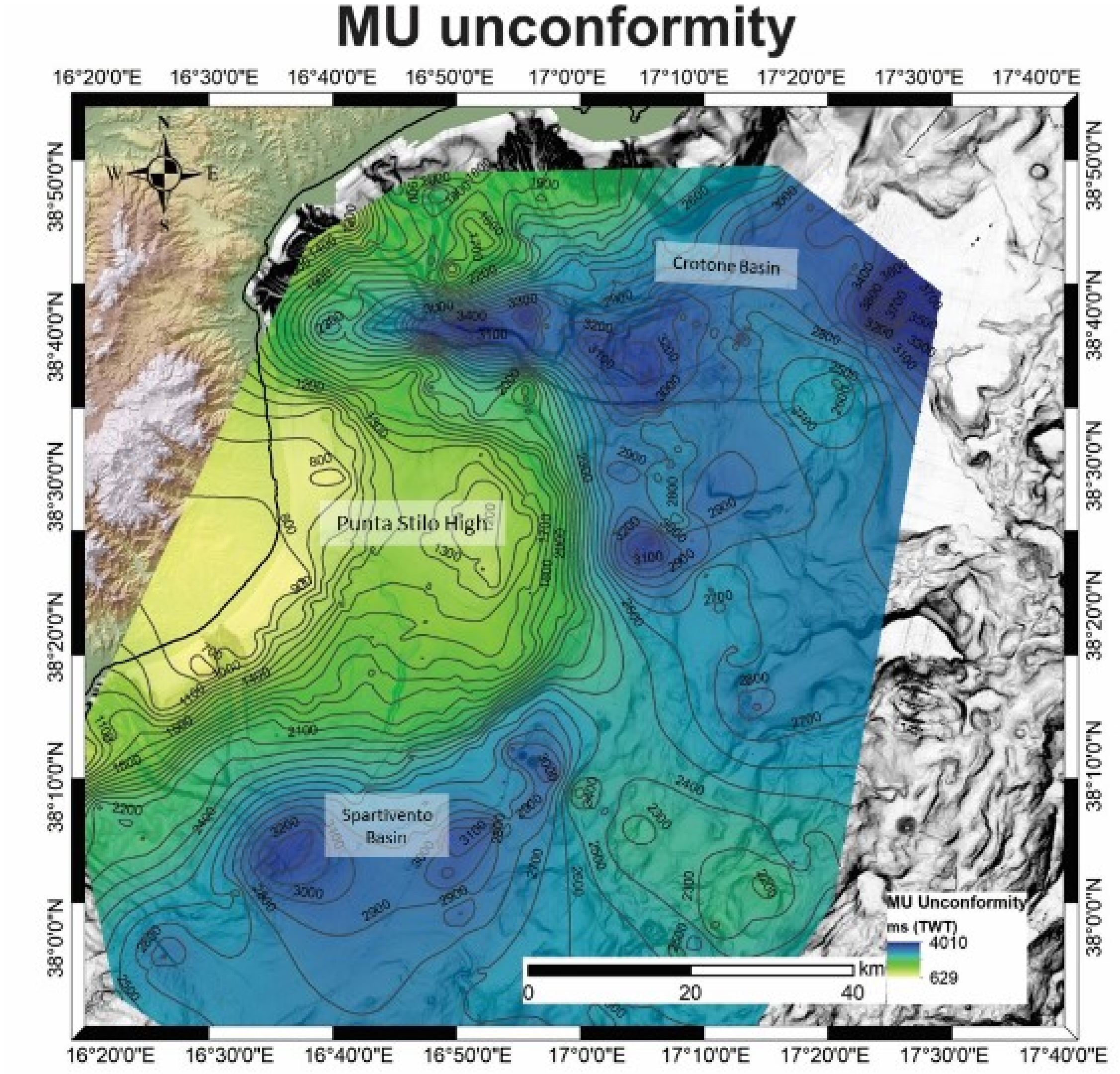

Figure 4-26:computed grid of the depth of the MU unconformity. Contour lines represents isochrons every 100 ms (TWT). Yellow areas are shallower zones that become deeper to the dark blue color.

MPCU: it is a low amplitude, continuous reflector gently dipping seaward with onlap terminations above it (Figure 4-27). This unconformity has been identified in the offshore southern part of the Crotone basin, and tentatively in the Spartivento basin, at the downslope area at the southern flank of the Punta Stilo (Figure 4-28). In the Crotone offshore basin the unconformity lies between 1.5 to 3.2 s TWT depth (Figure 4-29) and deepens moving seaward to the SE (Figure 4-29). This unconformity was related to previous studies (Consolaro et al., 2013; Praeg et al., 2009; Rossi and Sartori, 1981; Zecchin et al., 2015, 2012) and interpreted to be of Middle Pliocene in age, constrained at ca. 3.7-3.6 Ma.

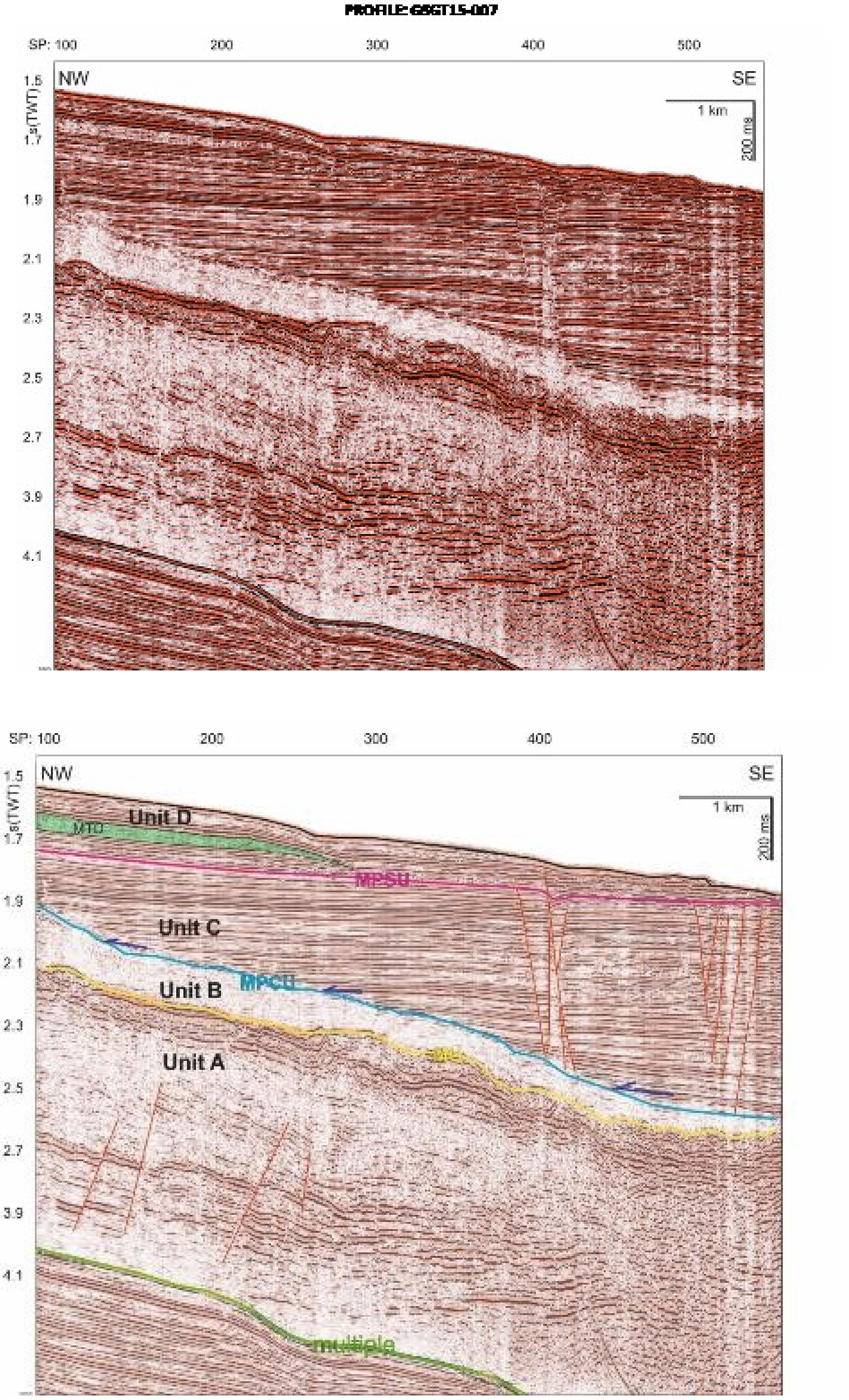

Figure 4-27: seismic profile GSGT15-007. On top the uninterpreted profile on the bottom the interpreted profile with the main unconformities and seismic units (see Figure 4-24 for the location of the profile).

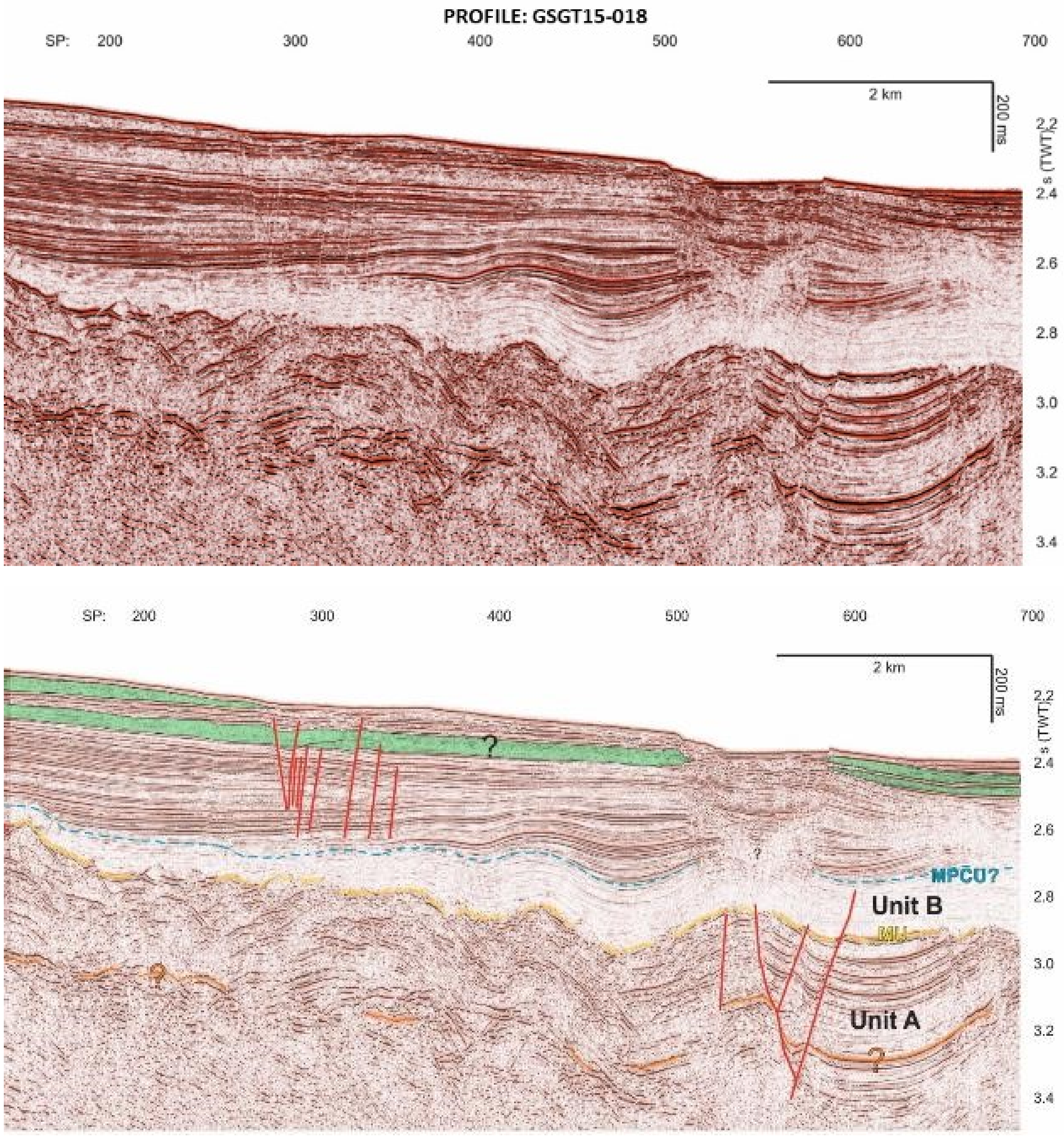

Figure 4-28: seismic profile GSGT15-018. On top the uninterpreted profile on the bottom the interpreted profile with the main unconformities and seismic units (see Figure 4-24 for the location of the profile).

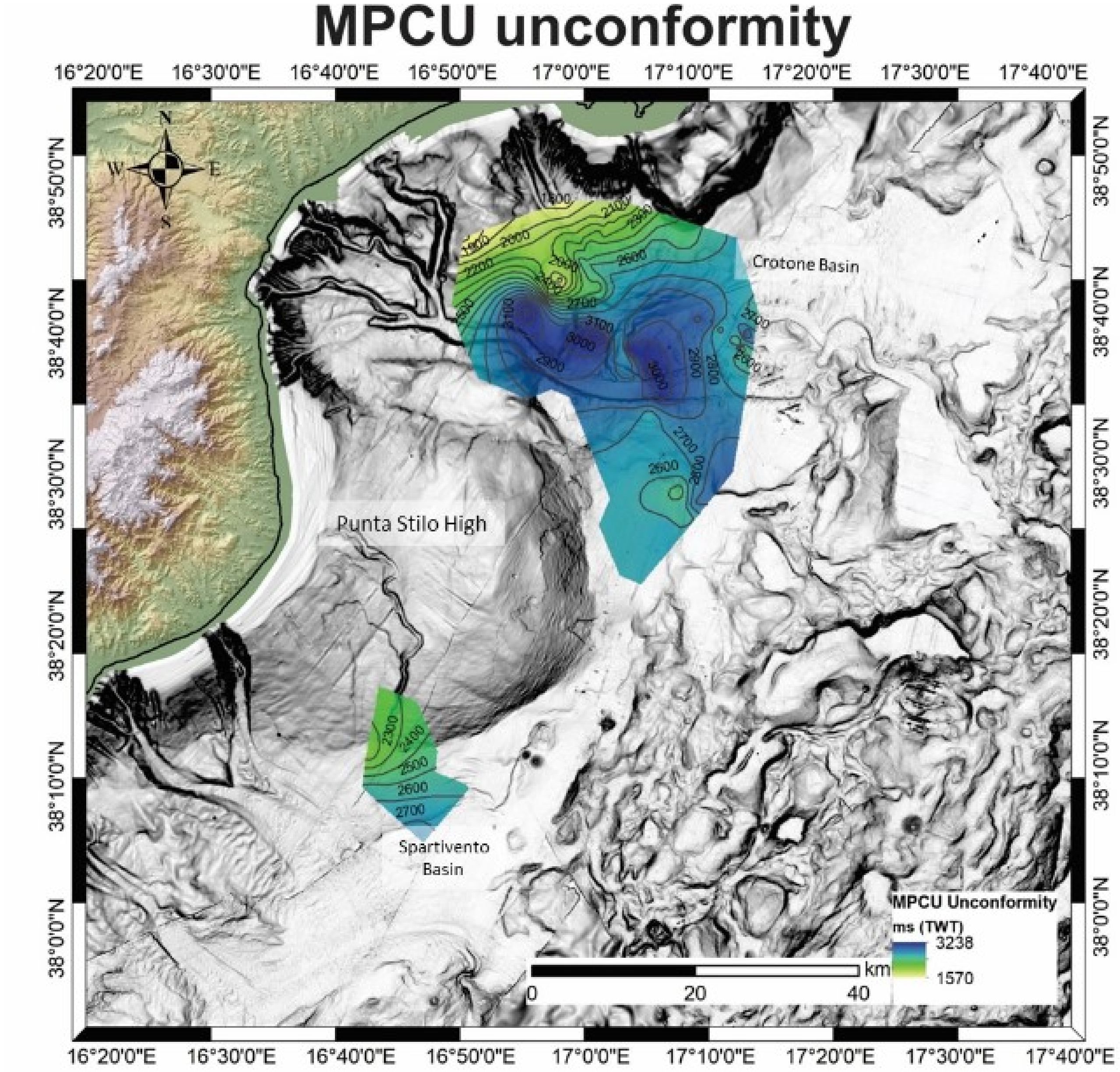

Figure 4-29: computed grid of the depth of the MPCU unconformity. Contour lines represents isochrons every 100 ms (TWT). Yellow areas are shallower zones that become deeper to the dark blue color.

MPSU: is characterized by a medium to high amplitude and medium frequency concordant reflector, that extends from the shallow area on top of the Punta Stilo high to the deeper basins of the Crotone and Spartivento. As for the MU unconformity it is shallower on the Punta Stilo high (Figure 4-25 and Figure 4-30) where it is a concordant reflector and deepens towards the forearc basin floor in the Crotone offshore basin and in the Spartivento basin (Figure 4-30). On the Punta Stilo high, it is 0.4 s TWT deep while it deepens up to 3.1 s TWT in the Crotone and Spartivento basins (Figure 4-30). Correlation with previous studies on the Crotone-Spartivento basin (Praeg et al., 2009; Zecchin et al., 2015, 2012) suggests that this unconformity is of Middle-Pleistocene in age, at ca. 1.2-1.1 Ma.

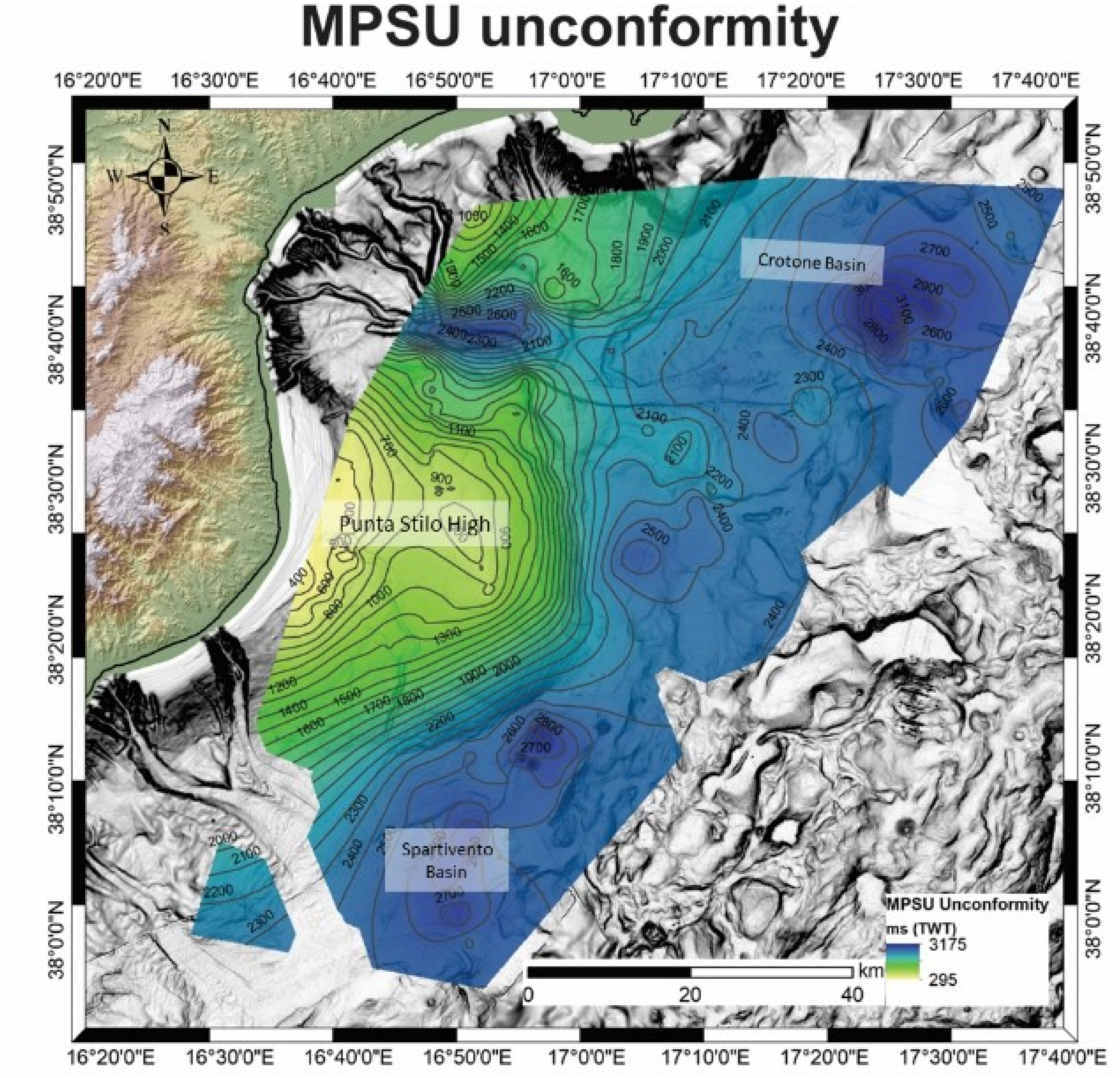

Figure 4-30: computed grid of the MPSU unconformity. Contour lines represents isochrons every 100 ms (TWT). Yellow areas are shallower zones that become deeper to the dark blue color.

U: is characterized by a strong erosional truncation of the top lapping underlying reflectors (Figure 4-31), that in some portions is interrupted by low reflectivity zones, that masks its presence and makes difficult to trace its prosecution along the SBP profiles. Grid map of the U unconformity shows that this unconformity is present across most of the continental shelf, ranging in depth between 0.058 s to 0.4321 s TWT (Figure 4-32), shallower in the inner part of the continental shelf and deepening moving seaward. The unconformity appears to terminate near the shelf break, except on the Punta Stilo high, where it spans up to the upper continental slope (Figure 4-32). This unconformity has already been recognized in adjacent areas and is inferred to represent the sea level fall related to the LGM (Romagnoli and Gabbianelli, 1990; Zecchin et al., 2011b).

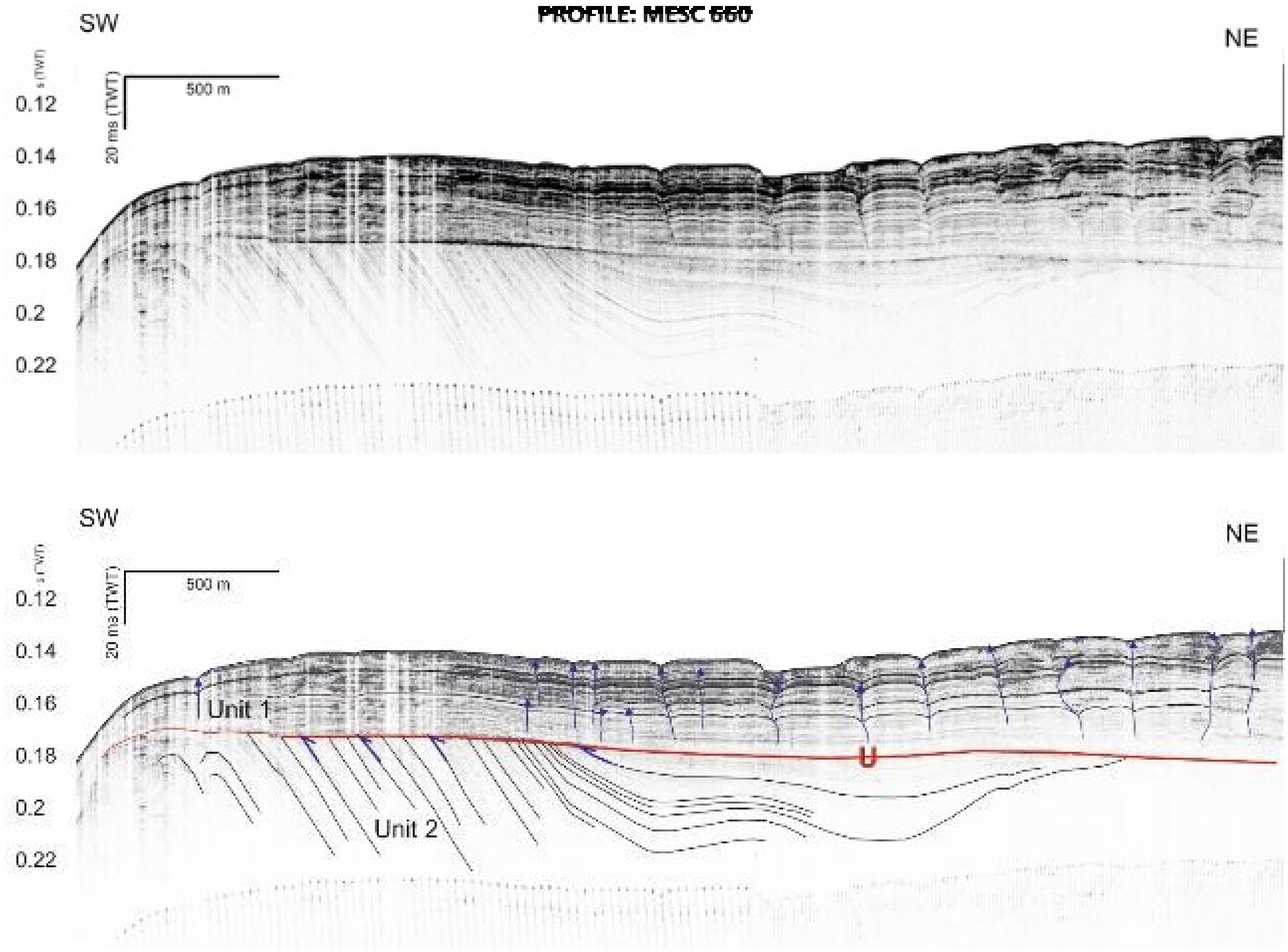

Figure 4-31: uninterpreted and interpreted MAGIC 660 sub-bottom profile showing the U unconformity and the two Units divided by it, Unit 1 on top and Unit 2 above. Note also the occurrence of inferred fluid migration pathways (blue arrows). For the position refer to Figure 4-32.

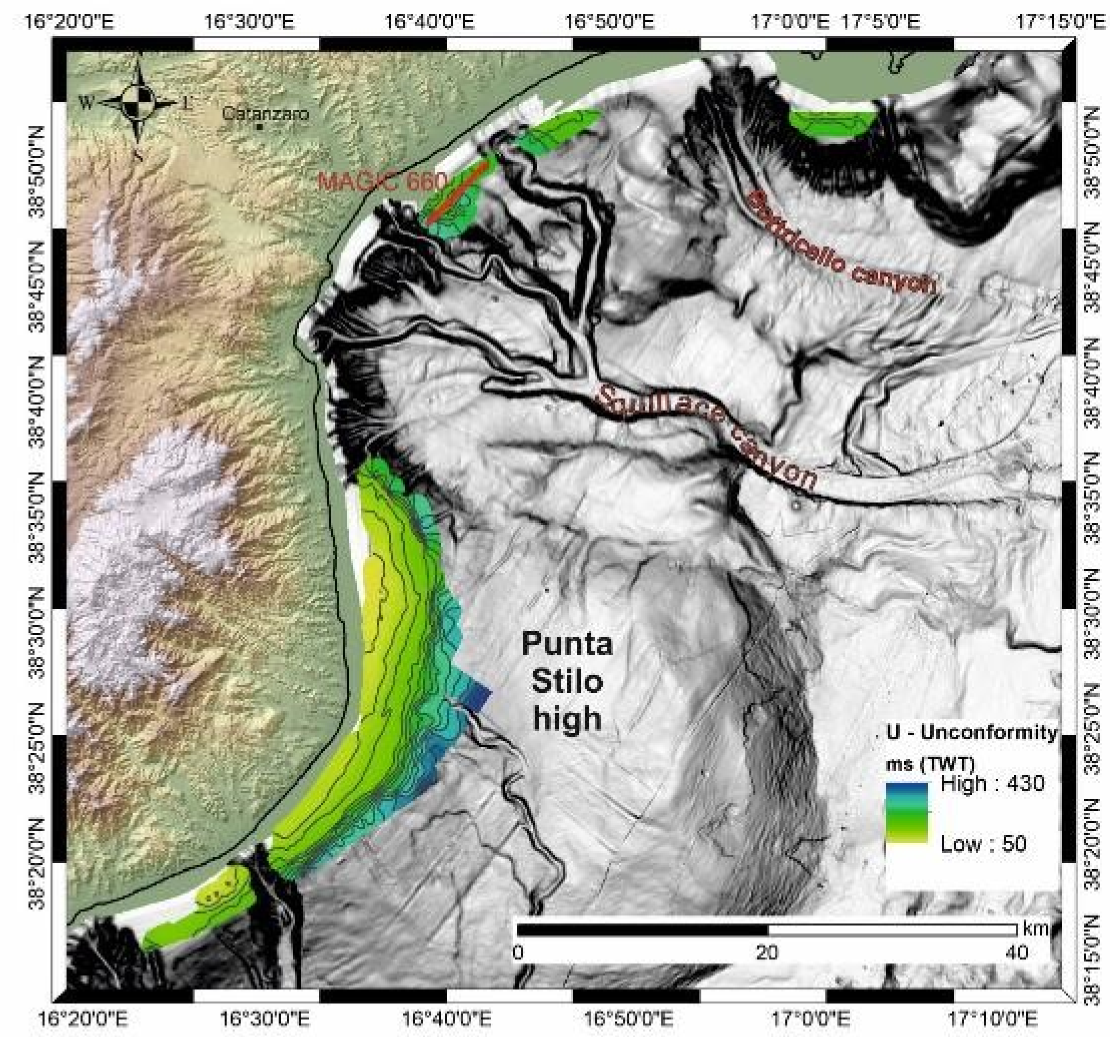

Figure 4-32: image showing the extension of the U unconformity. Note that U unconformity is mostly confined on the continental shelf and is absent within the canyon system. Furthermore, it ceases in correspondence of the shelf brake, except on the Punta Stilo high, where it prosecutes up to the upper continental shelf.

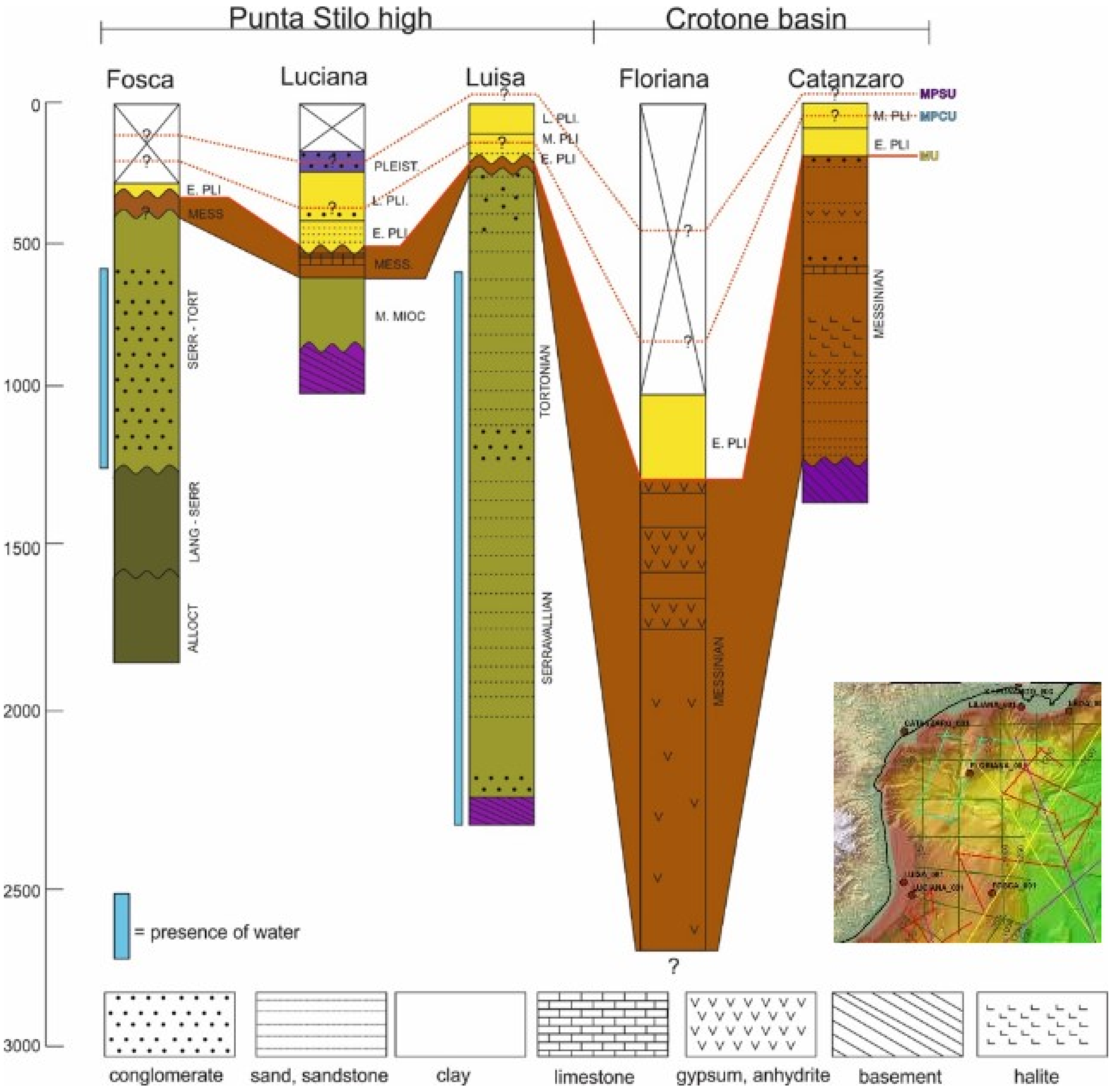

Figure 4-33: interpreted wells used for the correlation with the seismic stratigraphy of the area (see inset for the location of the wells). Figure modified after Capozzi et al., (2012).

4.2.2 Seismic Units

The four unconformities divide the stratigraphic sequence into 6 seismic units, named A, B, C, D, Unit 1 and Unit 2, moving upward with the stratigraphic succession. Units A, B, C, D are mapped on MCS data while Unit 1 and 2 are found on the SBP profiles.

Unit A: is characterized by medium to high amplitude reflectors, with medium to low frequency oblique discontinuous reflectors, sometimes disrupted by stacked sub vertical faults, as in the case of the southern part of the Punta Stilo high (Figure 4-34). In the Crotone basin unit A is more characterized by chaotic facies with some acoustically low reflectivity zones (Figure 4-35 and Figure 4-37). On the Punta Stilo packages of oblique high amplitude chaotic and discontinuous reflectors toplap to the MU unconformity (Figure 4-25). Unit A is bounded on top by the MU unconformity (Figure 4-27) while the bottom surface has not been identified because of the low penetration of the data and in other cases because masked by multiple reflections. For this reason, it was not possible to compute an isopach map. Because the top of this unit corresponds with the MU unconformity, that this unit could be associated to the Messinian deposits. In the Crotone basin they are mostly represented by a thick, more than 1 km, sequence of clays interbedded by thinner layers made of gypsum and anhydrate (Floriana well in Figure 4-33). The Messinian unit is reported to 1355 m b.s.l.f. up to the end of the well, around 2625 m b.s.l.f. Three thin layers of gypsum and anhydrate are reported at the top of the Messinian unit, between 1355 to 1378 m b.s.l.f. (23 m thick), the thicker layer between 1547 to 1717 m b.s.l.f. (170 m thick), and the deepest between 1845 to 1901 m b.s.l.f. (56 m thick).

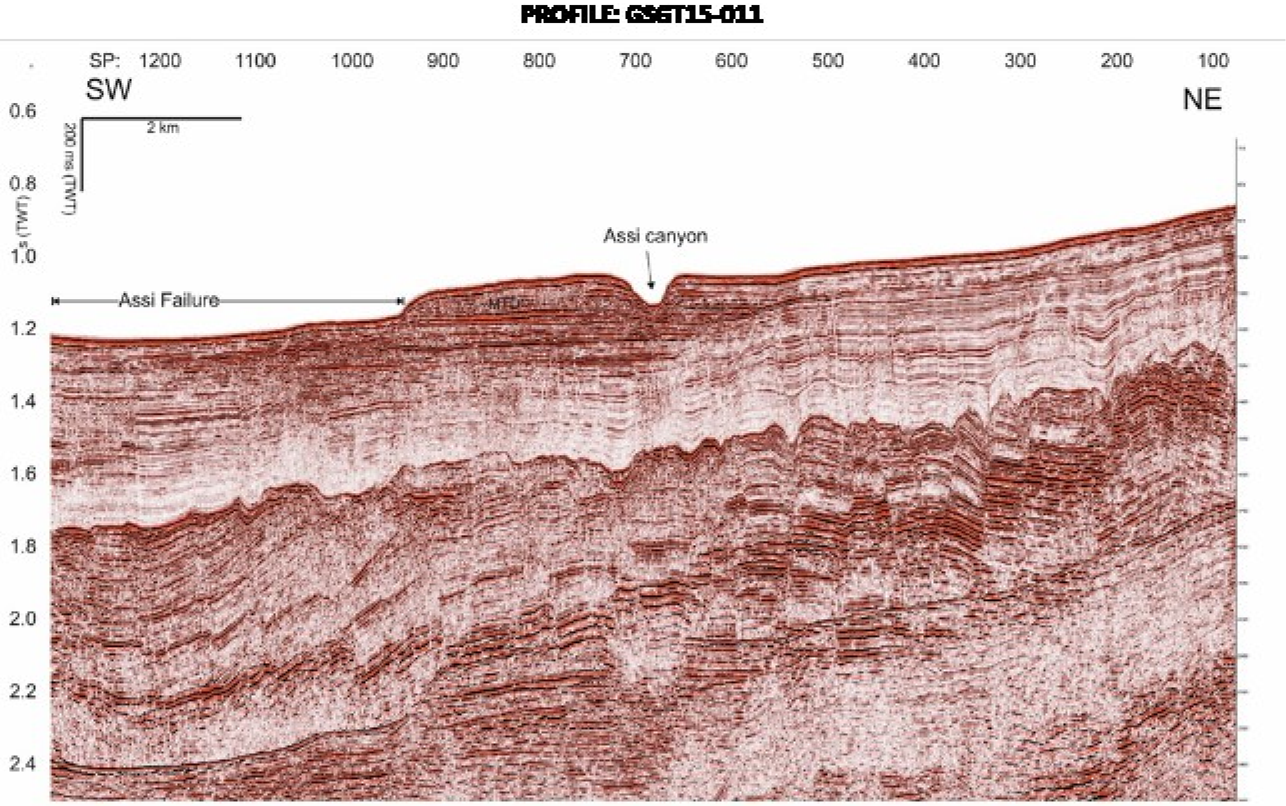

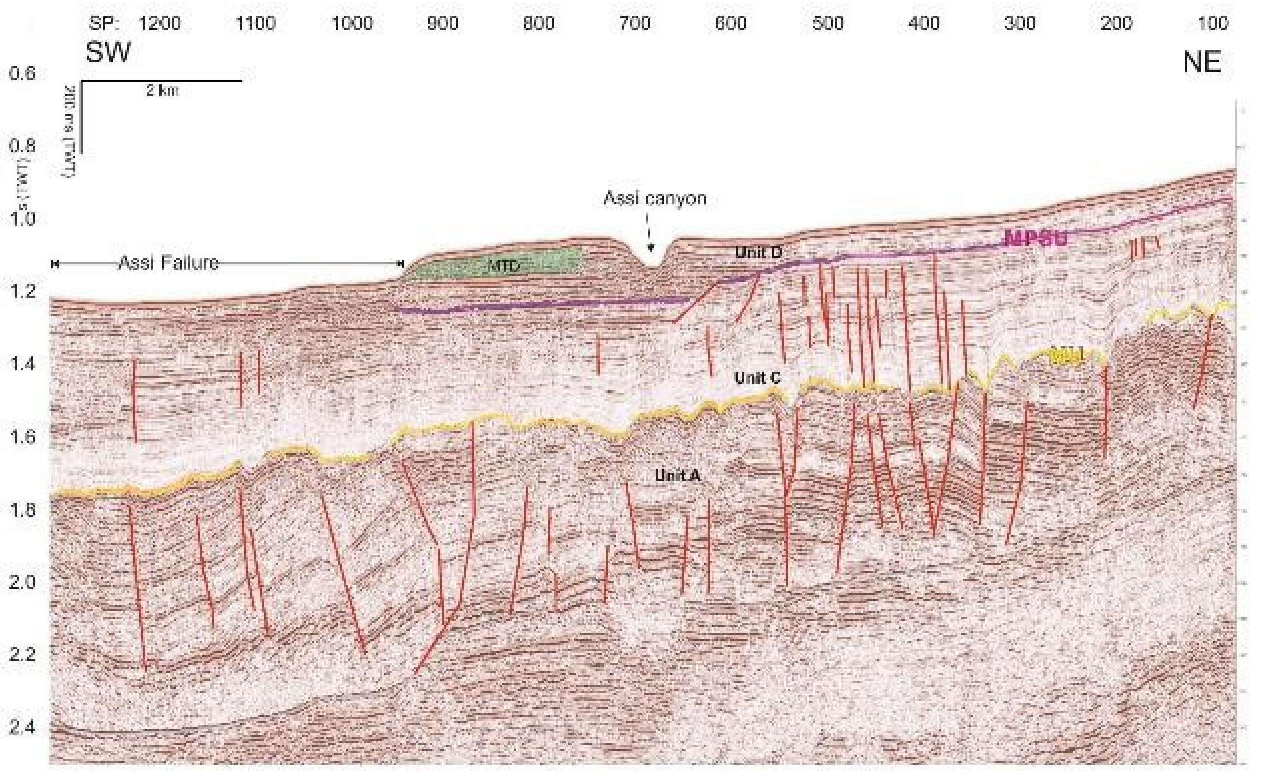

Figure 4-34: seismic profile GSGT15-011. On top the uninterpreted profile on the bottom the interpreted profile with the main unconformities and seismic units (see Figure 4-24 for the location of the profile).

Unit B: this unit is characterized by a layer of low reflectivity, with low amplitude and low frequency discontinuous reflectors, generally dipping seaward (Figure 4-27). The unit is clearly identifiable at the toe of the Crotone Megaslide (Figure 4-27) while moving seaward becomes less recognizable, due to a change of the seismic facies. This unit has been identified only in the Crotone basin and in the Spartivento basin, south of the Punta Stilo high (Figure 4-36). Unit B is bounded at the bottom by the MU unconformity while on top is bounded by the MPCU unconformity (Figure 4-27). Computed isopach map show a variable thickness of the unit, from ca. 50 ms TWT to a maximum of ca. 1s TWT, with a dominant thickness between 100 and 200 ms TWT (Figure 4-36). The maximum thickness occurs at three sub-circular areas, two in the Crotone basin between the Squillace and Bottricello canyon systems, and one in front of the downslope area of the eastern flank of the Punta Stilo high. In the case of the two sub-circular thicker areas in the Crotone basin, correspond to a diapir-like structure (Figure 4-35). Correlation with adjacent well Floriana, suggests that this unit is made up of Early Pliocene clays. (Figure 4-33). Unit B is reported between 2.6 to 2.9 s TWT b.s.l.f., thinning toward the lower slope of the Punta Stilo high and it is characterized by two buried folds decreasing in size moving towards the slope of the Punta Stilo high. In this area, the top of the unconformity is not clearly identifiable, except at the lower slope of the Punta Stilo high, where a weak discordant layer gently dipping seaward is observed (Figure 4-28). The geometry and acoustic character are similar to what has been observed in the Crotone basin. This unconformity has been interpreted to represent the MPCU unconformity. Furthermore, the mean thickness of unit B in this area ranges between 100 to 200 ms TWT, as in the Crotone basin.

PROFILE: GSGT15-001

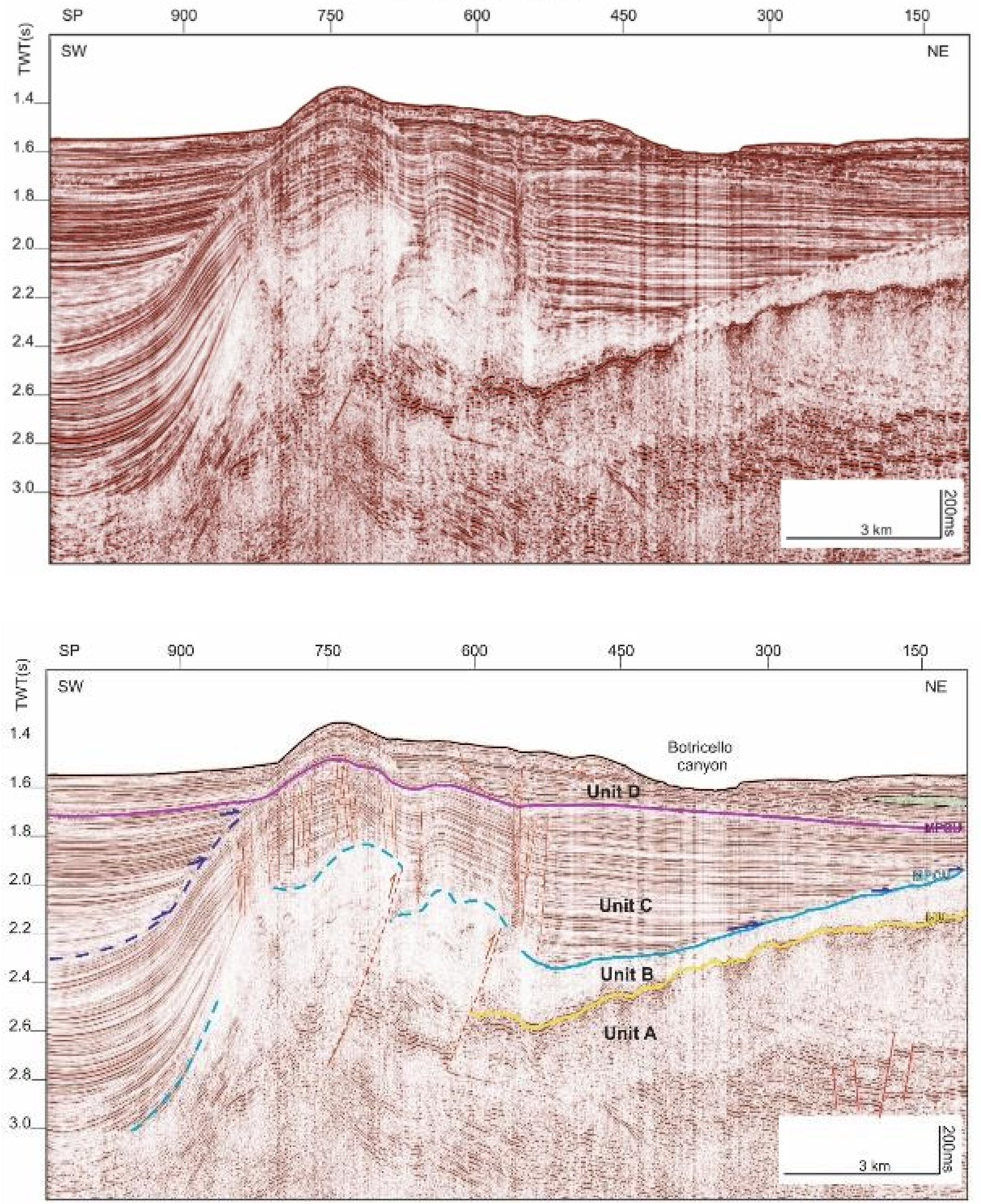

Figure 4-35: seismic profile GSGT15-001. On top the uninterpreted profile on the bottom the interpreted profile with the main unconformities, the seismic units and the diapir-like structure (shot point 650 – 800). See Figure 4-24 for the location of the profile).

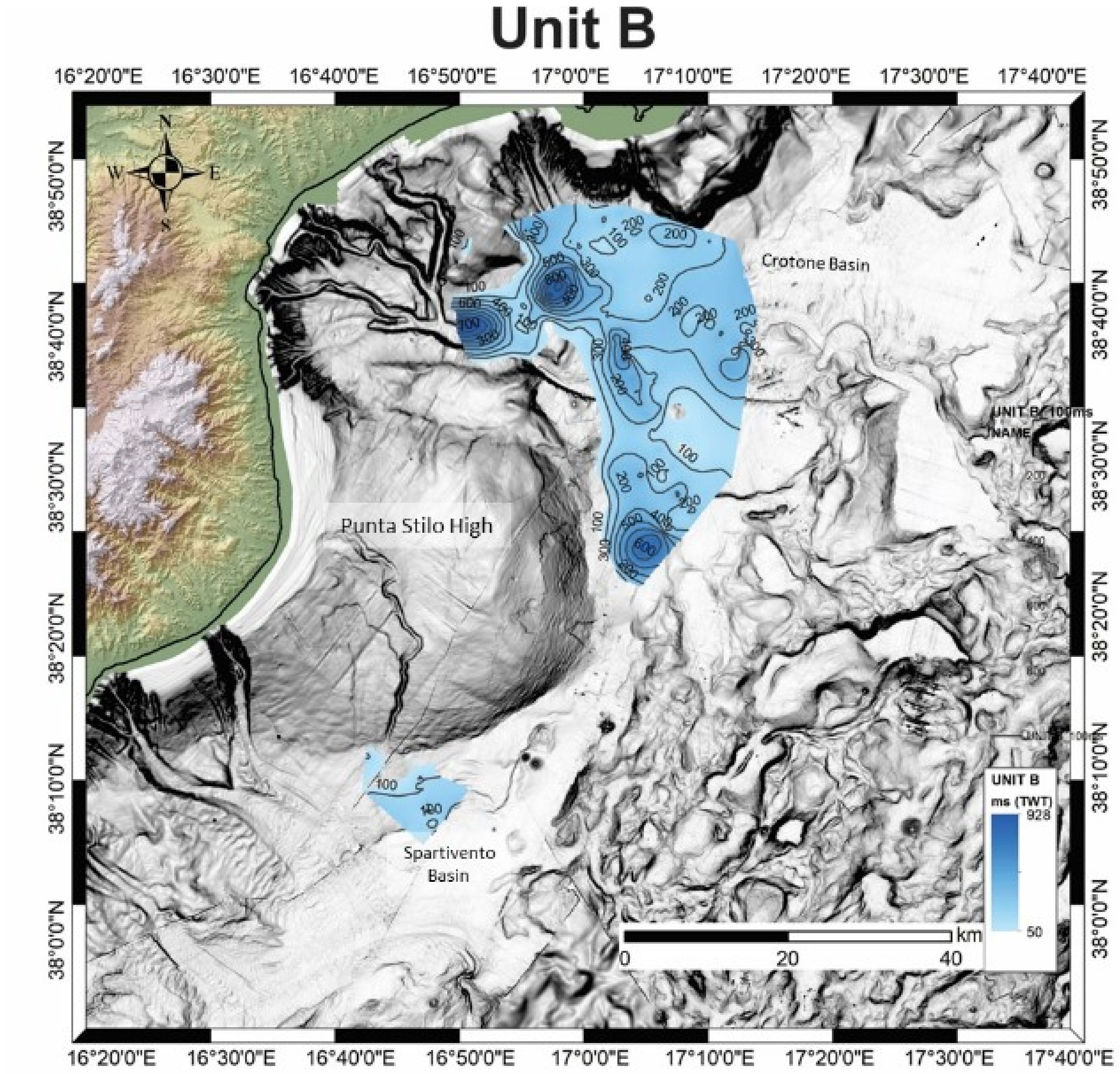

Figure 4-36: thickness map of the seismic Unit B. Darker areas represents thicker areas. Contour lines represent isopacks, every 100 ms (TWT)

Unit C: this seismic unit is characterized by high amplitude, parallel to sub parallel continuous with high to medium frequency reflectors. Unit C is identifiable both in the Crotone and Spartivento basins as well as in the shallower areas of the continental slope and the Punta Stilo high (Figure 4-25, Figure 4-27). Unit C is bounded at the bottom by the MPCU unconformity or, where unit A is absent, by the MU unconformity (Figure 4-37). On top unit C is bounded by the MPSU almost concordant unconformity. Unit C is thicker in the Crotone basin with a maximum of ca. 1.2s TWT and becomes thinner moving upslope and on the Punta Stilo high, where the mean thickness is ca. 500 ms TWT (Figure 4-39). Series of vertical to subvertical faults, in some cases to form conjugate faults are recurrent in this unit: most of the faults seems to terminate upward in proximity of the top of this unit, against the MPSU unconformity (Figure 4-37). On the Punta Stilo High, stacked subvertical faults and acoustic anomalies in form of vertical low frequency and chaotic chimneys suggest the presence of fluid migration pathways (Figure 4-38). On the Punta Stilo high, the Fosca well (Figure

4-33) indicates that unit C is made up of mostly clay layers with the occurrence of intercalated sand and sandstone and conglomerates close to the shelf break (Luciana and Luisa wells in Figure 4-33). Unit C is interpreted to be Lower-Pliocene to Middle Pleistocene in age.

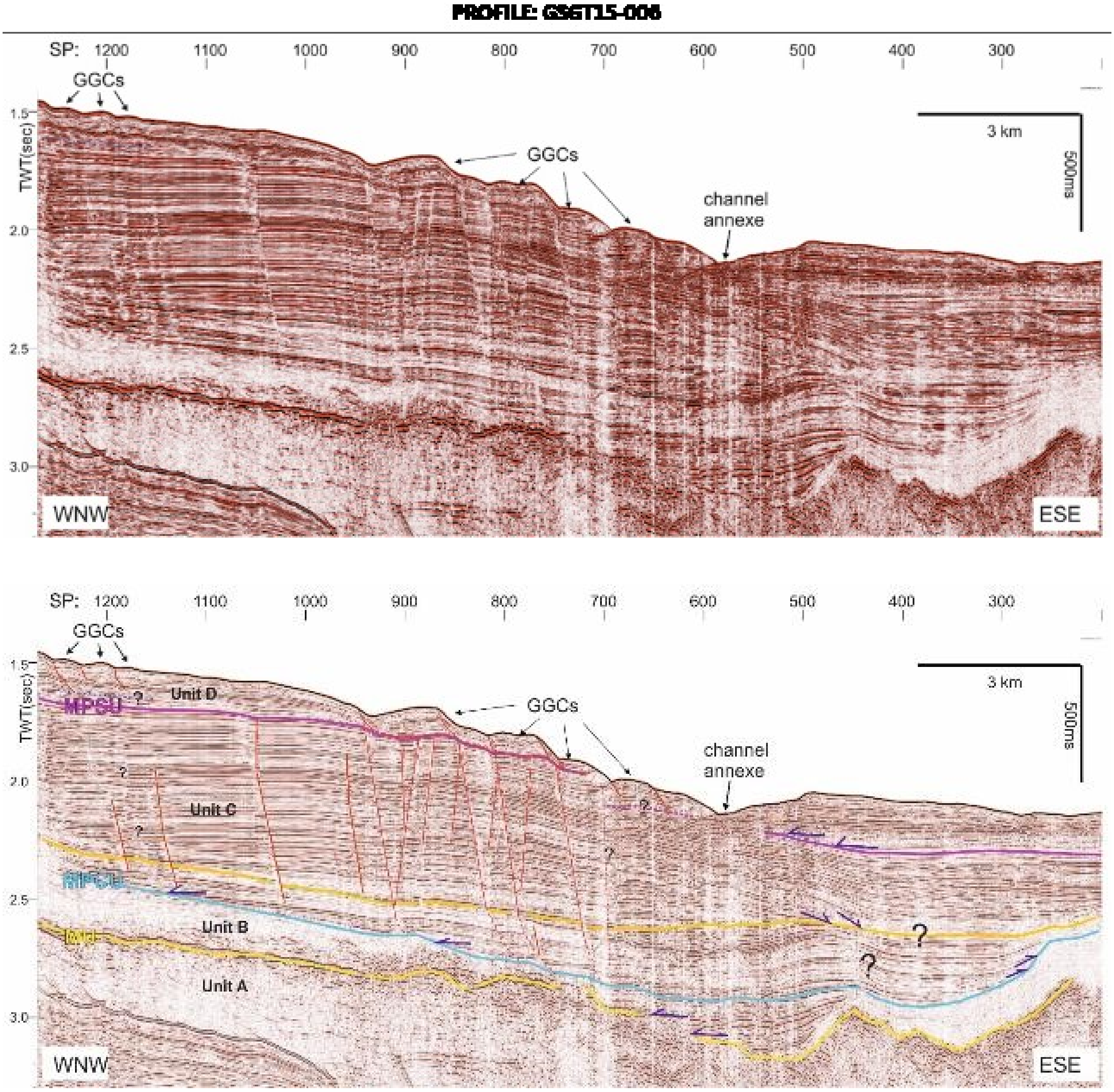

Figure 4-37: seismic profile GSGT15-006. On top the uninterpreted profile on the bottom the interpreted profile with the main unconformities and the seismic units (see Figure 4-24 for the location of the profile).

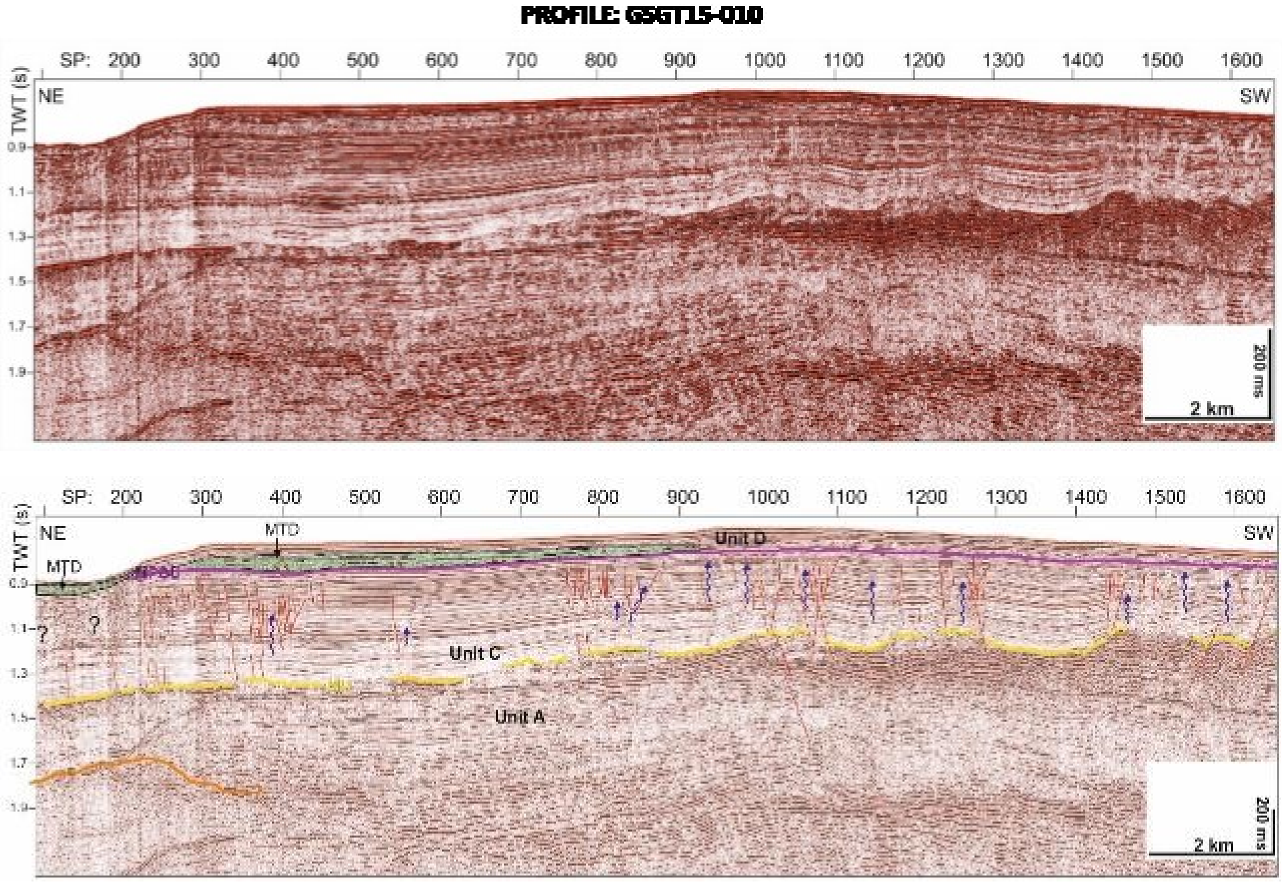

Figure 4-38: seismic profile GSGT15-010. On top the uninterpreted profile on the bottom the interpreted profile with the main unconformities and the seismic units (see Figure 4-24 for the location of the profile). Blue wiggle arrows represent fluid migration pathways

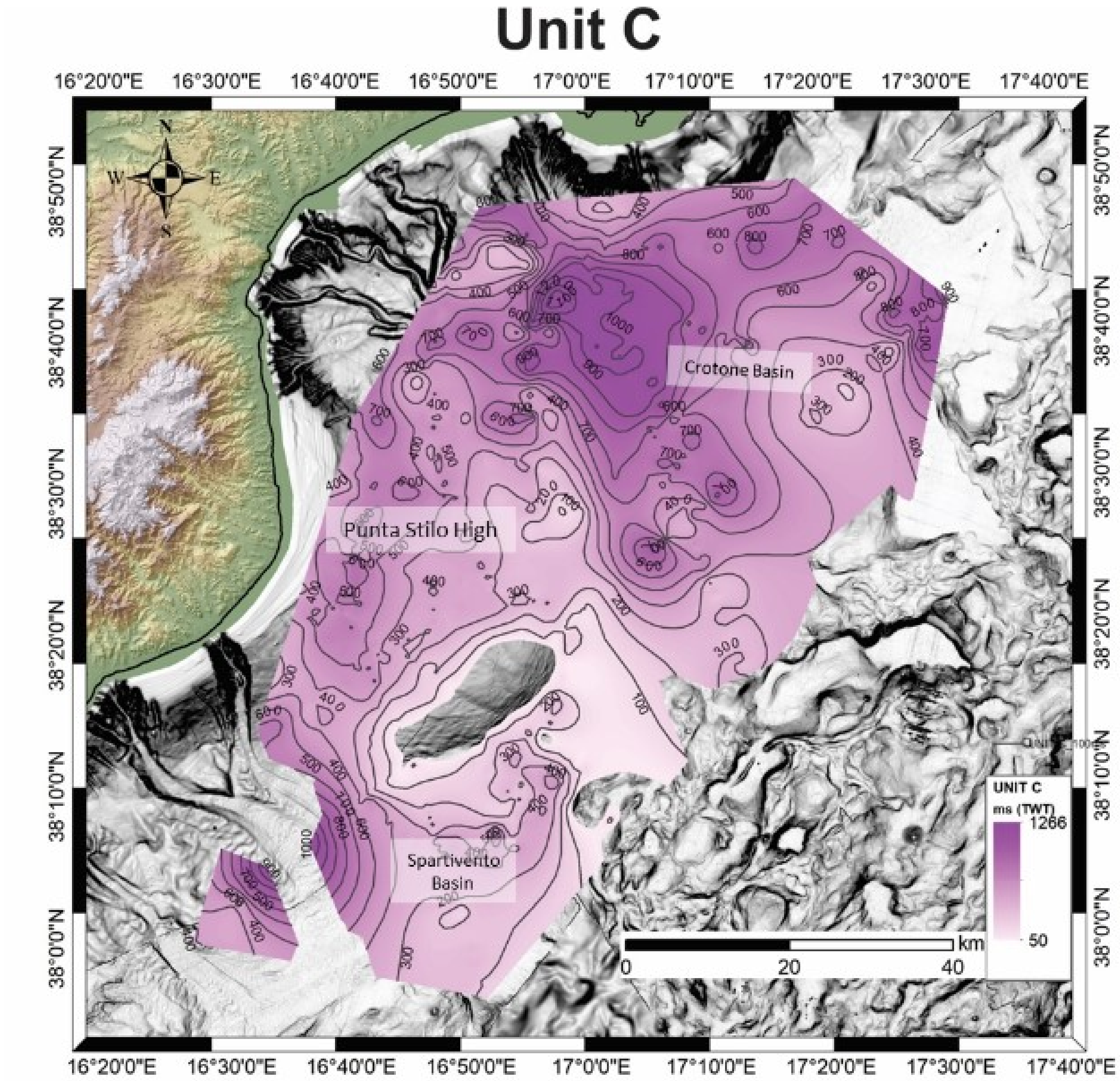

Figure 4-39: thickness map of the seismic Unit C. Darker areas represents thicker areas. Contour lines represent isopacks, every 100 ms (TWT).

Unit D: the unit is characterized by generally discontinuous reflectors with medium to low frequency and medium to high amplitude, with a parallel to subparallel wavy patterns. Unit D is bounded on top by the seafloor and on the bottom by the MPSU unconformity (Figure 4-27 and Figure 4-38). Unit D varies from 50 ms TWT to a maximum of 1 sec TWT in the Crotone basin on Squillace canyon (Figure 4-40). The mean thickness value is between 150-300 ms TWT. In this unit, seismically chaotic bodies have been identified to interrupt seismic reflection packages and interpreted to be MTDs (Figure 4-25 and Figure 4-38). These chaotic bodies have been found at the base and on top of the Punta Stilo high. Unit D is interpreted to be Upper Pleistocene to Holocene in age.

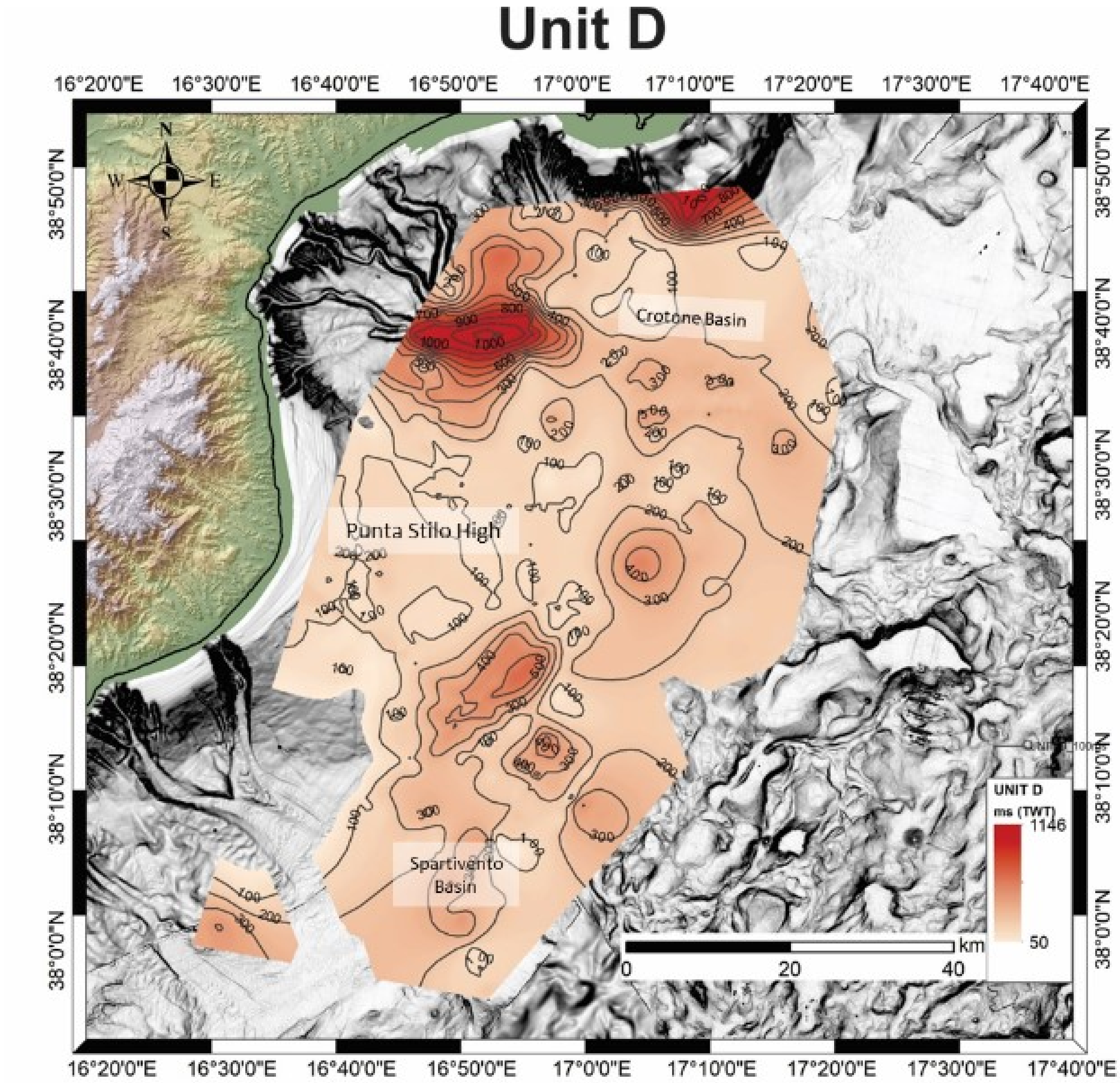

Figure 4-40: thickness map of the seismic Unit D. Contour lines represent isopacks, every 100 ms (TWT).

Unit 2 usually appear as high amplitude continuous package of parallel to sub-parallel reflectors of high amplitude in places folded (Figure 4-41). The unit is bounded on top by the U unconformity while on the bottom no surface has been identified, probably due to the limited penetration of the SBP profiles.

Unit 1 is characterized by horizontal to sub horizontal continuous high amplitude reflectors that onlap or downlap to the U unconformity at low angles (Figure 4-41). Unit 1 is bounded at the base by the U unconformity, on top by the seafloor.

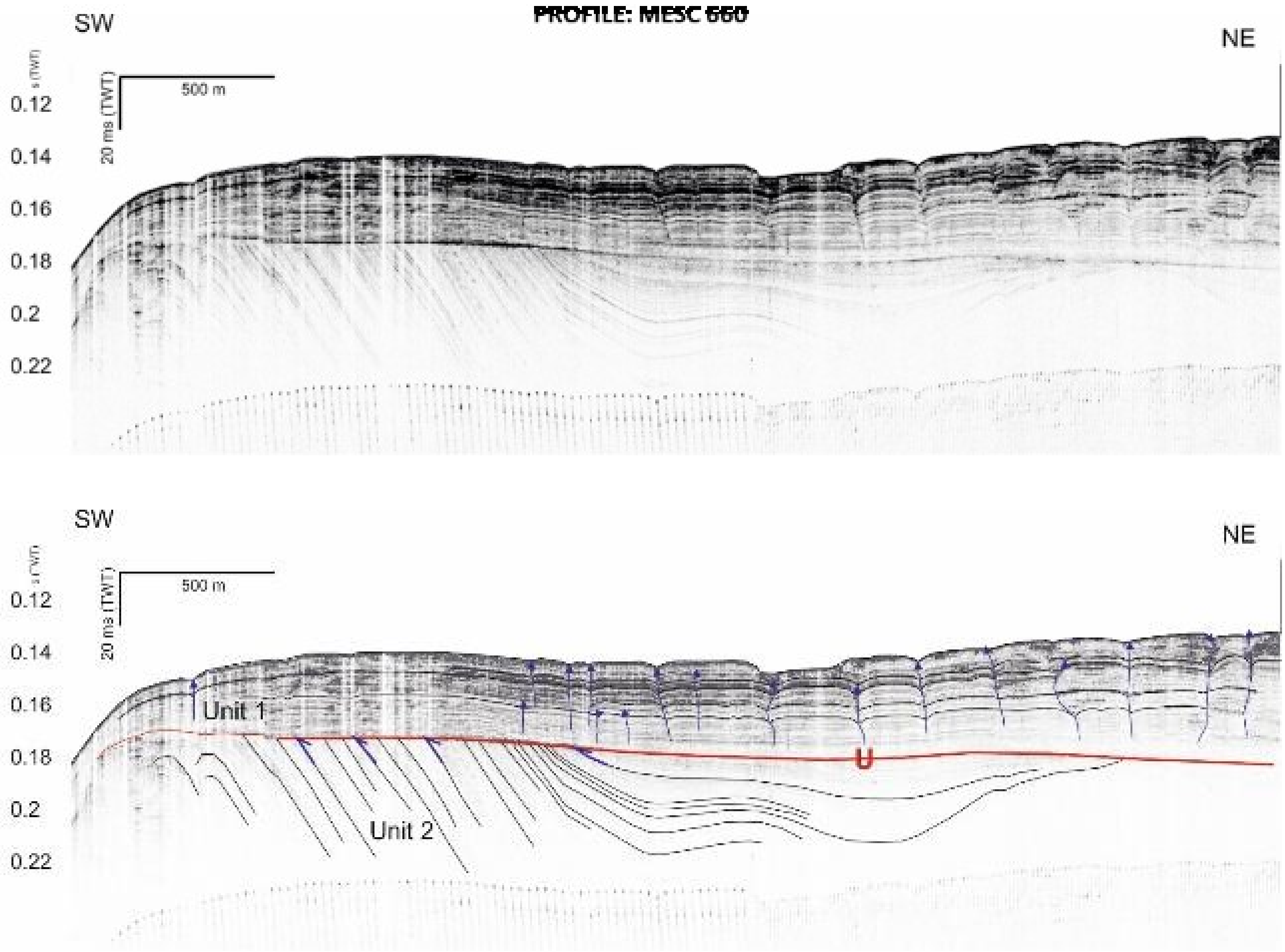

Figure 4-41: uninterpreted and interpreted MAGIC 660 sub-bottom profile showing the U unconformity and the two Units divided by it, Unit 1 on top and Unit 2 above. Note also the occurrence of inferred fluid migration pathways (blue arrows). For the position refer to Figure 4-32.

4.3 Features of mass movements in the Crotone – Spartivento forearc basin

Based on the analysis of multibeam data, sub-bottom profile and seismic data, it was possible to classify three kinds of mass movements in the study area: submarine landslides (SLs), headwall and sidewall scarps within the canyons (HSS) and slope parallel stratified ridges (SPSR).

4.3.1 Submarine landslides (SLs)

SLs affect two main areas: the Punta Stilo open slope and the basin floor. This type of mass movement is characterized by the occurrence of slide scarps, usually in form of single isolated arcuate or more complex slide scarps, and the presence of downslope MTDs (Figure 4-42). In many cases data coverage did not allow an identification of both slide scars and MTDs, so that it was not possible to reconstruct the failure event. Morphometric analysis has been conducted on the scarps and MTDs.

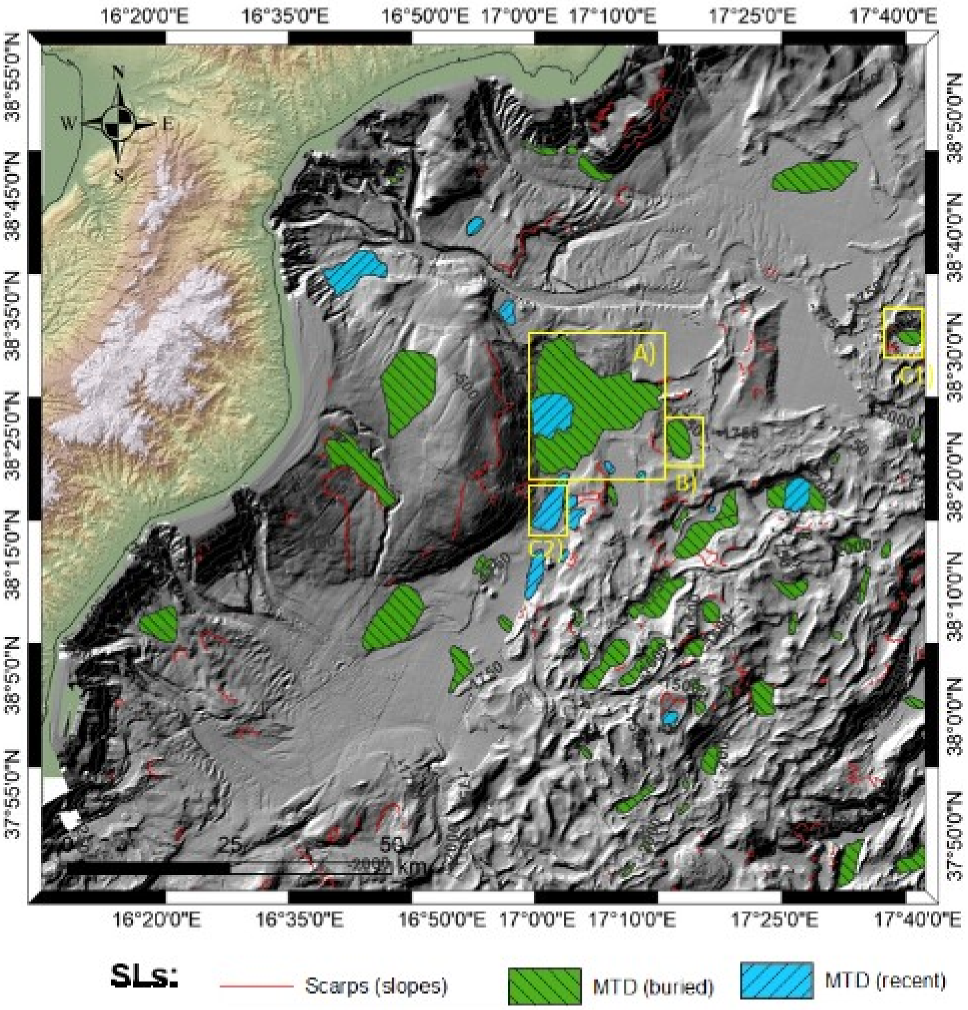

Figure 4-42: hill shade map of the study area showing the slide scarps and MTD characterizing the SLs mass movements. Green areas refer to buried MTDs, while light blue area to recent MTDs. Yellow boxes refer to the location of the MTD described from figure 4.44 to figure 4.47.

SLs scarps (Figure 4-43) appear as a single arcuate or more complex features. Where complexes occur, it is not clear if these scarps can be the considered as a product of several coalescent scarps or as a single scarp.

SLs scarps range from 300 meters to a maximum of 16 km length (Figure 4-44) and have been found in the continental slope with gradients >5°, on the slopes of morphological highs on the forearc basin floor, in the steep slopes that bordered the basins, and in the canyon systems. The two major SLs scarps are found on the flanks of the Punta Stilo high.

Morphometric analysis conducted on MTDs allowed to classify them into 3 categories: A) lens, B) layered, C) mixed MTDs.

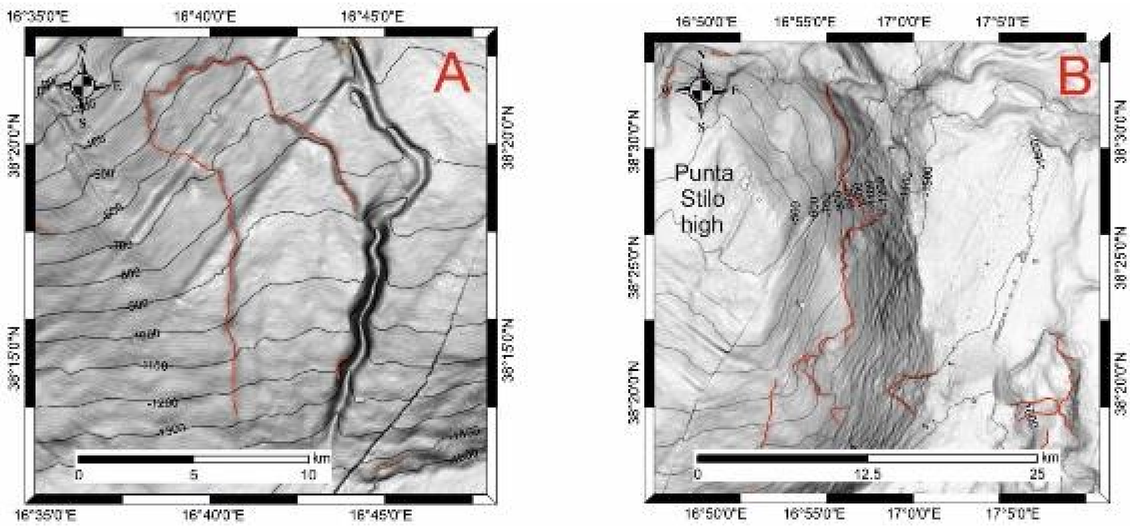

Figure 4-43: image showing examples of the two different slides scarps of the Sls classified according to their shape: A) single isolated slide scarp, B) complex isolated slide scarps.

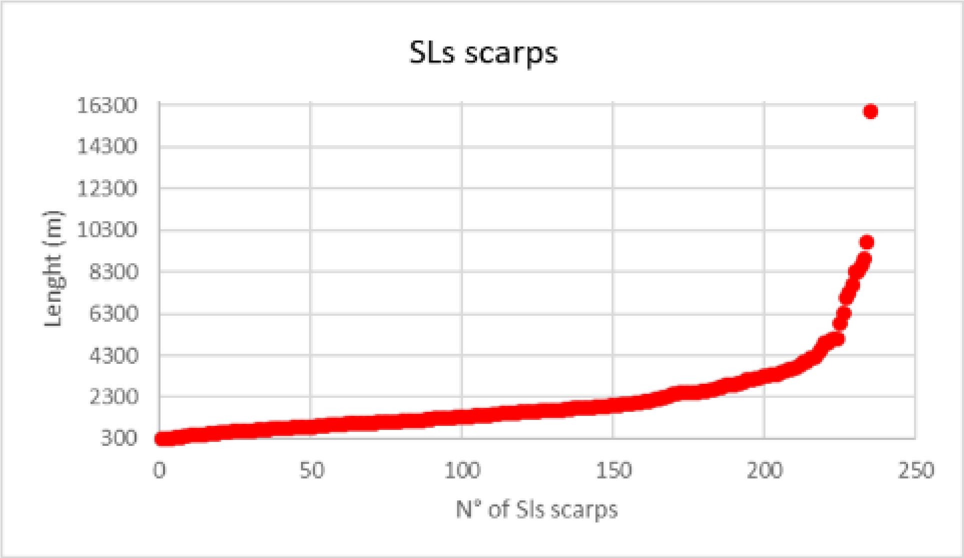

Figure 4-44: table showing SLs scarps length range.

A) **Lens-shaped MTDs** are characterized by an irregular geometry, thinning laterally to pinch out within undisturbed sediments (Figure 4-45). The top boundary is an irregular roughly convex upward continuous surface, if buried sediments are draping on it. The bottom boundary is an irregular surface that usually cuts reflectors below suggesting erosion related to the dynamic failure and energy of the failure event. In some cases, the small depressions and concavities are found, with abrupt steps that cuts and interrupt the reflectors below the bottom boundary (Figure 4-45). This type of MTD has been found at the downslope area on the eastern flanks of the Punta Stilo high.

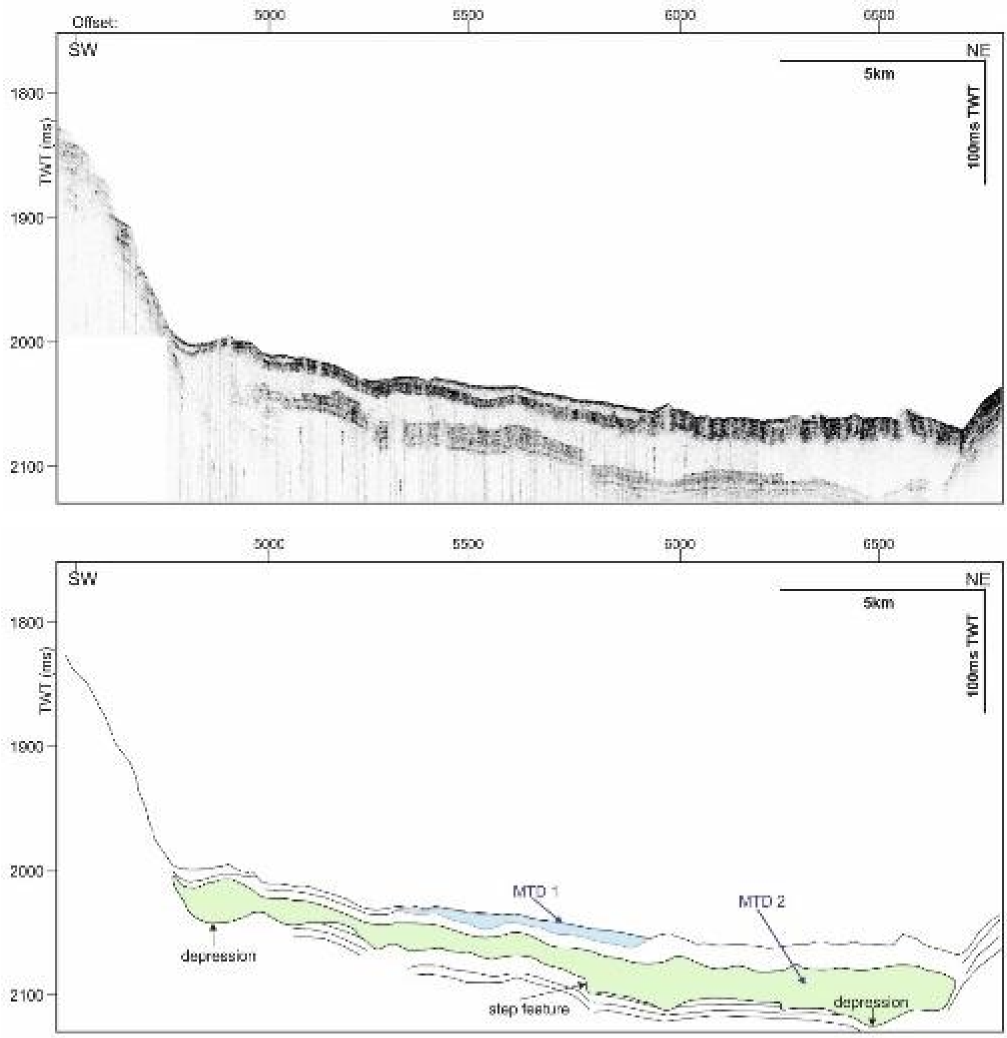

Figure 4-45: interpreted and uninterpreted profile of an irregular MTD at the downslope area of the Punta Stilo high. The recent MTD is smaller in size in respect of the buried MTD (see red box A in Figure 4-42 for the location of the MTDs).

B) **Tabular MTDs** are characterized by acoustically transparent bodies, with no appreciable lateral variations in thickness (Figure 4-46). The bottom and top boundaries are usually flat, parallel to sub parallel surfaces, mostly concordant with the reflector pattern under the bottom surface and above the top surface. For the bottom boundary this characteristic can be associated to absence of erosion, suggesting “low energy” deposits. These bodies seem to occupy all the available space, terminating against lateral inclined slope surfaces. Tabular MTDs are common in the basins that characterize the corrugated area.

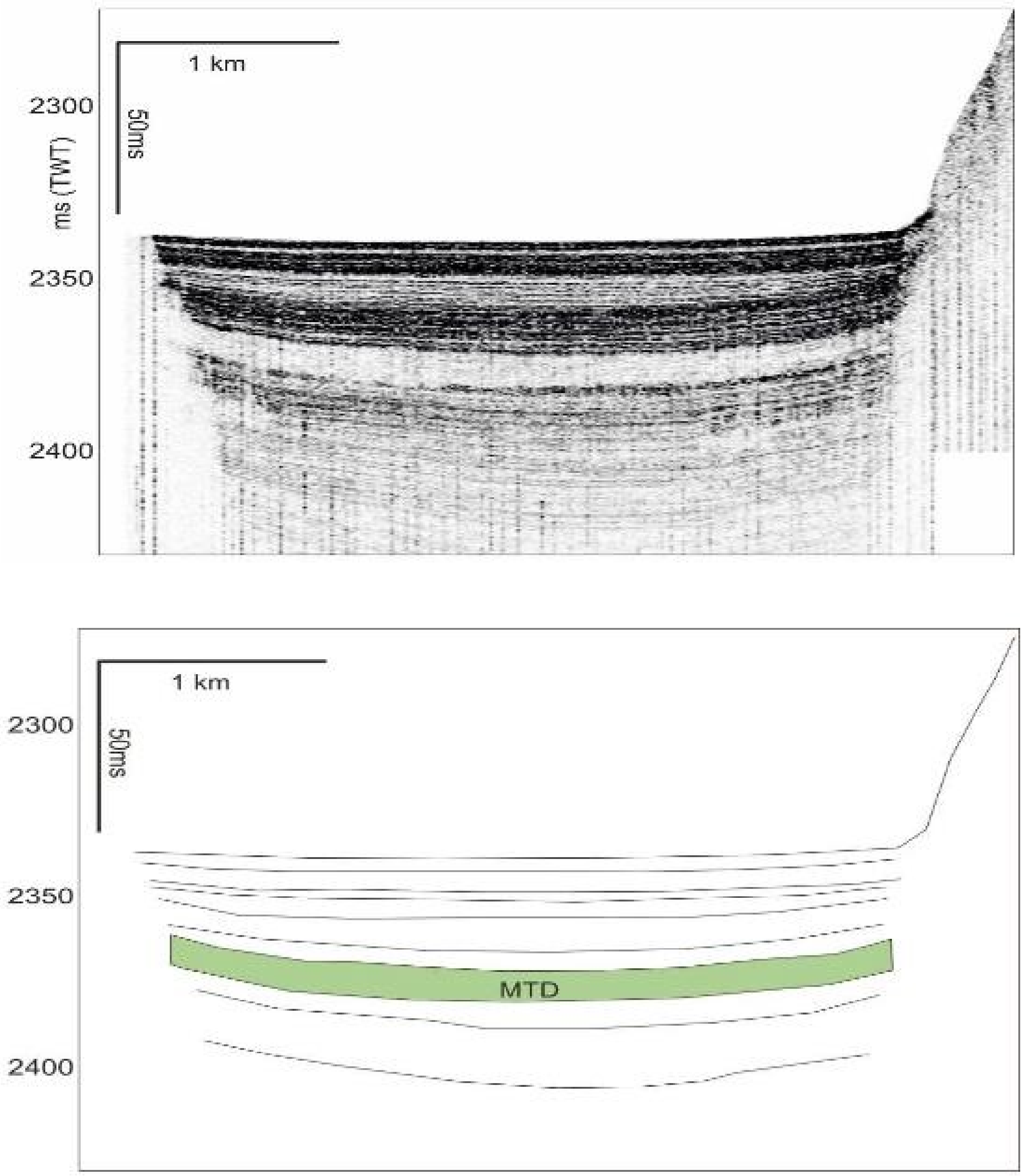

Figure 4-46:interpreted and uninterpreted tabular MTDs (see red box B in Figure 4-42 for the location of the MTDs)

C) **Mixed MTDs** are represented by acoustically transparent deposits where it is possible to recognize a weak internal reflector that separates MTDs (Figure 4-47), or where there is no clear reflector but the geometry suggests a distinction between layered and lens-shaped MTDs (Figure 4-47 and Figure 4-48). These Mixed MTDs might record events that occurred in a relatively short period of time. This type of MTDs are mostly found in the basins in the corrugated area.

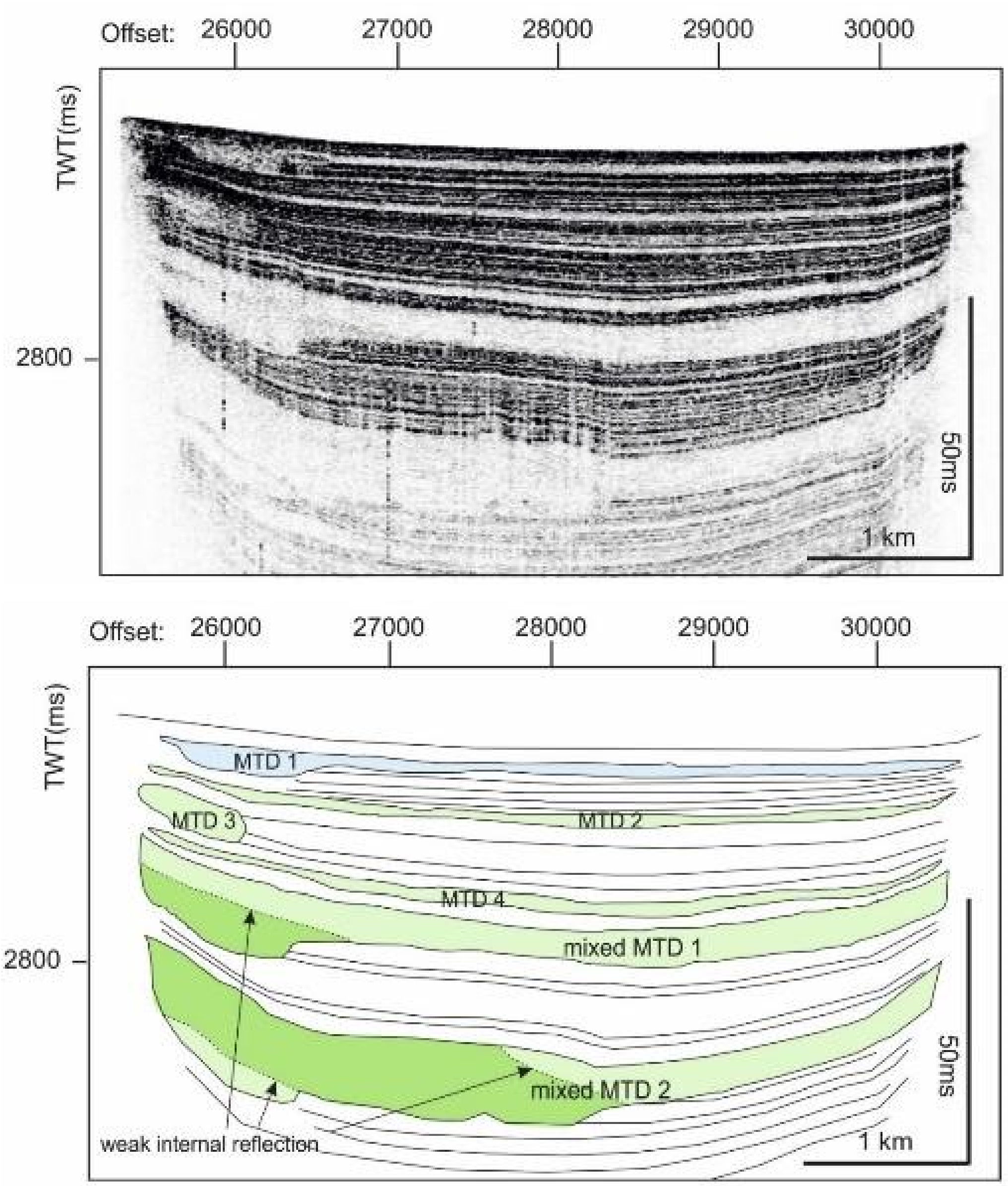

Figure 4-47: uninterpreted and interpreted tabular MTDs where internal reflection suggests multiple MTDs (see red box C1 in Figure 4-42 for the location of the MTDs).

The mapped MTDs have areas ranging from 1 to 100 km^2 (Figure 4-49). Most MTDs have been found to occur at the downslope areas of the forearc basin floor, where the wider MTDs have been identified: on the downslope flanks of the Punta Stilo high they have areas of 55 km^2 up to 240 km^2. In the corrugated domain, most of the small basins and depression are characterized by the occurrence of MTDs. A few examples are also present on the continental slope, where MTDs occur in areas of gentler gradients (3°) around the Squillace canyon system (Figure 4-42). Other MTDs are identified on top of the Punta Stilo high (Figure 4-42) and between the Caulonia Siderno and Bovalino La Verde canyon systems.

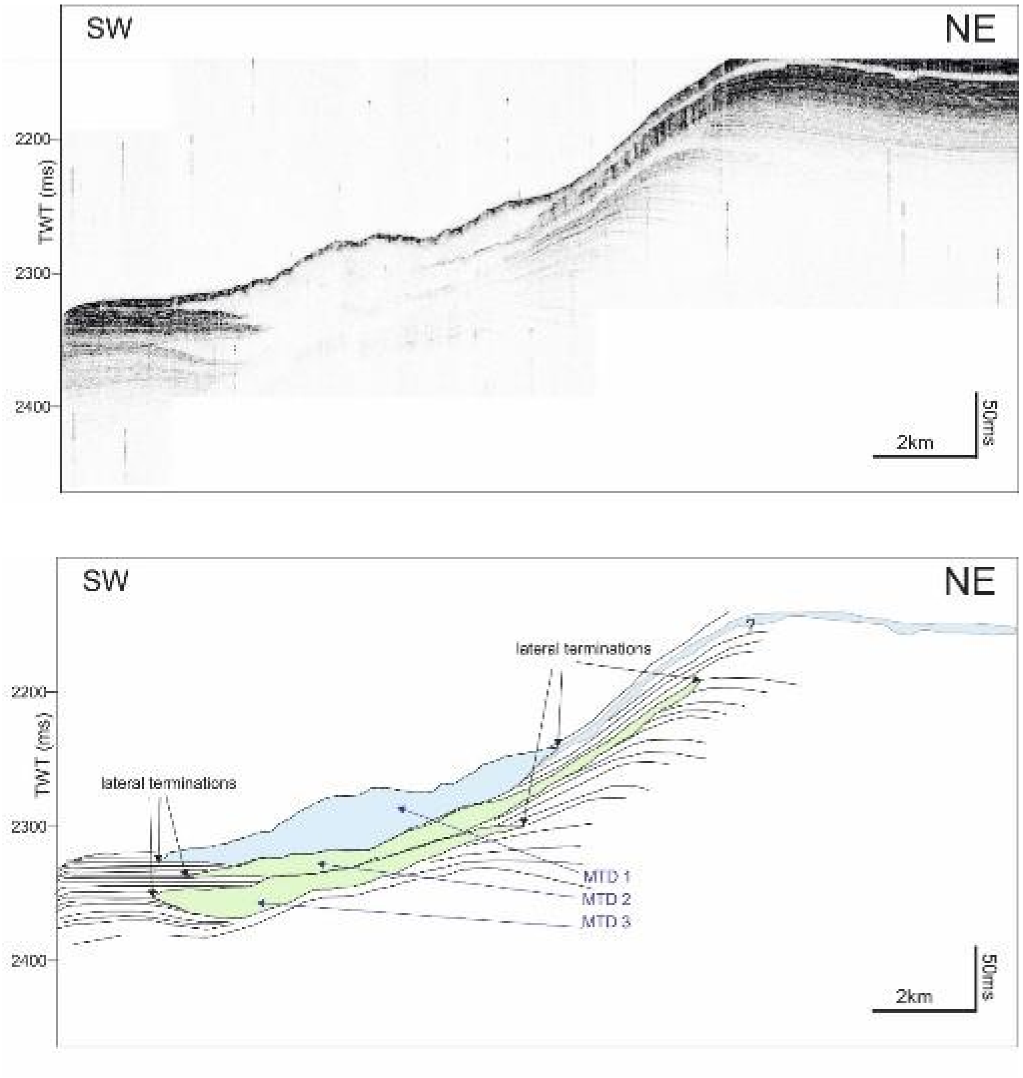

Figure 4-48: uninterpreted and interpreted mixed MTDs, closely stacked where the top and bottom surfaces of each acoustically transparent body are difficult to identify (see red box C2 in Figure 4-42for the location of the MTDs).

In addition to the spatial distribution of the MTDs, a temporal distribution is recorded by stacked MTDs that vary from 2 to a maximum of 4 stacked events, in some cases identifiable as individual acoustically transparent bodies separated by bedded reflectors (Figure 4-47), in other cases superimposed with top and bottom layers that may be difficult to identify (Figure 4-48). Stacked MTDs generally show that buried MTDs are of greater area, from 10^7 to 10^9 m^3 whereas recent MTDs are smaller, indicating a reduced magnitude of failure events over time (Figure 4-51). Where multichannel seismic data are available, MTDs are found to occur mostly in seismic unit D, above the MPSU unconformity (Figure 4-25, Figure 4-34, Figure 4-38).

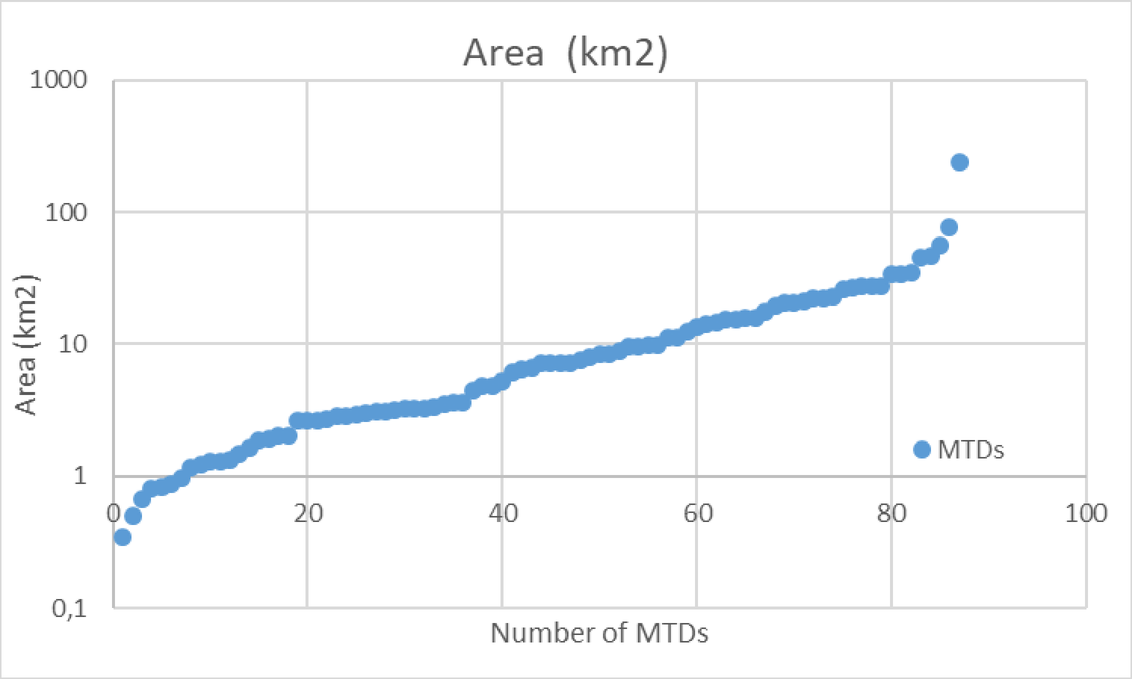

Figure 4-49: graph showing the area of the MTDs identified in the study area. Most MTDs detected have areas of tens of square km2 (area is expressed as a logarithmic scale)

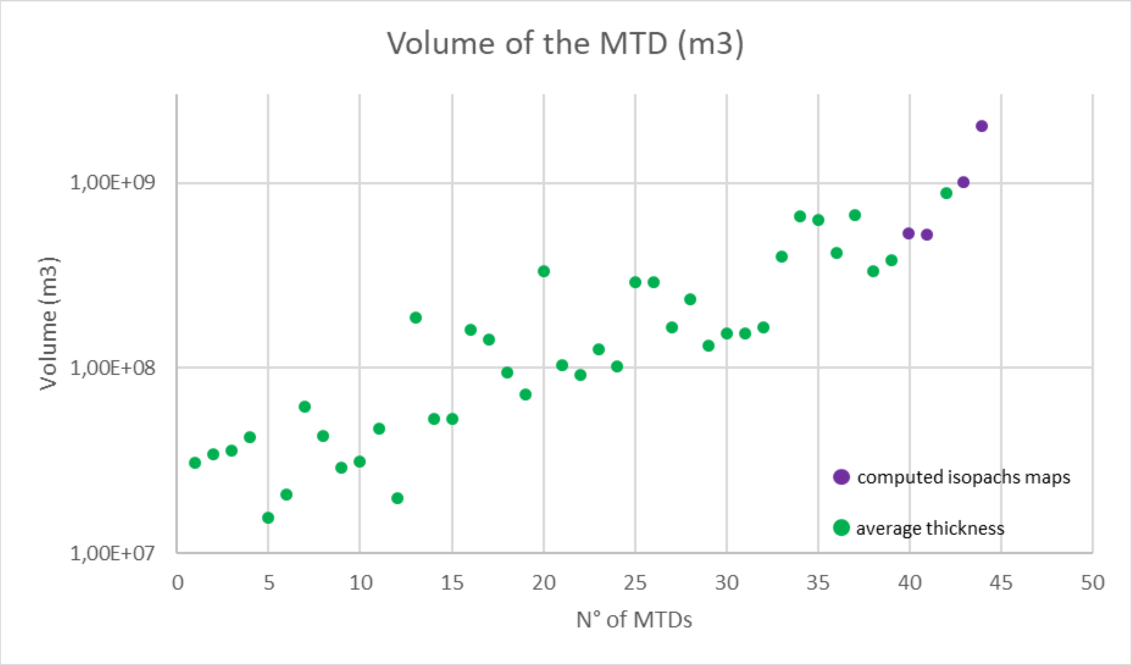

Figure 4-50 graph showing the estimated volume of the MTDs detected in the study area. Green dots refer to volumes calculated using the area and the mean thickness, purple dots volumes calculated interpolating top and bottom surfaces

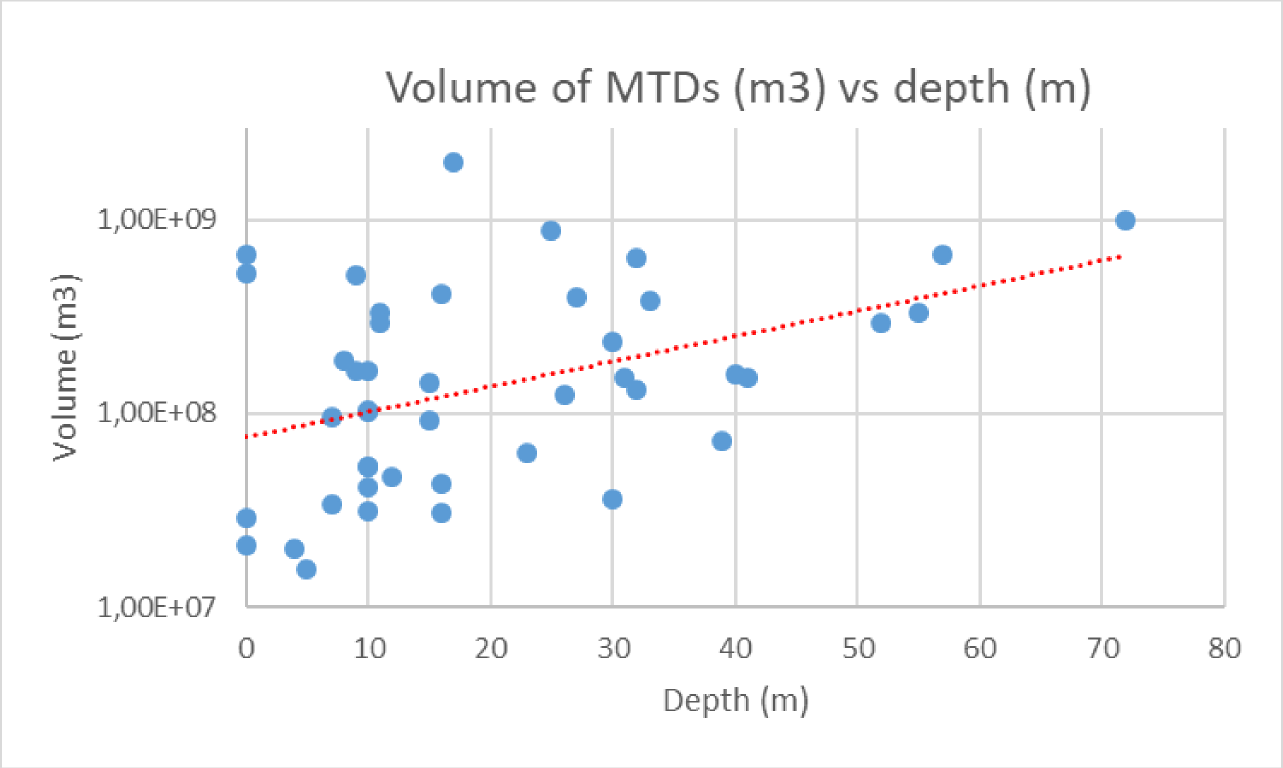

Figure 4-51:graph showing the relation between the MTDs and their depth below the seafloor. As depth increases, the size of the MTDs increases as well, as shown by the red trend line.

MTDs recognized on multichannel seismic data exhibit features of internal configuration, continuity, external geometry and amplitude strength. Compared to sub-bottom profiles, multichannel seismic reflection data provide more information about the MTD, because some internal reflection are present, in respect to sub-bottom profiles, that in the presence of MTD return acoustic transparent or fuzzy to hyperbolic facies.

MTDs exhibit geometries similar to those observed on sub-bottom profiles, varying from lens-shaped to tabular. In some cases, it is possible to recognize typical structures related to the deformation of the MTD. Thrust and folds are found in the toe zone of the MTD, like for example the MTD that lies at the base of the eastern flank of the Punta Stilo high (Figure 4-53), while normal and listric faults are found at the head domain of the MTD (Figure 4-53), for example at deeper MTD at downslope area of the Assi failure (Figure 4-55H). In other cases, discontinuous parallel to sub parallel with low amplitude reflectors are reported (Figure 4-54).

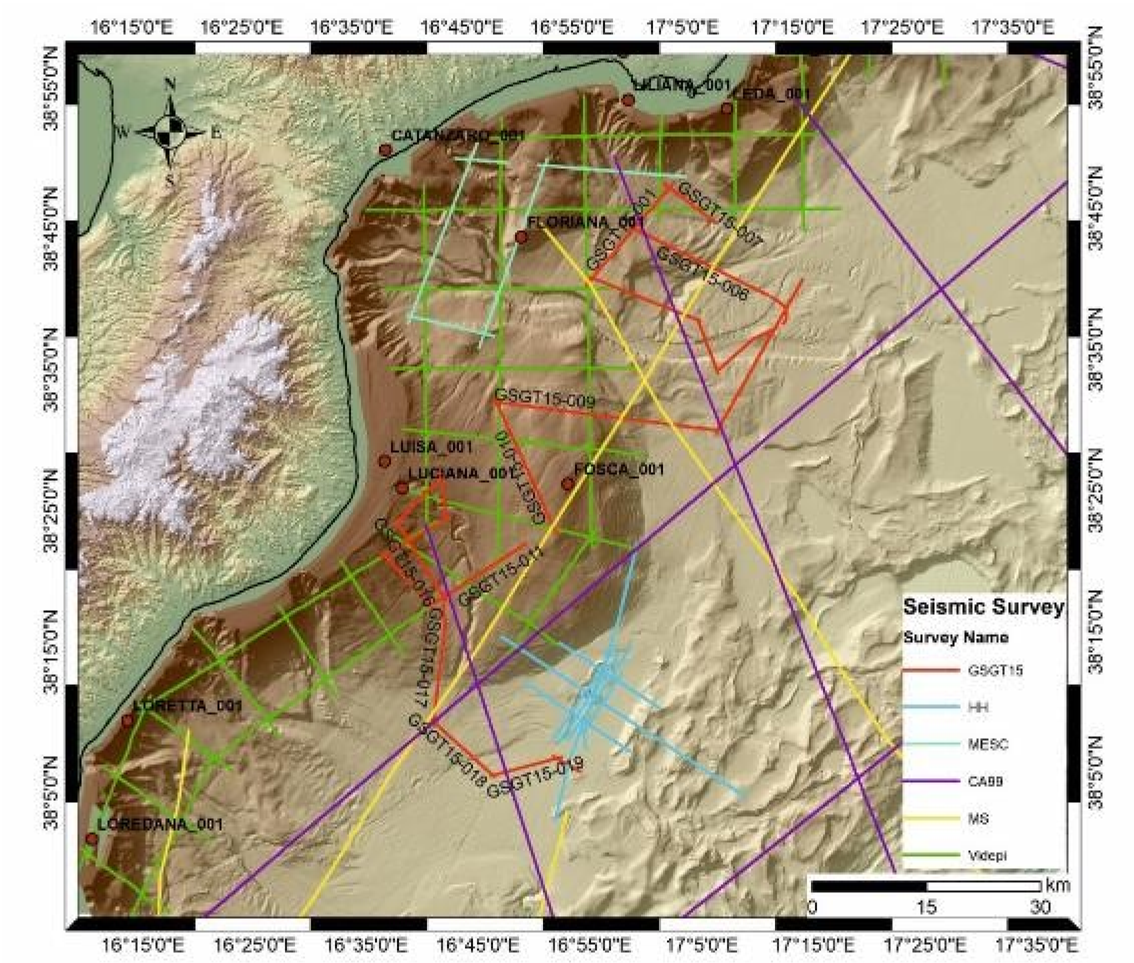

Figure 4-52: bathymetric map with the seismic dataset for the location reference of the profiles and the available wells

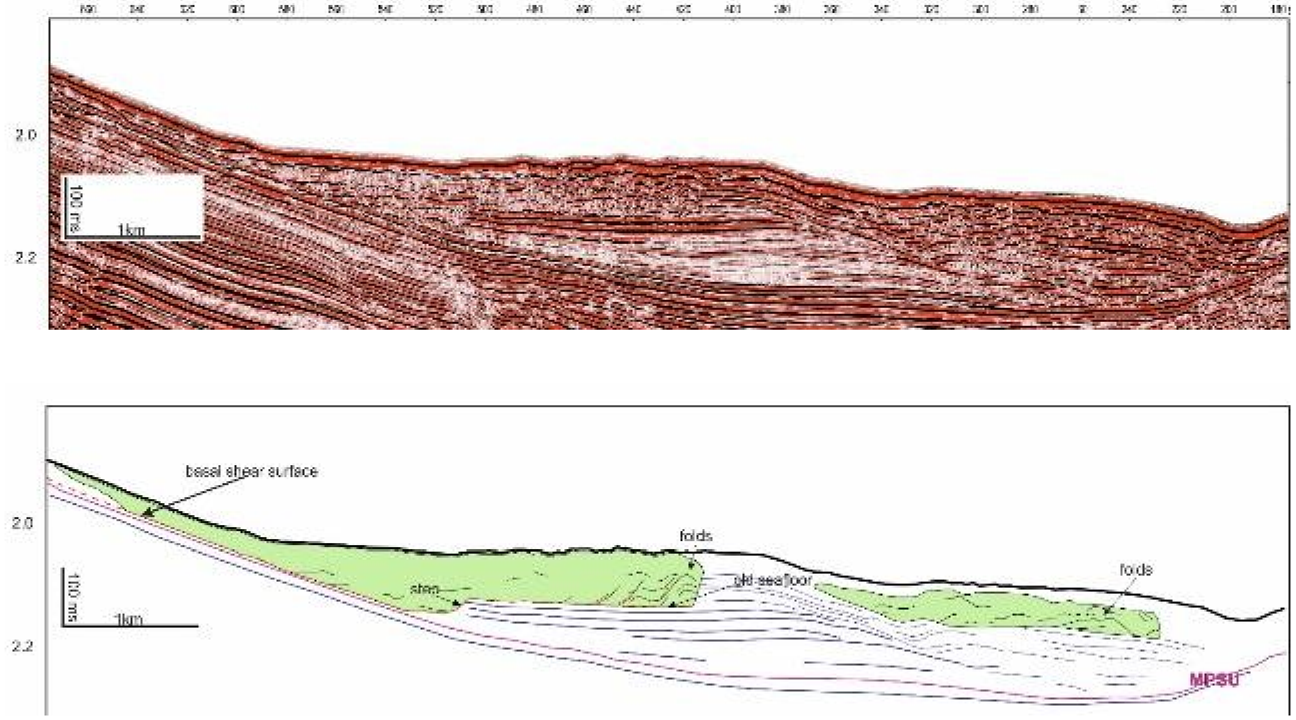

Figure 4-53: irregular MTDs (zoomed part of the GSGT15_009 profile in Figure 4-52, from SP 100 to 600).

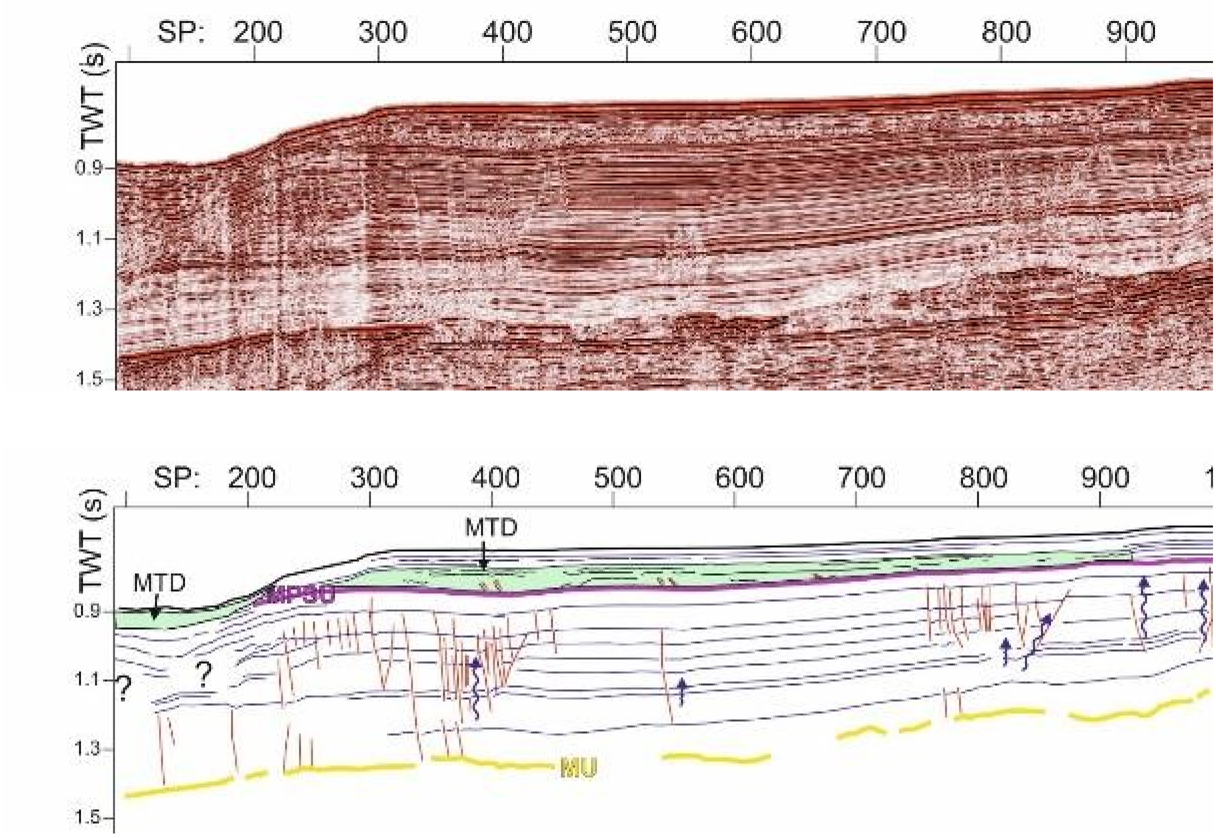

Figure 4-54: (zoomed part of the GSGT15_010 profile in Figure 4-52, from SP 200 to 900). Blue wiggle arrows indicate fluid migration pathways

For the Sls, thanks to the GSGT15 survey campaign, that acquired *ad hoc* data to investigate the mass movements, it was possible to investigate two submarine landslides, the Assi failure and the newly named Punta Stilo failure.

Assi failure

The Assi failure lies 8 km offshore from the Calabrian coast on slopes > 5°. The headwall scarps are found between 250-500 m b.s.l. with an arcuate elongate slide scar 50 m high, 6 km wide with sidewall scarps reaching the base of slope at ca. 1500 m b.s.l., 16 km long, with another scarp visible on the backward area respect to the headwall scarp (Figure 4-55A). In particular, the eastern lateral scarp of the Assi failure at ca. 850 m b.s.l.is interrupted by the Assi canyon (Figure 4-55A). Sub bottom data (Figure 4-55B) and a profile on the bathymetric map (Figure 4-55C) that cross transversally the slide, show two clear abrupt steps on the bathymetric map. On the eastern side, out of the slide area, it is possible to identify a MTD visible on seismic profiles GSGT15-11 (Figure 4-55E). Seismic profiles GSGT15-11 and GSGT15-16_18 show a continuous high amplitude reflector that is lying ca. 40 milliseconds (TWT) below the actual seafloor on the translational domain (the yellow dotted line in Figure 4-55E, Figure 4-55F and Figure 4-55G). This reflector extends from the translational domain up to the back-area respect to the headwall scarp. On the upper translational domain, a slide block is present, evidenced in the bathymetric data as an elongated body 25 m high, and 500 m wide and 1.2 km long. On the translational domain, a chaotic lens shape body is present (Figure 4-55E and Figure 4-55F). Moving at the base of the slope, three stacked MTDs have been found, with different geometries and internal configuration, numbered starting from the shallower to the deeper. MTD 1. MTD 2, MTD 3 (Figure 4-55E and Figure 4-55H). MTD 1 and MTD 2 appear as respectively elongated lens and layered shaped bodies, with MTD 2 also affected by series of faults. Finally, MTD 3 shows some internal reflection. For MTD 1, it was possible to interpolate an area across the profiles and calculate an area of 55 km^2 with an estimated volume of ca. 1 km^3. The volume estimation was made using an interval velocity of 1500 m/s. In seismic data, some acoustic anomalies in form of vertical seismic wipeouts are observed below the upper translational domain, that affect Unit C (Figure 4-55F and Figure 4-55G). MTD 1 and MTD 2 are separated by a thin package of reflectors.

Punta Stilo failure

The Punta Stilo slide lies 30 km offshore the Calabrian coast on the eastern flank of the Punta Stilo high. The headwall scarp extends with an irregular shape parallel to the slope for ca. 16 km, with an average height of 50 m in water depths between 850-1000 m b.s.l. (Figure 4-56A). The headwall scarp is identifiable as an abrupt step on the bathymetric profile (Figure 4-56B). Sub-bottom and multichannel seismic reflection profiles show a clear truncation of reflectors in correspondence of the headwall scarp (Figure 4-56C, Figure 4-56F, and Figure 4-56G): in sub-bottom profile M112-1 (Figure 4-56C) the scarp marks the transition from the bedded undisturbed echo-type above the scarp to the hyperbolic echofacies downslope in the translational domain (Figure 4-56C). In seismic profile GSGT15-009, a clear truncation of reflectors is visible in correspondence of the headwall scarp (Figure 4-56F). The absence of any draping sedimentation on the headwall scarp suggest two possibilities: that the headwall scarp is relatively recent or low sedimentation rate occurred after the slope failure. Under the slide scarp, around ca. 1.3 s TWT, a high amplitude reflector could correspond to a basal shear surface (Figure 4-56F and Figure 4-56G) on which the failure took place.

Smaller and deeper (below 1000 m b.s.f.) slide scars (tens of meters wide and less than 5 km long) are also reported on the same slope, probably related to successive events (Figure 4-56A). At the base of the slope, two MTDs have been identified and numbered progressively from the shallower to deeper. MTD 1 with an area of ca. 31 km^2, with no evidence of drape sedimentation above it. MTD 2 is also visible on the sub-bottom profile (Figure 4-56E). MTD 2 has a ca. 240 km^2 extension and lies at the base of the eastern flank of the Punta Stilo high. For this case, it was possible to map the bottom and top surfaces of the MTD and to estimate a volume of ca. 4 km^3. The isochron map of the MTD 2 shows a thicker area at the center of the MTD that becomes thinner moving towards the limits of the MTD. The maximum thickness calculated is ca. 50 ms TWT (Figure 4-56H); within the MTD presence of thrusts or fold like structures is deforming the toe of the MTD 2 reflectors

(Figure 4-56E). Both the two MTD occur within the seismic unit D, above the MPSU unconformity (Figure 4-56).

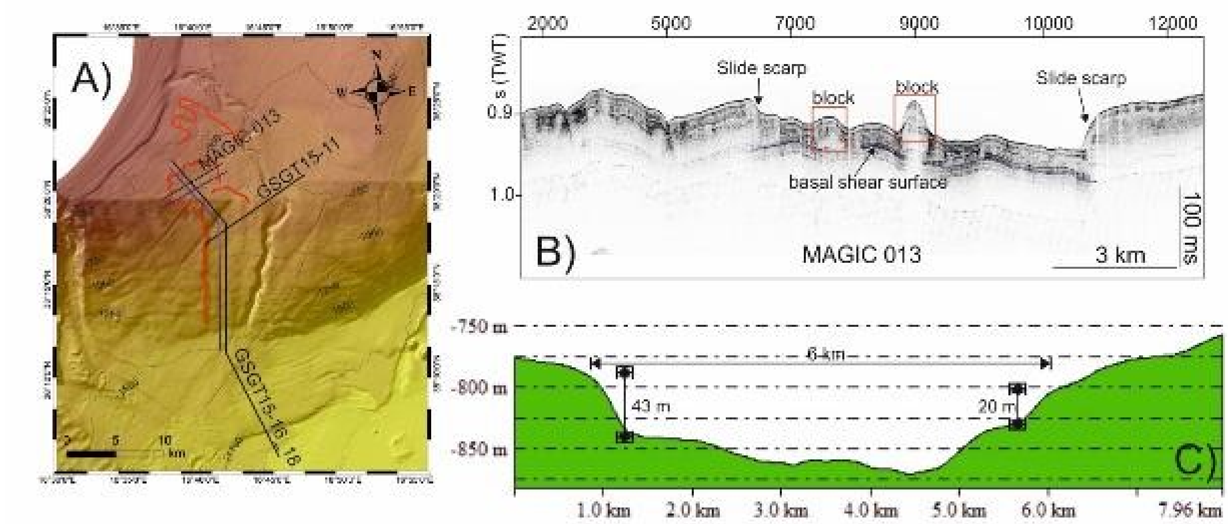

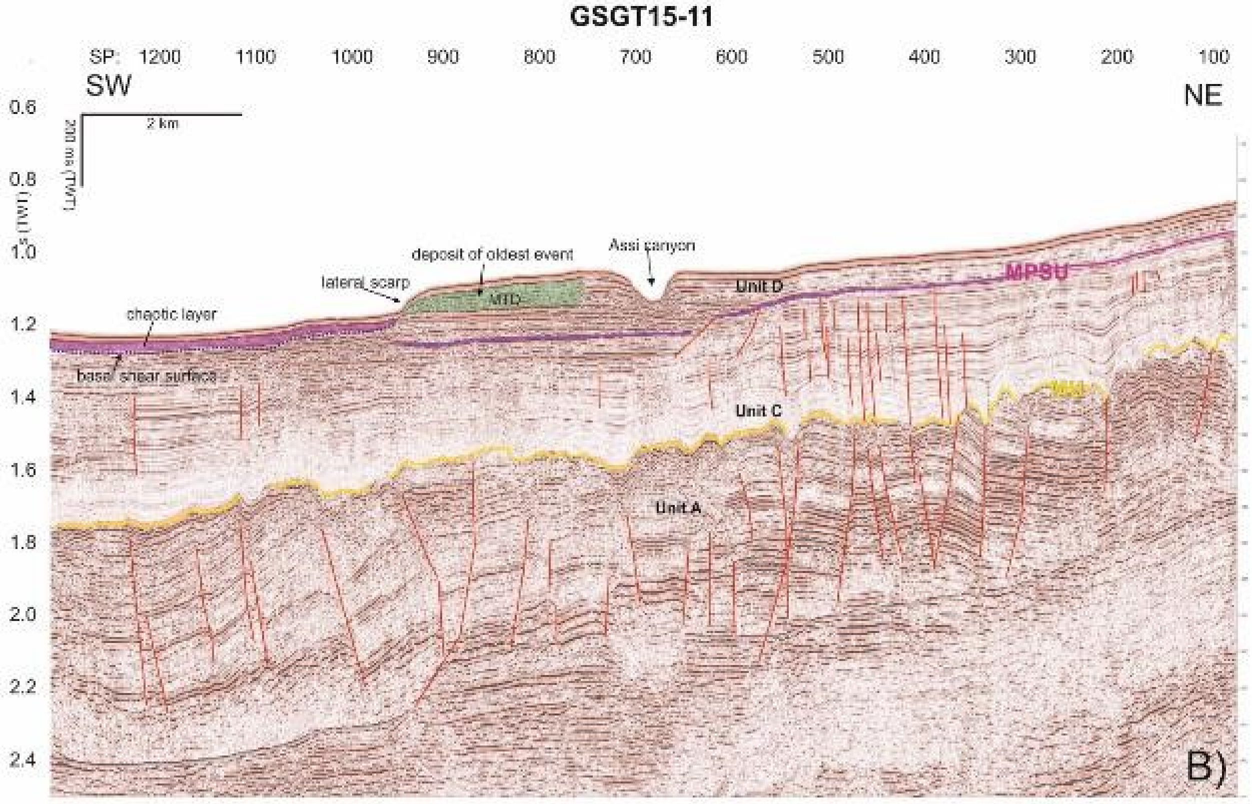

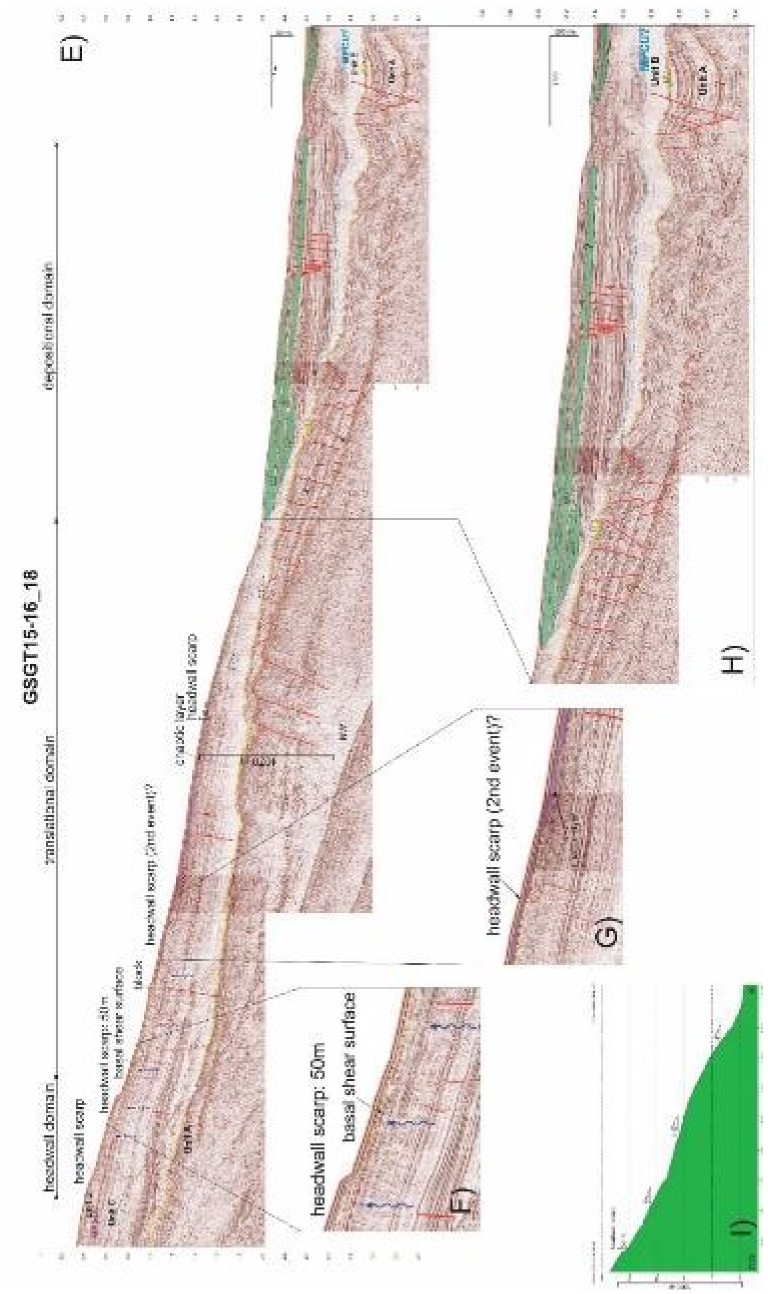

Figure 4-55 A) bathymetric view of the Assi failure: red lines are the headwall and sidewall scarps, black lines refer to the location of the seismic profiles (fig. 4.54 B, D, E) while blue lines refers to topographic profiles, longitudinal (fig. 4.54 C) and cross section (fig. 4.54 I) on the Assi failure. B) sub bottom profile cross cutting the translational domain (see fig. A for location). C) transverse topographic profile across the translational domain. D) seismic profile GSGT15-11 across the Assi failure. E) seismic profile GSGT15-16_18 across the Assi failure (see fig. A for location) F) zoomed image on the headwall scarp showing also the basal shear surface (yellow dotted line). G) zoomed image on the likely headwall scarp associated to the 2nd event. H) zoomed image on the MTDs of profile 3. I) longitudinal topographic profile across the Assi failure

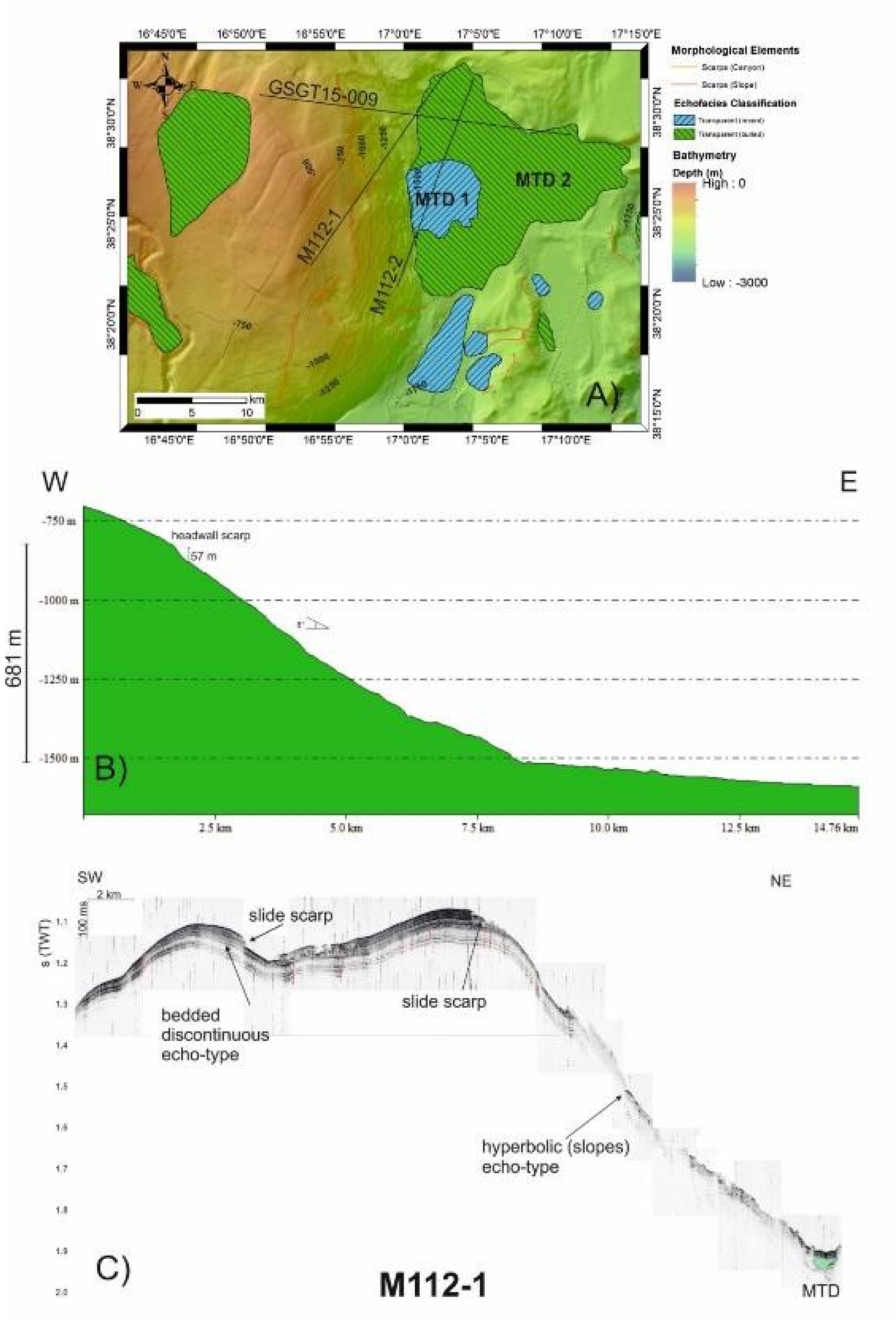
16°45'0"E
16°50'0"E
16°55'0"E
17°0'0"E
17°5'0"E
17°10'0"E
17°15'0"E
38°30'0"N
38°25'0"N
38°20'0"N
38°15'0"N
N
W
E
S
GSGT15-009
M112-1
M112-2
MTD 1
MTD 2
-500
-750
-1000
-1250
-1750
km
0
5
10
A)
Morphological Elements
Scarps (Canyon)
Scarps (Slope)
Echofacies Classification
Bathymetry
Depth (m)
High : 0
Low : -3000
W
E
-750 m
-1000 m
-1250 m
-1500 m
681 m
headwall scarp
57 m
6°
B)
2.5 km
5.0 km
7.5 km
10.0 km
12.5 km
14.76 km
SW
NE
2 km
100 ms
s (TWT)
1.1
1.2
1.3
1.4
1.5
1.6
1.7
1.8
1.9
2.0
slide scarp
slide scarp
bedded discontinuous echo-type
hyperbolic (slopes) echo-type
MTD
C)
M112-1

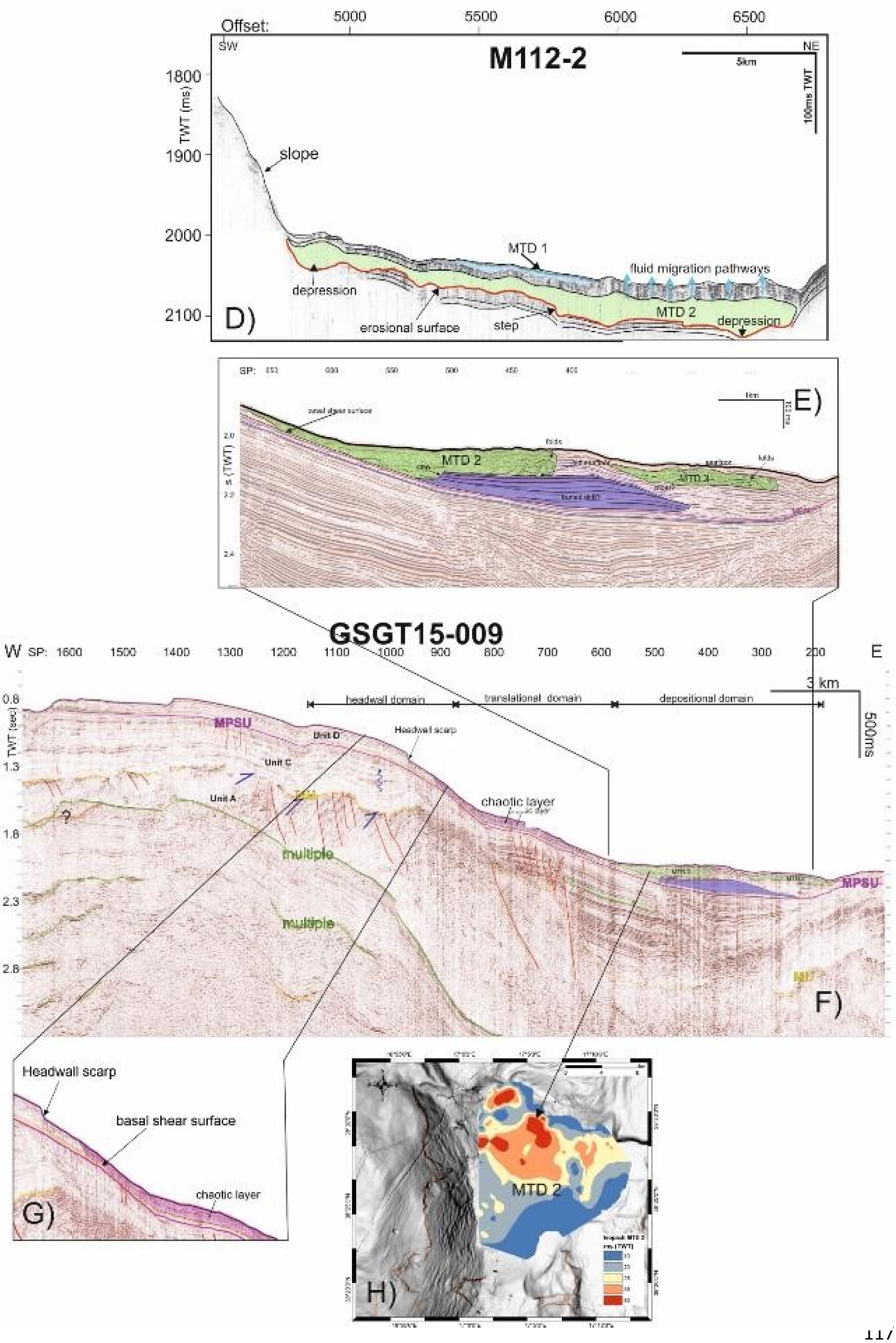
Offset:
5000
5500
6000
6500
SW
NE
M112-2
5km
100ms TWT
TWT (ms)
1800
1900
2000
2100
slope
MTD 1
fluid migration pathways
depression
erosional surface
step
MTD 2
depression
D)
SP:
E)
MTD 2
MTD 3
buried drift
GSGT15-009
W
E
SP: 1600
1500
1400
1300
1200
1100
1000
900
800
700
600
500
400
300
200
3 km
500ms
TWT (sec)
0.8
1.3
1.8
2.3
2.8
headwall domain
translational domain
depositional domain
MPSU
Unit D
Unit C
Unit A
Headwall scarp
chaotic layer
multiple
multiple
MPSU
F)
Headwall scarp
basal shear surface
chaotic layer
G)
MTD 2
H)

Figure 4-56: A) bathymetric view of the Punta Stilo failure: red lines are the scarps of the slides, black lines refer to the location of profile 1, profile 2 and profile 3, green and blue areas represents respectively buried and recent MTD. B) profile along the longitudinal profile of the failure (see profile 2 in fig. A for location). C) profile 1: sub-bottom profile crossing the Punta Stilo failure and showing the echo-types on the slide area. Note incision of the seafloor due to the slide scarp and a lateral termination of a MTD (see figure A for the location of the profile). D) profile 2: sub-bottom profile showing the subsurface expression of the MTD 2 (see figure A for location of the profile). E) zoomed image of the MTD 2 and MTD 3 at the downslope area of the Punta Stilo failure. F) profile 3: seismic profile along the longitudinal profile of the Punta Stilo failure (see fig. A for location). G) zoomed detail of the profile 3 on the basal shear surface. H) computed isochron map (expressed in ms, TWT) of the MTD 2, showing the thickness of the MTD 2 (colors refer to different thickness values, refer to the legend for the different thickness intervals)

Upslope the headwall scarps of both the Assi and Punta Stilo failures, sub-bottom and seismic data suggest the presence of fluids migration pathways (Figure 4-57). On the seismic profiles, results show stacked sub vertical fault systems with a decrease in frequency content, amplitude strength and phase continuity. The occurrence of such indicators could be related to the presence of fluids, as fluid migration pathways. However, only unit C seems to be affected by the presence of these seismic anomalies, that are sealed in correspondence of the MPSU unconformity. These patterns are identifiable on seismic profiles GSGT15-009 and GSGT15-010. The presence of overpressure fluids is also reported by the Fosca well (Figure 4-33), located ca. 3 km on the east respect to the GSGT15-010 profile; between ca. 980 to 1650 meters below the seafloor (m.b.s.f.). In sub bottom profiles the presence of gassy sediments is revealed by near-seabed acoustic anomalies in form of diffuse seismic blanking and wipeouts: this is clearly identifiable on the shelf areas (Figure 4-23).

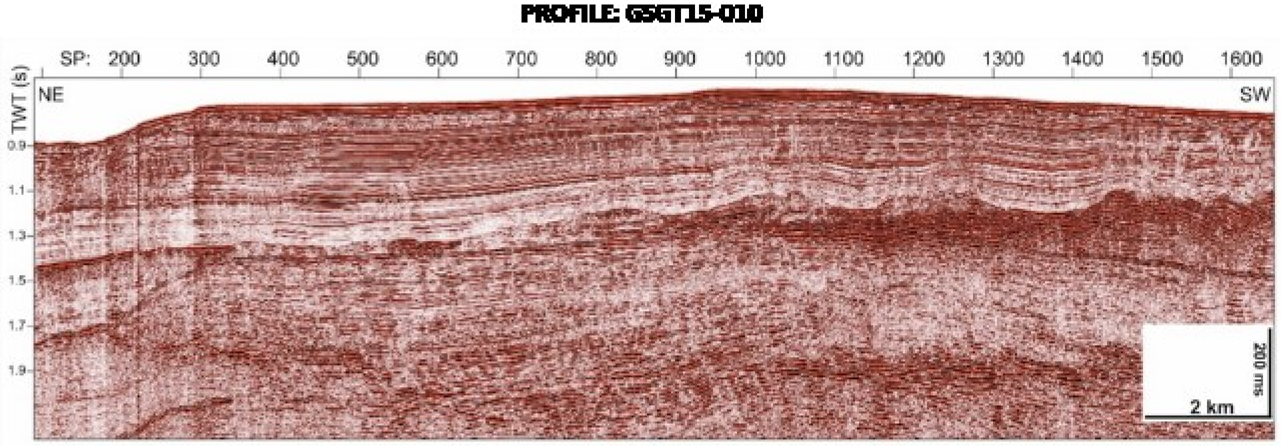

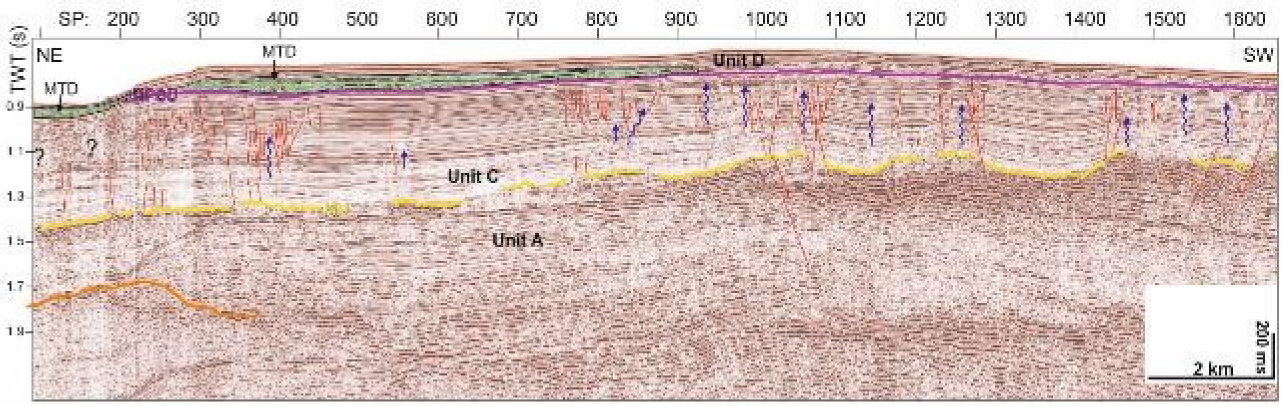

Figure 4-57: GSGT15-010 profile showing the interpreted fluid migration pathways (blue wiggle arrows). See Figure 4-52 for location of the profile.

4.3.2 Headwall and sidewall canyons slides (HSSs)

Headwall and sidewall slides occur within the canyon systems. They are identifiable as morphological scarps that range from tens to maximum of ca. 3 km (Figure 4-58) in length and are mostly found into the headwall domains and sidewall domains, in form of nested arcuate single scarps, overlapping in a downslope direction (Figure 4-59A, Figure 4-60A, Figure 4-60B).

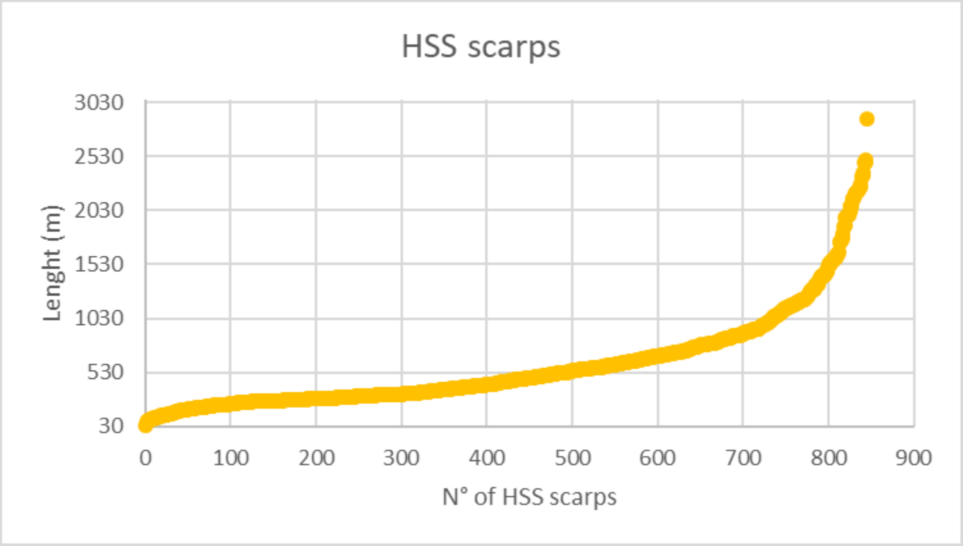

Figure 4-58: graph reporting the length of HSSs scarps mapped in the headwall and sidewall canyon slopes.

In particular they occur in the steep slopes (>10°) of the headwall canyons, that deeply incise the continental slope and the shelf break. Spatial distribution shows that they develop along the dip slope direction of the slope. The most striking example is provided by Squillace and Bottricello canyon systems (Figure 4-59A, Figure 4-60A, Figure 4-60B). In these two canyons, the steep slopes of the headwalls are widely incised by the morphological scarps. Sub bottom profiles are characterized by the hyperbolic and hyperbolic (slope) echo-type (Figure 4-59B, Figure 4-60C, Figure 4-60D) which can be associated by erosional processes and mass movements or to roughness of the seafloor (Table 4-1). On the headwall domains they appear as stacked morphological scarps along the dip slope direction, while on the sidewall canyon, especially in the main body, they appear stacked along the parallel slope direction. The occurrence of these morphological scarps is not related to the presence of MTDs at the downslope area.

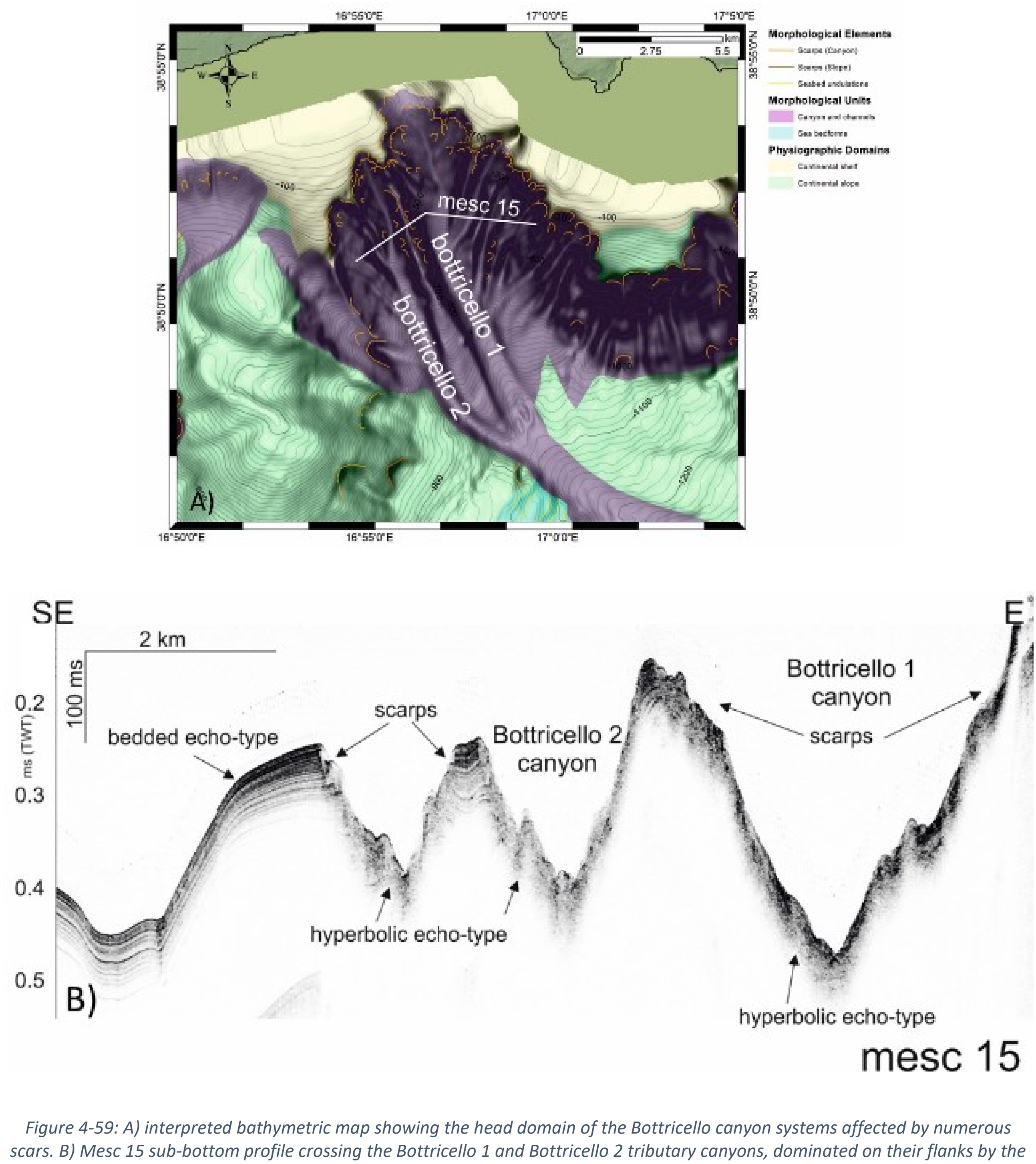

Figure 4-59: A) interpreted bathymetric map showing the head domain of the Bottricello canyon systems affected by numerous scars. B) Mesc 15 sub-bottom profile crossing the Bottricello 1 and Bottricello 2 tributary canyons, dominated on their flanks by the hyperbolic echo-type and the occurrence of scars at their upper part (see figure on top for the location of the profile)

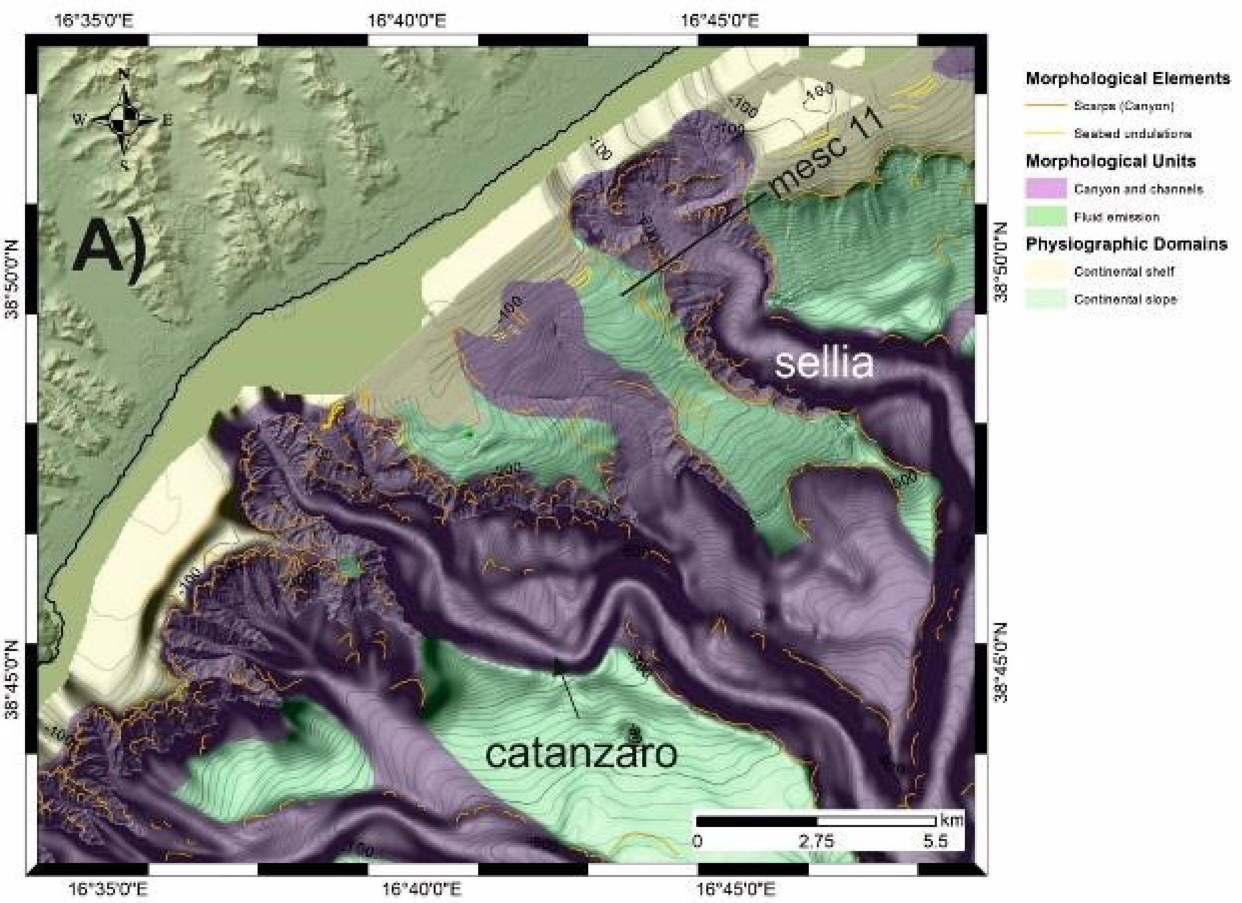
A)
16°35'0"E
16°40'0"E
16°45'0"E
38°50'0"N
38°45'0"N
N
S
W
E
mesc 11
sellia
catanzaro
-100
-200
-300
-400
-500
-600
km
0
2.75
5.5
Morphological Elements
Scarps (Canyon)
Seabed undulations
Morphological Units
Canyon and channels
Fluid emission
Physiographic Domains
Continental shelf
Continental slope

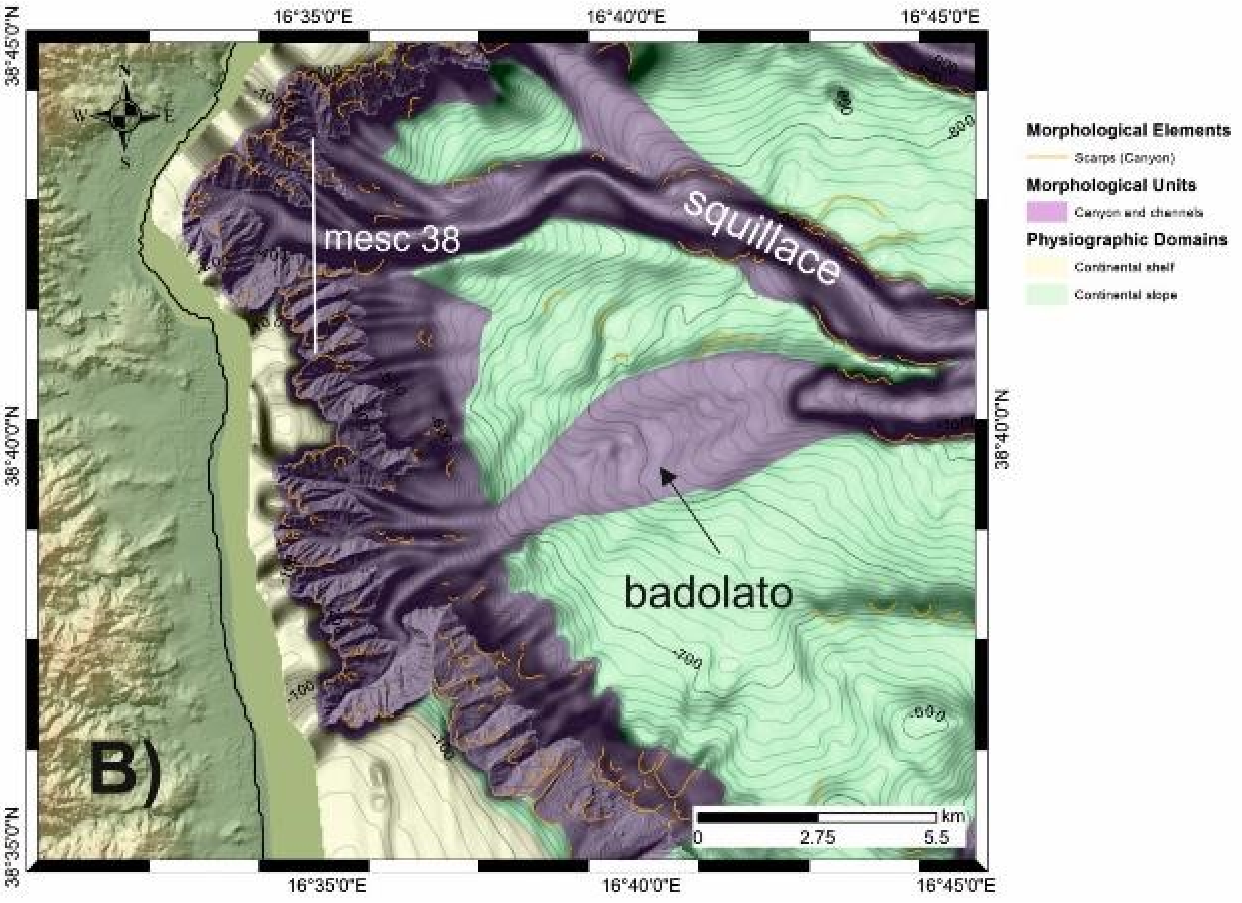
B)
16°35'0"E
16°40'0"E
16°45'0"E
38°45'0"N
38°40'0"N
38°35'0"N
N
S
W
E
mesc 38
squillace
badolato
-100
-400
-600
-700
-800
km
0
2.75
5.5
Morphological Elements
Scarps (Canyon)
Morphological Units
Canyon and channels
Physiographic Domains
Continental shelf
Continental slope

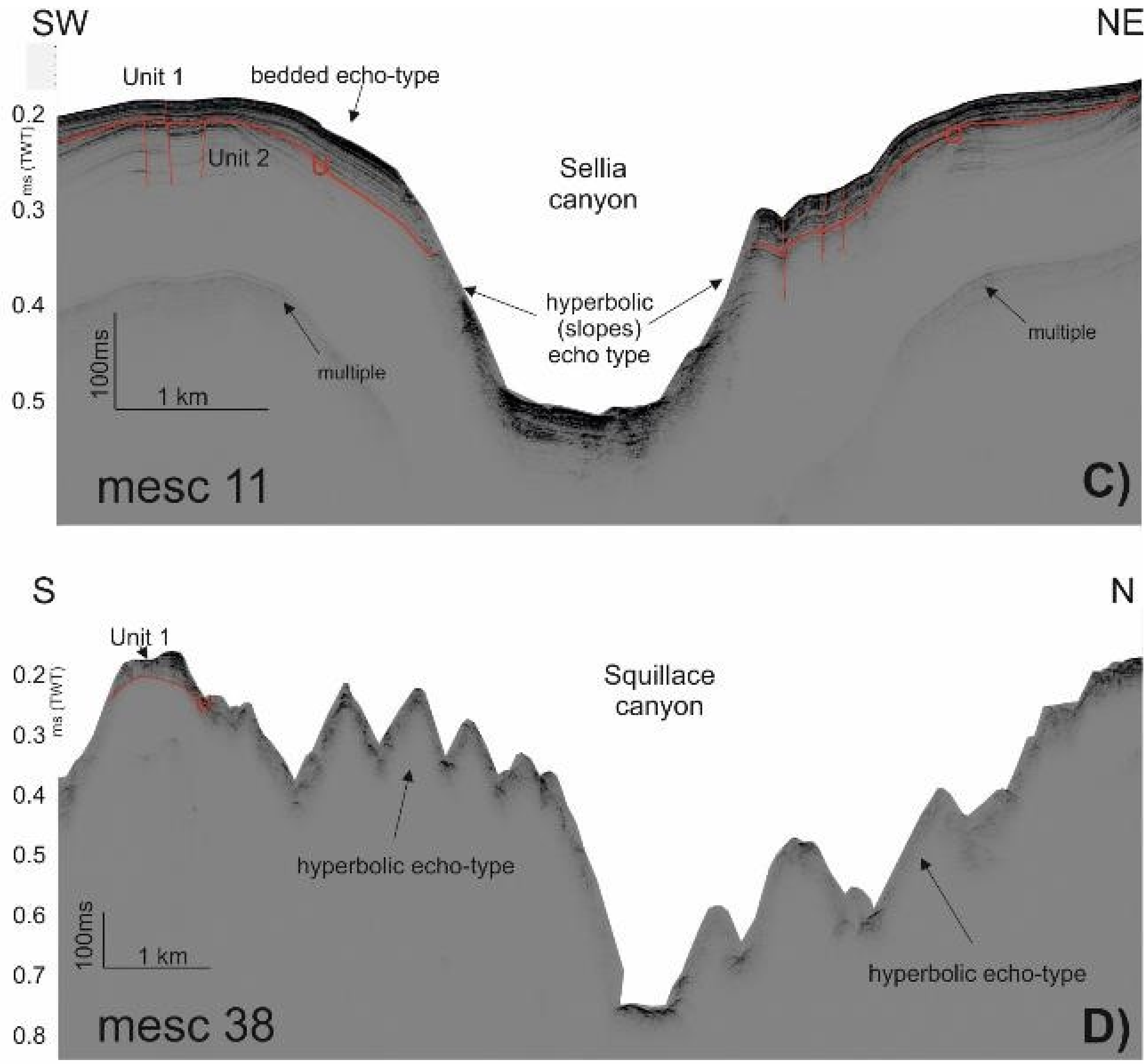

Figure 4-60: A) and B) interpreted bathymetric maps on the Squillace canyon head, characterized by its four tributary canyons. Note the numerous scarps affecting the steep slopes (>10°) of the headwall domains. C) and D) sub-bottom profiles cross cutting the Sellia and Squillace tributary canyons: note the dominance of the hyperbolic echo-type that characterizes the headwall areas of the Squillace canyon systems. In figure C) it also possible to note the U unconformity and how it deepens in proximity of the Sellia tributary canyon flanks and does not continue within the canyon system.

4.3.3 Slope parallel stratified ridges (SPSR)

In the offshore Crotone basin slope parallel undulations occur on a slope area of ca. 3° between the Bottricello canyon and the Squillace canyon, between 1100 to 1600 m b.s.l. On bathymetric data they appear as undulations between hundreds of meters to 1.8 km in length with heights from 5 to 36 m (Figure 4-61). Sub-bottom profiles show continuous stratified sediments associated to the bedded-discontinuous echo-type, locally interrupted by seaward dipping surfaces (Figure 4-61E). Seismic profile GSGT15-006 shows the occurrence of inferred normal fault systems that in some cases intersect to form conjugate system (Figure 4-61B and

Figure 4-61C). Faults dipping seaward affect the entire unit C and seems to terminate above the MU unconformity (Figure 4-61C); below the slope parallel undulations visible on bathymetric data (Figure 4-61C), these faults affect also unit D, reaching the seafloor, while the branches that are dipping landward conjugate with the seaward faults around 2.2 to 2.4 s TWT (Figure 4-61C). On unit D are visible displaced rotated blocks bounded by the normal faults (Figure 4-61B and Figure 4-61C). Moving landward, series of parallel folded reflectors are also present, with the amplitude and degree of the folding decreasing in depth and disappearing around 1600-1650 ms TWT (Figure 4-61C).

The same structures are identified also in seismic profile GSGT15-001 (Figure 4-62C), that extends from the flank of a diapiric like structure (between 700 to 450 shot point of seismic profile GSGT15-01 shown in Figure 4-62C) and interrupt in coincidence of the Bottricello canyon (Figure 4-62C). In both profiles, this package of folds affects only unit D and seems to gradually decrease in amplitude moving toward the MPSU unconformity. The diapir like structure can be described as an asymmetric SW-NE elongated structure, with a more elongated southwestern flank with reflectors terminating in onlap against it and a gentler northeastern flank. This structure affects all the seismic units, deforming the reflector of units D and C, while in the inner part, i.e. at the core of the structure is made up of unit B and unit A (Figure 4-62C). Unit B appears completely deformed with thickness values that vary from an average 200 ms TWT on the unperturbed part that gently dips towards the diapir-like structure to a maximum of 500 ms TWT at the core of the structure. Unit C appears bended with a decreasing thickness moving towards the central part of the structure, that from a maximum thickness of ca. 700 ms TWT on the northwestern and southeastern side to a ca. 400 ms in correspondence of the upper part of the structure. Reflectors are thinner and interrupted by series of sub vertical faults that terminate near the MPSU unconformity (Figure 4-62C). This structure has also a bathymetric expression in form of a dome like feature, 1. 93 km long, with the SW flank ca. 130 m high and the NE flank 50 m high (Figure 4-62C).

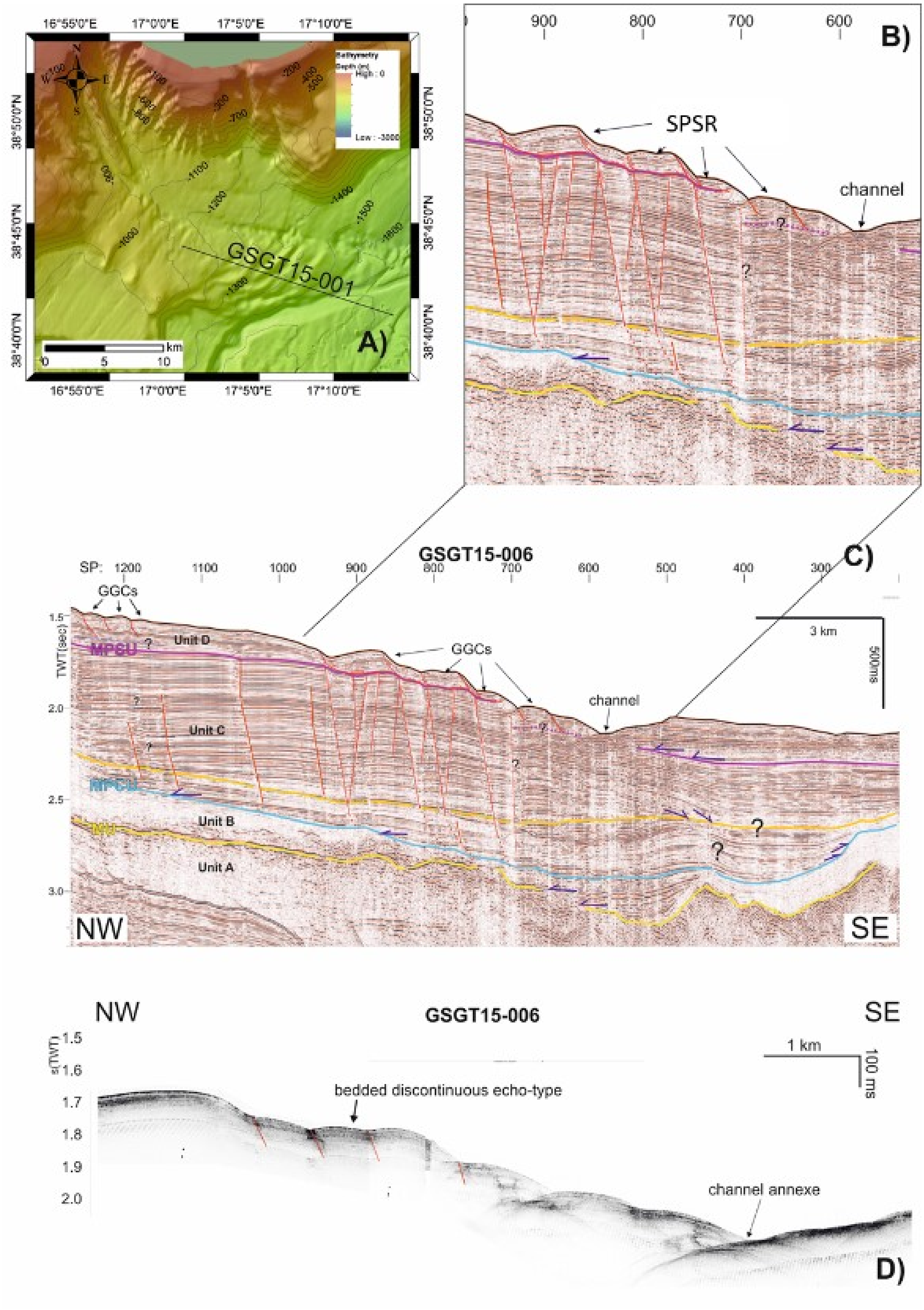

Figure 4-61: A) bathymetric map showing the position of profile 1 and profile 2. B) zoomed image of figure 6.5-4 C showing the SPSRs. C) profile 1: seismic profile cutting transversally the slope parallel undulations of figure A. D) profile 2: sub-bottom profile crossing the slope parallel undulations between the Bottricello canyon and the channel annexe, in the Crotone Spartivento basin (see figure A for location of the profile)

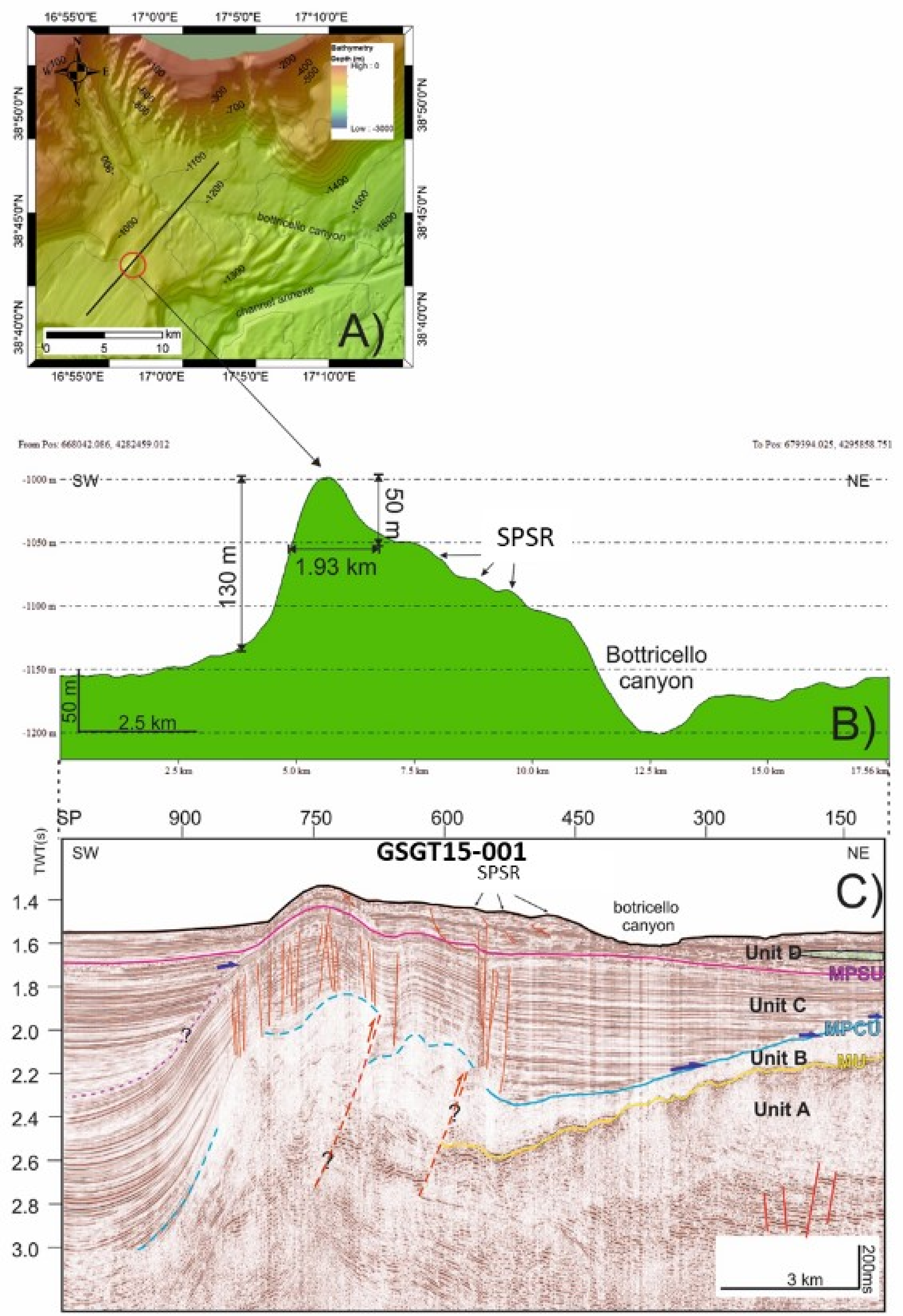

Figure 4-62: A) bathymetric map showing the SPU and the location of the bathymetric profile and seismic profile. B) bathymetric profile showing the morphological seabed expression of the diapir like structure. C) seismic profile GSGT15-001, with the SPSRs and the diapir like structure. See figure A for location of the profile.

5 Discussion

The temporal distribution of mass movements reveals that most of them occur above the MPSU regional unconformity, estimated to be of Middle Pleistocene age. This allows to make hypothesis on the relation of mass movements to the geodynamic evolution of the margin. The MPSU is a regional unconformity that marks the initiation of a new cycle of tectonic activity of the entire Calabrian Arc characterized by a general subsidence of the basin and an important and differential km-scale uplift of the Calabria region with rates up to 1mm/y, the roll-back of the subduction zone and arc trench migration. Such an interplay between subsidence of the more distal areas and uplift of the inner Calabrian arc could have caused tilting of intermediate areas, i.e. the actual continental shelf and slope, causing mass movements. The idea to be investigated is how uplift can be the responsible for causing mass movements. This is presented focusing on different preconditioning and triggering factors, critically assessed to propose a model of the development of mass movements during the Plio-Quaternary evolution of the Crotone-Spartivento basin.

5.1 Slope steepening

Increasing slope steepness favors the initiation of slope instabilities, thus giving rise to the onset of slope failures in form of the three types of mass movements observed.

The km scale differential uplift of Calabria has been recognized by the findings of raised Pleistocene marine terraces in the onshore Crotone basin (Zecchin et al., 2004), by means of GPS measurements (Antonioli et al., 2006) and by the recognition of the three regional scale Plio-Quaternary unconformities in the onshore basins (Roda, 1964; van Dijk, 1990; Zecchin et al., 2015) of Middle Pliocene, Early Pliocene and Middle Pleistocene age.

Slope steepening has been invoked as a potential pre-conditioning factor in many other geological settings and margins, both active and passive; examples can be found in the active Cretan margin (Strozyk et al., 2010) or the passive Brazilian margin (dos Reis et al., 2016; Silva et al., 2016). Strozyk et al., (2010) reported several MTDs found in mid-slope positions on the northeastern Cretan margin, interpreted to be originated by the deposition of coherent sediment masses with retrogressive upslope behavior. The Cretan basin is a large forearc basin of the Hellenic subduction zone bordered on the south by the island of Crete: while the basin is going under a subsidence that started in Late Miocene times and is progressively decreasing, the island of Crete is characterized by a rapid uplift of 6 mm/y (Ganas and Parsons, 2009). The location of MTDs has been proposed to be controlled by the progressive steepening of the slopes, due to the uplift of Crete coupled with the subsidence of the Kamilonisi Basin. Silva et al., (2016) present a study on MTDs in the offshore Foz do Amazonas Basin, as part of a larger mass transport deposits (MTDs). The Foz do Amazonas Basin is characterized by high sediment inputs by the Amazon river since Upper Miocene times that lead to the formation of the broad Amazon fan characterized by sedimentation rates ranging from 0.5 to 1mm/y in interglacial periods up to 50 mm/y during glacial periods (Silva et al., 2010 and references therein). The upper part of the Amazon fan is undergoing gravitational collapse, resulting in an inner belt of extensional tectonics consisting of listric normal seaward-dipping faults while to seaward a belt of compressional folds and thrusts along the upper submarine fan. Below the compressional belt MTDs extend for hundreds of kilometers seaward across slopes with gradients of 3-6˚, not in themselves sufficient to provoke slope failures. Silva et al. (2010) and Silva et al. (2016) identified slope steepening as a potential conditional factors of sediment instabilities over the last 10.5 Ma. In this case, slope steepening was not caused by an interplay between uplift and subsidence like in the case of the Cretan margin, but due to the high and increasing sedimentation rates during Pleistocene times. These two examples taken from both active and passive margins characterized by different geological settings prove how slope steepening is considered a potential pre-conditioning factor in the initiation of mass movements, and in particular in relation to slope failures as consequences of slope instabilities. However, the literature provides numerous other examples where slope steepening as being invoked as a potential pre-conditioning factor, such as in the offshore southern central Chile (Völker et al., 2012), in the glaciated margins offshore Eastern Canada (Li et al., 2012) . Comparison of the Calabrian Arc with the two examples described above, poses good premises in indicating that it might have played an important role in pre-conditioning slope failures. In fact, many similarities can be found, from the high gradients of the slope areas, to tectonics settings, involving subduction and subsidence. In the study area most of the slide scarps identified occur on slopes areas with gradients greater than 5°. This is valid both for the SLs (5-10°), and for HSSs (10-15°). Considering that slope steepening influences the balance between shear strength and stress strain, leading to slope instabilities and finally to slope failure it is likely that slope areas characterized by steep slopes are in a condition of instability, being the slopes over the angle of repose of the sediments, and thus favorable to generate slope instabilities. Making a direct comparison with the case of the Cretan margin, both forearc basins are characterized by a long-term (Ma) uplift (Table 5-1), respectively of the Cretan island and the Calabrian region, coupled with a general subsidence of the basins, i.e. the Kamilonisi and Crotone-Spartivento basins. Both the uplift started during Middle Pleistocene times (Table 5-1). Among these similarities on the tectonics and duration of the events, important differences can be found in the uplift rates, being 1 mm/y for the Calabrian Arc while for the island of Crete estimated to be 6 times more (6mm/y)(Ganas and Parsons, 2009) (Table 5-1), and in the mean 3°-6° for the Kamilonisi Basin and 5°-10° for the Crotone - Spartivento basin (Table 5-1). This comparison allows to make some observations regarding possible relationships between uplift rates, duration of the uplift, slope steepness and mass movements. Both the cases suggest that slope steepening plays an important role, beyond a big difference in the uplift rate.

Table 5-1: table comparing the Hellenic and Calabrian arc in terms of uplift rate, uplift initiation, mean slope steepness values of the slope areas and the MTD volumes.

	Uplift rate (mm/y)	Uplift initiation	Slope steepness (range)	MTD volumes (km3)
Hellenic Arc	6	Middle Pleistocene	3°-6°	0,1 - 2,5
Calabrian Arc	1	Middle Pleistocene	5°-10°	0,01 - 4

Strozyk et al (2010) had also pointed out that slope parallel bedding could enhance slope steepening in favoring translational mass movement along well-defined slide planes of over 5° inclination. In the Crotone -

Spartivento basin, echofacies analysis shows the bedded discontinuous echo-type to be prevalent in undisturbed areas, while seismic profile shows slope parallel sediment bedding, especially along the Punta Stilo high flanks (Figure 4-20, Figure 4-25). This echofacies can be associated to hemipelagic sedimentation, where the most prevalent sediments are clay and silt with the possible occurrence of more sandy layers in relation to sea-level oscillations. According to Lee et al., (2009) clayey and silty sediments more commonly fail under undrained conditions, and steep slopes are needed due to their high shear stress resistance. Regarding steep slopes, the Crotone-Spartivento basin is characterized by slope with gradients >5°.

5.2 Sea level change

Another regional factor to be considered is climate change, expressed as sea level variation. Climatic change and sea level variations can play a role in pre-conditioning slope failures. The literature provides many case studies on different geological margins, where sea level variations have been invoked as a preconditioning factor, such as in the North Atlantic (Owen et al., 2007b) where Late Pleistocene submarine mass movements have been influenced by climatic change and sea level oscillation, in the Mediterranean Sea (Urgeles and Camerlenghi, 2013) where a correlation is proposed between largest failures and low stand periods, or sea level rise during interglacial periods for the Holocene Storegga (Kremer et al., 2017; Smith et al., 2013b). However, as noted in the introduction, the role played by sea level change is still not clear. In particular, the debate is related to when mass movements occur during the sea level cycle. Posamentier and Kolla (2003) suggested that mass movements can be related to sea level low stands, when sedimentation at the shelf edge is inferred to be at its maximum and water overload weight is reduced, resulting in a typical deep-water stratigraphic succession that comprises debris flow deposits at the base corresponding to the initial period of relative sea-level fall, frontal- splay-dominated sections and then leveed- channel-dominated sections that correspond to the subsequent period of late low stand and early relative sea-level rise, respectively. Smith et al (2013) assert that the rapid sea level rise during the early Holocene has likely been an important factor in the development of the Storegga Slide. However, based on a global distribution of landslides in the last 180 k years, no significant correlations can be found between the temporal distribution of the submarine landslides and sea level oscillations (Urlaub et al., 2013b).

In the case of the Crotone Spartivento basin the role played by sea level oscillations is difficult to assess, due to limited age constraints on observed mass failures. However, an attempt is here made to correlate the timing of mass movements in the Crotone-Spartivento basin with a sea-level curve, considering the following limitations: a rough age estimate based only on a stratigraphic reconstruction, as well as a global sea-level curve that doesn't take into account local variations. The only useful age information is given by the MPCU unconformity, which marks the onset of the mass movements in this area. This is not enough to provide any relation between the sea level oscillations and the occurrence of the mass movements, because according to the global sea level curve, during Quaternary times, the Crotone-Spartivento basin has experienced several cycles of sea level oscillations (Antonioli et al., 2004; Cucci, 2004; Lajoie et al., 1991; Waelbroeck et al., 2002),(Figure 5-1A). Considering the limit of our age model, it is not possible to find a correlation between sea level stages and the occurrence of the mass movements. However, considering a lower frequency sea level oscillations (Figure 5-1B), the Crotone Spartivento basin has been experienced a progressive sea level rise, from lower levels related to the Messinan salinity crisis, up to the LGM, the last evidence in the stratigraphic succession of a relative sea level low stand, and associated to a shallow unconformity present in the continental shelf of the Crotone Spartivento basin (Figure 5-2). This could suggest that the mass movements might have occurred in a relative sea level rise.

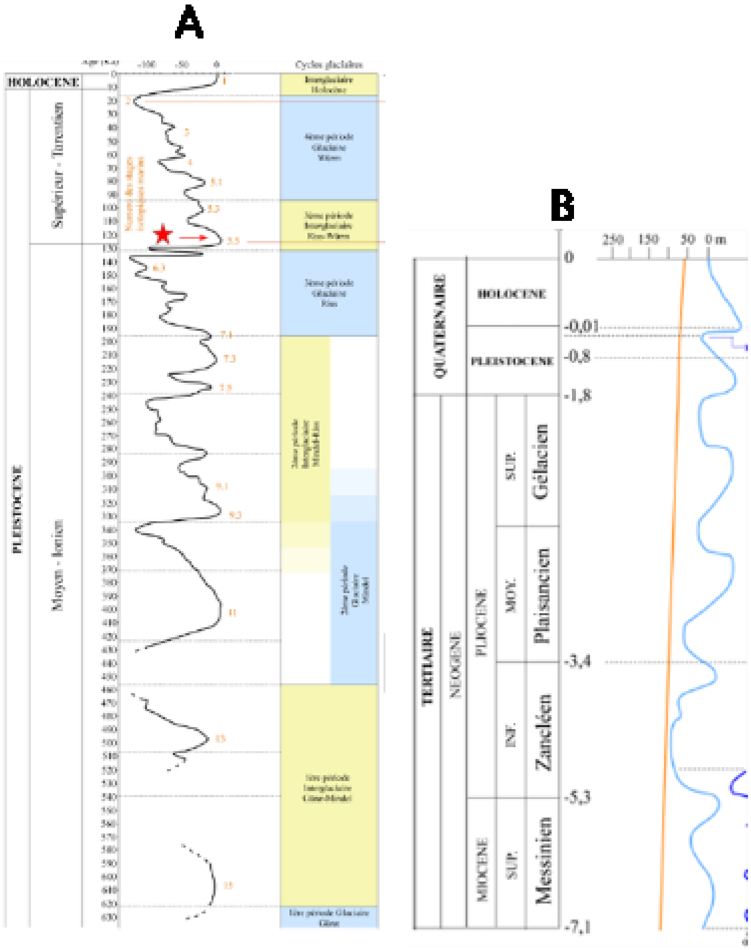

Figure 5-1: global curve of the sea level (Antonioli et al., 2004; Cucci, 2004; Waelbroeck et al., 2002). Image from Coste et al., (2014). The orange line in figure B represent the general trend of sea level rising from Messinian to Quaternary times.

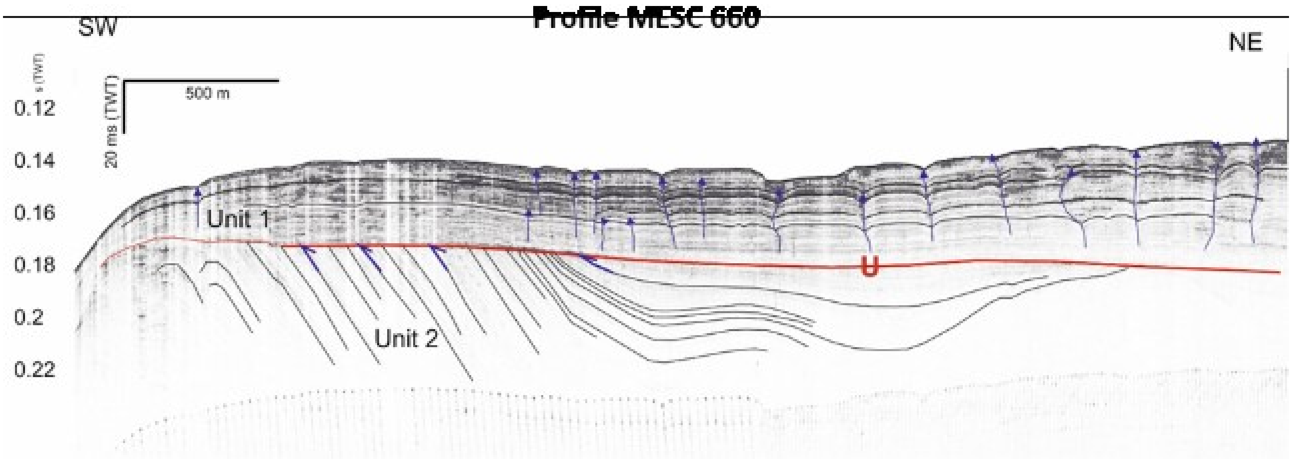

Figure 5-2: profile showing the U unconformity related to the LGM event (for location refer to figure 4.32 of chapter 4)

5.3 Overpressure fluids

Slope steepening or sea level change are not considered a sufficient cause of mass movements on active or passive margins but are likely to interact with other long-term geological processes, such as high sedimentation rates, presence of overpressure fluids, gas hydrates or weak layers. In this regard, results presented above have provided the occurrence of acoustic anomalies in form of vertical chimneys and wide areas of seismic blanking. Fluids, through geological and hydrological processes can induce excess in pore pressure, thus reducing shear strength. Fluid migration pathways associated to faults have been inferred to be present in the seismic units C and D, in particular on the Punta Stilo high, on the rear areas of the Punta Stilo and Assi failure headwall scarps. Areas characterized by seismic blanking are found in the shallow sediments on the inner continental shelf areas, probably associated to gassy sediments (Morelli et al., 2011). However, no evidence of fluid migration to seabed features has been identified in this area, such as the occurrence of pockmarks. This is probably related to the presence of more impermeable layers that could prevent or inhibit fluids ascent up to the seafloor. Impermeable layers could act as caps so that fluids are stopped in migration upward and start to propagate laterally on more permeable layers, thus generating overpressures that are known to weaken the sediments and lead to slope destabilization. Overpressured fluids are reported elsewhere in the Crotone-Spartivento basin: examples of features testifying their occurrence are the numerous mud volcanoes found in the area (Ceramicola et al., 2014b; Loher et al., 2018b, 2018a; Praeg et al., 2009), where deeply rooted over pressured sediments are suggested to be the source of the extruded mud breccias, presumably pre-Messinian and Messinian units, extruded due to compressive phases occurred in the mid-Pliocene.

Examples of repeated slope failures linked to fluid migration can be found in the western Mediterranean Sea, on the Eivissa Channel, with the Ana Slide complex (Berndt et al., 2012; Lastras et al., 2004b). Here evidence of fluid seepage has been identified, from several features, including seafloor pockmarks (Lastras et al., 2004b) and subsurface seismic anomalies related to gas and fluid migration pathways and gas clouds (Berndt et al., 2012). The Eivissa Channel is reported to be prone to slope failure by the recognition of several slope failures (Lastras et al., 2004b). Berndt et al., (2002) found a new landslide in the same location of the Ana Slide, occurred with ca. 100 ky before the Ana Slide and interpreted a same failure mechanism. According to Berndt et al., (2002) fluid migration is responsible for the slope failure, due to a weak layer that acted as a slide plane for both the two slides. This layer has been weakened in response to impermeable barriers that allowed accumulations of fluids migrating from a deeper gas cloud, formed through an upward migration of fluids rich in gas along fault planes opened during Quaternary rifting phases (Berndt et al., 2012). A similar mechanism can be proposed for the Crotone-Spartivento basin, where fluids migrated from the deeper Messinian and pre-Messinian shales into younger sediments, through series of fault systems generated by the contraction events that occurred during the Plio-Quaternary evolution of the basin. The absence of seafloor seepage features, such as pockmarks, suggests that fluid could be trapped by impermeable layers that stopped the upward migration. This seems to occur in proximity of the MPSU, or at the base of the Unit D, where most of the fault systems cease. On these layers, fluids could have migrated laterally over time, lowering the shear strength of the sediments due to overpressures.

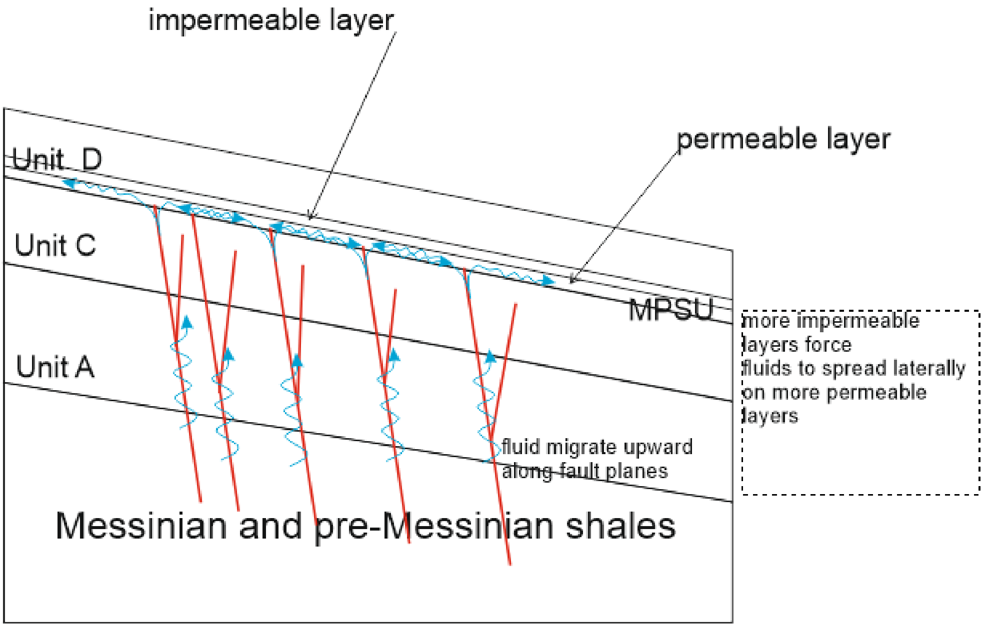

Figure 5-3: sketch showing the fluid migration. The deeper pre-Messinian and Messinian units are the source of fluids, that migrate upwards exploiting the faults systems that affect the Plio-Quaternary sequence. When a more permeable layer is capped by a impermeable cap, fluids starts to migrate laterally.

5.4 Mass movements in relation to the evolution of the margin

The model proposed is that the Calabrian uplift seems to have played a major role, not itself, but rather influencing the geological settings of the Crotone-Spartivento basin. After the Messinian Salinity Crisis ended up ca. 5.33 Ma the Crotone Spartivento basin experienced four tectono-stratigraphic episodes, each characterized by a general subsidence forearc basin interrupted by phases of uplift and tilting (Consolaro et al., 2013; Roda, 1964; Zecchin et al., 2015). These cycles are bounded by three main regional unconformities, named MPCU, EPSU and MPSU (Zecchin et al., 2015), identified in the Crotone-Spartivento basin as well as to other Calabrian basins (Zecchin et al., 2015)(Figure 5-5). Of these three unconformities, two have been recognized in this study, the Middle Pliocene and the Middle Pleistocene. In addition to those unconformities, the erosional top Messinian unconformity has been recognized, alternatively interpreted as the base of the Plio-Quaternary sequence. These unconformities have been described and correlated to the works of Zecchin et al., (2015) and Praeg et al., (2009), where the Middle Pliocene corresponds to the MPCU and the Middle Pleistocene correspond to the MPSU. The first cycle lasts from the Late Messinian / Early Pliocene to the Middle Pliocene. During Early Pliocene the Crotone-Spartivento basin was characterized by an hemipelagic sedimentation, with low sedimentation rates, described to be around 12-15 cm/yr (Consolaro et al., 2013)(Figure 5-4A). This condition of a relatively low sedimentation rate during the Early Pliocene is a common characteristic for most of the Mediterranean drill sites (Cita et al., 1999) and has been associated to the absence of terrestrial input from rivers due to the very rapid sea-level rise that abruptly terminated the Messinian salinity crisis. Only during the Late Pliocene, a new equilibrium between erosion and sedimentation was re-established, testified by increased sedimentation rates in the majority of Mediterranean drill sites (Cita et al., 1999). In the case of the Crotone-Spartivento basin this occurred in the Middle Pliocene, around 3.7 to 3.6 Ma, when the basin experienced a major change in the sedimentation rate, from 15-20 cm/yr up to 50-60 cm/yr (Consolaro et al., 2013) (Figure 5-4B). This change occurs in correspondence of the MPCU unconformity, that records the initiation of the spreading of the back-arc Vavilov basin and marks the beginning of the second tectonic cycle. This change in the sedimentation rate can be observed in the Crotone offshore basin, comparing the thicknesses of the two seismic units B and C. Unit B spans from the Late Messinian to Early Pliocene while Unit C spans from Middle Pliocene to Middle Pleistocene. Unit C is thicker than Unit B and are separated by the MPCU unconformity, that marks the transition from a low to high sedimentation rate. This high sedimentation generated a thick layer of sediments, that due to their excessive and abrupt loading could have affected the Messinian and pre-Messinian shales, inducing overpressure in fluid-rich layers. The tilting of the basin due to uplift and subsidence of the basin might have led to the generation of fault systems, that facilitate the upward migration of overpressure fluids (Figure 5-4C). This uplift was leaded by a contractional transpressional tectonic phase known as puncticulata event (Zecchin et al., 2015). The MPCU marks the initiation of the second cycle, that terminated in correspondence of the EPSU unconformity, when a second phase of uplift occurred ca. 2.5 Ma and stopped the subsidence of the basin. During Gelasian times the Crotone-Spartivento basin experienced a lowering of its level, that led to a relative sea level rise while uplift was active. This lowering increased the water column loading on the sediments. This loading exerted additional pressures on the sediments, favoring the generation of overpressure, in particularly in sediments that might have been rich in fluids, such the Messinian and pre-Messinian shales. Slope steepening is slowly increasing due to the 3.6 and 2.5 Ma events of uplifts. Coeval with the Gelasian drowning event contractional tectonics occur, as a response of the opening of the Marsili basin. Contractional events produces faults within the sediments thus favoring the upward migration of over pressured fluids (Figure 5-4D). At this time the interplay between tectonics and fluid migration generated the first mass movements.

This third cycle ends in correspondence of the MPSU, between 1-0.7 Ma, coeval with the onset of regional scale trans tensional fault systems (Del Ben et al., 2007; Massari and Prosser, 2013; van Dijk et al., 2000; Zecchin et al., 2012). The MPSU corresponds to the onset of the last cycle, characterized by a prolonged and still active uplift of the Calabria region, with uplift rates up to 1 mm/yr (Figure 5-4E). This uplift led to the subaerial exposure of the inner part of the Crotone basin, due to its tilting. The general subsidence of the basin coupled with the uplift led to an increased steepening of the slope areas. Compressional tectonics ceased, and most of the fault systems identified cease in correspondence with the MPSU. Overpressure fluids continued their upward migration up to the bottom of unit D, where likely more impermeable layers obstructed their upward migration. Overpressure fluids started to migrate laterally, probably in more permeable layers. Slope steepening led sediments having a reduced angle of repose, already decreased by the presence of fluids. This led to the formation of weak layers. At this point, sediments on slope areas were very weakened. However, a triggering factor was needed to induce mass movements. This could be found in the general seismicity associated to the subduction and plate dynamics of the Calabrian Arc.

Mass movements occur only in the last tectonostratigraphic cycle. Each cycle is defined by episodes of uplift that interrupted longer phases of subsidence of the basin, and if uplift is inferred to be a major cause of the initiation of the mass movements, one might think that every cycle in the Plio-Quaternary evolution would be affected by mass movements. Two hypotheses can be considered, from lack of data to the evolution of margin. The multichannel seismic reflection data available cover parts of the basin and more data are needed to investigate the relation between the occurrence of mass movements and the evolution of the margin. On the other hand, lack of records could occur in a sedimentary sequence, especially in presence of unconformities, that can be referred as a lack of sedimentation, or erosion. In the last case this means that evidences of mass movements occurred before the MPCU could have been eroded and for these reasons no evidences of mass movements are found before the Middle Pleistocene unconformity. Another interpretation could be related to the timing and period of the uplifts that occurred during the Plio-Quaternary. The most recent uplift occurred has two peculiarities: it has been defined as a rapid uplift (Antonioli et al., 2006, 2004; Cavazza et al., 1997; Westaway, 1993) and since when it started 1-0.7 Ma is still active, and this is known by GPS measurements (Antonioli et al., 2006). One explanation could be related to the duration or rates of these uplift events, where probably those that occurred between cycles 1 – 3 did not last enough in order to cause slope failures.

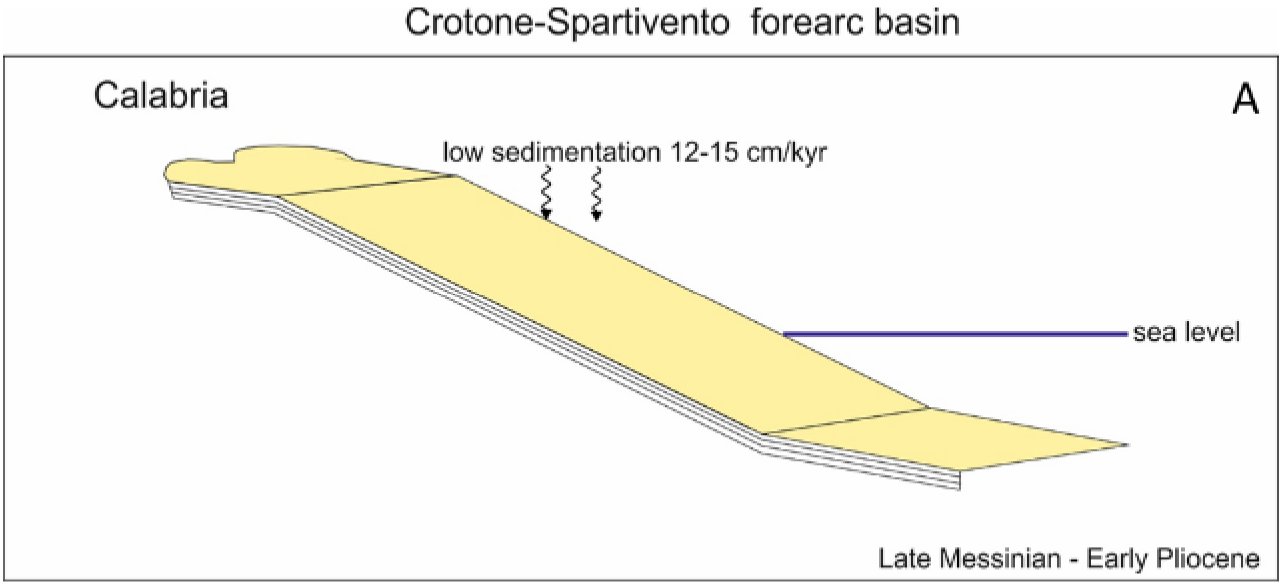
Crotone-Spartivento forearc basin
Calabria
A
low sedimentation 12-15 cm/kyr
sea level
Late Messinian - Early Pliocene

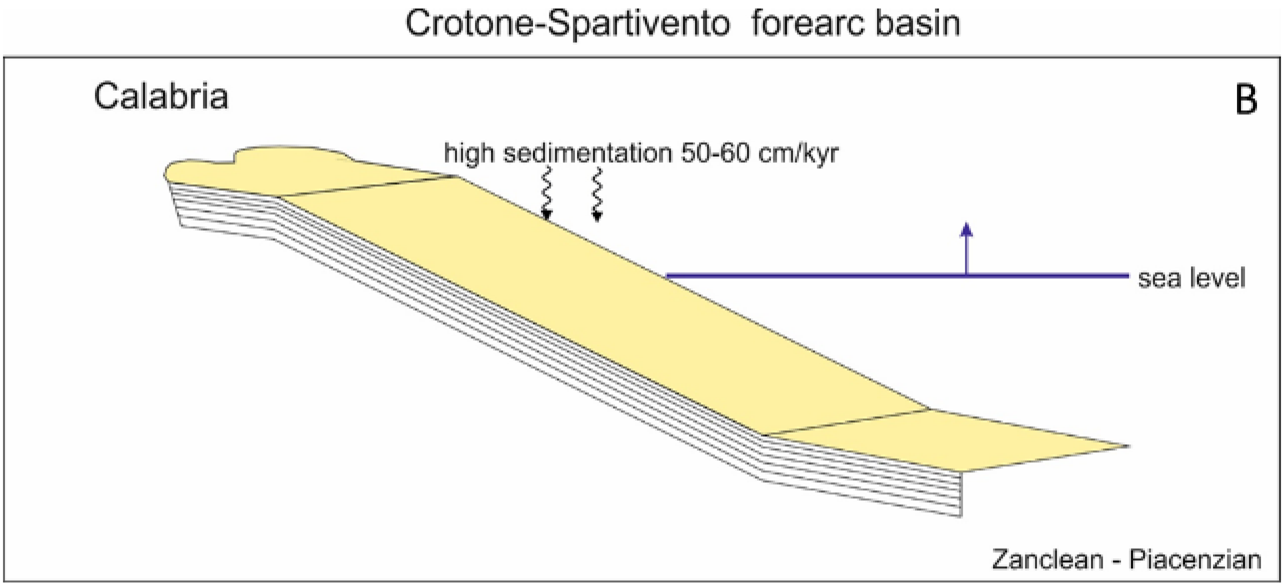
Crotone-Spartivento forearc basin
Calabria
B
high sedimentation 50-60 cm/kyr
sea level
Zanclean - Piacenzian

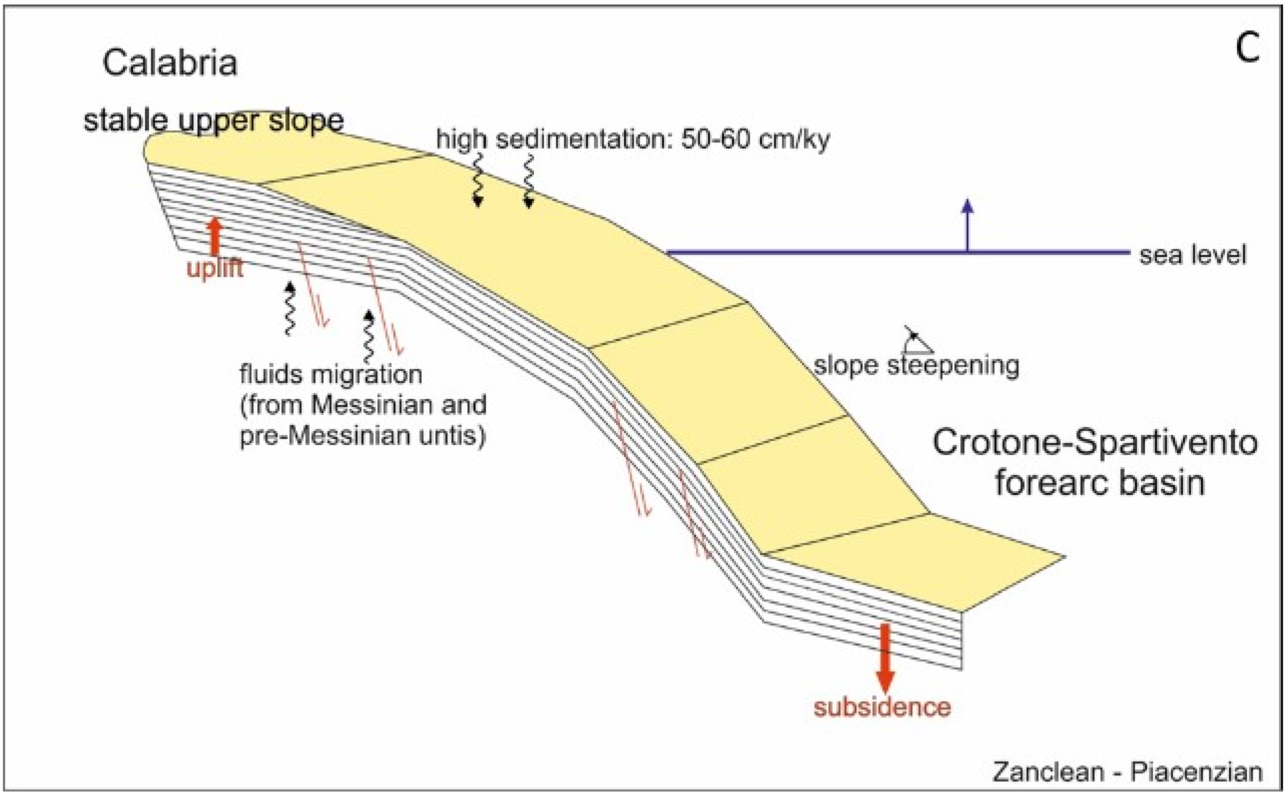
C
Calabria
stable upper slope
high sedimentation: 50-60 cm/ky
sea level
uplift
fluids migration
(from Messinian and
pre-Messinian untis)
slope steepening
Crotone-Spartivento
forearc basin
subsidence
Zanclean - Piacenzian

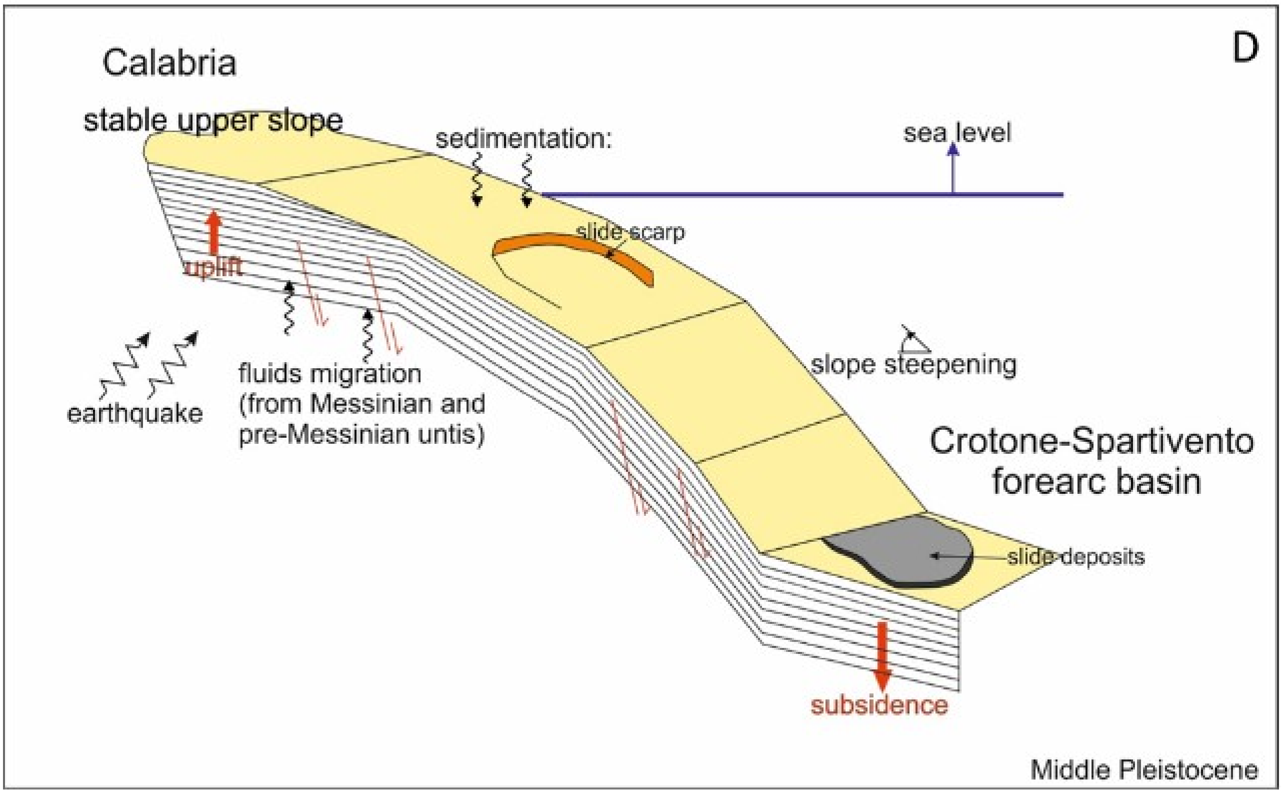
D
Calabria
stable upper slope
sedimentation:
sea level
slide scarp
uplift
earthquake
fluids migration
(from Messinian and
pre-Messinian untis)
slope steepening
Crotone-Spartivento
forearc basin
slide deposits
subsidence
Middle Pleistocene

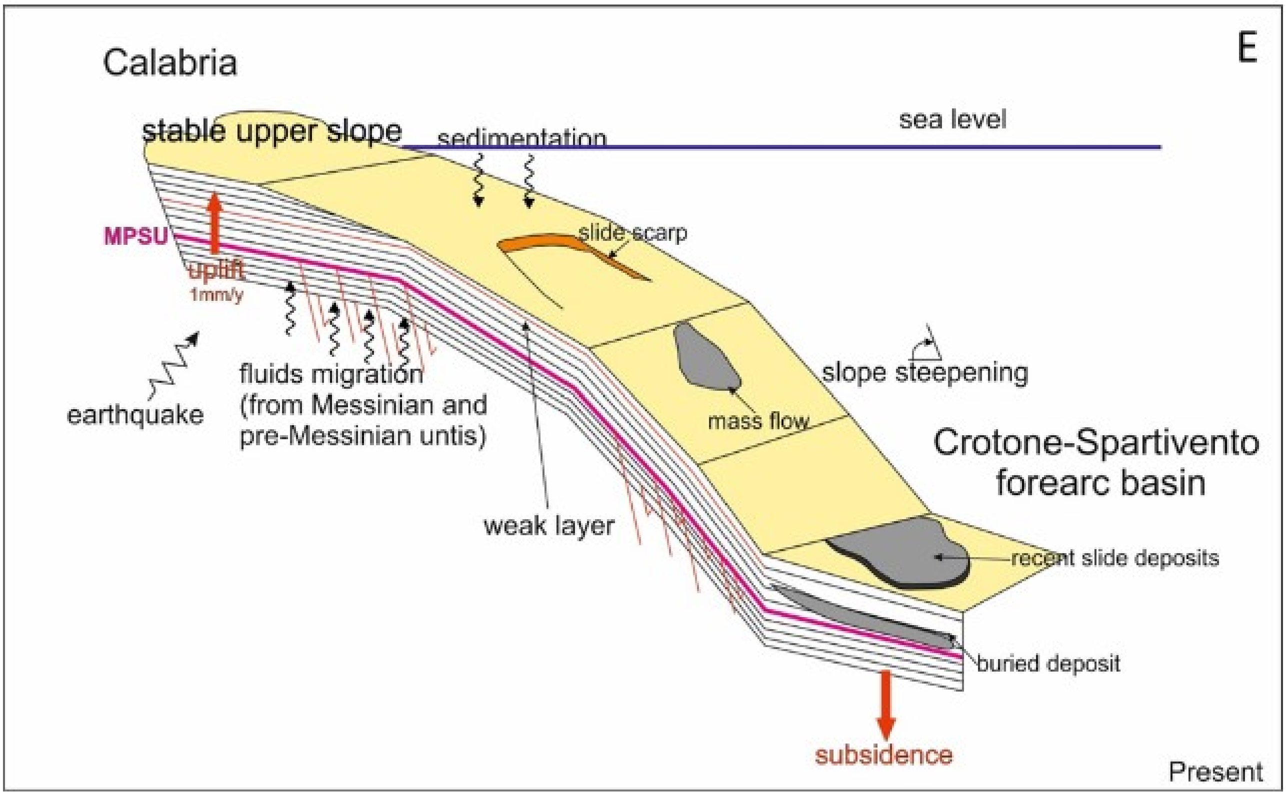

Figure 5-4: sequence showing the emplacement of the mass movements in the Crotone-Spartivento basin in relation to the Plio-Quaternary evolution of the margin at fixed time intervals: A) Late Messinian – Early Pliocene B-C) Zanclean Piacenzian D) Middle Pleistocene, E) present.

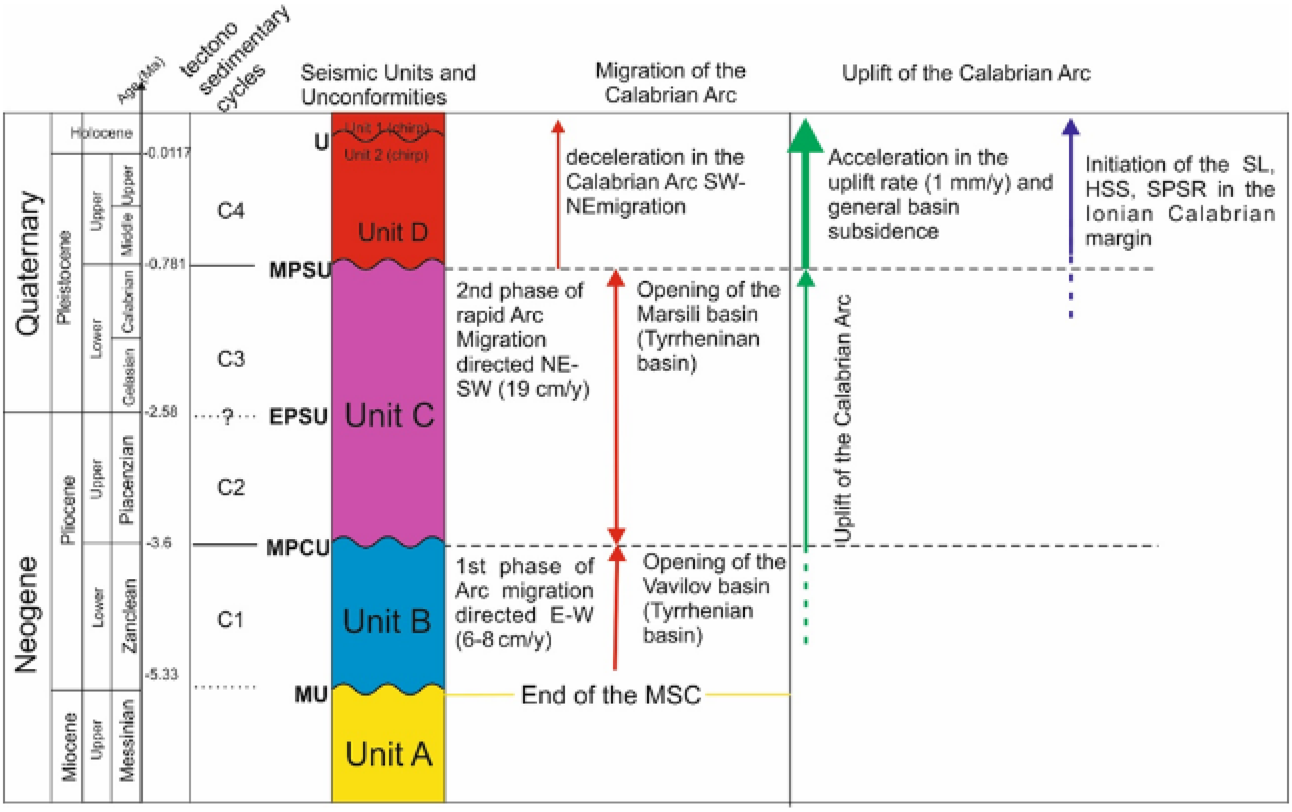

Figure 5-5: image showing the correlation between the seismic units and unconformities identified, the dynamics of the Calabrian Arc and the initiation of the mass movements in the Crotone-Spartivento forearc basin. The four regional unconformities are related

to the end of the MSC (MU) and to the four Plio-Quaternary tectonostratigraphic cycles related to the episodes of back-arc-spreading of the Vavilov and Marsili basin in the Tyrrhenian Sea (MPCU and MPSU). The U unconformity is related to the LGM, that led to the subaerial exposure of the inner continental shelf. mass movements occur in the last 1 Ma, after the MPSU, in relation to the last rapid and differential uplift that have characterized the Calabrian Arc.

5.5 Origin and development of the three mass movement types in the Crotone-Spartivento forearc basin

In the previous section mass movements were related to the geodynamics of the margin in order to propose a model for the onset of mass movements in the geological history of the Crotone Spartivento basin. In this chapter, the three types of mass movements are discussed, with particular reference to their morphologies and how they were emplaced.

The results allow a classification of mass movements according to different morphological features, which can also be used to reconstruct the mass movement type. In literature, morphologic features are described to develop as a response of a slope failure, and due to their dynamics, different types of failures produces different types of morphological features (Bull et al., 2009a; Clare et al., 2018; Moscardelli and Wood, 2008; Posamentier and Kolla, 2003b). For this reason, their identification and interpretation allow a reconstruction of the mass movement event.

5.5.1 Submarine landslides (SLs)

SLs are mainly characterized by the presence of slide scars and MTDs. The results show that slide scarps related to SLs range between 300 m to 16 km length, with MTD volumes ranging between 0.01 to 4 km^3. When a good correlation with the scarps found in the adjacent slopes can be established, it is observed that MTDs occur at short distances from them, suggesting that the failed material usually terminates its movement above the base of the slope: this is consistent with events like slide, slumps or debris flows, in which the cohesive material is not capable to travel on the lower gradients of the lower slope or the basin floor. Such events usually leave some acoustically recognizable features that provide evidence of the type of gravity failure, such as pinch-out geometries, thrusts or folds at the toe of MTDs, and in case of slumps and debris flows irregular top and bottom surfaces comprising low discontinuous to semi-transparent reflections (Bull et al., 2009b; Moscardelli and Wood, 2008). Mixed and lens-shaped MTDs show some of the seismic characteristic mentioned above, in particular they exhibit top and bottom irregular surfaces (Figure 4-45 and Figure 4-48), lens MTDs shows pinch-out geometries (Figure 4-48) and irregular MTDs are characterized by internal deformation in form of thrusts and folds at the toe of the MTD (Figure 4-53). This is consistent with an interpretation where lens and mixed MTDs could represent slumps and/or debris flows. In this regard, other information can be detected analyzing the toe region of the MTD. According to Frey-Martinez et al., (2006) two contrasting styles can be found: frontally emerged and frontally confined. These two styles can provide different information on the type and dynamic of the failure. An example is provided by the MTD of the Punta Stilo failure (Figure 4-56): the thrust and folds at its toe region (Figure 4-56H) can be due to the fact that during its failing, the material has encountered a morphostructural obstacle, where the confinement occurs where a positive topographic feature provides the necessary resisting forces to prevent further translation. A similar case has been observed by Trincardi and Argnani (1990) within the Gela Slide in the Plio-Quaternary foredeep of Sicily. In this regard, the buried MTD found at the downslope area of the Punta Stilo failure is mostly confined to the downslope area and narrows at its distal toe in correspondence of morphological obstacles on its sides. MTDs are also characterized by the occurrence of a basal shear surface, that develops due to progressive shear failure at the bottom surface of the MTD, thus separating deformed, chaotic and disrupted strata from the undeformed continuous strata of the substrate or coherent deposits down-dip. The basal interaction of MTDs with the underlying substrate is widely documented from seismic data (Alves et al., 2014; Bull et al., 2009b; Gee et al., 2005; Posamentier and Martinsen, 2011) However, basal shear surfaces can be complex, and localized deformation has been described in the substrate. In particular, some MTDs show irregular bottom surfaces that can be interpreted as erosional surfaces. The occurrence of an erosional surface can be related to coherent masses or flows capable of eroding the seabed. The erosional base has not been observed in all MTDs but only those that exhibit lens and mixed shapes (Figure 4-48, Figure 4-45), whereas tabular MTDs (Figure 4-46) show no signs of their passage in the strata below their basal surfaces. Erosional bottom surfaces can be associated to failure events as shear failures like slide, slumps or debris flow. According to their position at the downslope areas, the morphology discussed above, this supports the idea that they could be interpreted as more plastic flows, capable of eroding the underlying deposits, like slumps or debris flow (Figure 5-6B). For the layered MTDs where the top and bottom surfaces are concordant with the bedded sediments and no evidence of irregular surfaces is identified, one explanation is that the type of failed material is different, with lower energy, such as fluidized flows or turbidites capable of hydroplaning. Fluidized flow develop when the hydrodynamic water pressure at the front of the flow increases and is transferred down from the front of the flow into the underlying bed (Posamentier and Martinsen, 2011; Sobiesiak et al., 2018). The basal shear stress produced by the translation of the flow is not transferred into the substrate via the lubricant layer due to the large difference in viscosity, thus leaving the top surfaces almost unperturbed. Due to their more fluid behavior, these types of flows tend to spread laterally producing more regular MTDs, with top and bottom surfaces concordant with the sedimentation fill (Figure 5-6A)

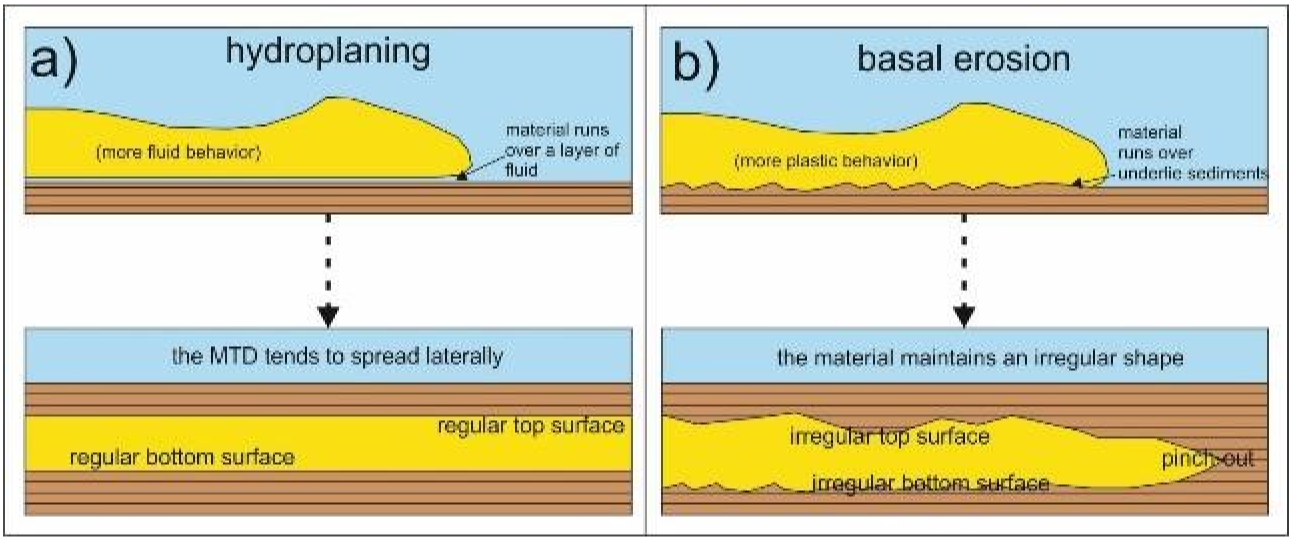

Figure 5-6: cartoon showing how different processes involving different type of flows can lead to the deposition of different MTD characterized by different morphologies, i.e. regular vs irregular top and bottom surfaces and body shape.

Wipeouts have been identified in some of the transparent buried bodies (Figure 4-19). They occur in the bedded sediments overlying the buried transparent deposits. This type of seismic anomalies have been observed in many cases, like in the Demerara abyssal plain (Loncke et al., 2009), in the Gela Basin in the Sicily Channel (Minisini D. and Trincardi F., 2009), in the Scotia Sea (Ruano et al., 2014). They can be interpreted as fluid migration or fluid ascents pathways. In the Crotone-Spartivento forearc basin, the best example is provided by the Punta Stilo MTD, where stacked seismic wipeouts occur (Figure 4-56D). Different hypothesis can be made about the nature of these fluid ascents. One is that the fluids were generated by dewatering of the MTD during later sedimentary overloading (Loncke et al., 2009). This implies that the MTD is partially filled by fluids. If this is the case, one possibility is that the failing material was enriched in fluids during its downslope movement so that the failure evolve from a more cohesive initial stage as a slide to a more plastic behavior as debris flows or slumps. A second hypothesis is that the fluids come from the sediments under the mass transport deposit as a result of loading by the MTDs, leading to a generation of high pore pressures and consequent upward migration of fluids. An example of this was reported for the twin slides of the Gela basin (Minisini D. and Trincardi F., 2009), where the occurrence of fluids pathways within the sediments overlying the MTDs was inferred to be derived by the sediments beneath the MTD itself. In our case, due to the lack of data, it was not possible to exclude either hypothesis.

5.5.1.1 *Case studies: the Assi and Punta Stilo slope failures*

The Assi failure has been studied by means of geophysical data acquired in 2009 by Ceramicola et al., (2014). Results show a three phases failure: the first and older event was associated with the headwall scarps on the upper slope and the failed material represented by the MTD reported on the middle slope (Figure 4-55A); the second event was associated with the N-S slide scarp found in the mid slope; the third event was associated with NW-SE headwall scarp. New data acquired in 2015 on the Assi failure allowed the evaluation of a prominent high amplitude reflector in respect to the above reflectors of Unit D (Figure 4-55E and Figure

4-55F), interpreted as possible glide plane. This glide plane is identified at the seismic profiles crossing longitudinally the Assi failure and could be linked to the two phases of the Assi failure. The high amplitude could be due to several factors, i.e. an abrupt change in the lithology or diagenetic processes at this boundary, a passage of the flow over the top of the surface may have compacted it, thereby increasing its density and consequently its impedance. Alternatively, the slide may have left rubble on the surface that, although smaller than the vertical resolution, creates substantial sound diffraction resulting in strong reflection.

The identification of three MTDs at the downslope area of the Assi failure suggest that at least three events occurred in this area. This is suggested by the fact that the three MTDs are separated by packages of reflectors, likely representing hemipelagic sedimentation (Figure 4-55H): they appear as very thin sequences suggesting that MTD was deposited as a consequence of a slope failure in a very short period of time. The MTDs of the Assi failure are characterized by a variety of shapes and features. The deeper MTD (MTD 3 of Figure 4-55H) shows some internal reflections and the presence of normal faults and deformed reflectors: such features could be compatible with a scenario where a mass of cohesive material slides on a gliding plane accompanied by internal deformation. In contrast MTD 1 and MTD 2 can be associated with slope failures which started as slides that rapidly transformed into debris flows. The transition into turbidites and hemipelagic sediments is seen on the seismic data by the occurrence of well-stratified seismic reflections at the distal edge of the slide deposits (Figure 4-55H). This interpretation is consistent with the model of the dynamics of the Assi failure proposed by Ceramicola et al., (2014), with the oldest phase associated with the scarps in the upper slope followed by two other failures, the youngest having formed by a retrogressive failure. In particular, the reduced size of MTD 3 can be interpreted as the toe of the first event or as a part of the slide deposit. The older event is associated with the presence of a MTD on the upper slope, on the eastern flank of the two younger failure events (Figure 4-55B). Furthermore, Ceramicola et al., (2014) suggested that the last two events characterized by a retrogressive failure events occurred over a very short period of time, i.e. 1450 y, with the first event dated 4300 years ago and the second event dated 2850 years ago. In this regard, MTD 1 and MTD 2 are separated by ca. 18 ms TWT of high amplitude reflectors probably related to hemipelagic sedimentation between the two events, that could be consistent with a short time interval. However, in absence of an accurate sedimentation rate and core data, it is not possible to precisely date the two events.

The Punta Stilo slide consists of two stacked events, a large buried MTD and a more recent MTD, smaller in size. As with the Assi failure, stacked MTDs suggests that this flank of the Punta Stilo high is prone to repeated failure events. However, in this case no-evidence of retrogressive headwall scarps have been found, rather the presence of smaller scarps on the lower slope suggests that repeated failures occur. The scarp on the upper slope coincides with an area where slope gradient increases from less than 6° to more than 10° moving downslope, suggesting there might be a relation between slope steepness and the failure event. Morphometric analysis showed that MTD 2 can be interpreted as a debris flow and the presence of an erosional bottom surface suggests that the flow was capable of scouring the surface at the base of the slope.

5.5.2 Headwall and sidewalls canyons slides (HSS)

Diffuse morphological scarps have been mapped within the six canyon systems described (chapter 4.1.2). They are smaller than the slide scars identified for SLs, ranging in length from tens of meters up to ca. 5 km (Figure 4-58). Headwall and sidewall canyon slide scars are observed to occur as nested slide scars, in particular, on the headwalls domains of the canyon systems (Figure 4-59 and Figure 4-60), with the more affected canyon headwall represented by the Squillace canyon (Figure 4-59B). The occurrence of these slide scarps can be associated with slope failures that occur in the steep slopes of the canyons. Slope failure is one of the processes through which the canyons are experiencing the development and widening of their systems. In particular, the presence of multiple scarps within the headwalls of the canyons can be interpreted as recurrent slope failure events, testifying to active erosion in the headwall domains of the canyons. This idea is also supported by the echofacies analysis, that shows how the canyon systems are mostly characterized by hyperbolic and rough echo-types, typically associated with active erosional processes (Table 4-1) (Damuth, 1975, 1980a; Gaullier and Bellaiche, 1998; Loncke et al., 2009).

Canyon headwall erosion is an erosional process that affects submarine canyons. The reasons why these areas are under erosion can be related to many processes, like storms waves that induce wave, earthquakes, hyperpycnal flows generated during flash-flood events (Casalbore et al., 2011, 2014b). Erosional processes in canyon headwalls are important for many reasons, because the eroded material feeds the canyon itself and thus is a source of sediments that are discharged in deeper areas. In particular, the reason erosional processes are present at the headwall domains is because the canyon is active and tends to reach its equilibrium profile, such processes can be related to the activity of the margin, with more dynamic canyons an indication of active margins. In this regard, a study of the Calabrian Arc by Coste et al., (2014) highlighted that the canyon systems can be considered active and are related to the evolution of the margin. In particular, Coste et al., (2014), suggested that the initiation of the canyons dated from the last tectonic cycle, i.e. from the mid-Pleistocene, as a response to strong uplift coupled with the subsidence of the forearc basin. This result highlights the role played by uplift in this area, which was responsible for the development of both canyons and mass movements. The model here proposed is that the canyons are characterized by active and retrogressive erosion at their headwalls and sidewalls because of the slope steepening induced by the uplift, as already stated on the previous chapter. This process is enhanced by the presence of gassy sediments or shallow fluid, as testified by the seismic blanking occurring all along the continental shelf, except on the canyon heads, where probably the sediments have been eroded. The absence of any MTDs within the canyons and the occurrence of fan shaped bodies at the canyon mouths, suggest that failed material is transported seaward by the canyons.

Canyons are sensitive to sea level variations, including the lowered sea levels of the last glacial maximum ca. 20000 years ago. On the continental shelf evidence of this event is provided by the U unconformity (Figure 4-31) ,which has been interpreted to record subaerial exposure (Romagnoli and Gabbianelli, 1990; Zecchin et al., 2011a). During the LGM, sea level was ca. 120 m lower than present: this would have cause erosional processes on the continental shelf by subaerial river systems (Figure 5-7). These paleo valleys could be responsible for the current canyons that occur in these zones, within which erosion probably remained dominant even after the LGM (Posamentier et al., 1988; Posamentier and Vail, 1988). This could explain why canyons developed in determined areas of the margin. This inherited situation could be related to different types of sediments, likely buried sandy fluvial strata, probably less cohesive and easily erodible, favoring the development of recurrent slope failures inferred by the occurrence of diffuse slide scarps. Furthermore, sub-bottom profiles show the occurrence of wide areas characterized by acoustically transparent anomalies, interpreted as indicators of overpressurefluids migration pathways. The combination of inherited paleo-valleys with the presence of diffuse fluid migration, can be related to the occurrence of repeated and frequent slope failures in the steep canyon headwalls (Figure 5-7).

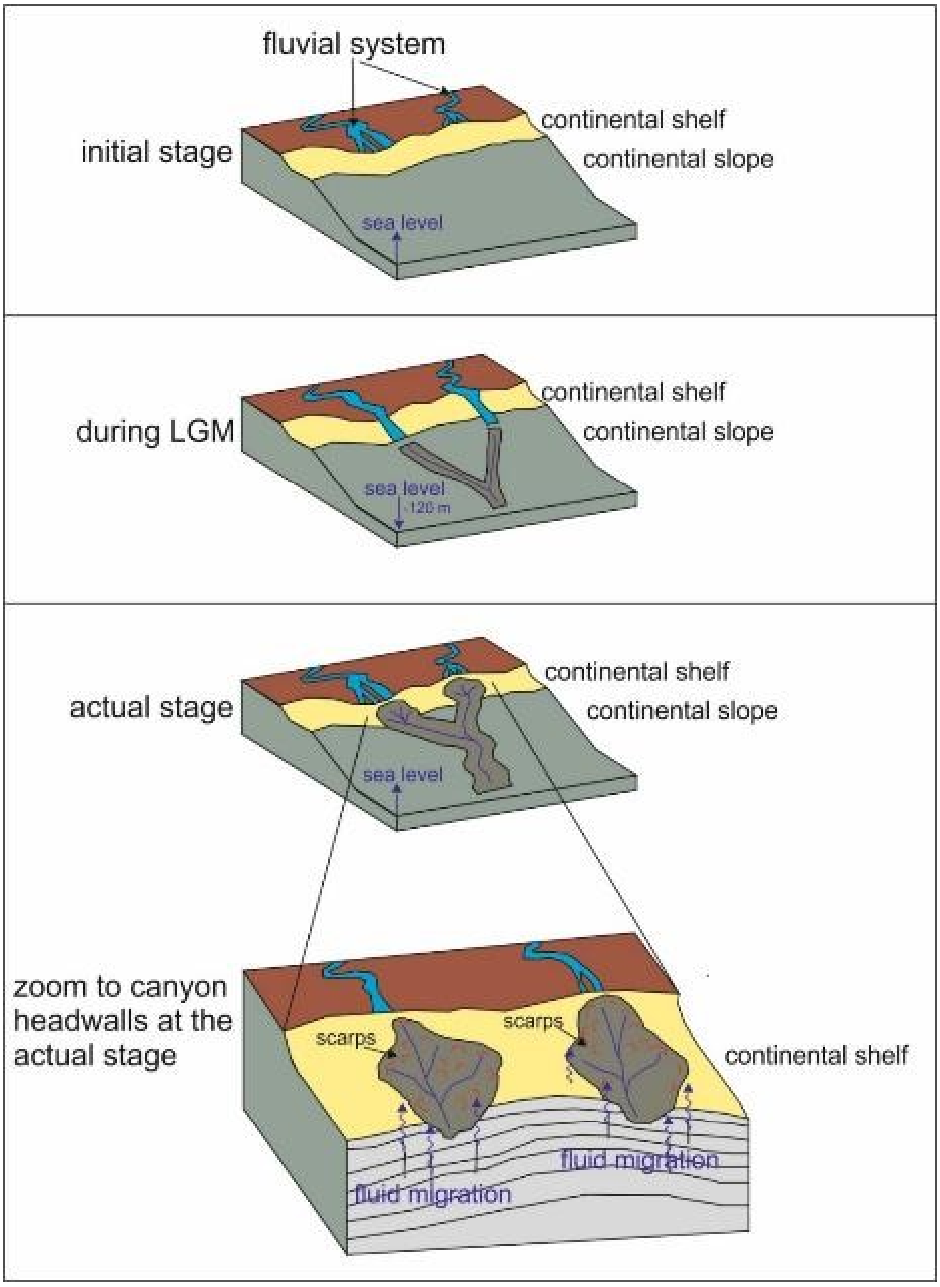

Figure 5-7: cartoon showing the incision and formation of the paleo valleys inherited by the canyon headwalls from the LGM stage and inferred to play a role in combination with the fluids that trigger or precondition the HSSs (modified from Coste et al., 2014).

During the LGM the sea level is low, and the subaerial system incise the continental shelf, generating valleys and likely depositing sandy fluvial sediments. When the LGM ends, canyon take advantage of the inherited paleo valleys and impose over them. The sandy sediments are weakened by the overpressures generated by the fluid migration, thus accelerating and emphasizing the erosions on the continental shelf.

The absence of MTDs within the canyon systems poses the question of where all the failed material is deposited. Echofacies analysis coupled with analysis of seabed morphology suggests that the failed material is trapped by the tributary channels at the headwall domain and subsequently transported by the main conduits to the basin floor, where rough echo types are observed to dominate in the basin floor. According to Damuth (1975) and Damuth and Hayes (1977), the rough and hyperbolics echofacies types provide information about the sand/silt ratio, where a quantitative relationship exists between the amount of coarser, bedded terrigenous sediments, i.e. sand/silt/ and gravel, in the upper few meters of the seafloor. According to their results, regions characterized by a rough echofacies have a ratio of coarser terrigenous sediments which is higher. On the other hand, regions characterized by the two other echo-types, i.e. the bedded and rough bedded have less coarse sediments. Finally, the rough echofacies can also be attributed to areas where erosional processes are dominant. One explanation is that a huge amount of sediments is transported by the canyon in form of flows capable to travel for long distances, in the order of tens of km, in form of confined flows and once they reach the mouth of the canyon, they spread out in form of non-confined flows and sediments are delivered. However, the lack of data between the coastline and the bathymetric map, precludes information about the possible connection of the canyons systems with their subaerial counterpart, although the data show that, except for the Assi canyon, all the canyon systems are deeply indented into the continental shelf, suggesting strong erosion by the canyons.

5.5.3 Slope parallel stratified ridges (SPSR)

Slope parallel stratified ridges have been identified at three areas in the Crotone-Spartivento fore-arc basin. This type of processes can be recognized on the seafloor as slope parallel undulations (SPUs Figure 4-14) 1 to 2 km wide and tens of meters high (from ca. 34 to 16 m, Figure 4-14B), and extends above low gradient slopes at the lower continental slope, between 1° -3°. SPSRs are associated with the bedded discontinuous echofacies (Figure 4-20). This type of echofacies can be associated to creeping-like features triggered by different geological processes and structures. In fact, in the Crotone basin an SPSR can be related to a diapir-like structure and to the presence of faults (Figure 4-61 and Figure 4-62). In the first case (Figure 4-61) SPSR can be related to development of a diapir-like structure, where vertical migration could have led to slope steepening and gravitational acceleration due to compressive forces exerted by the buried diapir at its flanks, exceeding a threshold for the stability of the sediments that are lying on the diapir flank: probably shears stress overcome shear strengths, leading to creeping behavior, that did not evolve into more dynamic failures like slides or flows due to the very low gradient (Figure 5-8). In the second case (Figure 4-62), the hypothesis is that creeping is due to the reactivation of previous fault planes, that coupled with a basal shear surface on the lower boundary of the creeping masses, found in correspondence of the MPSU unconformity, led to slow gravity gliding (Figure 5-8). The occurrence of such structures and the morphological seabed expression exclude that they can be interpreted as sediment waves, defined as large-scale depositional sea bedforms that develops as a consequence of a flowing current at the seafloor (Wynn and Stow, 2002). These type of sea bedforms usually have undulations in which the thickness is larger on their upper slope wave flank than on the downslope flank (Ercilla et al., 2002), because the wave sequence is sourced from the upper slope areas (Wynn and Stow, 2002). In the presence of creeping, the undulations have identical flanks with no variation in thickness and no lateral migration (Lee and Chough, 2001). In this study, the undulations seems not to display upslope migration, with constant thickness of the reflector, that are not continuous in cases of submarine creep because of the presence of local faults within the troughs (Lee and Chough, 2001). Based on the morphology and internal structures, they can be interpreted as seafloor undulations formed by slow gravity-driven submarine creep. These type of features, has been observed in many other geological settings, as offshore Israel (Almagor and Wiseman, 1982), in the Canadian Beaufort Sea (Hill et al., 1982), in a plateau area offshore south Korea in the East Sea (Lee and Chough, 2001). Creeping processes can lead to the concomitant deformation of the stratified sediments in form of folding. Local faults could develop due to accumulated strain by the creeping forces. When the deformation of the sediments is active, a basal shear zone would be formed in proximity of the lower boundary of the strata.

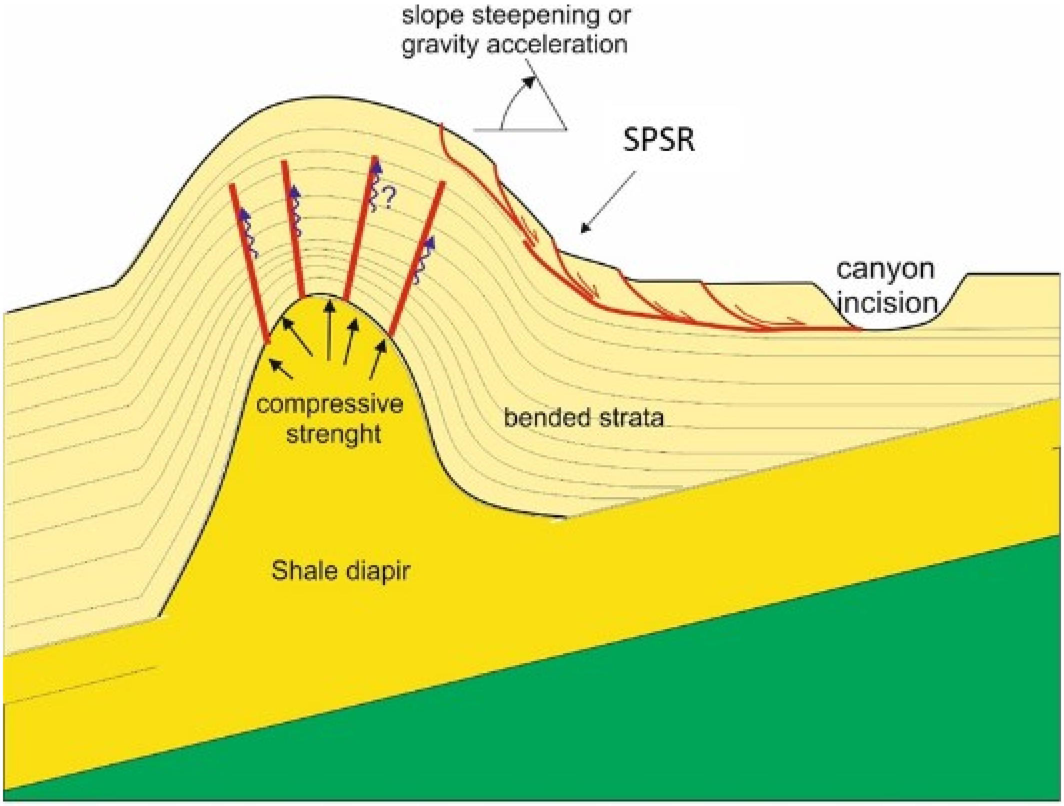

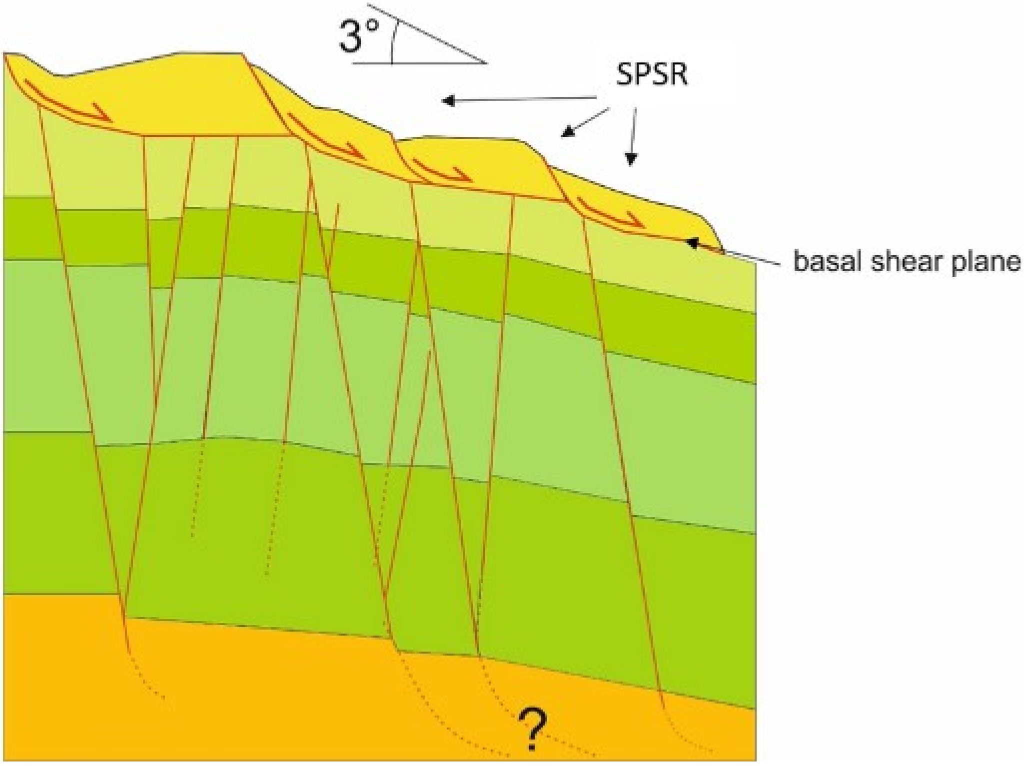

Figure 5-8: cartoon depicting the creeping masses in relation to the two different processes: on the top SPSRs develop as a response to the presence of a shale diapir structure, responsible for the development of compressive strength, faults on top of its and slope steepening or gravity acceleration due to slope steepening is leading to the failure on its flank. In the second case (bottom figure) reactivation of previous fault planes coupled with the development of a basal gliding plane seems to be the factor that led to the creeping features.

6 Conclusions

This thesis presented a study of mass movements in the Crotone Spartivento forearc basin, Ionian Sea. The study is based on the integration of different types of existing and newly acquired seafloor and subsurface geophysical data combined with well logs. The study has been conducted through a morphological analysis aimed at identifying and map the different mass movements, an echofacies analysis to reconstruct the main seafloor processes and a stratigraphic interpretation to date the occurrence of mass wasting in the Plio-Quaternary succession of the basin.

The different analysis performed, allowed to classify the mass movements occurring in the Crotone-Spartivento forearc basin, based on different geomorphological features: three main types of seafloor mass movements named as: 1) submarine landslides (SLs), 2) headwall and sidewall canyon slides (HSSs) and 3) slope parallel stratified ridges (SPSR) were recognized.

SLs are interpreted as slope failures, that occur on slopes areas with gradients > 5°. SLs are characterized by slide scarps upslope of mass transport deposits (MTDs). Two largest features occurr at the flanks of the Punta Stilo high, represented by the previously identified Assi failure and the newly described Punta Stilo failure. Morphometric analysis of the shape, geometry and position of the slide scarps and the MTDs suggest that: 1) SLs failure mechanism can be associated to slope failure in form debris flows with a plastic behavior that could evolve to more turbulent flows, likely turbidites. 2) Slope failures are recurrent events due to the presence of stacked MTDs. According to the decreasing in size from the buried to recent MTDs, it is suggested that there is a decreasing magnitude of slope failure events.

HSSs are represented by slide scarps that occur on steep (>10°) slopes on the headwalls and sidewalls of canyon systems. HSSs are characterized by nested or coalescent slide scarps and by the absence of MTDs at the downslope area. Nested slide scarps provide evidence of active and repeated erosion within the canyon systems. The most striking case is the Squillace canyon system, which has the widest headwall and greatest length of all the canyons in the forearc basin. Headwall domains are characterized by retrogressive erosion in form of repeated failure events where a combination of inherited paleo-valleys on which the canyon headwall developed and presence of fluids within the shallow areas of the continental shelf act as a pre-conditioning factors, weakening the sediments and thus emphasizing the process. Compared to SLs, HSSs are characterized by smaller events, as testified by the smaller slide scarps, but probably more frequent due to the high number of slide scarps. The absence of MTDs suggests that the failed material is discharged to the basin floor in form of non-confined flows, such as turbidites, capable of traveling from the headwall domains located at the continental shelf to the floor of the basin.

SPSRs are characterized by slope parallel undulations at the seaflore, that develop on low gradient slopes (<5°) on the lower continental slope, both in the Crotone and Spartivento basins. SPSRs are inferred to represent slow gravity driven processes in form of creeping. This type of feature is observed in two areas, which have common features, but are interpreted to have been triggered by two different subsurface mechanisms. In the first case the development of a mud diapir caused slope steepening; the diapir is related to pre-Messinian and Messinian shales and associated to compressional events that occurred during the Plio-Quaternary evolution of the margin. In the second case the cause is related to the reactivation of previous buried normal faults and the occurrence of a glide plane which combined favored the displacements and gliding of blocks; these faults are the product of the geodynamic evolution of the margin, related to the Plio-Quaternary compressive events that affected the Crotone-Spartivento forearc basin.

Seismostratigraphic analysis allowed an examination of the relation between mass movements and the Plio-Quaternary evolution of the margin. Three major unconformities and four seismic units were identified, and correlated with the stratigraphic succession known from available wells and previous works on the study area as well as the uplifted succession exposed in adjacent onshore areas. The three unconformities, respectively named MU, MPCU and MPSU bound seismic units that have been named Unit A, Unit B, Unit C and Unit D. The three seismic unconformities record important tectonic phases related to the geodynamic evolution of the Crotone Spartivento basin. The MU unconformity, dated between 5.6 to 5.3 Ma ago, lies near the base of the Plio-Quaternary succession and is inferred to mark the end of the Messinian Salinity Crisis (MSC) or respectively the onset of the Plio-Quaternary stratigraphic succession. The MPCU unconformity is related to a first phase of uplift of the Calabrian Arc and subsidence of the Crotone-Spartivento forearc basin due to the trench migration and back arc spreading of the Vavilov basin because of rollback of the subduction slab. The MPSU is inferred to mark a second phase of uplift and deformation started 1.1 to 1.2 Ma and correlated with the opening of the Marsili basin. A new unit has been identified, Unit B, inferred to mark the transition from the sea-level fall of the MSC and the return of marine conditions. Of particular interest is Unit D, that is the unit in which all the three mass movements classified have been identified. Unit D represents the last stage of the evolution of the margin, in which a rapid uplift affected the Calabrian region and it is supposed to be the main cause of the initiation of mass movements identified.

The results of this study provide a reconstruction of the spatial and temporal distribution of mass movements in the Crotone-Spartivento basin, posing new evidences on the relation existing between the emplacement of mass movements and the evolution of the margin. However, some questions still remain open and future work is needed for a better characterization and comprehension of the mass movements in relation to the failure dynamics.

7 Bibliography

Akinci, L., Sawyer, D., 2016. Deriving the Rate of Salt Rise at the Cape Fear Slide Using New Seismic Data, in: Submarine Mass Movements and Their Consequences, Advances in Natural and Technological Hazards Research. Springer, Cham, pp. 393–400. https://doi.org/10.1007/978-3-319-20979-1_39

Almagor, G., Wiseman, G., 1982. Submarine Slumping and Mass Movements on the Continental Slope of Israel, in: Saxov, S., Nieuwenhuis, J.K. (Eds.), Marine Slides and Other Mass Movements, NATO Conference Series. Springer US, Boston, MA, pp. 95–128. https://doi.org/10.1007/978-1-4613-3362-3_7

Alves, T.M., Strasser, M., Moore, G.F., 2014. Erosional features as indicators of thrust fault activity (Nankai Trough, Japan). Mar. Geol. 356, 5–18. https://doi.org/10.1016/j.margeo.2013.07.011

Anasetti, A., Winkelmann, D., Krastel, S., Bialas, J., Brückmann, W., 2012. The BGR Slide Off Costa Rica: Preconditioning Factors, Trigger, and Slide Dynamics, in: Submarine Mass Movements and Their Consequences, Advances in Natural and Technological Hazards Research. Springer, Dordrecht, pp. 289–299. https://doi.org/10.1007/978-94-007-2162-3_26

Antonioli, F., Ferranti, L., Lambeck, K., Kershaw, S., Verrubbi, V., Dai Pra, G., 2006. Late Pleistocene to Holocene record of changing uplift rates in southern Calabria and northeastern Sicily (southern Italy, Central Mediterranean Sea). Tectonophysics 422, 23–40. https://doi.org/10.1016/j.tecto.2006.05.003

Antonioli, F., Segre, A.G., Sylos Labini, S., 2004. New data on Late Holocene uplift rate in Calabria and Messina Straits area, Italy. Quat. Nova 8, 45–67.

Argnani, A., Cimini, G.B., Frugoni, F., Monna, S., Montuori, C., 2016. The role of continental margins in the final stages of arc formation: Constraints from teleseismic tomography of the Gibraltar and Calabrian Arc (Western Mediterranean). Tectonophysics 677–678, 135–152. https://doi.org/10.1016/j.tecto.2016.03.037

Bellwald, B., Hjelstuen, B.O., Sejrup, H.P., Haflidason, H., 2016. Postglacial Mass Failures in the Inner Hardangerfjorden System, Western Norway, in: Submarine Mass Movements and Their Consequences, Advances in Natural and Technological Hazards Research. Springer, Cham, pp. 73–82. https://doi.org/10.1007/978-3-319-20979-1_7

Berndt, C., Costa, S., Canals, M., Camerlenghi, A., de Mol, B., Saunders, M., 2012. Repeated slope failure linked to fluid migration: The Ana submarine landslide complex, Eivissa Channel, Western Mediterranean Sea. Earth Planet. Sci. Lett. 319–320, 65–74. https://doi.org/10.1016/j.epsl.2011.11.045

Blanc, P.-L., 2002. The opening of the Plio-Quaternary Gibraltar Strait: assessing the size of a cataclysm. Geodin. Acta 15, 303–317. https://doi.org/10.1016/S0985-3111(02)01095-1

Bohrmann, G., Bachmann, K., Buchheister, S., Candoni, O., Ceramicola, S., Loher, M., Meinecke, G., Renken, J., Spiesecke, U., von Wahl, T., Wintersteller, P., 2016. Report and preliminary results of R/V POSEIDON cruise POS499, Calabrian Mud Volcanoes, Catania (Italy) – Catania (Italy), 04 May – 22 May, 2016. Berichte MARUM – Zent. Für Mar. Umweltwissenschaften Fachbereich Geowiss. Univ. Brem. 1–76.

Bonardi, G., Cavazza, W., Perrone, V., Rossi, S., 2001. Calabria-Peloritani terrane and northern Ionian Sea, in: Anatomy of an Orogen: The Apennines and Adjacent Mediterranean Basins. Springer, Dordrecht, pp. 287–306. https://doi.org/10.1007/978-94-015-9829-3_17

Brothers, D.S., Luttrell, K.M., Chaytor, J.D., 2013. Sea-level–induced seismicity and submarine landslide occurrence. Geology 41, 979–982. https://doi.org/10.1130/G34410.1

Buenz, S., Mienert, J., Berndt, C., 2003. Geological controls on the Storegga gas-hydrate system of the mid-Norwegian continental margin. Earth Planet. Sci. Lett. 209, 291–307. https://doi.org/10.1016/S0012-821X(03)00097-9

Buffett, B.A., 2000. Clathrate Hydrates. Annu. Rev. Earth Planet. Sci. 28, 477–507. https://doi.org/10.1146/annurev.earth.28.1.477

Bull, S., Cartwright, J., Huuse, M., 2009a. A review of kinematic indicators from mass-transport complexes using 3D seismic data. Mar. Pet. Geol. 26, 1132–1151. https://doi.org/10.1016/j.marpetgeo.2008.09.011

Bull, S., Cartwright, J., Huuse, M., 2009b. A review of kinematic indicators from mass-transport complexes using 3D seismic data. Mar. Pet. Geol. 26, 1132–1151. https://doi.org/10.1016/j.marpetgeo.2008.09.011

Camerlenghi, A., Urgeles, R., Erchilla, G., Brückmann, W., 2007. Scientific Ocean Drilling Behind the Assessment of Geo-Hazards from Submarine Slides. Sci. Drill. https://doi.org/10.2204/iodp.sd.4.14.2007

Capozzi, R., Artoni, A., Torelli, L., Lorenzini, S., Oppo, D., Mussoni, P., Polonia, A., 2012. Neogene to Quaternary tectonics and mud diapirism in the Gulf of Squillace (Crotone-Spartivento Basin, Calabrian Arc, Italy). Mar. Pet. Geol. 35, 219–234. https://doi.org/10.1016/j.marpetgeo.2012.01.007

Casalbore, D., Bosman, A., Chiocci, F.L., Ingrassia, M., Macelloni, L., Sposato, A., Martorelli, E., 2016. New Insights on Failure and Post-failure Dynamics of Submarine Landslides on the Intra-slope Palmarola Ridge (Central Tyrrhenian Sea), in: Submarine Mass Movements and Their Consequences, Advances in Natural and Technological Hazards Research. Springer, Cham, pp. 93–101. https://doi.org/10.1007/978-3-319-20979-1_9

Casalbore, D., Bosman, A., Ridente, D., Chiocci, F.L., 2014. Coastal and Submarine Landslides in the Tectonically-Active Tyrrhenian Calabrian Margin (Southern Italy): Examples and Geohazard Implications, in: Submarine Mass Movements and Their Consequences, Advances in Natural and Technological Hazards Research. Springer, Cham, pp. 261–269. https://doi.org/10.1007/978-3-319-00972-8_23

Casalbore, D., Chiocci, F.L., Mugnozza, G.S., Tommasi, P., Sposato, A., 2011. Flash-flood hyperpycnal flows generating shallow-water landslides at Fiumara mouths in Western Messina Strait (Italy). Mar. Geophys. Res. 32, 257. https://doi.org/10.1007/s11001-011-9128-y

Catalano, R., Doglioni, C., Merlini, S., 2001. On the Mesozoic Ionian Basin. Geophys. J. Int. 144, 49–64. https://doi.org/10.1046/j.0956-540X.2000.01287.x

Cavazza, W., Barone, M., 2010. Large-scale sedimentary recycling of tectonic mélange in a forearc setting: The Ionian basin (Oligocene–Quaternary, southern Italy). GSA Bull. 122, 1932–1949. https://doi.org/10.1130/B30177.1

Cavazza, W., Blenkinsop, J., De Celles, P.G., Patterson, R.T., Reinhardt, E.G., 1997. Stratigrafia e sedimentologia della sequenza sedimentaria oligocenica-quaternaria del bacino calabro-ionico. Boll Soc Geol It 116, 51–77.

Ceramicola, S., Praeg, D., Coste, M., Forlin, E., Cova, A., Colizza, E., Critelli, S., 2014a. Submarine Mass-Movements Along the Slopes of the Active Ionian Continental Margins and Their Consequences for Marine Geohazards (Mediterranean Sea), in: Submarine Mass Movements and Their Consequences, Advances in Natural and Technological Hazards Research. Springer, Cham, pp. 295–306. https://doi.org/10.1007/978-3-319-00972-8_26

Ceramicola, S., Praeg, D., Cova, A., Accettella, D., Zecchin, M., 2014b. Seafloor distribution and last glacial to postglacial activity of mud volcanoes on the Calabrian accretionary prism, Ionian Sea. Geo-Mar. Lett. 34, 111–129. https://doi.org/10.1007/s00367-013-0354-y

Ceramicola, S., Tinti, S., Zaniboni, F., Praeg, D., Planinsek, P., 2012. Reconstruction of a submarine landslide and related tsunami from morpho-bathymetry and sub-bottom data on the Ionian Calabrian margin (Mediterranean Sea). Rendiconti Online Soc. Geol. Ital. 21, 953–954.

Cernobori, L., Hirn, A., McBride, J.H., Nicolich, R., Petronio, L., Romanelli, M., STREAMERS/PROFILES Working Group, 1996. Crustal image of the Ionian basin and its Calabrian margins. Tectonophysics 264, 175–189.

Chiarabba, C., Jovane, L., DiStefano, R., 2005. A new view of Italian seismicity using 20 years of instrumental recordings. Tectonophysics 395, 251–268. https://doi.org/10.1016/j.tecto.2004.09.013

Chiocci, F.L., Cattaneo, A., Urgeles, R., 2011. Seafloor mapping for geohazard assessment: state of the art. Mar. Geophys. Res. 32, 1–11. https://doi.org/10.1007/s11001-011-9139-8

Chiocci, F.L., Ridente, D., 2011. Regional-scale seafloor mapping and geohazard assessment. The experience from the Italian project MaGIC (Marine Geohazards along the Italian Coasts). Mar. Geophys. Res. 32, 13–23. https://doi.org/10.1007/s11001-011-9120-6

Cita, M.B., Corselli, C., 1990. Messinian paleogeography and erosional surfaces in Italy: an overview. Palaeogeogr. Palaeoclimatol. Palaeoecol. 77, 67–82. https://doi.org/10.1016/0031-0182(90)90099-S

Cita, M.B., Racchetti, S., Brambilla, R., Negri, M., Colombaroli, D., Morelli, L., Ritter, M., Rovira, E., Sala, P., Bertarini, L., Sanvito, S., 1999. Changes in the sedimentation rates in all Mediterranean drillsites document basin evolution and support starved basin conditions after early Zanclean flood., in: Memorie Della Società Geologica Italiana. pp. 145–159.

Clare, M., Chaytor, J., Dabson, O., Gamboa, D., Georgiopoulou, A., Eady, H., Hunt, J., Jackson, C., Katz, O., Krastel, S., León, R., Micallef, A., Moernaut, J., Moriconi, R., Moscardelli, L., Mueller, C., Normandeau, A., Patacci, M., Steventon, M., Urlaub, M., Völker, D., Wood, L., Jobe, Z., 2018. A consistent global approach for the morphometric characterization of subaqueous landslides. Geol. Soc. Lond. Spec. Publ. SP477.15. https://doi.org/10.1144/SP477.15

Clare, M.A., Talling, P.J., Challenor, P.G., Hunt, J.E., 2016. Tempo and Triggering of Large Submarine Landslides: Statistical Analysis for Hazard Assessment, in: Lamarche, G., Mountjoy, J., Bull, S., Hubble, T., Krastel, S., Lane, E., Micallef, A., Moscardelli, L., Mueller, C., Pecher, I., Woelz, S. (Eds.), Submarine Mass Movements and Their Consequences. Springer International Publishing, Cham, pp. 509–517. https://doi.org/10.1007/978-3-319-20979-1_51

Consolaro, C., Macrì, P., Massari, F., Speranza, F., Fornaciari, E., 2013. A major change in the sedimentation regime in the Crotone Basin (Southern Italy) around 3.7–3.6Ma. Palaeogeogr. Palaeoclimatol. Palaeoecol. 392, 398–410. https://doi.org/10.1016/j.palaeo.2013.09.022

Coste, M., 2014. Les processus s edimentaires, depuis la pente continentale jusqu'au bassin, en contexte de tectonique active : analyse compar ee entre la Marge Calabro-Ionienne et la Marge Ligure durant les derniers 5 Ma. Earth Sciences. Université Nice Sophia Antipolis.

Cucci, L., 2004. Raised marine terraces in the Northern Calabrian Arc (Southern Italy): a ~ 600 kyr-long geological record of regional uplift. Ann. Geophys. 47. https://doi.org/10.4401/ag-3350

D'Agostino, N., D'Anastasio, E., Gervasi, A., Guerra, I., Nedimović, M.R., Seeber, L., Steckler, M., 2011. Forearc extension and slow rollback of the Calabrian Arc from GPS measurements. Geophys. Res. Lett. 38, n/a-n/a. https://doi.org/10.1029/2011GL048270

Damuth, J.E., 1994. Neogene gravity tectonics and depositional processes on the deep Niger Delta continental margin. Mar. Pet. Geol. 11, 320–346. https://doi.org/10.1016/0264-8172(94)90053-1

Damuth, J.E., 1980a. Use of high-frequency (3.5-12 kHz) echograms in the study of near-bottm sedimentation processes in the deep-sea: a review. Mar. Geol. 38, 51–75.

Damuth, J.E., 1980b. Quaternary Sedimentation Processes in the South China Basin as Revealed by Echo-Character Mapping and Piston-Core Studies, in: The Tectonic and Geologic Evolution of Southeast Asian Seas and Islands. American Geophysical Union (AGU), pp. 105–125. https://doi.org/10.1029/GM023p0105

Damuth, J.E., 1975. Echo character of the western equatorial atlantic floor and its relationship to the dispersal and distribution of terrigenous sediments. Mar. Geol. 18, 17–45.

Dan, G., Sultan, N., Savoye, B., 2007. The 1979 Nice harbour catastrophe revisited: Trigger mechanism inferred from geotechnical measurements and numerical modelling. Mar. Geol. 245, 40–64. https://doi.org/10.1016/j.margeo.2007.06.011

Deiana, G., Meleddu, A., Paliaga, E., Todde, S., Orrù, P.E., 2015. Landslides and pockforms of southern sardinian margin. Geomorphol. Soc. 0. https://doi.org/10.13125/gfs-1901

Del Ben, A., Barnaba, C., Taboga, A., 2007. Strike-slip systems as the main tectonic features in the Plio-Quaternary kinematics of the Calabrian Arc. Mar. Geophys. Res. 29, 1–12. https://doi.org/10.1007/s11001-007-9041-6

dos Reis, A.T., Silva, C.G., Gorini, M.A., Leão, R., Pinto, N., Perovano, R., Santos, M.V.M., Guerra, J.V., Jeck, I.K., Tavares, A.A.A., 2016. The Chuí Megaslide Complex: Regional-Scale Submarine Landslides on the Southern Brazilian Margin, in: Lamarche, G., Mountjoy, J., Bull, S., Hubble, T., Krastel, S., Lane, E., Micallef, A., Moscardelli, L., Mueller, C., Pecher, I., Woelz, S. (Eds.), Submarine Mass Movements and Their Consequences. Springer International Publishing, Cham, pp. 115–123. https://doi.org/10.1007/978-3-319-20979-1_11

Dugan, B., Flemings, P.B., 2000. Overpressure and Fluid Flow in the New Jersey Continental Slope: Implications for Slope Failure and Cold Seeps. Science 289, 288–291. https://doi.org/10.1126/science.289.5477.288

Duggen, S., Hoernle, K., Bogaard, P. van den, Rüpke, L., Morgan, J.P., 2003. Deep roots of the Messinian salinity crisis. Nature 422, 602–606. https://doi.org/10.1038/nature01553

Dunbar, C.O., Rodgers, D., 1957. Principles of Stratigraphy. John WIley Sons 356. https://doi.org/10.1017/S0016756800070291

Edelmann, H., 1968. An underwater sound source with higher seismic efficiency. Geophys Prospect 16, 474–490.

Elger, J., Berndt, C., Rüpke, L., Krastel, S., Gross, F., Geissler, W.H., 2018. Submarine slope failures due to pipe structure formation. Nat. Commun. 9. https://doi.org/10.1038/s41467-018-03176-1

Elverhøi, A., Blasio, F.V. de, Butt, F.A., Issler, D., Harbitz, C., Engvik, L., Solheim, A., Marr, J., 2002. Submarine mass-wasting on glacially-influenced continental slopes: processes and dynamics. Geol. Soc. Lond. Spec. Publ. 203, 73–87. https://doi.org/10.1144/GSL.SP.2002.203.01.05

Embley, R.W., 1976. New evidence for occurrence of debris flow deposits in the deep sea. Geology 4, 371–374. https://doi.org/10.1130/0091-7613(1976)4<371:NEFOOD>2.0.CO;2

Ercilla, G., Casas, D., 2012. Submarine Mass Movements: Sedimentary Charaterization and Controlling Factors.

Ercilla, G., Wynn, R.B., Alonso, B., Baraza, J., 2002. Initiation and evolution of turbidity current sediment waves in the Magdalena turbidite system. Mar. Geol. 192, 153–169. https://doi.org/10.1016/S0025-3227(02)00553-4

Faccenna, C., Becker, T.W., Lucente, F.P., Jolivet, L., Rossetti, F., 2001. History of subduction and back arc extension in the Central Mediterranean. Geophys. J. Int. 145, 809–820. https://doi.org/10.1046/j.0956-540x.2001.01435.x

Fei, A., 2013. Slope stability along active and passive continental margins: a geotechnical approach. Faculty of Geoscience of Bremen University.

Feng, Y., Steinberg, J., Reshef, M., 2017. The Messinian evaporites in the Levant Basin: lithology, deformation and its evolution. Presented at the EGU General Assembly Conference Abstracts, p. 376.

Frey-Martínez, J., Cartwright, J., James, D., 2006. Frontally confined versus frontally emergent submarine landslides: A 3D seismic characterisation. Mar. Pet. Geol. 23, 585–604. https://doi.org/10.1016/j.marpetgeo.2006.04.002

Gallais, F., Gutscher, M.-A., Klaeschen, D., Graindorge, D., 2012. Two-stage growth of the Calabrian accretionary wedge in the Ionian Sea (Central Mediterranean): Constraints from depth-migrated multichannel seismic data. Mar. Geol. 326–328, 28–45. https://doi.org/10.1016/j.margeo.2012.08.006

Gamboa, D., Alves, T., Cartwright, J., 2012. Seismic-Scale Rafted and Remnant Blocks over Salt Ridges in the Espírito Santo Basin, Brazil, in: Submarine Mass Movements and Their Consequences, Advances in Natural and Technological Hazards Research. Springer, Dordrecht, pp. 629–638. https://doi.org/10.1007/978-94-007-2162-3_56

Ganas, A., Parsons, T., 2009. Three-dimensional model of Hellenic Arc deformation and origin of the Cretan uplift. J. Geophys. Res. Solid Earth 114. https://doi.org/10.1029/2008JB005599

Garcia-Castellanos, D., Estrada, F., Jiménez-Munt, I., Gorini, C., Fernàndez, M., Vergés, J., Vicente, R.D., 2009. Catastrophic flood of the Mediterranean after the Messinian salinity crisis. Nature 462, 778–781. https://doi.org/10.1038/nature08555

Garcia-Castellanos, D., Villaseñor, A., 2011. Messinian salinity crisis regulated by competing tectonics and erosion at the Gibraltar arc. Nature 480, 359–363. https://doi.org/10.1038/nature10651

Gargani, J., Rigollet, C., 2007. Mediterranean Sea level variations during the Messinian salinity crisis. Geophys. Res. Lett. 34. https://doi.org/10.1029/2007GL029885

Gaullier, V., Bellaiche, G., 1998. Near-Bottom Sedimentation Processes Revealed by Echo-Character Mapping Studies, Northwestern Mediterranean Basin. AAPG Bull. 82, 1140–1155.

Gautier, F., Clauzon, G., Suc, J.-P., Cravatte, J., Violanti, D., 1998. Age et durée de la crise de salinité messinienne. Comptes-Rendus L'Académie Sci. Paris 1103–1109.

Gee, M.J.R., Gawthorpe, R.L., Friedmann, J.S., 2005. Giant striations at the base of a submarine landslide. Mar. Geol. 214, 287–294. https://doi.org/10.1016/j.margeo.2004.09.003

Gee, M.J.R., Gawthorpe, R.L., Friedmann, S.J., 2006. Triggering and Evolution of a Giant Submarine Landslide, Offshore Angola, Revealed by 3D Seismic Stratigraphy and Geomorphology. J. Sediment. Res. 76, 9–19. https://doi.org/10.2110/jsr.2006.02

Gee, M.J.R., Uy, H.S., Warren, J., Morley, C.K., Lambiase, J.J., 2007. The Brunei slide: A giant submarine landslide on the North West Borneo Margin revealed by 3D seismic data. Mar. Geol. 246, 9–23. https://doi.org/10.1016/j.margeo.2007.07.009

Goes, S., Giardini, D., Jenny, S., Hollenstein, C., Kahle, H.-G., Geiger, A., 2004. A recent tectonic reorganization in the south-central Mediterranean. Earth Planet. Sci. Lett. 226, 335–345. https://doi.org/10.1016/j.epsl.2004.07.038

Gorini, C., Montadert, L., Rabineau, M., 2015. New imaging of the salinity crisis: Dual Messinian lowstand megasequences recorded in the deep basin of both the eastern and western Mediterranean. Mar. Pet. Geol. 66, 278–294. https://doi.org/10.1016/j.marpetgeo.2015.01.009

Govers, R., Meijer, P., Krijgsman, W., 2009. Regional isostatic response to Messinian Salinity Crisis events. Tectonophysics 463, 109–129. https://doi.org/10.1016/j.tecto.2008.09.026

Grant, J.A., Schreiber, R., 1990. Modern swathe sounding and sub-bottom profiling technology for research applications: The Atlas Hydrosweep and Parasound Systems. Mar. Geophys. Res. 12, 9–19. https://doi.org/10.1007/BF00310559

Gueguen, E., Doglioni, C., Fernandez, M., 1998. On the post-25 Ma geodynamic evolution of the western Mediterranean. Tectonophysics 298, 259–269. https://doi.org/10.1016/S0040-1951(98)00189-9

Guillaume, B., Funiciello, F., Faccenna, C., Martinod, J., Olivetti, V., 2010. Spreading pulses of the Tyrrhenian Sea during the narrowing of the Calabrian slab. Geology 38, 819–822. https://doi.org/10.1130/G31038.1

Gutscher, M.-A., Dominguez, S., Lepinay, B.M. de, Pinheiro, L., Gallais, F., Babonneau, N., Cattaneo, A., Faou, Y.L., Barreca, G., Micallef, A., Rovere, M., 2015. Tectonic expression of an active slab tear from high-resolution seismic and bathymetric data offshore Sicily (Ionian Sea). Tectonics 35, 39–54. https://doi.org/10.1002/2015TC003898

Gutscher, M.-A., Kopp, H., Krastel, S., Bohrmann, G., Garlan, T., Zaragosi, S., Klaucke, I., Wintersteller, P., Loubrieu, B., Le Faou, Y., San Pedro, L., Dominguez, S., Rovere, M., Mercier de Lepinay, B., Ranero, C., Sallares, V., 2017. Active tectonics of the Calabrian subduction revealed by new multi-beam bathymetric data and high-resolution seismic profiles in the Ionian Sea (Central Mediterranean). Earth Planet. Sci. Lett. 461, 61–72. https://doi.org/10.1016/j.epsl.2016.12.020

Hampton, M.A., Bouma, A.H., 1977. Slope instability near the shelf break, Western Gulf of Alaska*. Mar. Geotechnol. 2, 309–331. https://doi.org/10.1080/10641197709379786

Hampton, M.A., Lee, H.J., Locat, J., 1996a. Submarine landslides. Rev. Geophys. 34, 33–59. https://doi.org/10.1029/95RG03287

Hampton, M.A., Lee, H.J., Locat, J., 1996b. Submarine landslides. Rev. Geophys. 34, 33–59. https://doi.org/10.1029/95RG03287

Hansen, L., L'heureux, J.S., Longva, O., 2011. Turbiditic, clay-rich event beds in fjord-marine deposits caused by landslides in emerging clay deposits – palaeoenvironmental interpretation and role for submarine mass-wasting. Sedimentology 58, 890–915. https://doi.org/10.1111/j.1365-3091.2010.01188.x

Hardage, B., 1985. Vertical seismic profiling. Lead. Edge 4, 59–59. https://doi.org/10.1190/1.1487141

Hill, P.R., Moran, K.M., Blasco, S.M., 1982. Creep deformation of slope sediments in the Canadian Beaufort Sea. Geo-Mar. Lett. 2, 163. https://doi.org/10.1007/BF02462758

Hovland, M., Gardner, J.V., Judd, A.G., 2002. The significance of pockmarks to understanding fluid flow processes and geohazards. Geofluids 2, 127–136. https://doi.org/10.1046/j.1468-8123.2002.00028.x

Hsü, K.J., Cita, M.B., Ryan, W.B.F., Dumitrica, P., Lort, J.M., Maync, W., Nesteroff, W.D., Pautot, G., Stradner, H., Wezel, F.C., Forese, C., Kaneps, A.G., 1973. The origin of the Mediterranean evaporite, in: Initial Reports of the Deep Sea Drilling Project, Covering Leg 13 of the Cruises of the Drilling Vessel Glomar Challenger Lisbon, Portugal to Lisbon, Portugal, August-October.

Hutchins, R.W., Mckeown, D.L., King, L.H., 1976. A Deep Tow High Resolution Seismic System for Continental Shelf Mapping. Geosci. Can. 3.

Huvenne, V.A.I., Croker, P.F., Henriet, J.-P., 2002. A refreshing 3D view of an ancient sediment collapse and slope failure. Terra Nova 14, 33–40. https://doi.org/10.1046/j.1365-3121.2002.00386.x

Jacobi, R.D., 1976. Sediment slides on the northwestern continental margin of Africa. Mar. Geol. 22, 157–173. https://doi.org/10.1016/0025-3227(76)90045-1

Jolivet, L., Augier, R., Robin, C., Suc, J.-P., Rouchy, J.M., 2006. Lithospheric-scale geodynamic context of the Messinian salinity crisis. Sediment. Geol. 188–189, 9–33. https://doi.org/10.1016/j.sedgeo.2006.02.004

Kawamura, K., Sakaguchi, A., Strasser, M., Anma, R., Ikeda, H., 2012. Detailed Observation of Topography and Geologic Architecture of a Submarine Landslide Scar in a Toe of an Accretionary Prism, in: Submarine Mass Movements and Their Consequences, Advances in Natural and Technological Hazards Research. Springer, Dordrecht, pp. 301–309. https://doi.org/10.1007/978-94-007-2162-3_27

Kokusho, T., Kojima, T., 2002. Mechanism for Postliquefaction Water Film Generation in Layered Sand. J. Geotech. Geoenvironmental Eng. 128, 129–137. https://doi.org/10.1061/(ASCE)1090-0241(2002)128:2(129)

Kremer, K., Usman, M.O., Satoguchi, Y., Nagahashi, Y., Vadakkepuliyambatta, S., Panieri, G., Strasser, M., 2017. Possible climate preconditioning on submarine landslides along a convergent margin, Nankai Trough (NE Pacific). Prog. Earth Planet. Sci. 4. https://doi.org/10.1186/s40645-017-0134-9

Krijgsman, W., Hilgen, F.J., Raffi, I., Sierro, F.J., Wilson, D.S., 1999. Chronology, causes and progression of the Messinian salinity crisis. Nature 400, 652–655. https://doi.org/10.1038/23231

Kvalstad, T.J., Andresen, L., Forsberg, C.F., Berg, K., Bryn, P., Wangen, M., 2005. The Storegga slide: Evaluation of triggering sources and slide mechanics. Mar. Pet. Geol. 22, 245–256. https://doi.org/10.1016/j.marpetgeo.2004.10.019

Laberg, J.S., Camerlenghi, A., 2008. Chapter 25 The Significance of Contourites for Submarine Slope Stability, Developements in Sedimentology. Rebesco M., Camerlenghi A. https://doi.org/10.1016/S0070-4571(08)10025-5

Laberg, J.S., Vorren, T.O., Mienert, J., Haflidason, H., Bryn, P., Lien, R., 2003. Preconditions Leading to the Holocene Trænadjupet Slide Offshore Norway, in: Submarine Mass Movements and Their Consequences, Advances in Natural and Technological Hazards Research. Springer, Dordrecht, pp. 247–254. https://doi.org/10.1007/978-94-010-0093-2_28

Lajoie, K.R., Ponti, D.J., Powell, C.L., Mathieson, S.A., Sarna-Wojcicki, A.M., 1991. Emergent marine strandlines and associated sediments, coastal California; a record of Quaternary sea-level fluctuations, vertical tectonic movements, climate changes, and coastal processes, in: Quaternary Non-Glacial Geology: Conterminous United States. Geological Society of America. pp. 190–214.

Lastras, G., Canals, M., Urgeles, R., Hughes-Clarke, J.E., Acosta, J., 2004a. Shallow slides and pockmark swarms in the Eivissa Channel, western Mediterranean Sea. Sedimentology 51, 837–850. https://doi.org/10.1111/j.1365-3091.2004.00654.x

Lastras, G., Canals, M., Urgeles, R., Hughes-Clarke, J.E., Acosta, J., 2004b. Shallow slides and pockmark swarms in the Eivissa Channel, western Mediterranean Sea. Sedimentology 51, 837–850. https://doi.org/10.1111/j.1365-3091.2004.00654.x

Lee, H.J., 2005. Undersea landslides: extent and significance in the Pacific Ocean, an update. Nat. Hazards Earth Syst. Sci. 5, 877–892. https://doi.org/10.5194/nhess-5-877-2005

Lee, H.J., Locat, J., Desgagnés, P., Parsons, J.D., McAdoo, B.G., Orange, D.L., Puig, P., Wong, F.L., Dartnell, P., Boulanger, E., 2009. Submarine Mass Movements on Continental Margins, in: Continental Margin Sedimentation. Wiley-Blackwell, pp. 213–274. https://doi.org/10.1002/9781444304398.ch5

Lee, S.H., Chough, S.K., 2001. High-resolution (2–7 kHz) acoustic and geometric characters of submarine creep deposits in the South Korea Plateau, East Sea. Sedimentology 48, 629–644. https://doi.org/10.1046/j.1365-3091.2001.00383.x

Leslie, S.C., Mann, P., 2016. Giant submarine landslides on the Colombian margin and tsunami risk in the Caribbean Sea. Earth Planet. Sci. Lett. 449, 382–394. https://doi.org/10.1016/j.epsl.2016.05.040

Levesque, C., 2004. Preliminary overview of the morphology in the Saguenay Fjord with a particular look at mass movements. Proc. 57th Can. Geotech. Conf. Quebec 6, 23–30.

Lewis, K.B., 1971. Slumping on a Continental Slope Inclined at 1°–4°. Sedimentology 16, 97–110. https://doi.org/10.1111/j.1365-3091.1971.tb00221.x

L'Heureux, J.-S., Longva, O., Steiner, A., Hansen, L., Vardy, M.E., Vanneste, M., Haflidason, H., Brendryen, J., Kvalstad, T.J., Forsberg, C.F., Chand, S., Kopf, A., 2012. Identification of Weak Layers and Their Role for the Stability of Slopes at Finneidfjord, Northern Norway, in: Yamada, Y., Kawamura, K., Ikehara, K., Ogawa, Y., Urgeles, R., Mosher, D., Chaytor, J., Strasser, M. (Eds.), Submarine Mass Movements and Their Consequences. Springer Netherlands, Dordrecht, pp. 321–330. https://doi.org/10.1007/978-94-007-2162-3_29

Li, G., Campbell, D.C., Mosher, D., Piper, D.J.W., 2012. Comparison of Quaternary Glaciogenic Debris Flows with Blocky Mass-Transport Deposits in Orphan Basin, Offshore Eastern Canada, in: Yamada, Y., Kawamura, K., Ikehara, K., Ogawa, Y., Urgeles, R., Mosher, D., Chaytor, J., Strasser, M. (Eds.), Submarine Mass Movements and Their Consequences. Springer Netherlands, Dordrecht, pp. 723–733. https://doi.org/10.1007/978-94-007-2162-3_64

Locat, J., Lee, H.J., 2002. Submarine landslides: advances and challenges. Can. Geotech. J. 39, 193–212. https://doi.org/10.1139/t01-089

Locat, J., Leroueil, S., Locat, A., Lee, H., 2014. Weak Layers: Their Definition and Classification from a Geotechnical Perspective, in: Submarine Mass Movements and Their Consequences, Advances in Natural and Technological Hazards Research. Springer, Cham, pp. 3–12. https://doi.org/10.1007/978-3-319-00972-8_1

Lofi, J., Déverchère, J., Gaullier, V., Gillet, H., Gorini, C., Guennoc, P., Loncke, L., Maillard, A., Sage, F., Thinon, I., 2012. Seismic atlas of the "Messinian Salinity Crisis" markers in the Mediterranean and Black seas, Nouvelle Série.

Lofi, J., Gorini, C., Berne, S., Clauzon, G., Dos Reis, A.T., Ryan, W., Steckler, M., 2005. Erosional processes and paleo-environmental changes in the Western Gulf of Lions (SW France) during the Messinian Salinity Crisis. Mar. Geol. 217, 1–30. https://doi.org/10.1016/j.margeo.2005.02.014

Loher, M., Ceramicola, S., Wintersteller, P., Meinecke, G., Sahling, H., Bohrmann, G., 2018a. Mud Volcanism in a Canyon: Morphodynamic Evolution of the Active Venere Mud Volcano and Its Interplay With Squillace Canyon, Central Mediterranean. Geochem. Geophys. Geosystems 19, 356–378. https://doi.org/10.1002/2017GC007166

Loher, M., Marcon, Y., Pape, T., Römer, M., Wintersteller, P., dos, S.F., Praeg, D., Torres, M., Sahling, H., Bohrmann, G., 2018b. Seafloor sealing, doming, and collapse associated with gas seeps and authigenic carbonate structures at Venere mud volcano, Central Mediterranean. Deep-Sea Res. Part Oceanogr. Res. Pap. 137, 76–96. https://doi.org/10.1016/j.dsr.2018.04.006

Loncke, L., Droz, L., Gaullier, V., Basile, C., Patriat, M., Roest, W., 2009. Slope instabilities from echo-character mapping along the French Guiana transform margin and Demerara abyssal plain. Mar. Pet. Geol. 26, 711–723. https://doi.org/10.1016/j.marpetgeo.2008.02.010

Longhitano, S.G., Chiarella, D., Muto, F., 2014. Three-dimensional to two-dimensional cross-strata transition in the lower Pleistocene Catanzaro tidal strait transgressive succession (southern Italy). Sedimentology 61, 2136–2171. https://doi.org/10.1111/sed.12138

Longva, O., Janbu, N., Blikra, L.H., Bøe, R., 2003. The 1996 Finneidfjord Slide; Seafloor Failure and Slide Dynamics, in: Submarine Mass Movements and Their Consequences, Advances in Natural and Technological Hazards Research. Springer, Dordrecht, pp. 531–538. https://doi.org/10.1007/978-94-010-0093-2_58

Maesano, F.E., Tiberti, M.M., Basili, R., 2017. The Calabrian Arc: three-dimensional modelling of the subduction interface. Sci. Rep. 7, 8887. https://doi.org/10.1038/s41598-017-09074-8

Malinverno, A., Ryan, W.B.F., 1986. Extension in the Tyrrhenian Sea and shortening in the Apennines as result of arc migration driven by sinking of the lithosphere. Tectonics 5, 227–245. https://doi.org/10.1029/TC005i002p00227

Martinsen, O., 1994. Mass movements. Springer Netherlands, pp. 127–165. https://doi.org/10.1007/978-94-011-0731-0_5

Massari, F., Prosser, G., 2013. Late Cenozoic tectono-stratigraphic sequences of the Crotone Basin: insights on the geodynamic history of the Calabrian arc and Tyrrhenian Sea. Basin Res. 25, 26–51. https://doi.org/10.1111/j.1365-2117.2012.00549.x

Massari, F., Prosser, G., Capraro, L., Fornaciari, E., Consolaro, C., 2010. A revision of the stratigraphy and geology of the south-western part of the Crotone Basin (South Italy). Ital. J. Geosci. 353–384. https://doi.org/10.3301/IJG.2010.20

Masson, D.G., Harbitz, C.B., Wynn, R.B., Pedersen, G., Lovholt, F., 2006. Submarine landslides: processes, triggers and hazard prediction. Philos. Trans. R. Soc. Math. Phys. Eng. Sci. 364, 2009–2039. https://doi.org/10.1098/rsta.2006.1810

Masson, D.G., Wynn, R.B., Talling, P.J., 2010. Large Landslides on Passive Continental Margins: Processes, Hypotheses and Outstanding Questions, in: Submarine Mass Movements and Their Consequences, Advances in Natural and Technological Hazards Research. Springer, Dordrecht, pp. 153–165. https://doi.org/10.1007/978-90-481-3071-9_13

McAdoo, B.., Pratson, L.., Orange, D.., 2000. Submarine landslide geomorphology, US continental slope. Mar. Geol. 169, 103–136. https://doi.org/10.1016/s0025-3227(00)00050-5

McGee, T.M., 2000. Pushing the Limits of High-Resolution in Marine Seismic Profiling. J. Environ. Eng. Geophys. 5, 43–53. https://doi.org/10.4133/JEEG5.4.43

Micallef, A., Camerlenghi, A., Garcia-Castellanos, D., Otero, D.C., Gutscher, M.-A., Barreca, G., Spatola, D., Facchin, L., Geletti, R., Krastel, S., Gross, F., Urlaub, M., 2018. Evidence of the Zanclean megaflood in the eastern Mediterranean Basin. Sci. Rep. 8, 1078. https://doi.org/10.1038/s41598-018-19446-3

Minelli, L., Billi, A., Faccenna, C., Gervasi, A., Guerra, I., Orecchio, B., Speranza, G., 2013. Discovery of a gliding salt-detached megaslide, Calabria, Ionian Sea, Italy: ACTIVE SALT-DETACHED MEGASLIDE. Geophys. Res. Lett. 40, 4220–4224. https://doi.org/10.1002/grl.50818

Minelli, L., Faccenna, C., 2010. Evolution of the Calabrian accretionary wedge (central Mediterranean). Tectonics 29, n/a-n/a. https://doi.org/10.1029/2009TC002562

Minisini D., Trincardi F., 2009. Frequent failure of the continental slope: The Gela Basin (Sicily Channel). J. Geophys. Res. Earth Surf. 114. https://doi.org/10.1029/2008JF001037

Mitchum, R.M., Vail, P.R., 1977. Seismic Stratigraphy and Global Changes of Sea Level: Part 7. Seismic Stratigraphic Interpretation Procedure: Section 2. Application of Seismic Reflection Configuration to Stratigraphic Interpretation 165, 135–143.

Morelli, D., Cuppari, A., Colizza, E., Fanucci, F., 2011. Geomorphic setting and geohazard-related features along the Ionian Calabrian margin between Capo Spartivento and Capo Rizzuto (Italy). Mar. Geophys. Res. 32, 139–149. https://doi.org/10.1007/s11001-011-9130-4

Moscardelli, L., Wood, L., 2015. Morphometry of mass-transport deposits as a predictive tool. Geol. Soc. Am. Bull. B31221.1. https://doi.org/10.1130/B31221.1

Moscardelli, L., Wood, L., 2008. New classification system for mass transport complexes in offshore Trinidad. Basin Res. 20, 73–98. https://doi.org/10.1111/j.1365-2117.2007.00340.x

Moscardelli, L., Wood, L., Mann, P., 2008. Mass-transport complexes and associated processes in the offshore area of Trinidad and Venezuela. AAPG Bull. 90, 1059–1088. https://doi.org/10.1306/02210605052

Mosher, D.C., Simpkin, P.G., 1999. Environmental Marine Geoscience 1. Status and Trends of Marine High-Resolution Seismic Reflection Profiling: Data Acquistion. Geosci. Can. 26.

Mulder, T., 2011. Gravity Processes and Deposits on Continental Slope, Rise and Abyssal Plains, in: Developments in Sedimentology. Elsevier, pp. 25–148. https://doi.org/10.1016/B978-0-444-53000-4.00002-0

Mulder, T., Cochonat, P., 1996. Classification of Offshore Mass Movements. SEPM J. Sediment. Res. Vol. 66. https://doi.org/10.1306/D42682AC-2B26-11D7-8648000102C1865D

Nardin, T.R., Hein, F.J., Girsline, D.S., Edwards, B.D., 1979. A review of mass movement processes, sediement and acoustic characteristics, and contrasts in slope and base-of-slope systems versus canyon-fan-basin floor system. SEPM (Society for Sedimentary Geology), pp. 61–73. https://doi.org/10.2110/pec.79.27.0061

O'Leary, D.W., 1991. Structure and morphology of submarine slab slides: Clues to origin and behavior. Mar. Geotechnol. 10, 53–69. https://doi.org/10.1080/10641199109379882

Owen, M., Day, S., Maslin, M., 2007a. Late Pleistocene submarine mass movements: occurrence and causes. Quat. Sci. Rev. 26, 958–978. https://doi.org/10.1016/j.quascirev.2006.12.011

Owen, M., Day, S., Maslin, M., 2007b. Late Pleistocene submarine mass movements: occurrence and causes. Quat. Sci. Rev. 26, 958–978. https://doi.org/10.1016/j.quascirev.2006.12.011

Patacca, E., Sartori, R., Scandone, P., 1990. Tyrrhenian basin and Apenninic arcs: kinematic relations since Late Tortonian times. Mem Soc Geolg Ital 45, 425–451.

Polonia, A., Torelli, L., Artoni, A., Carlini, M., Faccenna, C., Ferranti, L., Gasperini, L., Govers, R., Klaeschen, D., Monaco, C., Neri, G., Nijholt, N., Orecchio, B., Wortel, R., 2016. The Ionian and Alfeo–Etna fault zones: New segments of an evolving plate boundary in the central Mediterranean Sea? Tectonophysics 675, 69–90. https://doi.org/10.1016/j.tecto.2016.03.016

Polonia, A., Torelli, L., Mussoni, P., Gasperini, L., Artoni, A., Klaeschen, D., 2011. The Calabrian Arc subduction complex in the Ionian Sea: Regional architecture, active deformation, and seismic hazard. Tectonics 30. https://doi.org/10.1029/2010TC002821

Posamentier, H.W., Jersey, M.T., Vail, P.R., 1988. Eustatic controls on clastic deposition I. Conceptual framework. SEMP Spec. Pub. 42 Sea-Level changes an Integrated approach, 127–136.

Posamentier, H.W., Kolla, V., 2003a. Seismic Geomorphology and Stratigraphy of Depositional Elements in Deep-Water Settings. J. Sediment. Res. 73, 367–388. https://doi.org/10.1306/111302730367

Posamentier, H.W., Kolla, V., 2003b. Seismic Geomorphology and Stratigraphy of Depositional Elements in Deep-Water Settings. J. Sediment. Res. 73, 367–388. https://doi.org/10.1306/111302730367

Posamentier, H.W., Martinsen, O., 2011. The Character and Genesis of Submarine Mass-Transport Deposits: Insights from Outcrop and 3D Seismic Data. SEPM (Society for Sedimentary Geology), pp. 7–38. https://doi.org/10.2110/sepmsp.096.007

Posamentier, H.W., Vail, P.R., 1988. Eustatic controls on clastic deposition II – sequence and system track models. Soc Econ Paleontol Miner. Spec Pub Sea level changes an integrated approach, 110–124.

Praeg, D., Ceramicola, S., Barbieri, R., Unnithan, V., Wardell, N., 2009. Tectonically-driven mud volcanism since the late Pliocene on the Calabrian accretionary prism, central Mediterranean Sea. Mar. Pet. Geol., Mud Volcanism: Processes and Implications 26, 1849–1865. https://doi.org/10.1016/j.marpetgeo.2009.03.008

Pratson, L.., Laine, E.P., 1989. The relative importance of gravity-induced versus current-controlled sedimentation during the Quaternary along the Mideast U.S. outer continental margin revealed by 3.5 kHz echo character. Mar. Geol. 89, 87–126. https://doi.org/10.1016/0025-3227(89)90029-7

Presti, D., Billi, A., Orecchio, B., Totaro, C., Faccenna, C., Neri, G., 2013. Earthquake focal mechanisms, seismogenic stress, and seismotectonics of the Calabrian Arc, Italy. Tectonophysics 602, 153–175. https://doi.org/10.1016/j.tecto.2013.01.030

Prior, D.B., Bornhold, B.D., Johns, M.W., 1984. Depositional Characteristics of a Submarine Debris Flow. J. Geol. 92, 707–727.

Puig, P., Ogston, A.S., Mullenbach, B.L., Nittrouer, C.A., Parsons, J.D., Sternberg, R.W., 2004. Storm-induced sediment gravity flows at the head of the Eel submarine canyon, northern California margin. J. Geophys. Res. Oceans 109. https://doi.org/10.1029/2003jc001918

Roda, C., 1964. Distribuzione e facies dei sedimenti Neogenici nel Bacino Crotonese. Geol Roman 3, 319–366.

Rogers, K.G., Goodbred, S.L., 2010. Mass failures associated with the passage of a large tropical cyclone over the Swatch of No Ground submarine canyon (Bay of Bengal). Geology 38, 1051–1054. https://doi.org/10.1130/g31181.1

Romagnoli, C., Gabbianelli, G., 1990. Late Quaternary sedimentation and soft-sediment deformation features in the Corigliano Basin, North Ionian Sea (Mediterranean). G. Geol. 52, 33–53.

Rossi, S., Sartori, R., 1981. A seismic reflection study of the External Calabrian Arc in the northern Ionian Sea (eastern Mediterranean). Mar. Geophys. Res. 4, 403–426. https://doi.org/10.1007/BF00286036

Roveri, M., Flecker, R., Krijgsman, W., Lofi, J., Lugli, S., Manzi, V., Sierro, F.J., Bertini, A., Camerlenghi, A., De Lange, G., Govers, R., Hilgen, F.J., Hübscher, C., Meijer, P.T., Stoica, M., 2014. The Messinian Salinity Crisis: Past and future of a great challenge for marine sciences. Mar. Geol. 352, 25–58. https://doi.org/10.1016/j.margeo.2014.02.002

Royden, L., Faccenna, C., 2018. Subduction Orogeny and the Late Cenozoic Evolution of the Mediterranean Arcs. Annu. Rev. Earth Planet. Sci. 46, 261–289. https://doi.org/10.1146/annurev-earth-060115-012419

Ruano, P., Bohoyo, F., Galindo-Zaldívar, J., Pérez, L.F., Hernández-Molina, F.J., Maldonado, A., García, M., Medialdea, T., 2014. Mass transport processes in the southern Scotia Sea: Evidence of paleoearthquakes. Glob. Planet. Change 123, 374–391. https://doi.org/10.1016/j.gloplacha.2014.06.009

Ryan, W.B.F., 2011. Geodynamic responses to a two-step model of the Messinian salinity crisis. Bull. Société Géologique Fr. 182, 73–78. https://doi.org/10.2113/gssgfbull.182.2.73

Ryan, W.B.F., 2009. Decoding the Mediterranean salinity crisis. Sedimentology 56, 95–136. https://doi.org/10.1111/j.1365-3091.2008.01031.x

Ryan, W.B.F., 1976. Quantitative evaluation of the depth of the western Mediterranean before, during and after the Late Miocene salinity crisis. Sedimentology 23, 791–813. https://doi.org/10.1111/j.1365-3091.1976.tb00109.x

Sartori, R., 2003. The Tyrrhenian back-arc basin and subduction of the Ionian lithosphere. Episodes 26, 21–46.

Sartori, R., 1990. The main results of OPD Leg 107 in the frame of Neogene to Recent geology of peri-Tyrrhenian areas, in: Proceedings of the Ocean Drilling Program. Scientific Results, Ocean Drilling Program. Kastens, K.A., Mascle, J., et al., College Station, Texas, pp. 715–730.

Sawyer, D., Akinci, L., Nikolinakou, M.A., Heidari, M., 2015. Links and Feedbacks between Salt Diapirs, Hydrates, and Submarine Landslides: Example from Cape Fear, offshore North Carolina, U.S.A. Presented at the 2015 AGU Fall Meeting, Agu.

Scarfì, L., Barberi, G., Barreca, G., Cannavò, F., Koulakov, I., Patanè, D., 2018. Slab narrowing in the Central Mediterranean: the Calabro-Ionian subduction zone as imaged by high resolution seismic tomography. Sci. Rep. 8, 5178. https://doi.org/10.1038/s41598-018-23543-8

Seed, H.B., Rahman, M.S., 1978. Wave-induced pore pressure in relation to ocean floor stability of cohesionless soils. Mar. Geotechnol. 3, 123–150. https://doi.org/10.1080/10641197809379798

Selvaggi, G., Chiarabba, C., 1995. Seismicity and P-wave velocity image of the Southern Tyrrhenian subduction zone. Geophys. J. Int. 121, 818–826. https://doi.org/10.1111/j.1365-246X.1995.tb06441.x

Shanmugam, G., 2016. Slides, Slumps, Debris Flows, Turbidity Currents, Hyperpycnal Flows, and Bottom Currents ☆, in: Reference Module in Earth Systems and Environmental Sciences. Elsevier. https://doi.org/10.1016/B978-0-12-409548-9.10884-X

Silva, C.C., dos Reis, A.T., Perovano, R.J., Gorini, M.A., dos Santos, M.V.M., Jeck, I.K., Tavares, A.A.A., Gorini, C., 2016. Multiple Megaslide Complexes and Their Significance for the Miocene Stratigraphic Evolution of the Offshore Amazon Basin, in: Lamarche, G., Mountjoy, J., Bull, S., Hubble, T., Krastel, S., Lane, E., Micallef, A., Moscardelli, L., Mueller, C., Pecher, I., Woelz, S. (Eds.), Submarine Mass Movements and Their Consequences. Springer International Publishing, Cham, pp. 49–60. https://doi.org/10.1007/978-3-319-20979-1_5

Silva, C.G., Araújo, E., Reis, A.T., Perovano, R., Gorini, C., Vendeville, B.C., Albuquerque, N., 2010. Megaslides in the Foz do Amazonas Basin, Brazilian Equatorial Margin, in: Mosher, D.C., Shipp, R.C., Moscardelli, L., Chaytor, J.D., Baxter, C.D.P., Lee, H.J., Urgeles, R. (Eds.), Submarine Mass Movements and Their Consequences. Springer Netherlands, Dordrecht, pp. 581–591. https://doi.org/10.1007/978-90-481-3071-9_47

Sloan, E.D., 2003. Fundamental principles and applications of natural gas hydrates. Nature 426, 353–359. https://doi.org/10.1038/nature02135

Smith, D.E., Harrison, S., Jordan, J.T., 2013a. Sea level rise and submarine mass failures on open continental margins. Quat. Sci. Rev. 82, 93–103. https://doi.org/10.1016/j.quascirev.2013.10.012

Smith, D.E., Harrison, S., Jordan, J.T., 2013b. Sea level rise and submarine mass failures on open continental margins. Quat. Sci. Rev. 82, 93–103. https://doi.org/10.1016/j.quascirev.2013.10.012

Sobiesiak, M.S., Kneller, B., Alsop, G.I., Milana, J.P., 2018. Styles of basal interaction beneath mass transport deposits. Mar. Pet. Geol. 98, 629–639. https://doi.org/10.1016/j.marpetgeo.2018.08.028

Strozyk, F., 2009. Submarine landslide in active margin environments - slope stability vs. neotectonic activity on the northeastern margin of Crete, eastern Mediterranean. University of Bremen.

Strozyk, F., Strasser, M., Krastel, S., Meyer, M., Huhn, K., 2010. Reconstruction of retreating mass wasting in response to progressive slope steepening of the northeastern Cretan margin, eastern Mediterranean. Mar. Geol. 271, 44–54. https://doi.org/10.1016/j.margeo.2010.01.008

Sultan, N., Cochonat, P., Canals, M., Cattaneo, A., Dennielou, B., Haflidason, H., Laberg, J.S., Long, D., Mienert, J., Trincardi, F., Urgeles, R., Vorren, T.O., Wilson, C., 2004a. Triggering mechanisms of slope instability processes and sediment failures on continental margins: a geotechnical approach. Mar. Geol. 213, 291–321. https://doi.org/10.1016/j.margeo.2004.10.011

Sultan, N., Cochonat, P., Foucher, J.-P., Mienert, J., 2004b. Effect of gas hydrates melting on seafloor slope instability. Mar. Geol., COSTA - Continental Slope Stability 213, 379–401. https://doi.org/10.1016/j.margeo.2004.10.015

Sultan, N., Voisset, M., Marsset, B., Marsset, T., Cauquil, E., Colliat, J., 2007. Potential role of compressional structures in generating submarine slope failures in the Niger Delta. Mar. Geol. 237, 169–190. https://doi.org/10.1016/j.margeo.2006.11.002

Tortorici, L., 1982. Lineamenti geologico-strutturali dell’arco Calabro-Peloritano. Rendiconti Della Soc. Ital. Mineral. E Petrol. 38, 927–940.

Trincardi, F., Normark, W.R., 1989. Pleistocene Suvero slide, Paola basin, southern Italy. Mar. Pet. Geol. 6, 324–335. https://doi.org/10.1016/0264-8172(89)90029-9

Tripsanas, E., Bryant, W., A. Phaneuf, B., 2004. Slope-instability processes caused by salt movements in a complex deep-water environment, Bryant Canyon area, northwest Gulf of Mexico. Aapg Bull. - AAPG BULL 88, 801–823. https://doi.org/10.1306/01260403106

Tripsanas, E.K., Bryant, W.R., Phaneuf, B.A., 2004. Depositional processes of uniform mud deposits (unifites), Hedberg Basin, northwest Gulf of Mexico: New perspectives. AAPG Bull. 88, 825–840.

Tripsanas, E.K., Bryant, W.R., Prior, D.B., Phaneuf, B.A., 2003. Interplay Between Salt Activities and Slope Instabilities, Bryant Canyon Area, Northwest Gulf of Mexico | SpringerLink, in: Submarine Mass Movements and Their Consequences, Advances in Natural and Technological Hazards Research. Locat J., Mienert J., Boisvert L. (eds).

Urgeles, R., Camerlenghi, A., 2013. Submarine landslides of the Mediterranean Sea: Trigger mechanisms, dynamics, and frequency-magnitude distribution. J. Geophys. Res. Earth Surf. 118, 2600–2618. https://doi.org/10.1002/2013JF002720

Urgeles, R., Locat, J., Sawyer, D.E., Flemings, P.B., Dugan, B., Binh, N.T.T., 2010. History of Pore Pressure Build Up and Slope Instability in Mud-Dominated Sediments of Ursa Basin, Gulf of Mexico Continental Slope, in: Submarine Mass Movements and Their Consequences, Advances in Natural and Technological Hazards Research. Springer, Dordrecht, pp. 179–190. https://doi.org/10.1007/978-90-481-3071-9_15

Urlaub, M., Talling, P.J., Masson, D.G., 2013a. Timing and frequency of large submarine landslides: implications for understanding triggers and future geohazard. Quat. Sci. Rev. 72, 63–82. https://doi.org/10.1016/j.quascirev.2013.04.020

Urlaub, M., Talling, P.J., Masson, D.G., 2013b. Timing and frequency of large submarine landslides: implications for understanding triggers and future geohazard. Quat. Sci. Rev. 72, 63–82. https://doi.org/10.1016/j.quascirev.2013.04.020

Urlaub, M., Zervos, A., Talling, P.J., Masson, D.G., Clayton, C.I., 2012. How Do ∼2° Slopes Fail in Areas of Slow Sedimentation? A Sensitivity Study on the Influence of Accumulation Rate and Permeability on Submarine Slope Stability, in: Submarine Mass Movements and Their Consequences, Advances in Natural and Technological Hazards Research. Springer, Dordrecht, pp. 277–287. https://doi.org/10.1007/978-94-007-2162-3_25

Vail, P.R., Jr, R.M.M., Iii, S.T., 1977. Seismic Stratigraphy and Global Changes of Sea Level: Part 3. Relative Changes of Sea Level from Coastal Onlap: Section 2. Application of Seismic Reflection Configuration to Stratigrapic Interpretation 165, 63–81.

van Dijk, J.P., 1991. Basin dynamics and sequence stratigraphy in the Calabrian Arc (Central Mediterranean); records and pathways of the Crotone Basin. Geol. En Mijnb. 70, 187–201.

van Dijk, J.P., 1990. Sequence stratigraphy, kinematics and dymanic geohistory of the Crotone Basin (Calabrian Arc, central Mediterranean): an integrated apporach. Mem Soc Geolg Ital 44, 259–285.

van Dijk, J.P., Bello, M., Brancaleoni, G.P., Cantarella, G., Costa, V., Frixa, A., Golfetto, F., Merlini, S., Riva, M., Torricelli, S., Toscano, C., Zerilli, A., 2000. A regional structural model for the northern sector of the Calabrian Arc (southern Italy). Tectonophysics 324, 267–320. https://doi.org/10.1016/S0040-1951(00)00139-6

van Dijk, J.P., Okkes, M., 1991. Neogene tectono-stratigraphy and kinematics of Calabrian basins; implications for the geodynamics of the Central Mediterranean. Tectonophysics 196, 23–60.

Varnes, D.J., 1978. Slope movement types and processes, in: Schuster, R.L., Krizek, R.J. (Eds.), Landslides, Analysis and Control, Special Report 176. Washington, pp. 11–33.

Veeken, P.H.C., 2006. Seismic Stratigraphy, Basin Analysis and Reservoir Characterisation, Volume 37 - 1st Edition, 1st ed.

Völker, D., Geersen, J., Behrmann, J.H., Weinrebe, W.R., 2012. Submarine Mass Wasting Off Southern Central Chile: Distribution and Possible Mechanisms of Slope Failure at an Active Continental Margin, in: Yamada, Y., Kawamura, K., Ikehara, K., Ogawa, Y., Urgeles, R., Mosher, D., Chaytor, J., Strasser, M. (Eds.), Submarine Mass Movements and Their Consequences. Springer Netherlands, Dordrecht, pp. 379–389. https://doi.org/10.1007/978-94-007-2162-3_34

Waelbroeck, C., Labeyrie, L., Michel, E., Duplessy, J.C., McManus, J.F., Lambeck, K., Balbon, M., Labracherie, M., 2002. Sea-level and deep water temperature changes derived from benthic foraminifera isotopic records. Quat. Sci. Rev. 21, 295–305. https://doi.org/10.1016/S0277-3791(01)00101-9

Westaway, R., 1993. Quaternary uplift of southern Italy. J. Geophys. Res. Solid Earth 98, 21741–21772. https://doi.org/10.1029/93JB01566

Wynn, R.B., Stow, D.A.V., 2002. Classification and characterisation of deep-water sediment waves. Mar. Geol. 192, 7–22. https://doi.org/10.1016/S0025-3227(02)00547-9

Yamada, Y., Kawamura, K., Ikehara, K., Ogawa, Y., Urgeles, R., Mosher, D., Chaytor, J., Strasser, M., 2012. Submarine Mass Movements and Their Consequences, in: Submarine Mass Movements and Their Consequences, Advances in Natural and Technological Hazards Research. Springer, Dordrecht, pp. 1–12. https://doi.org/10.1007/978-94-007-2162-3_1

Zecchin, M., Accaino, F., Ceramicola, S., Civile, D., Critelli, S., Lio, C.D., Mangano, G., Prosser, G., Teatini, P., Tosi, L., 2018. The Crotone Megalandslide, southern Italy: Architecture, timing and tectonic control. Sci. Rep. 8, 7778. https://doi.org/10.1038/s41598-018-26266-y

Zecchin, M., Caffau, M., Civile, D., Critelli, S., Di Stefano, A., Maniscalco, R., Muto, F., Sturiale, G., Roda, C., 2012. The Plio-Pleistocene evolution of the Crotone Basin (southern Italy): Interplay between sedimentation, tectonics and eustasy in the frame of Calabrian Arc migration. Earth-Sci. Rev. 115, 273–303. https://doi.org/10.1016/j.earscirev.2012.10.005

Zecchin, M., Caffau, M., Di Stefano, A., Maniscalco, R., Lenaz, D., Civile, D., Muto, F., Critelli, S., 2013a. The Messinian succession of the Crotone Basin (southern Italy) II: Facies architecture and stratal surfaces across the Miocene–Pliocene boundary. Mar. Pet. Geol. 48, 474–492. https://doi.org/10.1016/j.marpetgeo.2013.08.013

Zecchin, M., Caffau, M., Roda, C., 2011a. Relationships between high-magnitude relative sea-level changes and filling of a coarse-grained submarine canyon (Pleistocene, Ionian Calabria, Southern Italy): Coarse-grained submarine canyon fill in Southern Italy. Sedimentology 58, 1030–1064. https://doi.org/10.1111/j.1365-3091.2010.01194.x

Zecchin, M., Ceramicola, S., Gordini, E., Deponte, M., Critelli, S., 2011b. Cliff overstep model and variability in the geometry of transgressive erosional surfaces in high-gradient shelves: The case of the Ionian Calabrian margin (southern Italy). Mar. Geol. 281, 43–58. https://doi.org/10.1016/j.margeo.2011.02.003

Zecchin, M., Civile, D., Caffau, M., Muto, F., Di Stefano, A., Maniscalco, R., Critelli, S., 2013b. The Messinian succession of the Crotone Basin (southern Italy) I: Stratigraphic architecture reconstructed by seismic and well data. Mar. Pet. Geol. 48, 455–473. https://doi.org/10.1016/j.marpetgeo.2013.08.014

Zecchin, M., Nalin, R., Roda, C., 2004. Raised Pleistocene marine terraces of the Crotone peninsula (Calabria, southern Italy): facies analysis and organization of their deposits. Sediment. Geol. 172, 165–185. https://doi.org/10.1016/j.sedgeo.2004.08.003

Zecchin, M., Praeg, D., Ceramicola, S., Muto, F., 2015. Onshore to offshore correlation of regional unconformities in the Plio-Pleistocene sedimentary successions of the Calabrian Arc (central Mediterranean). Earth-Sci. Rev. 142, 60–78. https://doi.org/10.1016/j.earscirev.2015.01.006

8 Table of figures